

Proprioceptive reflexes and neurological disorders

Alfred C. Schouten

Proprioceptive reflexes and neurological disorders

Proefschrift

ter verkrijging van de graad van doctor
aan de Technische Universiteit Delft,
op gezag van de Rector Magnificus prof. dr ir J.T. Fokkema,
voorzitter van het College voor Promoties,
in het openbaar te verdedigen op dinsdag 25 mei 2004 om 15:30 uur
door

Alfred Christiaan SCHOUTEN

werktuigkundig ingenieur
geboren te Dordrecht, Nederland.

Dit proefschrift is goedgekeurd door de promotor:
Prof. dr F.C.T. van der Helm

Toegevoegd promotor:
Dr J.J. van Hilten

Samenstelling promotiecommissie:

Rector Magnificus,	Technische Universiteit Delft, voorzitter
Prof. dr F.C.T. van der Helm,	Technische Universiteit Delft, promotor
Dr J.J. van Hilten,	Technische Universiteit Delft, toegevoegd promotor
Prof. dr ir M.H.G. Verhaegen,	Technische Universiteit Delft
Prof. dr T. Sinkjær,	Aalborg University
Prof. dr J.H. Arendzen,	Universiteit Leiden
Prof. dr ir D.F. Stegeman,	Katholieke Universiteit Nijmegen
Prof. dr ir P.P.J. van den Bosch,	Technische Universiteit Eindhoven
Prof. dr ir H.G. Stassen,	Technische Universiteit Delft, reservelid

Het onderzoek beschreven in dit proefschrift is mede mogelijk gemaakt door financiële ondersteuning van de Nederlandse organisatie voor wetenschappelijk onderzoek, medische wetenschappen (NWO-MW, project nummer: 902-36-084). De pols manipulator beschreven in dit proefschrift is mede mogelijk gemaakt door een gift van Medtronic.

ISBN 90-77595-41-4

Copyright 2004, A.C. Schouten, Delft, The Netherlands.

All rights reserved. No part of this book may be reproduced by any means, or transmitted without the written permission of the author. Any use or application of data, methods and/or results etc., occurring in this report will be at the user's own risk.

Contents in brief

1	Introduction	1
2	Experimental approach	13
3	Proprioceptive reflexes in patients with complex regional pain syndrome	25
4	Proprioceptive reflexes in patients with Parkinson's disease	35
5	Design of perturbation signals for the estimation of spinal reflexes	47
6	Quantifying spinal reflexes in vivo during postural control	59
7	Design of a torque-controlled wrist manipulator	83
8	Quantifying proprioceptive reflexes at the wrist	97
9	Proprioceptive reflexes at the wrist in patients with Parkinson's disease	119
10	Analysis of reflex modulation with a biological neural network	129
11	Reflections	151

Contents

Contents in brief	iii
Contents	v
1 Introduction	1
1.1 Introduction	2
1.2 Human motion control	2
1.2.1 Neurons	2
1.2.2 Muscles	4
1.2.3 Proprioceptors	4
1.2.4 Postural control	7
1.2.5 Identifying human joint dynamics	9
1.3 Neurological disorders	10
1.3.1 Complex regional pain syndrome	10
1.3.2 Parkinson's disease	10
1.4 Goal and approach	11
1.5 Thesis outline	11
2 Experimental approach	13
2.1 Introduction	14
2.2 Materials and methods	14
2.2.1 Apparatus	14
2.2.2 Procedures	15
2.2.3 Data processing	16
2.3 Discussion	22
3 Proprioceptive reflexes in patients with complex regional pain syndrome	25
3.1 Introduction	26
3.2 Materials and methods	26
3.2.1 Subjects	26
3.2.2 Apparatus	27
3.2.3 Procedures	27
3.2.4 Data processing	28
3.3 Results	30
3.3.1 WB disturbances and intrinsic parameters	30
3.3.2 NB1 disturbances	31

3.3.3	NB2 disturbances	31
3.4	Discussion	32
4	Proprioceptive reflexes in patients with Parkinson's disease	35
4.1	Introduction	36
4.2	Materials and methods	36
4.2.1	Subjects	36
4.2.2	Apparatus	36
4.2.3	Procedures	37
4.2.4	Data processing	39
4.3	Results	41
4.3.1	Nonparametric FRFs	41
4.3.2	Intrinsic and reflexive parameters	45
4.4	Discussion	45
5	Design of perturbation signals for the estimation of spinal reflexes	47
5.1	Introduction	48
5.2	Materials and methods	48
5.2.1	Subjects	48
5.2.2	Apparatus	48
5.2.3	Procedures	48
5.2.4	Data processing	51
5.3	Results	53
5.3.1	Isometric experiments	53
5.3.2	Main experiment	53
5.4	Discussion	57
6	Quantifying spinal reflexes in vivo during postural control	59
6.1	Introduction	60
6.2	Materials and methods	60
6.2.1	Subjects	60
6.2.2	Apparatus	61
6.2.3	Procedures	61
6.2.4	Data processing	63
6.3	Results	71
6.3.1	Activation dynamics	71
6.3.2	Nonparametric FRFs	71
6.3.3	Intrinsic and reflexive parameters	77
6.4	Discussion	79
6.4.1	Methodology	79
6.4.2	Functionality of reflexes	80
6.4.3	Comparison with previous work	80

7	Design of a torque-controlled wrist manipulator	83
7.1	Introduction	84
7.2	Materials and methods	84
7.2.1	Apparatus	84
7.2.2	Procedures	88
7.2.3	Data processing	90
7.3	Results	92
7.3.1	Controller settings	92
7.3.2	Estimation performance	93
7.4	Discussion	95
8	Quantifying proprioceptive reflexes at the wrist	97
8.1	Introduction	98
8.2	Materials and methods	98
8.2.1	Subjects	98
8.2.2	Apparatus	98
8.2.3	Procedures	98
8.2.4	Data processing	100
8.3	Results	107
8.3.1	Isometric experiments	107
8.3.2	Activation dynamics	107
8.3.3	Nonparametric FRFs	107
8.3.4	Intrinsic and reflexive parameters	113
8.4	Discussion	116
9	Proprioceptive reflexes at the wrist in patients with Parkinson's disease	119
9.1	Introduction	120
9.2	Materials and Methods	120
9.2.1	Subjects	120
9.2.2	Apparatus	120
9.2.3	Procedures	121
9.2.4	Data processing	122
9.3	Results	123
9.3.1	Nonparametric FRFs	123
9.3.2	Intrinsic and reflexive parameters	126
9.4	Discussion	128
10	Analysis of reflex modulation with a biological neural network	129
10.1	Introduction	130
10.2	Method	130
10.2.1	Simulation model	131
10.2.2	Procedures	139
10.2.3	Tools and languages	142
10.3	Results	143
10.3.1	Presynaptic inhibition candidate	143

10.3.2	Alternative deficiency candidate	144
10.4	Discussion	145
10.4.1	Model verifications	147
10.4.2	Presynaptic inhibition candidate	148
10.4.3	Alternative deficiency candidate	148
10.4.4	Conclusion	149
11	Reflections	151
11.1	Introduction	152
11.2	Results and conclusions	152
11.3	Recommendations and future directions	155
11.3.1	Medical applications	155
11.3.2	Effect of tasks and conditions	156
11.3.3	Future challenges	157
11.4	Epilogue	158
	References	159
	A Spiking vs. continuous time-signals	165
	Summary	169
	Samenvatting	173
	Dankwoord	177
	Curriculum vitae	179

List of abbreviations

ANOVA	analysis of variance
BNN	biological realistic neural network
CF	crest factor
CNS	central nervous system
CRPS	complex regional pain syndrome
CVA	cerebro vascular attack
DOF	degrees-of-freedom
DSP	digital signal processor
EMG	electromyography
FFT	fast Fourier transform
FRF	frequency response function
GTO	Golgi tendon organ
IEMG	integrated rectified EMG
NB	narrow bandwidth
NMS	neuromusculoskeletal
PD	Parkinson's disease
RMS	root-mean-square
RSD	reflex sympathetic dystrophy
RSI	repetitive strain injury
SD	standard deviation
SNR	signal-to-noise ratio
VAF	variance accounted for
WB	wide bandwidth

Chapter 1

Introduction

Proprioceptive reflexes play an important role during the control of movement and posture. Many studies suggest disturbed modulation of proprioceptive reflexes as the cause for the motor features present in neurological disorders. However no quantitative data exist to support the hypothesis. In this thesis methods are developed and evaluated to quantify proprioceptive reflexes in vivo during postural control. The prime goal of this thesis is to gain insight in the pathophysiology of motor disorders and to evaluate the method as a diagnostic tool. This chapter provides an introduction to relevant physiological and control engineering background. The last section of this chapter describes the outline of the thesis.

1.1 Introduction

Humans are capable of performing a large variation of movements and postures. The central nervous system (CNS), i.e. the 'brain' with the spinal cord, coordinates the muscles which generate the force required for movements. Even in the presence of unpredictable and unexpected external disturbances humans are able to perform the intended movement or to hold the intended posture. For example during walking at the beach, while a strong gale is blowing, the CNS must continuously react adjusting muscle tension not to fall over. Remarkably most of the time these corrections for the disturbances are fast and made unconsciously. Small sensory organs inside the body, called proprioceptors, inform the CNS about the actual movement of the body segments and play an important role in coordinated movement.

Movement disorders are commonly found with a brain disease, i.e. a neurological disorder. An example of such a movement disorder is tremor (shaking), as seen with Parkinson's disease. This thesis investigates the role of proprioceptive information in the development of the motor features with neurological disorders. This chapter provides the necessary background on human motion control such that the goal can be formulated. The chapter ends with an outline of the complete thesis.

1.2 Human motion control

From an engineering perspective the human neuromusculoskeletal system can be regarded as a robot, consisting of a linkage system (the skeleton) with motors (muscles), sensors (proprioceptors), and a control system (the CNS). The nerves and neurons are the wires and connectors, which transport the information from the proprioceptors to the CNS and from the CNS to the muscles. The CNS integrates intentions with information from the proprioceptor to coordinate movement of the skeleton by selectively (de-)activating muscles. Control engineers will directly recognize a feedback loop: the movement results from commands from the CNS, which on their turn (partly) depend on the movement sensed by the proprioceptors (proprioceptive feedback), i.e. there is a mutual interaction between CNS and limb movement.

1.2.1 Neurons

Neurons, or nerve cells, are the primary elements of the CNS. A typical neuron contains a cell body, dendrites and an axon, see Fig. 1.1. The cell body receives signals from other neurons via several short dendrites, and via one long axon (nerve) a signal can be sent to other neurons. The contact of the axon of a sending neuron to the dendrite of a receiving neuron is called a synapse. Three types of neurons play a role in human movement control: motoneurons, sensory neurons, and interneurons. Motoneuron, or efferent neurons, lie in the spinal cord and excite the muscle. Sensory, or afferent, neurons carry information from proprioceptors to the CNS. Interneurons are the largest group of neurons and comprise all other neurons.

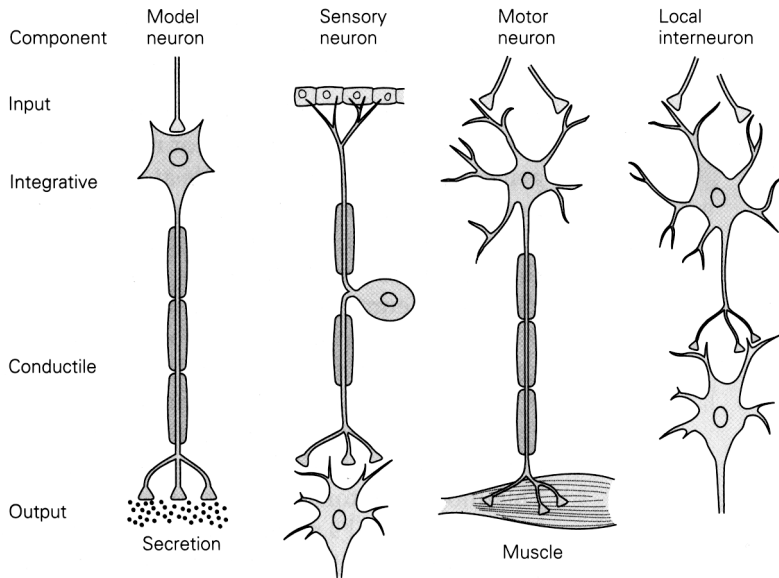


Figure 1.1: In general neurons have four major functional regions: an input region, an integrative part to process the input (the cell body), a conductive axon (nerve), and an output. Sensory neurons lack the input of other neurons, motoneurons innervate muscles, and interneurons often lack a long conductive nerve. (adapted from Kandel et al., 2000)

Interneurons get input and send output only to other neurons. Interneurons form complex networks to process sensory information and to generate muscle commands. The dendrites of one spinal motoneuron make around 10000 contacts with sensory and interneurons.

Information in the CNS is processed via electrochemical processes. In rest the electric potential in a cell body of a neuron is -80 mV compared to the extracellular fluids. When this potential is raised above a threshold of -60 mV a chain of reactions follows, resulting in an action potential. With an action potential the potential of the neuron quickly rises to 20 mV lasting approximately 1 ms and slowly decaying to the rest potential. This action potential is conducted over the axon typically with a speed of 1 to 100 m/s, depending on the diameter of the axon, or the nerve. Thicker nerves conduct faster. A neuron releasing an action potential is referred to as spiking of the neuron. As the width and height of this spike is fixed the information is present in the numbers of spikes per time unit, i.e. the spike rate.

When the action potential reaches the end of the axon, i.e. the synaptic terminal, neurotransmitters are released. These chemical neurotransmitters interact with the receptor molecules on the dendrites of the receiving neuron, resulting in a potential change in the receiving neuron. Depending on the type of neurotransmitter either the potential of the receiving neuron increases (excitatory synapses) or decreases

(inhibitory synapses). With an inhibitory synapse the potential in the receiving neuron is lowered, making it less sensitive for excitatory synapses from other neurons.

1.2.2 Muscles

Skeletal muscles provide the force needed to move and support the skeleton. The muscles are connected via tendons to the skeleton and are activated by the α -motoneurons located in the spinal cord. Most skeletal muscles consist of thousands parallel muscle fibres. The axons of the motoneurons innervate the muscle fibres at the endplates. One muscle is activated by several hundreds of motoneurons, each innervating a selected number of muscle fibres: a motor unit. An incoming action potential propagates relatively slow (3-5 ms) in both directions along the muscle fibres. As one action potential innervates many muscle fibres a single action potential results in electric activity that even can be recorded over the skin surface with electromyography (EMG).

Muscle fibres are complex structures, for this thesis it goes too far to describe the structure in high detail. The contractile force is produced by so-called cross bridges. Each muscle fibre contains contractile proteins, organized in thick and thin filaments. A thick filament is made up of about 250 myosin molecules, which each can bind to the thin filaments: a cross bridge. As Ca^{2+} facilitates the binding of the cross bridges, the force a muscle fibre generates depends on the intracellular concentration of Ca^{2+} . Under resting conditions the intracellular concentration of Ca^{2+} is kept low by active pumping into the sarcoplasmic reticulum, responsible for sequester and release of Ca^{2+} . With the arrival of an action potential Ca^{2+} is released. Periodic action potentials are necessary to obtain a constant concentration of Ca^{2+} and consequently a constant muscle force. The process of release and sequester of Ca^{2+} is not instantaneous and is called activation dynamics.

In 1938 Hill showed that with a constant activation level the muscle force depends on the length of the muscle and the stretch velocity, see Fig. 1.2. Huxley (1969) suggested that the force-length relationship originates from the overlap of thick and thin filaments, which is directly related to the number cross bridges available for binding. Furthermore Huxley suggested that shortening facilitates the unbinding of the cross bridges reducing the contractile force and vice versa, explaining the force-velocity relationship.

For small deviations, like in posture control the force-length and force-velocity relationship can be linearised and described with stiffness and damping. Higher activation levels generally result in higher stiffness and damping.

1.2.3 Proprioceptors

Proprioception is the unconscious perception of movement and spatial orientation arising from sensory organs (proprioceptors) within the body itself. Proprioceptors sense the movement and internal forces in the body. They include muscle spindles, Golgi tendon organs, joint sensors, skin receptors and the vestibular system.

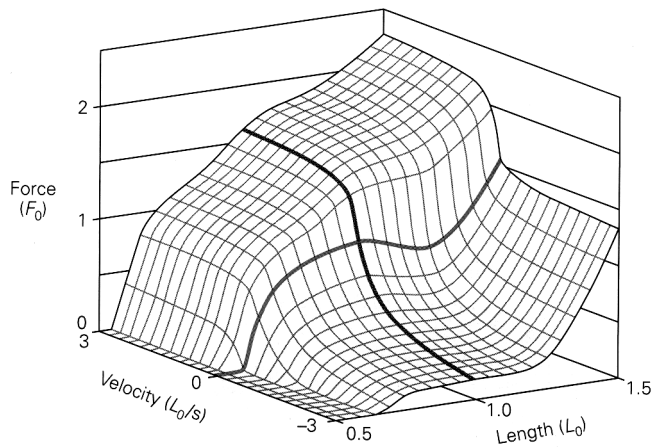


Figure 1.2: The muscle force is a function of muscle length and velocity, given a constant activation level. For most regions the slope for force-length relation is positive. (Adapted from Kandel et al., 2000)

Muscle spindles are located inside the muscle and provide information about muscle stretch and stretch velocity. Golgi tendon organs (GTOs) sense the tension in the tendon, which is directly related to the muscle force. Joint sensors are sensitive to the joint position. Skin, or tactile, receptors sense the pressure at the skin. And finally the vestibular system in the middle ear gives information about the acceleration of the head. The slowness of the joint and skin receptors makes them relatively unimportant for human motion control. Muscle spindles and GTOs are the most important proprioceptors for motion control of the human arm.

Muscle spindles

Muscle spindles are small sensory receptors within the muscle. As the muscle spindles lay in the muscle parallel to the muscle fibres, its stretch is proportional to the stretch of the muscle. The main components of a muscle spindle are the intrafusal muscle fibres, afferent sensory fibre endings and efferent motor fibre endings, see Fig 1.3A. The intrafusal muscle fibres are specialised muscle fibres and their central region is noncontractile. The sensory fibres endings spiral around the central region of the intrafusal muscle fibres and are responsive to stretch of these muscle fibres. γ -motoneurons innervate the intrafusal muscle fibres and changes the sensitivity of the sensory fibre endings to stretch.

A muscle spindle contains three types of intrafusal muscle fibres: dynamic nuclear bag fibres, static nuclear bag fibres, and nuclear chain fibres, see Fig 1.3B. Two types of afferent sensory fibres leave the muscle spindle: primary (Ia) and secondary (II) endings. Primary endings are most sensitive to stretch velocity and secondary endings to stretch. Primary endings make contact with all three types of intrafusal muscle fibres, the secondary ending make contact with static nuclear

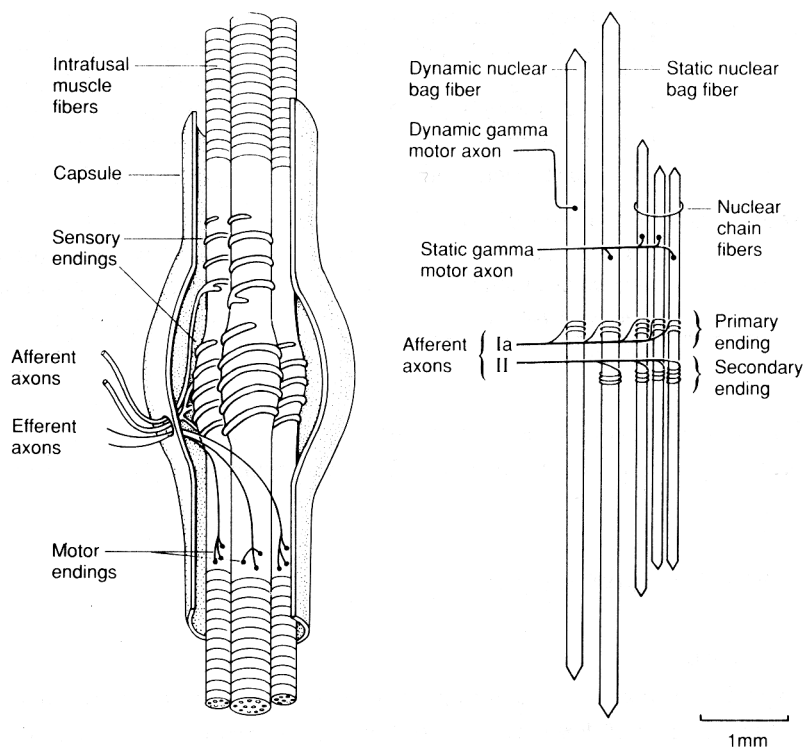


Figure 1.3: A. Physiology of a muscle spindle; B. The intrafusal fibres of a muscle spindle, see text for details. (Adapted from Kandel et al., 2000)

bag and nuclear chain fibres. Two types of γ -motoneurons innervate the intrafusal muscle fibres: static γ -motoneuron innervate both static nuclear bag fibres and nuclear chain fibres, dynamic γ -motoneuron only innervate the dynamic nuclear bag fibres. As the CNS can independently innervate both types of γ -motoneurons, the sensitivity of both sensory fibres can independently be set.

Golgi tendon organs

Golgi tendon organs (GTOs) are sensory receptors located at the junction between muscle fibres and tendon. Tendon organs are thin encapsulated structures and have one single afferent axon (Ib), see Fig. 1.4. The afferent ending diverges into many fine endings, which intertwines among the collagen fibres. Stretching of a GTO straightens the collagen fibres, compressing the nerve endings and causes them to fire. The stretch of a GTO depends on the load, which is proportional to the muscle force, as a GTO is in series with a muscle. Crago et al. (1982) showed that the spike rate of a GTO is linear with the muscle force.

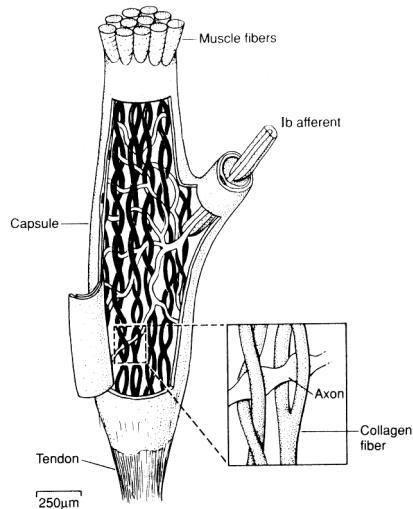


Figure 1.4: *Physiology of a Golgi tendon organ, see text for details. (Adapted from Kandel et al., 2000)*

1.2.4 Postural control

This thesis deals with postural control. Postural control is a specific case within human motion control. The human has to maintain a posture, i.e. an equilibrium position. During postural control two independent strategies contribute to stability and performance: (1) intrinsic properties of the muscles and (2) proprioceptive reflexes. With activation of a muscle not only the generated force increases, but also the visco-elasticity increases, i.e. the resistance to external disturbances. By co-activation of antagonistic muscles around a joint the joint remains in equilibrium and is less sensitive to disturbances. Proprioceptive reflexes from muscle spindles provide information about stretch and stretch velocity. This information is fed back to the motoneurons. A stretch after a perturbation results in selective activation and deactivation of the antagonistic muscles to restore the posture. Co-activation is very energy consuming as the muscles are constantly activated. Reflexes are energy efficient as the muscles are only activated in response to a present disturbance. Major drawback of reflexes is the time delay; reflexes are not instantaneous. It takes time to transport the signals over the nerves and to process the information. Also the force build-up in a muscle takes time (activation dynamics). From control engineering it is known that the effectiveness of time delayed feedback is limited as oscillations and instability must be avoided. Smaller delay, i.e. faster response, gives larger stability margins and consequently can be more effective.

Proprioceptive reflexes

A proprioceptive reflex is the contraction of a muscle, in response to stimuli from a proprioceptor. An example is the knee jerk, with a small tap just below the knee on the tendon the muscle is lengthened. This muscle lengthening is sensed by muscle spindles and automatically, unconsciously, the muscle contracts resulting in shortening of the muscle, opposing stretch.

Traditionally reflexes are categorized in three types according to the reflex latencies: short, medium, and long latency reflexes. The shortest possible feedback path is from the muscle spindles to the spinal cord and back to the muscle: the short latency reflex (e.g. the knee jerk). As this reflex loop is formed via the spinal cord and does not leave the spinal cord short latency reflexes are also called spinal reflexes. The delay of spinal reflexes is around 30-60 ms and mainly depends on length of the nerves, in distal joints the delay is larger than for proximal joints. Both medium and long latency reflexes are cortical reflexes, i.e. the cortex is part of the reflex arc, and typically have a delay of 60 ms and slower. Spinal reflexes have the greatest influence on the performance as the time delay is the smallest, giving large stability margins. Humans have the possibility to (unconsciously) change the reflex magnitude, even of spinal reflexes. With γ -activation the sensitivity of the muscle spindles can be set by the CNS. Furthermore with presynaptic inhibition of muscle spindle afferents the magnitude of the spinal reflex can be reduced (Stein and Capaday, 1988). This makes the CNS an adaptive controller, it does not only amplify and distribute the signals from proprioceptors to the α -motoneuron, but it also can adjust/modulate the gain of the amplifier.

Stability and performance

In human motion control the CNS must preserve stability and optimize performance. In general a controller has a good performance if the motion follows the desired/planned motion and disturbances have minimal influence on the motion. The first is expressed in the so-called control behaviour and the latter in the disturbance behaviour. For a good disturbance rejection the sensitivity for external disturbances must be low. In daily life external disturbances continuously act on the body. These disturbances can be large (a strong gale during walking at the beach) and can be small (the wind from a butterfly flapping its wings), but disturbances are always present.

Stability is a prerequisite for a good performance. Any system is stable or unstable, there is no intermediate. In postural control stability implies that the posture is robust to a perturbation. Instabilities will present as shaking of limbs or ultimately in fixed tonic postures. Instabilities can occur when the reflex magnitude is too large relative to the muscle cocontraction. With muscle cocontraction the joint visco-elasticity increases instantaneously, enlarging the stability margins. With proprioceptive reflexes the build-up of corrective force after a perturbation takes time depending on the neural time delay and the muscle activation dynamics. As a result of delay, there exist one frequency (a sine) where the corrective action, i.e. the

feedback, is opposite to perturbation (the input and output sine are shifted a half period compared to each other). The system is unstable if the amplitude of the corrective action at that frequency is larger than the perturbation, as the amplitude increases for every following period.

1.2.5 Identifying human joint dynamics

In human motion control one tries to identify the dynamics of the skeleton, muscles, sensors, and controller. It is the challenge to find the structure and the parameters of the controller and how it handles with different conditions and/or disturbances.

Position, forces and EMG of the muscles are the variables that can be observed noninvasively in humans. Furthermore position and force disturbances can be applied to perturb the posture and to provoke a response. With system identification a model of the system (joint dynamics) is obtained by analysis between input (position or force) and output (force or position, sometimes EMG). Two types of perturbations (input) can be distinguished, i.e. force and position perturbations. For technical systems there is no principal difference. However humans are highly adaptive and need a proper task instruction. Force disturbances require a position task and vice versa.

Position tasks (with force perturbations) are natural for the subject. They mimic daily life situations, and are superior to investigate the functionality of proprioceptive reflexes. The subject has to actively preserve stability and reflexes contribute to the performance. Note that in human motion control the function of the perturbation is twofold. Firstly it provides the input necessary to excite the system, allowing identification, and secondly the perturbation is part of the conditions to influence reflexive behaviour. As the CNS is an adaptive controller, weighting performance against effort, different perturbations will give different weights.

The neuromusculoskeletal system is highly nonlinear by nature, as the skeleton is a multi-link system and the muscles, proprioceptors, and neurons are all nonlinear. Most control engineering and system identification tools are only valid for linear systems. It is desirable to investigate the human neuromusculoskeletal system in a state that allows linearisation, so that linear tools can be used. Linearisation is allowed when small deviations around an equilibrium posture are concerned, for example during postural control.

To identify a system the system must be perturbed. Perturbation signals can be classified into transients and continuous signals. Continuous signals have the advantage that the human can tune its controller during the perturbation to maximize the performance (disturbance rejection). It is thought that after a few seconds the optimal setting is obtained (Van der Helm et al., 2002). With transient signals, like steps, it is unclear which reflex setting is measured. For the first transient disturbance the reflex setting from before the disturbance is recorded and after several tests the setting will possibly converge to an optimal setting for the given disturbance (learning). This implicates that many trials have to be performed before the subject is adapted to the applied transient perturbation, if he/she adapts at all. The interest of this study is the modulation of reflexive feedback and to exclude an-

ticipation, i.e. non-reflexive behaviour, the disturbances must be unpredictable. In this study we have chosen to use continuous random signals, *continuous* to allow modulation of the reflexes, and *random* to prevent anticipation.

1.3 Neurological disorders

1.3.1 Complex regional pain syndrome

Complex regional pain syndrome (CRPS), formerly known as reflex sympathetic dystrophy (RSD), is a painful condition that typically follows an injury to a limb, which can be minimal or severe (sprain/strain, fracture, contusion/crush injury), although in a number of patients no trauma can be identified. The syndrome manifests with variable combinations of pain, differences in skin colour and temperature, oedema and sweating (Paice, 1995; Ribbers et al., 1995). The syndrome may spread to other extremities. In addition to the sensory and autonomic signs and symptoms, patients may present or subsequently develop movement disorders (Van Hilten et al., 2001). One of the most common movement disorders is tonic dystonia of the affected limb(s) (Bhatia et al., 1993; Schwartzman and Kerrigan, 1990). Although the mechanism behind CRPS is still considered elusive, the evidence implicating involvement of inhibitory interneuronal circuits in the pathophysiology of tonic dystonia in patients with CRPS is compelling (Van Hilten et al., 2000).

1.3.2 Parkinson's disease

Parkinson's disease (PD) is a neurodegenerative disorder characterized by: tremor, bradykinesia, rigidity, and impaired postural reflexes. PD is seen predominantly in elderly people. In PD the dopamine producing cells in the substantia nigra are gradually lost. The substantia nigra is one of the principal nuclei in the basal ganglia of the CNS. The basal ganglia play a major role in voluntary movements and dopamine is one of the major neurotransmitters in the basal ganglia.

Current studies indicate that the reflex magnitude is modulated by presynaptic inhibition of muscle spindle afferents in the spinal cord, under control of higher centres in the CNS (Stein and Capaday, 1988). Consequently the loss of dopamine in higher centres of the CNS must also influence the reflex gain modulation. Reduced ability to presynaptically inhibit muscle spindle afferents will result in high reflexive feedback gains. The features of PD are in agreement with the consequences of extraordinary high reflexive feedback gains. High feedback gains make a system stiffer: rigidity. High feedback gains, in a time-delayed feedback loop, result in oscillatory behaviour: tremor. High feedback gains hamper performance and tend to keep the joint in its equilibrium: bradykinesia.

1.4 Goal and approach

Motor features are common with neurological disorders. Abnormalities of muscle tone are an integral component of many chronic neurological disorders. Where muscle tone is clinically defined as the force with which a muscle resists being lengthened. Dystonia, rigidity, and spasticity are three different forms of hypertonia, i.e. abnormally high muscle tone. Many studies suggest that the motor features of neurological disorders in general and hypertonia specifically results from exaggerated proprioceptive reflexes. However no quantitative data are available to support this hypothesis.

The prime goal of this project is to gain insight in the pathophysiology of the neurological disorders with hypertonia. The objective is met by quantifying the proprioceptive reflexes for two neurological disorders, which each is related to one form of hypertonia: complex regional pain syndrome (CRPS), dystonia; and Parkinson's disease (PD), rigidity. Proprioceptive reflexes will be quantified with the shoulder manipulator to get insight of the pathophysiology and to show the potential of the methods as a diagnostic tool. To measure a more distal joint and to be more flexible in the future a new, mobile, wrist manipulator will be developed.

1.5 Thesis outline

Except this Chapter, Chapter 2 and the last Chapter, all Chapters are written as autonomous chapters and can be read individually. In **Chapter 2** the shoulder manipulator and the experimental methods to quantify proprioceptive reflexes are described in detail. Chapters 3-6 and 10 concern about reflexes at the shoulder and 7-9 about reflexes at the wrist. **Chapter 11** draws up the balance and discusses possible future directions.

In **Chapter 3** proprioceptive reflexes around the shoulder in patients suffering from complex regional pain syndrome (CRPS) are assessed. To provoke different reflex gain settings the bandwidth of the force disturbance signal is varied, while subjects were asked to '*minimize the deviations*'. Reflex gains are quantified by fitting a model onto the mechanical admittance. In **Chapter 4** the modulation of proprioceptive reflexes in patients with Parkinson's disease (PD) is investigated. The external damping, imposed by the manipulator, is varied, while a wide bandwidth force disturbance is applied. External damping reduces the oscillations due to tremor, one of the symptoms of PD, which otherwise would dominate and deteriorate the recordings.

In **Chapter 5** and **6** the method to quantify proprioceptive reflexes is substantially improved. The original method relied on the analysis of the endpoint admittance and prior assumptions were needed to separate intrinsic and reflexive contributions. Inclusion of the reflexive impedance, i.e. the dynamic relationship between position and EMG, removed the need for prior assumptions. To estimate the reflexive impedance reliably special force disturbance signals were designed as described in Chapter 5. In Chapter 6 the method to quantify the intrinsic and

reflexive parameters is developed.

For most neurological disorders the motor features starts at distal joints and may affect more proximal joints as the disease develops. A wrist manipulator is developed to measure reflexes at the wrist. The design of the wrist manipulator is described in **Chapter 7**. In **Chapter 8** the newly developed wrist manipulator is used to quantify reflexes at the wrist for healthy subjects, using the improved method (Chapter 5 and 6). In **Chapter 9** the proprioceptive reflexes at the wrist are quantified for patients suffering from Parkinson's disease.

In **Chapter 10** a biological realistic neural network is built and connected with a muscle-limb model to investigate the reflex gain modulation. By removing specific neural connection(s) it is tried to replicate the results of Chapter 3 and to investigate which connection(s) might be responsible for the observed results in patients with CRPS.

Chapter 2

Experimental approach

In this thesis proprioceptive reflex gains are quantified during postural control. Continuous random force disturbances are applied by means of a manipulator (the shoulder manipulator), while subjects are instructed to 'minimize the deviations' of the handle. The results were analysed in frequency domain with the frequency response function (FRF) of the mechanical admittance, expressing the dynamic relation between force disturbance and handle position. The mechanical response to an external force disturbance comprises intrinsic (muscle) and reflexive properties. The parameters of the intrinsic visco-elasticity and proprioceptive feedback gains are obtained by fitting a model onto the mechanical response. By either changing the bandwidth of the force disturbance or the external dynamics imposed by the manipulator different reflex settings are provoked. This chapter describes the shoulder manipulator, the model for human posture control, and the procedure to obtain the intrinsic and reflexive parameters.

2.1 Introduction

Recently, a method has been developed that allows the quantitative assessment of proprioceptive reflex gains at the shoulder during posture tasks (Van der Helm et al., 2002; Brouwn, 2000). In this method continuous random force disturbances are applied, via a handle, to the arm, while the subject is instructed to '*minimize the position deviations*' resulting from the force disturbances. Subjects will counteract the disturbances with cocontraction of all muscles around the shoulder girdle, and also proprioceptive reflexes are involved. The method allows the quantification of both the intrinsic muscle visco-elasticity and the magnitude of the proprioceptive reflexes. By changing the frequency content of the force disturbance, different reflex gain settings are provoked. Model studies show that healthy subjects modulate the reflex gains to optimally suppress the deviations resulting from the disturbances (De Vlugt et al., 2001; Schouten et al., 2001). A follow-up study showed that subjects will also modulate reflex gain with external damping (De Vlugt et al., 2002). Major advantages of force perturbations (and consequently position tasks) are that the task is natural and motivating for the subject. In contrast to the often used position perturbations the subject has to preserve stability actively. Furthermore a position task is unambiguous and functional to the usage of proprioceptive reflexes, i.e. requiring maximum stiffness, demanding high cocontraction and pronounced reflexive feedback.

2.2 Materials and methods

2.2.1 Apparatus

With the shoulder manipulator force disturbances are applied to the hand by means of a linear manipulator, see Fig. 2.1 (Ruitenbeek and Janssen, 1984; Van der Helm et al., 2002). The subject sits in a chair and holds a handle with the right hand. The subject can move the handle of the manipulator for- and backwards, resulting in ante-/retroflexion of the shoulder joint. The height of the chair is adjusted so that the forearm is in-line with the piston of the actuator. Subjects had to hold their right arm in 90 degrees flexion. This position is defined as the neutral, or reference, position.

The hand force exerted by the subject, $f_h(t)$, is measured by a force transducer mounted between the handle and the piston of the hydraulic actuator. From the force applied by the subject the controller generates the handle position, $x_h(t)$, making a force controlled manipulator. The electronic controller of the hydraulic actuator compensates for the dynamics of the actuator and to the subject the manipulator behaves like an external mass-spring-damper system. The parameters for mass (m_e), damper (b_e), and spring (k_e) are adjustable between limits (m_e : 0.6-10 kg; b_e : 0-200 Ns/m; k_e : 0-125 N/m). Additionally an external force disturbance, $d(t)$, can be added to the hand force.

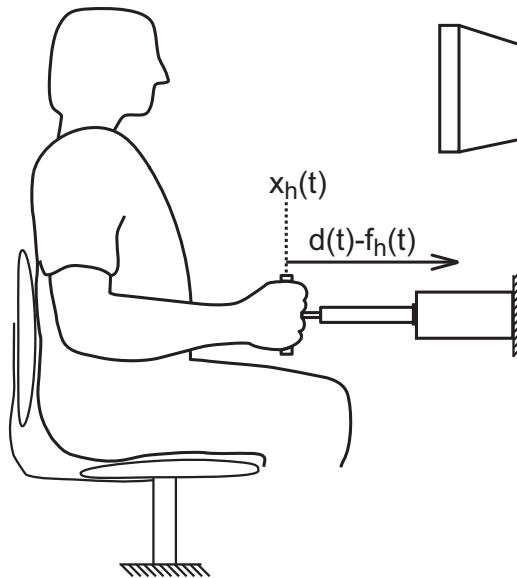


Figure 2.1: Experimental set-up; the subject sits on a chair and holds the handle with the right hand. The subject can move the handle for- and backwards. The hand force $f_h(t)$ applied to the hydraulic manipulator is measured by a force transducer mounted between the handle and the piston. The manipulator controls the position of the handle $x_h(t)$ and is based on the hand force, the external force disturbance $d(t)$ and the simulated external dynamics (also environment). To assist the subject the actual position of the handle is shown on the display.

2.2.2 Procedures

Subjects had to hold the handle and were instructed to ‘minimize the displacements’ of the handle, while continuous random force disturbances (task *stiff*). The length of the disturbance was 40 s (reduced to 30 s in the extended method, see Chapters 5 and 6). The actual position of the handle was shown on a display to prevent drift and to inform the subject about the magnitude of the position deviations. The subjects experienced the task as natural and motivating. Only a few trials were necessary to get the subject acquainted with the manipulator. To obtain a better estimate for the mass of the arm, the task *slack* was used during some trials: the subject was asked not to react to the disturbances and to minimize any effort, resulting in minimal muscle activation.

To provoke different reflexive settings multiple trials were recorded in which the bandwidth of the force disturbance or the parameters of the manipulator were varied, see each Chapter for details. For each condition the magnitude of the disturbance signal was set by trial-and-error to get an approximately equal magnitude

for the position deviations. Generally four conditions can be distinguished:

- Wide bandwidth (WB) disturbance: signal with uniform power typically between 0.5 and 20 Hz.
- Narrow bandwidth disturbance type 1 (NB1): signal with uniform power between 0.5 Hz and a variable upper frequency.
- Narrow bandwidth disturbance type 2 (NB2): signals with power around a specific centre frequencies.
- External damping conditions: values for the damping imposed by the manipulator are set, while the WB signal is used as a disturbance.

The first condition (WB disturbance) with task *stiff* and no external damping is referred to as the reference condition.

2.2.3 Data processing

Signal recording and processing

During each trial the force disturbance $d(t)$, the position of the handle $x_h(t)$, the force at the handle $f_h(t)$, and the EMG of four relevant shoulder muscles (e_1 : m. pectoralis major, e_2 : m. deltoideus anterior, e_3 : m. deltoideus posterior, and e_4 : m. latissimus dorsi) were recorded and stored on computer. Before recording, the EMG signals were high pass filtered to remove DC components and movement artefacts (20 Hz, 3th order Butterworth), amplified, rectified and low pass filtered to prevent aliasing (200 Hz, 3th order Butterworth). All signals were recorded at 500 Hz with 12 bits resolution.

In Chapters 5 and 6 the EMG signals were digitally rectified and the EMG signals were recorded before rectifying. This required a higher sample frequency (2.5 kHz) and consequently a higher cut off for the anti-aliasing filter (1 kHz). Furthermore the signals were recorded with a higher resolution (16 bits).

Nonparametric analysis

To remove any transient response the first 3616 samples per channel (≈ 7 s) of each trial were omitted, as the objective is to investigate stationary behaviour, leaving 2^{14} samples ($T_{obs} \approx 33$ s) for analysis. Note that Chapters 5 and 6 use different numbers as both the trial length and sample rate are different (30 s, 2.5 kHz), see the chapters for details.

The position, force, and disturbance signals ($x_h(t)$, $f_h(t)$, $d(t)$) were Fourier transformed (via fast Fourier transform, FFT) and used to estimate the cross and

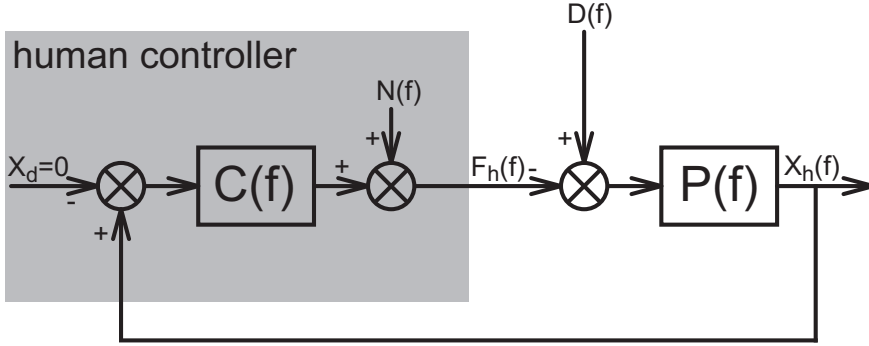


Figure 2.2: Block scheme of human posture control expressed in the frequency domain. $C(f)$: transfer function of arm dynamics; $P(f)$ transfer function of manipulator dynamics; $D(f)$ external force disturbance; $F_h(f)$ hand reaction force; $X_h(f)$ hand position (coincides with the manipulator handle); $N(f)$ model remnant; $X_d = 0$ reference position. The arm dynamics (grey box) are described by the linear transfer function, $C(f)$, together with the remnant $N(f)$, which is uncorrelated with $D(f)$.

auto spectral densities.

$$\hat{G}_{df}(f) = D(-f)F_h(f) = D^*(f)F_h(f) \quad (2.1)$$

$$\hat{G}_{dx}(f) = D(-f)X_h(f) = D^*(f)X_h(f) \quad (2.2)$$

$$\hat{G}_{dd}(f) = D(-f)D(f) = D^*(f)D(f) = |D(f)|^2 \quad (2.3)$$

$$\hat{G}_{xx}(f) = X_h(-f)X_h(f) = X_h^*(f)X_h(f) = |X_h(f)|^2 \quad (2.4)$$

in which $\hat{G}(f)$ denotes the estimated spectral densities (hat denotes estimate), and an asterisk denotes the complex conjugate. $X_h(f)$, $F_h(f)$, and $D(f)$ are the Fourier transforms of $x_h(t)$, $f_h(t)$, and $d(t)$ respectively. The resolution of frequency depends on the observation time and equals T_{obs}^{-1} , in this case approximately 0.03 Hz. The spectral densities were averaged over 4 adjacent frequencies to improve the estimates and to reduce the variance of the estimators (Jenkins and Watts, 1968). As a result the frequency resolution dropped to $\frac{4}{T_{obs}} \approx 0.12$ Hz.

Fig. 2.2 gives the closed loop block scheme of human posture control. The position of the manipulator's handle is force-controlled by the subject. The manipulator imposes a mass-spring-damper system and the human controls the position of the handle while force disturbances are applied. Because force disturbances were applied, interaction between the subject and manipulator existed (the position of the manipulator depended on both the dynamics of the subject and the external dynamics imposed by the manipulator). Because of this interaction closed loop iden-

tification algorithms were required to estimate the dynamics of the subject:

$$\hat{H}_{dx}(f) = \frac{\hat{G}_{dx}(f)}{\hat{G}_{dd}(f)} \equiv \frac{P(f)}{1 + P(f)C(f)} \quad (2.5)$$

$$\hat{H}_{df}(f) = \frac{\hat{G}_{df}(f)}{\hat{G}_{dd}(f)} \equiv \frac{P(f)C(f)}{1 + P(f)C(f)} \quad (2.6)$$

$$\hat{H}_{xf}(f) = \frac{\hat{G}_{df}(f)}{\hat{G}_{dx}(f)} \equiv C(f) \quad (2.7)$$

in which $\hat{H}_{xf}(f)$ is the estimated frequency response functions (FRF) of the arm impedance and $\hat{H}_{dx}(f)$ the estimated FRF of the combined admittance. As force perturbations are applied it is more natural to present the arm admittance (force as input, position as output), and so the impedance is inverted.

$$\hat{H}_{fx}(f) = \frac{\hat{G}_{dx}(f)}{\hat{G}_{dx}(f)} = \hat{H}_{xf}^{-1}(f) \quad (2.8)$$

In addition to the admittance the coherence $\hat{\gamma}^2(f)$ was estimated.

$$\hat{\gamma}^2(f) = \frac{|\hat{G}_{dx}(f)|^2}{\hat{G}_{dd}(f)\hat{G}_{xx}(f)} \quad (2.9)$$

The coherence represents a measure of the linearity and signal-to-noise ratio (SNR) as a function of frequency. By definition, the coherence varies between 0 and 1. A coherence of 1 at a certain frequency means that a linear relationship exists between input/output and that the signals contain no noise at that frequency. Possible causes of low coherence are voluntary activity during a trial, resulting in displacements or noise unrelated to the applied signal. Generally spoken, if the coherence is high over all relevant frequencies, a linear relationship exists and the human arm can be modelled with the aid of a linear model.

Quantifying intrinsic and reflexive properties

The dynamic behaviour of the neuromusculoskeletal system in response to external disturbances is the result of interactions between intrinsic (inertias of the limbs, passive visco-elasticity of tissues, and visco-elasticity of the antagonistic muscles) and reflexive (proprioceptive reflexes) parameters. Because intrinsic and reflexive properties coexist during most tasks, reflexes cannot be measured directly. An indirect method was used to separate intrinsic and reflexive parameters (Van der Helm et al., 2002). This method is based on two basic principles: (1) during the *stiff* task with the WB disturbance and no external damping (the reference condition) reflexive feedback is negligible and so only intrinsic properties remain and (2) for all *stiff* tasks the average muscle activation is constant, i.e. the intrinsic properties are constant, see Discussion for motivation. These principles imply that all changes in

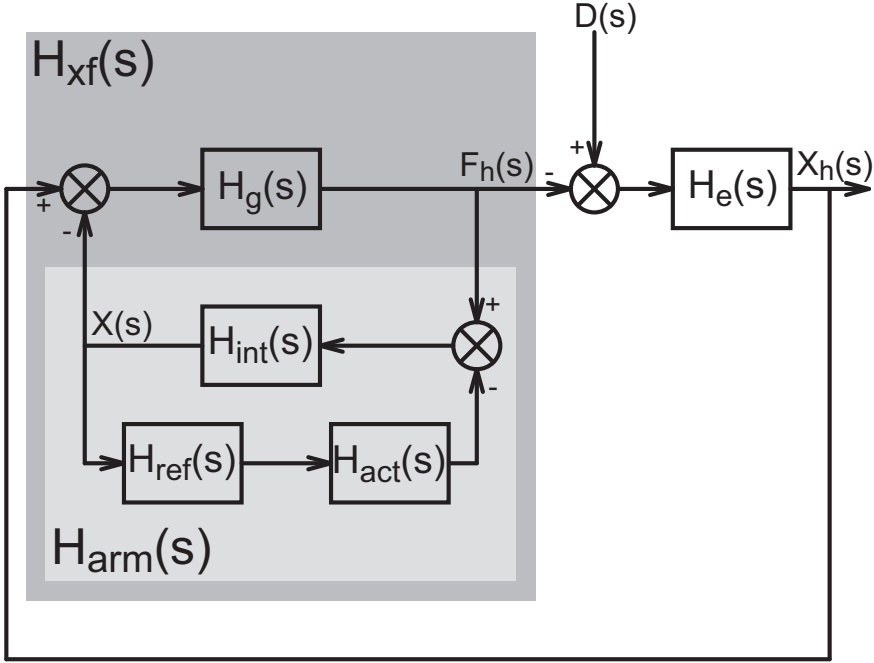


Figure 2.3: Neuromusculoskeletal model $H_{xf}(s)$ in conjunction with the environment $H_e(s)$. The external force disturbance $D(s)$, hand force $F_h(s)$, and position of the handle $X_h(s)$ are measured. $X(s)$ represents arm position, $H_g(s)$ grip dynamics, $H_{int}(s)$ intrinsic properties, $H_{act}(s)$ activation dynamics, and $H_{ref}(s)$ reflexive feedback. The light grey box represents the arm model, $H_{arm}(s)$, only. The dark grey box ($H_{xf}(s)$) is the model to describe the measured transfer function of the human arm, and $H_e(s)$ describes the dynamics imposed by the manipulator.

admittance during tasks with NB disturbances or external damping conditions, in comparison with WB disturbance and no external damping, can be attributed to proprioceptive feedback.

Fig. 2.3 gives the model for human posture control. The manipulator, $P(f)$ in Fig. 2.2, imposes an external environment, which is described as a second order mass-spring-damper system $H_e(s)$, with external mass m_e , external damping b_e , and external stiffness k_e .

$$H_e(s) = \frac{1}{m_e s^2 + b_e s + k_e} \quad (2.10)$$

The Laplace operator s equals $\lambda + j2\pi f$ in which $\lambda = 0$ because the initial transient response is not of interest in this study. The arm model (excluding the hand, light grey box in Fig. 2.3) is represented as a causal system with force as input and position as output. The interaction force, modelled as hand force f_h , that drives both the

arm and manipulator results from the hand grip dynamics H_g , and the difference between the handle position x_h and arm position x :

$$H_g(s) = b_g s + k_g \quad (2.11)$$

in which b_g and k_g are respectively the grip damping and grip stiffness. The hand grip dynamics, which describes the visco-elasticity of the fingers and skin, needs to be included because the grip is not infinitely rigid and influences the measured admittances. However, the grip is relatively stiff and only influences frequencies well above the eigenfrequency of the arm. The hand force minus the reflexive force (minus because of the negative feedback loop) inputs the intrinsic model. The intrinsic model H_{int} includes the (lumped) mass, passive visco-elasticity of tissues, and the visco-elasticity of the cocontracted muscles. For small displacements the intrinsic visco-elastic properties of muscles can be described by a linear spring-damper system (Winters et al., 1988).

$$H_{int}(s) = \frac{1}{ms^2 + bs + k} \quad (2.12)$$

in which m is the arm mass, b the arm damping, and k is the arm stiffness. The reflexive model $H_{ref}(s)$ consists of feedback gains for length (k_p) and velocity (k_v). A time delay τ_d of 25 ms is incorporated to model the transportation delay and neural processing time (Crago et al., 1976; Carter et al., 1990; Kirsch et al., 1993).

$$H_{ref}(s) = (k_v s + k_p) e^{-\tau_d s} \quad (2.13)$$

Activation dynamics of the muscles, $H_{act}(s)$, are incorporated in the model as a first order process with a time constant of 30 ms (Winters and Stark, 1985; Winters et al., 1988).

$$H_{act}(s) = \frac{1}{\tau_a s + 1} \quad (2.14)$$

Combining Eqs. 2.12-2.14 gives the admittance of the arm without the hand grip, $H_{arm}(s)$ (light grey box in Fig. 2.3).

$$\begin{aligned} H_{arm}(s) &= \frac{X(s)}{F_h(s)} = \frac{H_{int}(s)}{1 + H_{int}(s)H_{ref}(s)H_{act}(s)} \\ &= \frac{1}{ms^2 + bs + k + (k_v s + k_p) \frac{e^{-\tau_d s}}{\tau_a s + 1}} \end{aligned} \quad (2.15)$$

Including the hand grip dynamics gives the mechanical admittance of the arm, $H_{fx}(s)$.

$$H_{xf}(s, p) = \frac{F_h(s)}{X_h(s)} = \frac{H_g(s)}{1 + H_g(s)H_{arm}(s)} \quad (2.16)$$

$$H_{fx}(s, p) = \frac{X_h(s)}{F_h(s)} = H_{xf}^{-1}(s) = H_{arm}(s) + H_g^{-1}(s) \quad (2.17)$$

in which $H_{xf}(s)$ is the arm impedance, $H_{fx}(s)$ the arm admittance and p the parameter vector.

$$p = [m, b, k, b_g, k_g, k_v, k_p] \quad (2.18)$$

Note that in Figs. 2.2 and 2.3 the human is described as an impedance (force over position) and needs to be inverted to get the admittance (position over force).

The model parameters p are obtained by fitting the arm model $H_{fx}(s, p)$ onto the estimated FRF of the arm admittance $\hat{H}_{fx}(f)$ by minimizing a criterion function.

$$L(p) = \sum_k \hat{\gamma}^2(f_k) \left| \ln \hat{H}_{fx}(f_k) - \ln H_{fx}(f_k, p) \right|^2 \quad (2.19)$$

where k indexes the frequency vector. The criterion is evaluated over the frequencies where the disturbance contains power. The criterion is weighted with the coherence as a measure of the reliability of the FRF. Because of the large range of gain in the FRFs a least squares criterion with logarithmic difference is used (Pintelon et al., 1994).

The model for the complete system, i.e. human and manipulator, is described by the combined, or total, admittance:

$$\begin{aligned} H_{dx}(s) &= \frac{X_h(s)}{D(s)} = \frac{H_e(s)}{1 + H_e(s)H_{fx}^{-1}(s)} \\ &= \frac{1}{H_{fx}^{-1}(s) + m_e s^2 + b_e s + k_e} \end{aligned} \quad (2.20)$$

When the hand grip is assumed infinitely stiff the total dynamics are:

$$H_{dx, grip=\infty}(s) = \frac{1}{(m + m_e) s^2 + (b + b_e) s + k + \frac{e^{-\tau_d s}}{\tau_d s + 1} (k_v s + k_p)} \quad (2.21)$$

From this equation it can be seen that the external mass, stiffness, and damping acts in parallel to the arm mass, stiffness, and damping.

A second order system, like the intrinsic model (Eq. 2.12), can be parametrised in several ways. One is in terms of a mass, spring, and damper. Another is to express the eigenfrequency (f_0), relative damping (β), and gain (K).

$$H_{int}(s) = \frac{1}{ms^2 + bs + k} = \frac{K}{\omega_0^2 s^2 + 2\frac{\beta}{\omega_0} s + 1} \quad (2.22)$$

with

$$f_0 = \frac{\omega_0}{2\pi} = \frac{1}{2\pi} \sqrt{\frac{k}{m}}, \quad \beta = \frac{b}{2\sqrt{km}}, \quad K = \frac{1}{k} \quad (2.23)$$

with f_0 in Hz. The response of an underdamped system ($\beta < 1$) can contain oscillations, in contrast to an overdamped system ($\beta > 1$). When present, these oscillations will occur around the eigenfrequency of the system.

Model validation

To obtain a validity index for the estimated parameters of the model the variance accounted for (VAF) is used, in which a VAF value of 100% indicates that no differences exist between simulated and measured position and the observed behaviour is completely described by the model. First the model is simulated in time-domain with use of the applied force disturbance from the experiment and the estimated intrinsic and reflexive parameters to obtain the simulated position $\hat{x}_h(t)$. In the VAF the measured position $x_h(t)$, is compared to the simulated position according to:

$$\text{VAF} = 1 - \frac{\sum_{k=1}^n |x_h(t_k) - \hat{x}_h(t_k)|^2}{\sum_{k=1}^n |x_h(t_k)|^2} \quad (2.24)$$

In this formula, k indexes the (sampled) time vector. Note that the coherence and VAF are closely related. The coherence indicates whether a linear and noise free relation between disturbance and position exists and the VAF reflects the accuracy of the chosen (linear) model describing this relation. Hence low coherences for some frequencies, indication noise or nonlinearities, will always result in a low VAF. A low VAF despite high coherence indicates that the chosen linear model structure is not appropriate to describe the observed (linear) input-output behaviour.

2.3 Discussion

Frequency response functions (FRFs), like the admittance, describe the relation between input to output at each frequency. By definition the input with a (mechanical) admittance is force and the output position. FRFs can be depicted in so-called Bode diagrams. Fig. 2.4 gives the admittance of a mass-spring-damper system. A Bode diagram exists of two graphs, one for the gain and one for the phase. For a given frequency, i.e. a sine, the gain describes the ratio between the amplitudes of the input sine and the output sine. The phase describes the relative shift in time between these sines. For the lower frequencies, that is below the eigenfrequency, the admittance of a mass-spring-damper is dominated by the stiffness of the spring, the higher frequencies are dominated by the mass, and the intermediate frequencies by the damping.

As the FRF describes the relation between input and output signals at each frequency a lot of data points exist. Furthermore interpretation of a FRF can be difficult and the enormous number of data points makes comparisons between subject and conditions are almost impossible. It is desirable to describe the FRF with a limited number of parameters. When the relation between input and output is linear (expressed in the coherence) the data can be described with the aid of a linear model. Such a linear model generally has a limited number of parameters, facilitating comparisons. The model parameters are obtained by fitting the model onto the estimated FRF, following a minimisation criterion. In this thesis models based on current physiology are used. With this approach the input-output relation is described with a limited number of interpretable parameters.

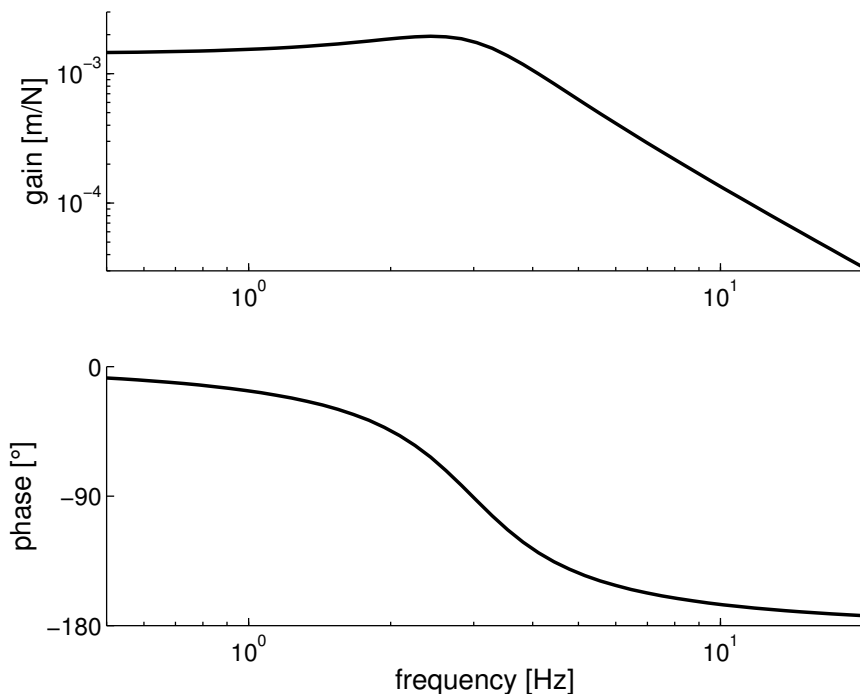


Figure 2.4: Bode diagram describing the FRF of a mass-spring-damper system ($m = 2$ kg, $b = 30$ Ns/m, $k = 700$ N/m). Upper: gain of the FRF; lower: phase of the FRF.

In the study of Van der Helm et al. (2002) force disturbances are applied with varying frequency content. The task instruction given to the subjects was to ‘*minimize the deviations*’. This task demands a high performance (expressed in a low admittance). Generally it was found that reflex gains increase when the disturbance bandwidth decreases. A follow-up study, where the external damping imposed by the manipulator was altered, showed that reflex gains increase with increasing external damping (De Vlugt et al., 2002).

Model studies show that the reflex gains were nearly optimal for the given condition (De Vlugt et al., 2001; Schouten et al., 2001). High feedback gains decrease the admittance at low frequencies at the cost of an oscillatory peak around the eigenfrequency. With a wide bandwidth disturbance (the reference condition) low reflex gains are desirable to avoid oscillations. When dealing with relatively slow disturbances (below the eigenfrequency of the arm: approximately 3 Hz) high reflex gains are optimal, as the eigenfrequency is not excited. With an external environment the performance is determined by the combined behaviour of arm and environment. External damping reduces possible oscillations of the arm, facilitating high feedback gains (De Vlugt et al., 2002).

Chapter 3

Proprioceptive reflexes in patients with complex regional pain syndrome

Alfred C. Schouten, Willem Johan T. van de Beek, J.J. (Bob) van Hilten,
Frans C.T. van der Helm
Experimental Brain Research 151:1-8 (2003)

Complex regional pain syndrome (CRPS) is a syndrome that frequently follows an injury and is characterized by sensory, autonomic and motor features of the affected extremities. One of the more common motor features of CRPS is tonic dystonia, which is caused by impairment of inhibitory interneuronal spinal circuits. In this study the circuits that modulate the gain of proprioceptive reflexes of the shoulder musculature are quantitatively assessed in nineteen CRPS patients, nine of whom presented with dystonia. The proprioceptive reflexes are quantified by applying two types of force disturbances: (1) disturbances with a fixed low frequency and a variable bandwidth and (2) disturbances with a small bandwidth around a prescribed centre frequency. Compared to controls, patients have lower reflex gains for velocity feedback in response to the disturbances around a prescribed centre frequency. Additionally, patients with dystonia lack the ability to generate negative reflex gains for position feedback, for these disturbances. Proprioceptive reflexes to the disturbances with a fixed low frequency and variable bandwidth present no difference between patients and controls. Although dystonia in the CRPS patients was limited to the distal musculature, the results suggest involvement of interneuronal circuits that mediate postsynaptic inhibition of the motoneurons of the proximal musculature.

3.1 Introduction

Complex regional pain syndrome (CRPS) is a painful condition that typically follows a minor injury to a limb although in a number of patients no trauma can be identified. In addition to the sensory and autonomic features, patients may present or subsequently develop tonic dystonia of the affected limb(s) (Bhatia et al., 1993; Schwartzman and Kerrigan, 1990; Van Hilten et al., 2001). Although the mechanism behind CRPS is still considered elusive, the evidence implicating involvement of inhibitory interneuronal circuits in the pathophysiology of tonic dystonia in patients with CRPS is compelling (Van Hilten et al., 2000). Recently, a method has been developed that allows the quantitative assessment of circuits that modulate the gain of proprioceptive reflexes of the upper extremity during posture tasks (Van der Helm et al., 2002, see also Chapter 2). In the current study, this method is applied to determine the possible involvement of spinal interneuronal circuits that control reflex gains of proprioceptive reflexes in the pathophysiology of CRPS.

3.2 Materials and methods

3.2.1 Subjects

Nineteen patients (15 women) with CRPS were evaluated with a mean (standard deviation, SD) age of 39.8 (11.7) years and a mean (SD) age of onset of 31.7 (10.9) years. All patients fulfil the criteria of CRPS in one or more of the extremities (Amadio et al., 1991). These criteria are the combination of diffuse pain, loss of hand function, and objective evidence of significant autonomic dysfunction. Results of the patients were compared to a group of ten healthy controls (2 women) with a mean (SD) age of 25.0 (2.4) years, which have been described previously by Van der Helm et al. (2002).

In fifteen patients signs and symptoms of CRPS are present in the right arm at the time of the assessments (see Table 3.1); two patients presented with CRPS of the right arm, but at the time of the experiment the signs and symptoms of CRPS had resolved; and in two patients the right arm was not affected. Features of CRPS involved one ($n = 2$), two ($n = 6$), three ($n = 1$) or all ($n = 10$) extremities. Motor signs that were noted during the neurological examination of the right arm included dystonia ($n = 9$), tremor ($n = 5$), myoclonic jerks ($n = 1$) and weakness ($n = 3$). Autonomic signs of the right arm were hyperhidrosis ($n = 7$), skin colour changes ($n = 6$), skin temperature changes ($n = 5$), and oedema ($n = 1$). Sensory signs included hypoaesthesia ($n = 10$), hyperaesthesia ($n = 2$), hypalgesia ($n = 9$), hyperalgesia ($n = 3$), and analgesia ($n = 1$). Sensory symptoms were pain ($n = 14$), numbness ($n = 14$), paraesthesia ($n = 11$), and a decreased or increased perception of the temperature of water ($n = 7$). In two patients the nails of the right arm had become brittle.

In view of the demonstrated involvement of inhibitory interneuronal circuits in CRPS patients suffering from dystonia, subgroups are defined on the presence or

Table 3.1: Main characteristics of the 19 patients with CRPS participating in this study.

patient	gender	age	CRPS in right arm	dystonia in right arm	tremor in right arm	evaluated
1	F	54	yes	no	no	yes
2	F	29	yes ^a	no	no	yes
3	F	46	yes	yes	no	no
4	F	42	yes	no	no	yes
5	F	55	yes	yes	no	yes
6	M	50	yes	yes	no	yes
7	F	34	yes	yes	yes	no
8	M	56	yes ^a	no	no	yes
9	F	29	yes	yes	no	yes
10	M	34	no	no	no	yes
11	M	48	yes	no	no	yes
12	F	19	yes	yes	yes	no
13	F	49	yes	no	no	yes
14	F	29	yes	no	yes	no
15	F	44	yes	no	no	no
16	F	50	yes	yes	no	yes
17	F	34	yes	yes	yes	no
18	F	27	yes	yes	yes	no
19	F	26	no	no	no	yes

^a At the time of the experiment the signs and symptoms of CRPS had resolved.

absence of dystonia in the right extremity (Van Hilten et al., 2000).

The medical ethics committee of the Leiden University Medical Centre approved the study and all patients gave informed consent to the experimental procedure.

3.2.2 Apparatus

Force disturbances were applied to the shoulder with a manipulator. The manipulator is extensively described in Chapter 2 and is introduced briefly. The subjects sat in a chair and had to hold a handle with their right hand. Movement of the handle resulted in ante-/retroflexion movements of the shoulder-joint. The controller of the manipulator compensated for the manipulator and only a small mass was apparent to the subject (0.6 kg, the damping and stiffness were negligible).

3.2.3 Procedures

The experiment consisted of 32 trials, lasting 40 s each. During 30 trials the subject was instructed to 'minimize the displacements' of the handle (task stiff), while continuous random disturbances with varying frequency content were applied as a force disturbance. The power of the random continuous disturbances was adjusted between the trials to limit the maximum amplitude of the displacements to approximately 1 cm, to allow linear model approximations. To motivate the subject the

reference position, which must be obtained by the subject, was presented as a horizontal line on a display together with a dot, which represents the actual position of the handle. To obtain a better estimate for the mass of the arm, the task *slack* was used during 2 of the 32 trials: the subject was asked not to react to the disturbances and to minimize any effort, resulting in minimal muscle activation.

Prior to the experiment each subject performed a few test trials to become accustomed to the task. As most of the trials require maximum effort of the subject (task *stiff*), sufficient time was given in between to prevent fatigue. The complete experiment for one subject, including instruction and pauses, lasted for approximately one and a half hours.

Disturbance signals

The continuous random disturbances, which were applied as a (force) disturbance, can be categorized into three types:

- Wide bandwidth (WB) disturbance: a signal with a uniform power between a lowest frequency (f_l) of 0.05 Hz and a highest frequency (f_h) of 20 Hz.
- Narrow bandwidth disturbance type 1 (NB1): a fixed f_l (0.05 Hz) and a f_h which varies from 1.3 to 3.8 Hz ($f_h = 1.3; 1.8; 2.3; 2.8; 3.3; 3.8$ Hz).
- Narrow bandwidth disturbance type 2 (NB2): a variable centre frequency (f_c) with a fixed bandwidth of 0.3 Hz ($f_c = 1.3; 1.8; 2.3; 3; 4; 5; 6; 7$ Hz).

Each of these 15 disturbances was applied twice during the task *stiff*, resulting in 30 trials. In the additional 2 trials in which the task *slack* was performed by the subject, only the WB disturbance was applied. The trials were presented in a predetermined random sequence that was identical for all subjects.

3.2.4 Data processing

Signal recording and processing

During each trial the force exerted by the subject $f_h(t)$, the position of the handle $x_h(t)$, and the applied force disturbance $d(t)$ were measured. All data were sampled at 500 Hz and stored on computer. To remove any transient response only the last 33 s of each trial (of 40 s) was used for data processing, as the objective of our investigations was to investigate stationary behaviour.

Nonparametric analysis

As the modelling was done in frequency domain, the data were converted from time to frequency domain. For each trial the arm admittance $\hat{H}_{f_x}(f)$ of the subject was estimated. In addition to the arm admittance, the coherence $\hat{\gamma}^2(f)$ of each trial was estimated and represents a measure of the linearity and signal-to-noise ratio per frequency. The estimators are given in Chapter 2.

As force disturbances are applied while subjects are instructed to maintain their posture, some drift of the position of the arm will occur. This drift is present at low frequencies (mainly below 0.5 Hz). Since drift is a time-variant phenomenon (i.e. nonlinear) the coherences for these frequencies can be low. Subjects having low coherences (that is below 0.6) for frequencies above 1 Hz in more than two trials were excluded.

Quantification of intrinsic and reflexive properties

The dynamic behaviour of the neuromusculoskeletal system in response to external disturbances is the result of interactions between intrinsic (inertias of the limbs, passive visco-elasticity of tissues, and visco-elasticity of the antagonistic muscles during the performance of the task) and reflexive (proprioceptive reflexes) properties. Because intrinsic and reflexive properties coexist during most tasks, reflexes can not be measured directly from the mechanical behaviour. An indirect method is used to separate intrinsic and reflexive parameters (Van der Helm et al., 2002, see also Chapter 2). This method is based on two basic principles: (1) during the *stiff* task with WB disturbance reflexive feedback is silent and so only intrinsic properties remain and (2) for all *stiff* tasks (both with WB and NB disturbances) the average muscle activation is constant, i.e. the intrinsic properties are constant. These principles imply that all changes in admittance during tasks with NB disturbances, in comparison with WB disturbance, can be attributed to proprioceptive feedback.

The intrinsic properties are modelled as a mass-spring-damper system, describing the lumped mass of the arm m , arm damping b , and the arm stiffness k . The visco-elasticity of the constantly activated muscles is included within b and k . The intrinsic model is extended with a model for the hand grip (grip stiffness k_g and grip damping b_g), which describes the linking of the arm to the manipulator. The reflexive model consists of feedback gains for length (k_p) and velocity (k_v). Activation dynamics of the muscles are incorporated as a first order process with a time constant of 30 ms. A time delay of 25 ms is incorporated to model the transportation delay and neural processing time. The derivation of the intrinsic and reflexive models is given in Chapter 2.

The parameters of the intrinsic arm model (m, b, k, b_g, k_g) are fitted on the admittances of the tasks with the WB disturbance, while neglecting the reflexive parameters. Furthermore the estimation of the intrinsic parameters of the tasks *stiff* and *slack* is combined, resulting in a better estimate for the one common parameter, the arm mass. The reflexive parameters (k_p, k_v) are fitted to the admittances of the tasks with NB disturbances, while the intrinsic parameters are fixed to the values estimated from the trials with WB disturbance task *stiff* (reference task). The criterion to fit the model to the observed admittances is given in Chapter 2.

Model validation

To obtain a validity index for the estimated parameters of the model the variance accounted for (VAF) is used, see Chapter 2. A VAF value of 100% indicates that

no differences exist between simulated and measured position and the observed behaviour is completely described by the model.

During the trials, some drift of the position of the arm will occur. In order to reduce the effect of the drift on the VAF, frequencies below 0.6 Hz have been removed from the recorded and simulated positions (by FFT, set low frequencies to zero, and inverse FFT), before calculating the VAF.

For some conditions, the performance of the neuromusculoskeletal system is greatly enhanced through modulation by proprioceptive reflexes. Theoretical studies of the proprioceptive reflexes (De Vlugt et al., 2001; Schouten et al., 2001) reveal that in case of high reflex gains the neuromusculoskeletal system will become boundary stable. This means that large deviations around the eigenfrequency (eigenfrequency arm ≈ 3 Hz) can occur, even when the disturbance does not excite the eigenfrequency. Consequently the recorded position will be dominated by deviations around the eigenfrequency, which would substantially lower the VAF. This phenomenon especially occurs for NB2 disturbances with f_c beyond the eigenfrequency. To reduce this effect, the recorded and simulated position for NB2 disturbances with $f_c \geq 4$ Hz are high pass filtered (by FFT, set frequencies until 3.5 Hz to zero, and inverse FFT), before calculating the VAF.

Statistical analysis

Differences in the intrinsic and reflexive parameters between patients and controls were evaluated using an unpaired two-sample Student's t -test for samples with unequal variances. A post hoc Bonferroni test was performed to correct for multiple comparisons ($n = 50$). P -values smaller than 0.001 are considered significant.

3.3 Results

Of the nineteen subjects, twelve can be analysed (Table 3.1). Seven patients can not be evaluated as the experiment was prematurely interrupted as a result of pain or severe spasms (Patients 3, 12 and 18) or as a result of low coherences for frequencies above 1 Hz in more than two trials (Patients 7, 14, 15 and 17).

3.3.1 WB disturbances and intrinsic parameters

The coherence is evaluated with a frequency resolution of ≈ 0.12 Hz (see Chapter 2). This means that in the range of interest (1-20 Hz) the coherence is evaluated at 156 frequency points. The coherence is considered high when it is higher than 0.8 for at least 90% of these points. In all controls the coherence is high for all trials. For most patients ($n = 7$) the coherence is high. In three patients the coherences were reasonable ($\hat{\gamma}^2(f) > 0.6$ for all frequencies) for all trials and two other patients had only a low coherence for the two trials with the task *slack*. For the task *stiff* all controls have a high VAF (above 80%), for task *slack* the VAF is slightly lower but always above 60% (above 80% for $n = 6$). For most patients (*stiff*: $n = 9$, *slack*:

Table 3.2: *Intrinsic parameters, mean (SD), patients with CRPS compared to healthy subjects. Italic boldface type indicates a significant difference between patients and controls ($p < 0.001$).*

description		controls ($n = 10$)		patients ($n = 12$)	
		stiff	slack	stiff	slack
m [kg]	total mass	1.98 (0.24)		2.12 (0.57)	
b [Ns/m]	arm damping	41.7 (7.4)	18.5 (5.3)	36.4 (15.1)	25.1 (10.7)
k [N/m]	arm stiffness	878 (172)	266 (144)	713 (234)	487 (223)
b_g [Ns/m]	grip damping	137 (44)	42 (16)	113 (49)	54 (26)
k_g [kN/m]	grip stiffness	20.8 (7.2)	3.8 (1.9)	8.5 (6.2)	4.0 (2.8)
β [-]	relative damping	0.51 (0.10)	0.42 (0.08)	0.48 (0.16)	0.43 (0.18)
f_0 [Hz]	eigenfrequency	3.34 (0.25)	1.80 (0.43)	2.90 (0.30)	2.35 (0.45)

$n = 8$) the VAF is above 60%. The patients having low VAF values (that is below 60%) also have low coherencies.

For both patients and controls, a slightly underdamped second order system is found for the admittances with WB disturbance. It is found that the eigenfrequency of the arm is significantly higher in controls as compared to patients during the task *stiff* (Table 3.2). Furthermore the stiffness of the hand grip (k_g) during the task *stiff* is significantly higher for controls. No further significant differences emerge between patients and controls concerning the intrinsic parameters.

3.3.2 NB1 disturbances

In all controls and patients, the coherences are higher than 0.7 for frequencies above 1 Hz. Most patients ($n = 10$) and all controls have high VAF values (above 60%) for $f_h \geq 1.8$ Hz. For $f_h = 1.3$ Hz the VAF is less than 60% in two controls and one patient.

In both patients and controls, high values for the length feedback gain, k_p , are found for low disturbance bandwidth, f_h , which gradually approach zero at the eigenfrequency (of approximately 3 Hz) (see Fig. 3.1). For both patients and controls, k_v has low positive values or equal zero for all f_h . Concerning the reflexive parameters for NB1 disturbances no significant differences emerge between patients and controls for one of the conditions.

3.3.3 NB2 disturbances

In all controls and patients, the coherences are higher than 0.9 at all centre frequencies. In all controls the VAF is higher than 60% for all f_c . Most patients ($n = 11$) have high VAF values (above 60%) for $f_c \leq 1.8$ Hz. For $f_c = 1.3$ Hz the VAF is lower than 60% in five patients.

In controls and patients without dystonia, k_p is negative for f_c higher than 1.5 Hz (see Fig. 3.2). Compared to controls and to patients without dystonia, patients

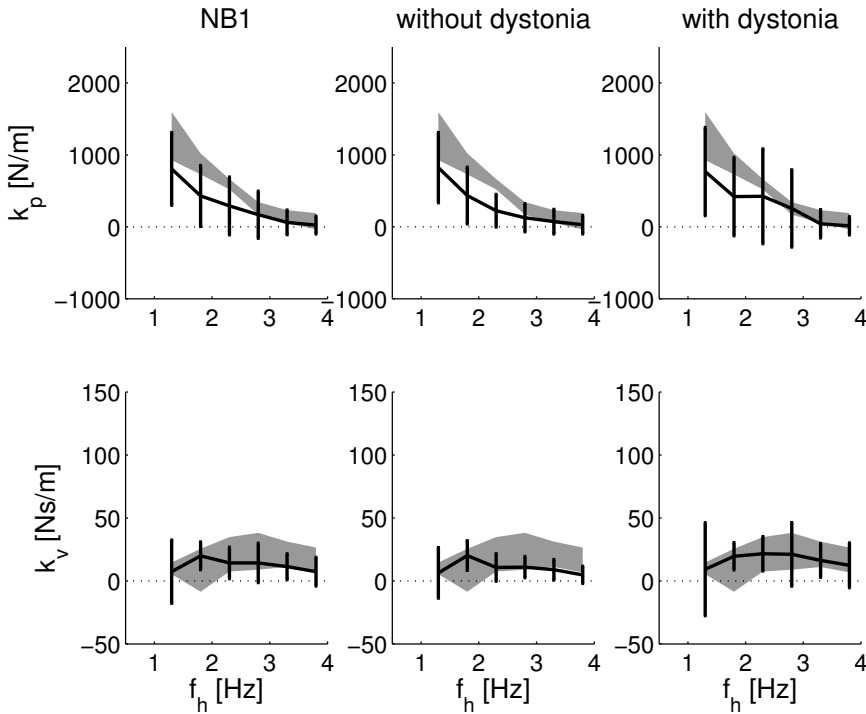


Figure 3.1: Mean reflexive parameters for NB1 disturbances. Left: CRPS patients ($n = 12$); middle: CRPS patients without a tonic dystonia ($n = 8$); right: CRPS patients with a tonic dystonia ($n = 4$). The error bars denote the means \pm SD. The grey area denotes the mean \pm SD of healthy subjects.

with dystonia of the upper extremity develop a less negative or even a positive k_p for these f_c values, the difference being significant for $f_c = 5$ Hz ($p < 0.001$). In controls high k_v values are found for low f_c and k_v gradually approaches zero for $f_c \approx 4$ Hz. Patients have a lower k_v for $f_c = 1.3, 1.8$ and 2.3 Hz, as compared to controls ($p < 0.001$).

3.4 Discussion

This study uses the method described by Van der Helm et al. (2002) to measure the modulation of reflexes in CRPS patients. In the method of Van der Helm et al. force disturbances are applied with varying frequency content. The authors found that by varying the frequency content the strength of the reflexes changes. When dealing with relatively slow disturbances (below the eigenfrequency of the arm: approximately 3 Hz) high reflex gains are desirable to decrease the admittances (De Vlugt et al., 2001; Schouten et al., 2001) and consequently suppress the force

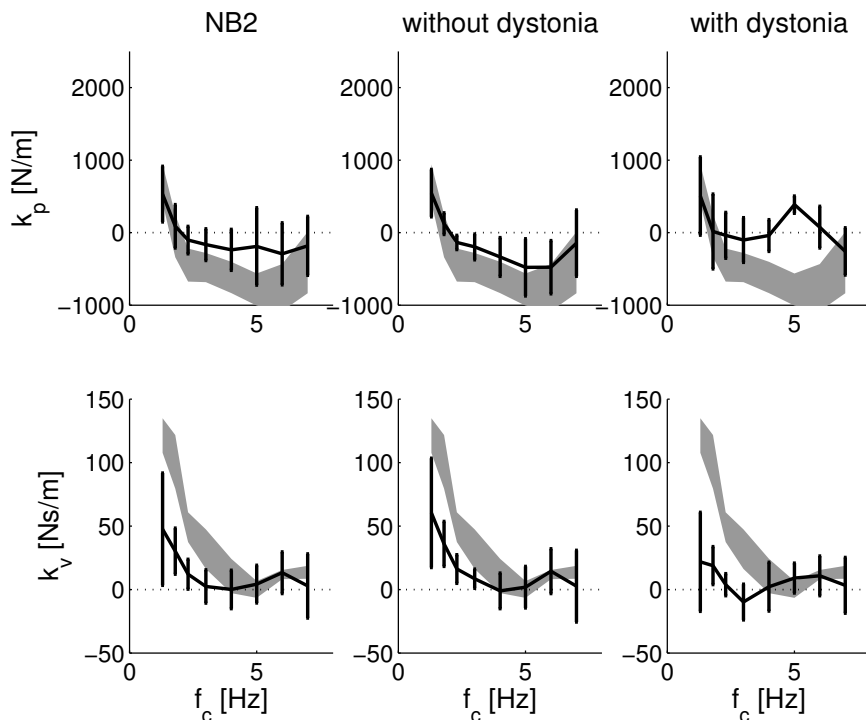


Figure 3.2: Mean reflexive parameters for NB2 disturbance. Left: CRPS patients ($n = 12$); middle: CRPS patients without a tonic dystonia ($n = 8$); right: CRPS patients with a tonic dystonia ($n = 4$). The error bars denotes the means \pm SD. The grey area denotes the mean \pm SD of healthy subjects.

disturbances. On the other hand, the effectiveness of the reflexive feedback for relatively fast disturbances (beyond the eigenfrequency) is limited or even counterproductive because of oscillatory behaviour, resulting from the time delays associated with proprioceptive reflexes (De Vlugt et al., 2001; Schouten et al., 2001).

In CRPS patients with dystonia, the reflex gains for position feedback (k_p) with application of NB2 disturbances are less negative and even become positive, in contrast to controls and patients without dystonia. Negative reflex gains in a negative feedback system imply reduced muscle activation upon stretching of the muscle. The mechanism of this reflex is unknown, but most likely results from (1) direct inhibition of the motoneuron (autogenic inhibition) or (2) excitation of the antagonistic motoneurons (reciprocal excitation). Both autogenic inhibition and reciprocal excitation have been discussed by Jankowska (1992) to be existing reflexive pathways. Model studies demonstrate that negative gains are optimal for the given disturbances and conditions (De Vlugt et al., 2001; Schouten et al., 2001).

Additionally, all patients show significantly lower reflex gains for velocity feed-

back (k_v) for centre frequencies of 1.3, 1.8 and 2.3 Hz as compared to controls. Controls have a high k_v for a low f_c and a low k_v for a high f_c , indicating that for NB2 disturbances they are able to modulate their response to changes in muscle stretch velocity. The lower k_v in patients for the lowest f_c indicates a smaller effect of afferent input on motoneuron activity, as compared to controls. Most likely this results from increased presynaptic inhibition (Stein and Capaday, 1988), although functional impairment of afferent fibres cannot be ruled out. Interestingly, both patients and controls do not modulate k_v in response to NB1 disturbances. The patients present no difference from controls in their ability to produce and inhibit positive reflex gains for position feedback on NB1 disturbances. Positive reflex gains are the result of a monosynaptic stretch reflex and are inhibited by interneuronal circuits that mediate presynaptic inhibition. With an increasing upper frequency limit of the NB1 disturbance the patients are able to modulate the monosynaptic stretch reflex to a degree similar to that found in controls, suggesting normal presynaptic inhibition of muscle spindle afferents on NB1 disturbances at the level of proximal arm musculature. This contrasts with previous findings indicating a decreased presynaptic inhibition in dystonia involving distal musculature of CRPS patients (Van Hilten et al., 2000). However, motoneurons innervating hand and finger muscles lack recurrent inhibition and have a higher proportion of β -innervation compared to motoneurons innervating proximal musculature, underscoring differences in neuronal circuits that regulate proximal and distal muscle tone (Illert et al., 1996; Katz et al., 1993).

With the current design, some limitations were encountered. First, seven out of 19 patients could not be analysed, including all five patients with a tremor. This indicates that the current setting is not applicable to patients with a tremor. Second, compared to controls, the patients have lower coherences for frequencies below 1 Hz. This may be explained by spasms, which occur at these low frequencies or non-intended voluntary activity. The latter is less likely because subjects were able to maintain the reference position. The coherence indicates whether there is a linear relation between disturbance and position and the VAF reflects the accuracy of the (linear) model describing this relation. Hence low coherences for some frequencies will always result in a low VAF.

Dystonia of CRPS generally progresses in the extremities from distal to proximal musculature (Schwartzman and Kerrigan, 1990). Although dystonia in the evaluated CRPS patients mainly affects the distal musculature, the results indicate involvement of the proximal musculature as well. At this level, the results suggest impairment of interneuronal circuits that mediate postsynaptic inhibition of the motoneurons.

Chapter 4

Proprioceptive reflexes in patients with Parkinson's disease

In this study the involvement of disturbed modulation of proprioceptive reflexes in Parkinson's disease (PD) was investigated. PD is a neurodegenerative disorder characterized by tremor, bradykinesia, rigidity, and impaired postural reflexes. With the gradual loss of dopamine producing brain cells the smooth initiation of movements and fine control of muscles vanish and subsequently the symptoms develop. In this study it is hypothesized that also the modulation of proprioceptive reflexes is involved in the development of the symptoms. The modulation of proprioceptive reflexes at the shoulder joint is assessed during postural control task. Force disturbances were applied via a handle while the subjects were instructed to 'minimize the deviations' of the handle. Several settings for the external damping, imposed by the manipulator, are applied. It is found that the intrinsic muscle stiffness is significantly larger in patients compared to healthy control subjects. In patients the position feedback gain does increase with external damping but not as steeply as in controls, indication that the range of reflex gain modulation is confined with PD.

4.1 Introduction

Parkinson's disease (PD) is a neurodegenerative disorder characterized by tremor, bradykinesia, rigidity, and impaired postural reflexes. As patients with PD progressively lose the coordination and activation of the muscles, it is hypothesized that also the ability to modulate the proprioceptive reflexes deteriorates.

Van der Helm et al. (2002) showed that the reflexive feedback gains increase with decreasing bandwidth of the force disturbance. The subjects had to '*minimize the deviations*' of the handle, while continuous random force disturbances were applied. The protocol has proven to be useful to get insight into the pathophysiology of complex regional pain syndrome (CRPS) (Schouten et al., 2003, see Chapter 3). However patients with tremor could not be evaluated as the tremor dominates the position. As tremor is one of the major symptoms of PD a different protocol needs to be applied to investigate reflex gain modulation in PD. In De Vlugt et al. (2002) the external dynamics imposed by the manipulator, i.e. how the manipulator '*feels*' to the subject, were altered. It was shown that proprioceptive reflexes increase with external damping. This damping protocol seems promising for assessing the reflexes in PD as the external damping will reduce to voluntary oscillations as seen with tremor.

In this study the modulation of proprioceptive reflexes in subjects with Parkinson's disease is assessed. It is hypothesized that in parkinsonian patients the range of proprioceptive reflex gain modulation is confined. Modulation of the reflexes is provoked by altering the external damping.

4.2 Materials and methods

4.2.1 Subjects

Experiments were conducted on a group of parkinsonian patients ($n = 10$; 8 men) with a mean (standard deviation, SD) age 55.1 (7.0) years. The main characteristics of the involved patients are summarized in Table 4.1. All patients were scored according to the Hoehn & Yahr scale and the individual scores for tremor and rigidity in the right arm are given (Hoehn and Yahr, 1967). Where zero on the Hoehn & Yahr scale indicates that no difference existed compared to healthy subjects, and four indicate severe impairment. All patients were on medication during the experiments. Results are compared to a group of normal, healthy subjects ($n = 19$; 11 men) with mean (SD) age of 32.1 (15.4).

The medical ethical committee of the Leiden University Medical Centre approved the study. All patients gave informed consent to the experimental procedure.

4.2.2 Apparatus

Force disturbances were applied to the shoulder with a manipulator. The manipulator is extensively described in Chapter 2 and is introduced briefly. The subjects

Table 4.1: *Main characteristics of the ten patients with Parkinson's disease participating in this study.*

patient	gender	age	Hoehn & Yahr	tremor in right arm	rigidity in right arm
1	M	59	2	1	2
2	M	60	2	0	2
3	M	52	2	1	2
4	M	64	2	0	2
5	M	55	2	0	2
6	F	43	2	1	2
7	M	63	3	1	2
8	M	53	2	0	1
9	M	45	2	0	3
10	F	57	2	0	1

sat in a chair and had to hold a handle with their right hand. Movement of the handle resulted in ante-/retroflexion movements of the shoulder-joint. To the subject the manipulator behaved like a mass-spring-damper system. The parameters of the spring (k_e), damper (b_e), and mass (m_e) are adjustable. In this study the mass is fixed to the minimum value ($m_e = 0.6$ kg), no stiffness was set ($k_e = 0$ N/m), and the damping (b_e) was altered during the experiments, see Procedures.

4.2.3 Procedures

The experiment consisted of a series of trials, which last 40 s each. The subjects were instructed to '*minimize the deviations*' of the handle (task *stiff*), while a continuous random force disturbance was applied. Five settings for external damping (b_e) were used: 0, 50, 100, 150, 200 Ns/m. Task *stiff* without external damping (0 Ns/m) is referred to as the reference condition. To obtain a better estimate for the arm mass, the setting with no external damping was repeated with task *slack*: the subject was asked not to react on the disturbances and to minimise effort, resulting in little muscle activation. Each setting was applied four times, making a total of 24 trials. For each setting the power of the force disturbance was adjusted such that the maximum amplitude of the position deviations was approximately 1 cm, facilitating linear model approximation. The trials were presented in random order.

Prior to the experiment each subject performed a few test trials to get acquainted with the experimental set-up. As most of the trials required maximum effort (task *stiff*), sufficient time was given in between the trials to prevent fatigue. The experiment for each subject lasted approximately one and a half hours.

Disturbance signal

The signal used as a force disturbance is a continuous random signal. The signal was designed in the frequency domain and transformed to time domain via the in-

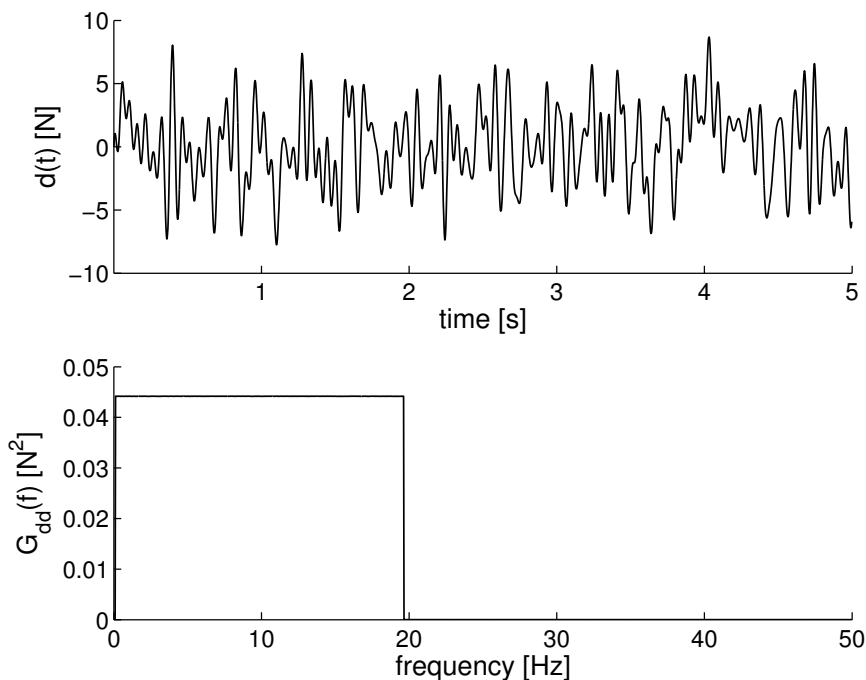


Figure 4.1: Force disturbance signal. Upper: first 5 s of the signal, $d(t)$; lower: power spectral density of the signal, $\hat{G}_{dd}(f)$.

verse fast Fourier transform. The power of the signal was taken uniformly between 0.1 and 20 Hz with a random phase, see Fig. 4.1. The resolution in frequency domain is equal to inverse of the observation time. To be able to observe all excited frequencies, the constructed signal must have the same length as the signal length used for analysis (in this study ≈ 33 s, see also Data processing. When the signals have equal length the analysed frequencies coincide. Finally, to obtain a 40 s signal the constructed signal (≈ 33 s) was repeated in time and cut at the precise length of 40 s.

When constructing the signal in this manner one has control over the exact properties of the signal, in contrast to a finite sequence of (filtered) white noise signal. Furthermore the estimates for the frequency response functions (FRFs) will be substantially better compared to use of (filtered) white noise (Schoukens et al., 1993; Pintelon and Schoukens, 2001).

4.2.4 Data processing

Signal recording and processing

During a trial the force disturbance $d(t)$, the position of the handle $x_h(t)$, and the applied force on the handle $f_h(t)$ were recorded. Further, the electromyographic (EMG) activity of four muscles was recorded, which contribute to the torque around the shoulder in ante-/retroflexion direction: m. pectoralis major, m. deltoideus anterior, m. deltoideus posterior and m. latissimus dorsi. Before digitizing the EMG signals were high pass filtered (20Hz, 3th order Butterworth), to remove DC components and movement artefacts, amplified, rectified, and low pass filtered with 200 Hz cut off (3th order Butterworth), to prevent aliasing. All signals were digitally recorded at 500 Hz with 12 bit resolution and stored on computer. This study investigates stationary behaviour and to remove any initial response only the last 2^{14} samples (≈ 33 s) from a trial are used for further analysis. This time window coincides with the original length of the constructed force disturbance signal (see Section 4.2.3).

The EMG signals were used to get an impression of the mean muscle activity, or cocontraction, during a trial. To do so the IEMG of each muscle during a trial is calculated.

$$\text{IEMG}_i = \frac{1}{n} \sum_{k=1}^n |e_i(t_k)| \quad (4.1)$$

in which e_i is the EMG signal of muscle i , k indexes the time vector, and n is the number of samples. The IEMG of each muscle is normalized so that the mean over the four repetitions during the reference condition, equals one. The mean EMG u_0 during a trial is defined as the mean of the normalized EMGs of the four muscles.

$$u_0 = \frac{1}{4} \sum_{i=1}^4 \frac{\text{IEMG}_i}{\text{IEMG}_{ref,i}} \quad (4.2)$$

in which $\text{IEMG}_{ref,i}$ denotes the IEMG for muscle i during the reference condition averaged over the four repetitions.

Nonparametric analysis

As the modelling was done in the frequency domain the data was transformed from time to frequency domain via fast Fourier transform (FFT). To reduce the noise in the recorded signals, the time signals for each condition were averaged over the four repetitions before FFT. For each condition the subject's arm admittance, $\hat{H}_{fx}(f)$, and the admittance of the combined system, i.e. the subject's arm and the external environment imposed by the manipulator, $\hat{H}_{dx}(f)$, were estimated. In addition the coherence $\hat{\gamma}^2(f)$ was estimated. The coherence gives a measure for how well the output of a system is linearly related to the input of the system. By definition the value for the coherence varies between 0 and 1. Nonlinearities and measurement noise decrease the coherence. The estimators are given in Chapter 2.

Quantification of intrinsic and reflexive properties

The dynamic behaviour of the neuromusculoskeletal system in response to disturbances is the result of interactions between intrinsic properties (inertias of the limbs, passive visco-elasticity of tissues, and visco-elasticity of the antagonistic muscles resulting from cocontraction) and proprioceptive reflexes. Because intrinsic and reflexive properties coexist during most tasks, reflexes can not directly be measured. An indirect method is used to separate intrinsic and reflexive parameters (Van der Helm et al., 2002; De Vlugt et al., 2002, see also Chapter 2). This method is based on two basic principles: (1) with a broadband disturbance and no external damping reflexive feedback will be small and negligible, i.e. only intrinsic properties remain and (2) for all *stiff* tasks the average muscle activation is constant, i.e. the intrinsic properties are constant. These principles imply that all changes in admittance during tasks with damping, in comparison without damping, can be attributed to proprioceptive feedback. The second principle is supported by the measured mean EMG, which indicates the actual co-activation during a condition.

The intrinsic properties are modelled as a mass-spring-damper system (lumped arm mass m , arm damping b , and arm stiffness k). The visco-elasticity of the co-activated muscles is included within b and k . The intrinsic model is extended with a model for the hand grip (grip stiffness k_g and grip damping b_g), which describes the linking of the arm to the manipulator. The reflexive model consists of feedback gains for length (k_p) and velocity (k_v). Activation dynamics of the muscles are incorporated as a first order process with a time constant of 30 ms. A time delay of 25 ms is incorporated to model the transportation delay and neural processing time. The derivation of the intrinsic and reflexive models is given in Chapter 2.

The intrinsic parameters (m, b, k, b_g, k_g) were estimated by fitting the arm model $H_{fx}(f)$ onto the measured arm admittance $\hat{H}_{fx}(f)$ in case of no external damping. Furthermore the estimation of the intrinsic parameters of the tasks *stiff* (the reference condition) and *slack* was combined, resulting in a better estimate for the one common parameter, the arm mass.

For all *stiff* conditions, including the reference condition, the reflexive parameters (k_p, k_v) were estimated using the intrinsic parameters. The intrinsic parameters were obtained from the reference condition and scaled with the mean EMG for that condition.

$$b = u_0 \cdot b_{ref} \quad (4.3)$$

$$k = u_0 \cdot k_{ref} \quad (4.4)$$

$$b_g = u_0 \cdot b_{g,ref} \quad (4.5)$$

$$k_g = u_0 \cdot k_{g,ref} \quad (4.6)$$

in which $_{ref}$ denotes the parameter values for the intrinsic parameters during the reference condition.

The model parameters were obtained by minimizing the following criterion

function:

$$L(p) = \sum_k \frac{\hat{\gamma}^2(f_k)}{1 + f_k} \left| \ln \hat{H}_{f_x}(f_k) - \ln H_{f_x}(f_k, p) \right|^2 \quad (4.7)$$

where k indexes the frequency vector and p is the parameter vector. Because of the large range of gain in the FRFs a least squares criterion with logarithmic difference was used (Pintelon et al., 1994). The criterion was weighted with the coherence to reduce emphasis on less reliable frequencies in the FRF and with $(1 + f_k)^{-1}$ to prevent excessive emphasis on the higher frequencies.

Model validation

To obtain a validity index for the parametrised model the variance accounted for (VAF) was used, see Chapter 2. The simulated position was obtained from evaluation of the parametrised model using the same force disturbance as used in the experiments. A VAF value of 100% indicates that no differences exist between simulated and measured position meaning that the observed behaviour is completely described by the model.

During the trials, some drift of the position of the arm will occur. In order to reduce the effect of the drift on the VAF, frequencies below 0.6 Hz have been filtered from the recorded and simulated positions (3th order high pass Butterworth), before calculating the VAF.

Statistical analysis

Differences for the intrinsic parameters between patients and healthy subjects were evaluated using unpaired two-sample Student's t -tests for samples with unequal variances. Differences for reflexive parameters are evaluated with a 2-way ANOVA. p -values smaller than 0.05 are considered significant.

4.3 Results

4.3.1 Nonparametric FRFs

In Figs. 4.2 and 4.3 the FRFs and coherences for a typical control subject and parkinsonian patient (patient 6) are given. For all healthy control subjects the coherence is high during all conditions (generally above 0.9 for all excited frequencies), indicating that the relation between disturbance and position is linear and the noise is small. The coherence is also high for all patients, although slightly lower than for the healthy controls. For the reference condition (left: $b_e = 0$ Ns/m) both the total admittance as the arm admittance of the control subject are well damped, as there is no distinct peak around the eigenfrequency. With increasing external damping the arm admittance decreases for the lower frequencies, i.e. becomes stiffer, at the cost

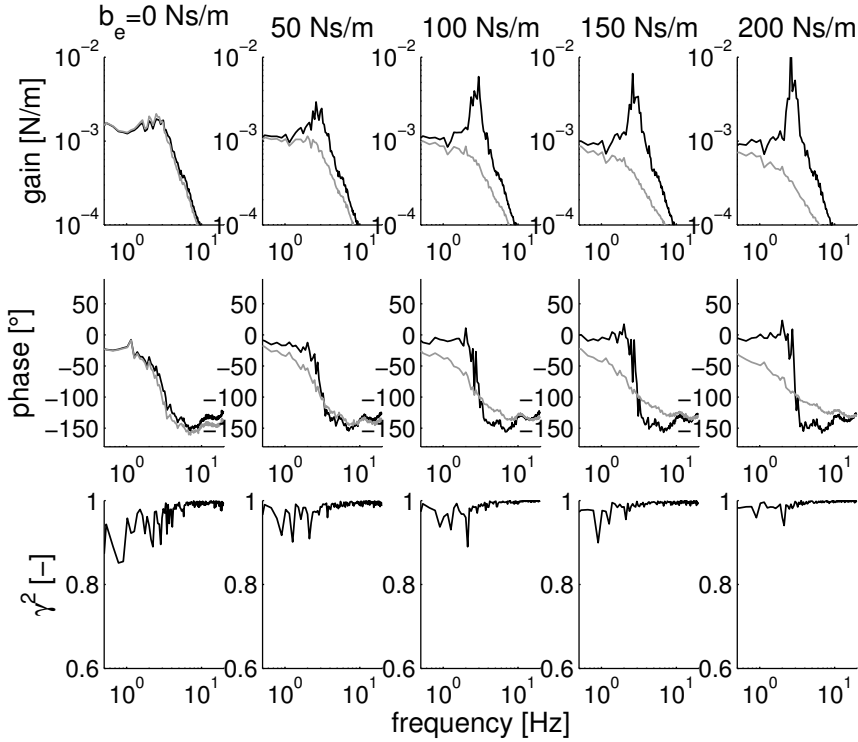


Figure 4.2: The FRFs and coherence of a typical healthy control subject. Grey lines: arm admittance $\hat{H}_{fx}(f)$; black lines: total admittance $\hat{H}_{dx}(f)$ and coherence $\hat{\gamma}^2(f)$.

of an oscillatory peak around the eigenfrequency, likely resulting from increased reflexes. The total admittance remains well damped for all conditions indicating that the performance is not deteriorated by the oscillatory peak in the arm admittance.

For the parkinsonian patient both the total admittance as the arm admittance are underdamped for the reference condition (a distinct peak is present around the eigenfrequency). The low relative damping of the total admittance worsens performance as oscillations around the eigenfrequency will occur. With increasing external damping the oscillatory peak of the arm admittance enlarges. This peak is even present in the total admittance for $b_e = 50$ Ns/m. Note that during the neurological examination a small tremor was present for this subject, see Table 4.1.

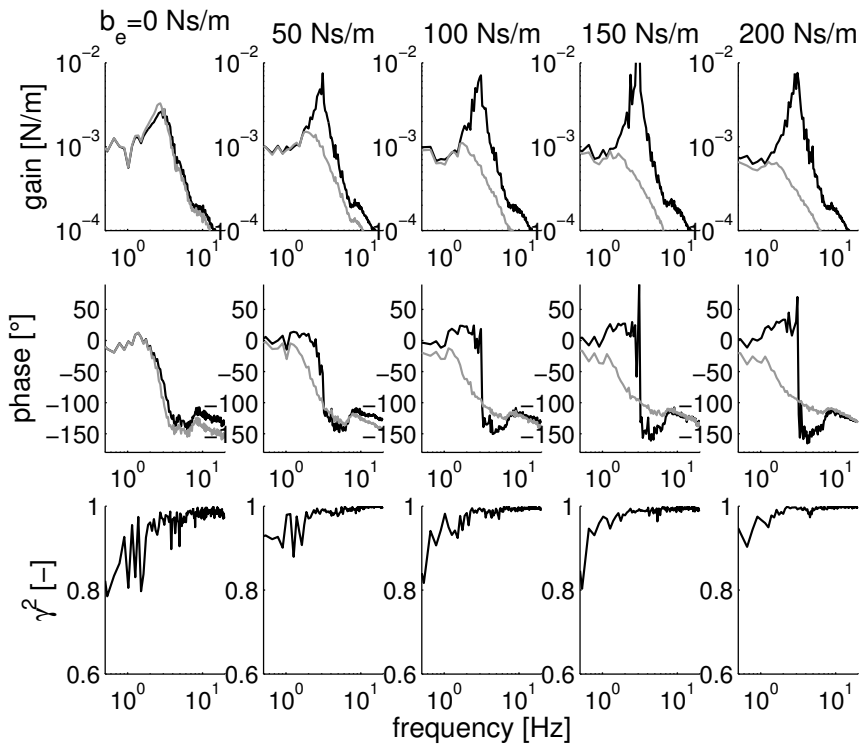


Figure 4.3: The FRFs and coherence of a typical parkinsonian patient (patient 6). Grey lines: arm admittance $\hat{H}_{fx}(f)$; black lines: total admittance $\hat{H}_{dx}(f)$ and coherence $\hat{\gamma}^2(f)$.

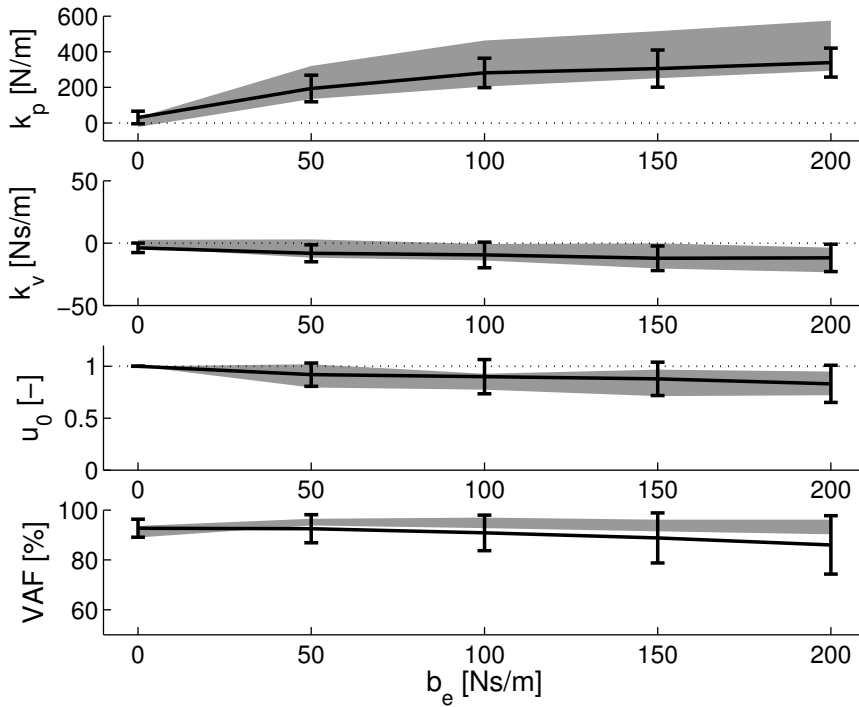


Figure 4.4: From top to bottom: position feedback gain k_p ; velocity feedback gain k_v ; mean EMG u_0 ; VAF. Grey area indicates the parameters for healthy control subjects (mean \pm SD) and the black line with the error bars show the means \pm SD for the PD patients.

Table 4.2: Mean (SD) intrinsic parameters of healthy controls and patients. The parameters given in *italic boldface type* are significantly different.

description		controls ($n = 19$)		patients ($n = 10$)	
		stiff	slack	stiff	slack
m [kg]	arm mass	1.96 (0.51)		2.35 (0.44)	
b [Ns/m]	arm damping	33.8 (10.4)	17.4 (6.7)	39.2 (10.9)	23.0 (7.1)
k [N/m]	arm stiffness	714 (139)	245 (123)	944 (237)	485 (120)
b_g [Ns/m]	grip damping	167 (51)	41 (25)	227 (75)	49 (18)
k_g [kN/m]	grip stiffness	11.0 (7.8)	2.6 (2.0)	10.9 (5.7)	3.3 (1.3)
β [-]	relative damping	0.46 (0.15)	0.16 (0.11)	0.42 (0.11)	0.11 (0.3)
f_0 [Hz]	eigenfrequency	3.07 (0.32)	1.72 (0.43)	3.24 (0.75)	2.32 (0.49)

4.3.2 Intrinsic and reflexive parameters

The estimated intrinsic parameters for both healthy subjects and patients are given in Table 4.2. The reflexive parameters, the mean EMG, and the VAF values are given in Fig. 4.4. The high VAF values show that the model predicts the observed behaviour very well. Because the coherence was slightly lower in case of the patients it was expected that the VAF values were slightly lower for the patients.

For both task *stiff* and *slack* the arm stiffness is significantly larger in parkinsonian patients. Furthermore the ratio of stiffness with task *stiff* and *slack* is smaller in patients (patients: 1.95, control: 2.91). For both patients and controls the position feedback gain k_p increased with increasing damping although this increase is less pronounced for the patients ($p < 0.02$, 2-way ANOVA).

4.4 Discussion

In this study intrinsic muscle parameters and proprioceptive reflex gains are quantified during postural control tasks. The modulation of reflexive feedback gains with external damping is investigated. It is found that in patients the position feedback gain k_p increases with external damping but not as steeply as in controls, indicating that the range of modulation is confined with PD. Furthermore the intrinsic muscle stiffness is higher, suggesting that reflexes are present during the reference condition.

This study considers postural control, with small variation around an equilibrium point, to allow linear modelling. Besides linear behaviour, the influence of disturbances other than the applied disturbance must be small in order to have a good estimate of the arm dynamics. Examples of uncorrelated disturbances are subject-induced steering or uncontrolled movements. For both the control subjects and the patients the coherence is high, indicating that the relation between disturbance and position is linear and the noise is small. The high coherence in patients shows that proprioceptive reflexes can be assessed in patients with PD.

The fact that the coherence is high in patients also implicates that the tremor seen in some of the patients is linearly related with the force disturbance. This means that the tremor is a property of the system involved and not the result of oscillations induced by the higher centres of the central nervous system (CNS), which would be uncorrelated with the force disturbance. This is also supported by the measured admittances, for some patients the dynamics are underdamped, meaning that even a small disturbance results in relatively large oscillations.

It is known that high feedback gain in a time-delayed feedback loop, like proprioceptive reflexes, result in oscillations around the eigenfrequency (De Vlugt et al., 2001; Schouten et al., 2001). The high coherence at the eigenfrequency and the poor damping indicate that the reflexes are present during the reference condition and responsible for the tremor. Consequently the assumption of negligible reflexes during the reference condition may result in an overestimation of the intrinsic parameters and an underestimation of the reflexive parameters. This implicates that

the increased stiffness in PD results from enhanced proprioceptive reflexes, which could be responsible from the rigidity observed in PD. The possible underestimation of the reflex gains does not influence the major finding of this study that the range of modulation is confined in patients suffering from PD. It even suggests that not the upper value of the position feedback gain is limited but the lower value of the feedback gain is limited.

With the current method prior assumptions are needed to separate intrinsic and reflexive contributions. To remove the need for prior assumptions the method could be extended by estimating the dynamic relation between position and EMG giving a direct measure for the proprioceptive reflexes. However special precaution needs to be taken to reduce the uncorrelated noise in the (rectified) EMG signals, or to increase the signal, i.e. the response to the continuous force disturbance, in the EMG recording.

Chapter 5

Design of perturbation signals for the estimation of spinal reflexes

Alfred C. Schouten, Erwin de Vlugt, Frans C.T. van der Helm
Submitted to *Journal of Neuroscience Methods*

This study aimed to identify the reflexive contribution during posture maintenance. Continuous random force disturbances were applied at the hand while the subjects were instructed to 'minimize the deviations' resulting from the force disturbances. The results were analysed in frequency domain with frequency response functions (FRFs). Two FRFs were evaluated: (1) the mechanical admittance and (2) the reflexive impedance, expressing the dynamic relation between position and muscle activation (assessed via electromyography, EMG). The reflexive impedance describes the muscle activation resulting from the position deviations and hence is a direct measure for proprioceptive reflexes. To record all relevant dynamical characteristics of the arm, wide bandwidth signals were used as force disturbance. Distributing the power of the signal over less frequencies within the bandwidth improved the signal-to-noise ratio (SNR) of the EMG recordings, facilitating reliable estimation of the reflexive impedance. The high coherence indicated that the relation between force disturbance and EMG was linear under the given conditions and improved with the SNR. The method of designing disturbance signals and the estimation of the reflexive impedance are useful for studies aiming to quantify spinal reflexes and to investigate the functionality of spinal reflexes.

5.1 Introduction

Continuous random force disturbances have proven to be useful to quantify spinal reflexes and so to investigate the functionality of reflexes (De Vlugt et al., 2002; Van der Helm et al., 2002; Schouten et al., 2003). However these studies, and other to quantify proprioceptive reflexes (Kearney et al., 1997; Mirbagheri et al., 2000; Zhang and Rymer, 1997), are all based on analyses of the dynamic relation between force and position (mechanical admittance) only and consequently assumptions are needed to separate the reflexive contributions from the mechanical admittance. Incorporation of the muscle activation might improve the procedures.

Force disturbances with position tasks are unambiguous and natural for the subject. High effort tasks, like *'minimize displacements'* demand high levels of co-contraction. This implicates that the variation in the muscle activation due to reflexes will be relatively small compared to the high tonic muscle activity. Muscle activation is easily recorded by surface electromyography (EMG). EMG, however, contains substantial noise, uncorrelated to the applied disturbance, and the small variations due to reflexes will be hard to identify. Goal of this study is to redesign the continuous signals used as force disturbances such that the dynamic relation between position and muscle activation (reflexive impedance) can be estimated reliably in addition to the mechanical admittance during postural control tasks.

5.2 Materials and methods

5.2.1 Subjects

Ten healthy subjects participated in the experiment (20-44 years, 4 women, 3 left handed). The experiments were conducted on the right arm only. All subjects gave informed consent prior to the procedure.

5.2.2 Apparatus

A manipulator was used to apply force disturbances to the shoulder joint. The manipulator is extensively described in Chapter 2 and is introduced briefly. The subjects sat in a chair and had to hold a handle with their right hand. Movement of the handle resulted in ante-/retroflexion movements of the shoulder joint. To the subject the manipulator behaved like a mass-spring-damper system. The parameters of the spring (k_e), damper (b_e), and mass (m_e) are adjustable. In this study the mass was fixed ($m_e = 1$ kg), no stiffness and damping were set ($k_e = 0$ N/m; $b_e = 0$ Ns/m).

5.2.3 Procedures

Subjects had to hold the handle and were instructed to *'minimize the displacements'* of the handle, while continuous random force disturbances were applied for 30 s. All subjects experienced the task as natural and motivating. Only a few trials were

necessary to get the subject acquainted with the manipulator. The actual position of the handle was shown on a display to assist and motivate the subjects and to prevent drift.

Six different signals were used as a force disturbance. All signals had a bandwidth of 0.5-20 Hz, which was sufficient to capture all relevant dynamics of the arm (Van der Helm et al., 2002). The force disturbances were composed as a sum of sines, the so-called multisine signals. These signals were designed to have a specified frequency content and by minimizing the crest factor (the compression, or compactness, of the signal) the power of the signal could be increased without changing signal amplitude (Schoukens et al., 1993; Pintelon and Schoukens, 2001; De Vlugt et al., 2003a). With cresting of multisine signals the (random) phases of the sines are optimized such that the crest factor is minimal. The crest factor is defined as the maximal amplitude of the signal divided by the root-mean-square (RMS) of the signal:

$$CF = \frac{\max |d(t)|}{RMS_d} \quad (5.1)$$

in which CF is the crest factor and RMS_d denotes the RMS of signal $d(t)$.

Random signals have crest factors in the range of 4 to 5, while optimized signals have crest factors around 2 (Pintelon and Schoukens, 2001). When the amplitude of the output is limited, e.g. the position deviations must be kept small, higher input power can be used with signals having an optimized crest factor. Higher input power generally results in a better SNR and consequently will improve the estimators for the frequency response functions (FRFs) between input and output.

The disturbance signals were 30 s in length and had a sample frequency of 2500 Hz. For analysis the first 9464 samples (≈ 4 s) were omitted to remove any initial transient response, leaving 2^{16} samples (≈ 26 s) for analysis. As a result of the limited observation time ($T_{obs} = 26.2144$ s $\equiv 2^{16}$ samples) a finite resolution in the frequency domain resulted ($\Delta f = T_{obs}^{-1} \approx 0.038$ Hz). As a result of the finite resolution in the frequency domain 508 sines existed in the bandwidth of 0.5-20 Hz. The method used to estimate the FRFs requires averaging over 4 adjacent frequency bands (see Sec. 5.2.4), resulting in 127 clusters of 4 adjacent frequencies, within the bandwidth.

In this study six different multisine signals were tested. The reference signal (WB127) had a full spectrum, i.e. uniform power in all clusters between 0.5 and 20 Hz. To further improve the SNR of the EMG, the number of cluster was gradually reduced from 64 to 22 clusters (WB64, WB43, WB32, WB26, and WB22). In all signals with reduced spectra the power was uniformly and equidistantly distributed over the signal bandwidth. In Fig. 5.1 the full spectrum signal and a reduced spectrum signal are shown. The power spectral densities indicates the distribution of signal power over the frequencies. Because in the reduced spectrum signals the power is distributed over less clusters, the power per frequency increases, while the total power and consequently the RMS of the signals are constant.

To obtain adequate linear model approximations the position deviations must

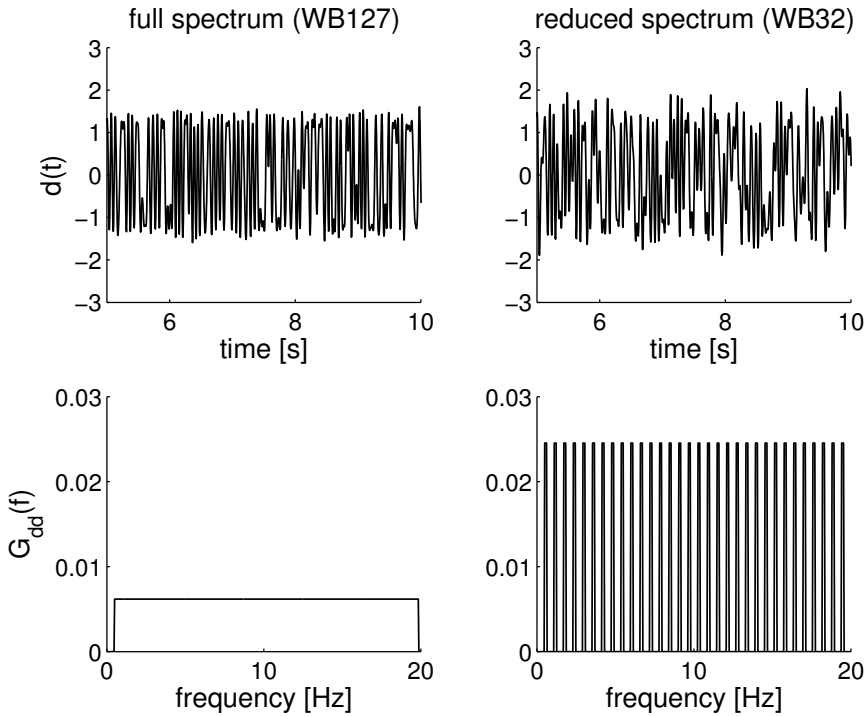


Figure 5.1: Left: full spectrum disturbance WB127; right: reduced spectrum disturbance WB32. Upper plots: 5 s fragment of the signals; lower plots: power spectral density of the signals. Both signals are scaled to have a RMS of one.

be kept small. Prior to the experiment the magnitude of the reference force disturbance was adjusted, by trial-and-error, to obtain a RMS for the hand position of approximately 3 mm. This signal magnitude was set once and was taken the same for all signals. Each force disturbance was applied four times resulting in 24 trials. The trials were presented in random order. In between the trials the subject was allowed to rest at any time.

The EMG amplitude differs for each muscle and each subject as a result of different anatomical and physiological conditions. To relate the EMG to muscle force the EMG to force ratios were determined from isometric push and pull tasks performed prior and after the experiment. The subjects had to maintain constant force levels for 10 s (-25, -20, -15, 0, 15, 20, 25 N) by pushing or pulling on the handle, while the handle was controlled to be in a fixed (rigid) position. During the isometric trials the force at the handle was shown on the display to assist the subject.

5.2.4 Data processing

Signal recording and processing

During a trial the force disturbance $d(t)$, the position of the handle $x_h(t)$, the force at the handle $f_h(t)$, and the EMG signals of four relevant shoulder muscles (e_1 : m. pectoralis major, e_2 : m. deltoideus anterior, e_3 : m. deltoideus posterior, and e_4 : m. latissimus dorsi) were recorded at 2500 Hz sample frequency and 16 bit resolution. Before recording the EMG signals were high pass filtered to remove DC components and movement artefacts (20 Hz, 3th order Butterworth) and low pass filtered to prevent aliasing (1 kHz, 3th order Butterworth). This study investigates stationary behaviour and to remove any initial transient effect the first 9464 samples (≈ 4 s) were eliminated, leaving 2^{16} samples (≈ 26 s) for further processing.

The EMG recordings of the muscles were used (1) to estimate the amount of co-activation during a trial expressed by the mean EMG u_0 and (2) to obtain the (lumped) muscle activation $a(t)$ to get a measure of the active state of the muscles at time t .

To improve the quality of the EMG signals a prewhitening filter was implemented, following the procedures as described in Clancy et al. (2002). With EMG the action potentials of the muscle fibres are recorded at the skin surface. As the action potential propagates over the muscle fibres, the recorded EMG will have a temporal distortion. In prewhitening an inverse filter is applied to decorrelate the recorded EMG and to restore the flat (white) spectrum. The power spectral densities of the EMG signals during the maximum isometric push and pull tasks were used to obtain the parameters of the prewhitening filter (6th order). The prewhitening filter was implemented as a moving average filter.

The integrated rectified EMG, IEMG, was calculated for each trial:

$$\text{IEMG}_i = \frac{1}{n} \sum_{k=1}^n |e_{w,i}(t_k)| \quad (5.2)$$

in which $e_{w,i}$ is the prewhitened EMG of muscle i , k indexes the time vector, and n is the number of samples. The mean EMG was calculated, according to:

$$u_0 = \frac{1}{4} \sum_{i=1}^4 \frac{\text{IEMG}_i}{\text{IEMG}_{ref,i}} \quad (5.3)$$

in which $\text{IEMG}_{ref,i}$ denotes the IEMG for muscle i during the reference disturbance (WB127) averaged over the four repetitions.

To calculate the (lumped) muscle activation the EMG signals were scaled and expressed in Newtons. For each muscle the EMG to force ratio K_i was obtained by fitting a straight line between the average forces and the average IEMGs of the isometric push/pull tasks, using a least squares criterion. In these calculations the negative forces were omitted when the ratios of the 'push' muscles were determined (m. pectoralis major and m. deltoideus anterior). And for the 'pull' muscles (m. deltoideus posterior and m. latissimus dorsi) the positive forces were omitted.

The muscle activation was obtained by combining the rectified prewhitened EMGs of the four recorded muscles:

$$a(t) = \frac{1}{2} (K_1 |e_{w,1}(t)| + K_2 |e_{w,2}(t)|) + \frac{1}{2} (K_3 |e_{w,3}(t)| + K_4 |e_{w,4}(t)|) \quad (5.4)$$

In this equation it is assumed that both ‘push’ muscles (1 and 2) had equal relevance and consequently the total push force was equal to the mean of both muscles. The same holds for the ‘pull’ muscles (3 and 4). Note that K_1 and K_2 are positive and K_3 and K_4 are negative, as the muscles operate in opposite directions.

Nonparametric analysis

The time records ($x_h(t)$, $f_h(t)$, $d(t)$, $a(t)$) of the four repetitions for one condition were averaged to reduce the noise in the signals. The signals were transformed to the frequency domain using the fast Fourier transform (FFT). Because force disturbances were applied, interaction between the subject and manipulator existed, i.e. the position of the handle depends on both the dynamics of the subject and the external environment imposed by the manipulator. Because of this interaction closed loop identification algorithms were required to estimate the FRFs of the mechanical admittance and reflexive impedance (Van der Helm et al., 2002; De Vlugt et al., 2003a). The FRFs were estimated by dividing the appropriate spectral densities:

$$\hat{H}_{fx}(f) = \frac{\hat{G}_{dx}(f)}{\hat{G}_{df}(f)} \quad (5.5)$$

$$\hat{H}_{xa}(f) = \frac{\hat{G}_{da}(f)}{\hat{G}_{dx}(f)} \quad (5.6)$$

in which \hat{G}_{dx} denotes the estimated cross spectral density between d and x_h (hat denotes estimate). \hat{H}_{fx} and \hat{H}_{xa} are estimates for the FRFs of the mechanical admittance and reflexive impedance respectively. The estimated spectral densities were averaged over 4 adjacent frequencies to improve the estimators (Jenkins and Watts, 1968). As a measure for reliability the coherences are calculated.

$$\hat{\gamma}_x^2(f) = \frac{|\hat{G}_{dx}(f)|^2}{\hat{G}_{dd}(f)\hat{G}_{xx}(f)} \quad (5.7)$$

$$\hat{\gamma}_a^2(f) = \frac{|\hat{G}_{da}(f)|^2}{\hat{G}_{dd}(f)\hat{G}_{aa}(f)} \quad (5.8)$$

$\hat{\gamma}_x^2$ and $\hat{\gamma}_a^2$ are estimates for the coherence for the handle position and muscle activation respectively. The coherence varies between 0 and 1 by definition and is reduced by noise and nonlinearities. All estimators for the FRFs and coherences were only evaluated at the frequencies where the force disturbance contained power, unless noted otherwise. The use of periodic multisines as a disturbance ensures that all spectral estimators are unbiased and have a relative low variance (Pintelon and Schoukens, 2001; De Vlugt et al., 2003a).

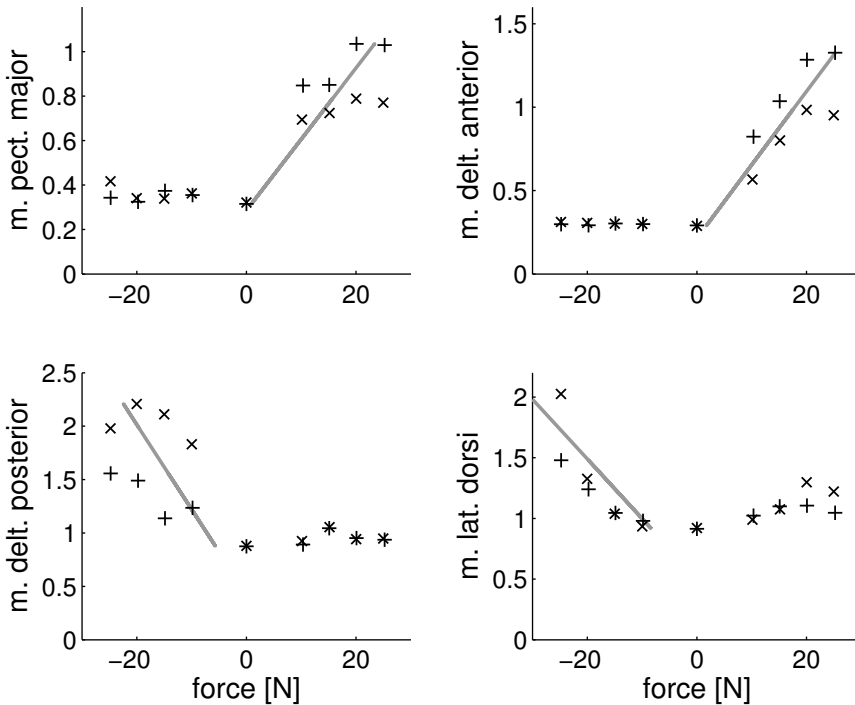


Figure 5.2: EMG to force ratios for a typical subject. Upper-left: *m. pectoralis major*; upper-right: *m. deltoideus anterior*; lower-left: *m. deltoideus posterior*; lower-right: *m. latissimus dorsi*. Average force is given on the X-axis, the corresponding IEMG on the Y-axis. Positive force corresponds with pushing. The 'x' and '+' denotes the IEMG of the push/pull tasks before and after the main experiment respectively; the slope of the line denotes the estimated EMG to force ratio.

5.3 Results

5.3.1 Isometric experiments

Fig. 5.2 shows the EMG to force relations for a typical subject. The *m. pectoralis major* and *m. deltoideus anterior* were active during pushing, while the *m. deltoideus posterior* and *m. latissimus dorsi* were relatively silent. On the active part of the EMG to force relation the EMG to force ratio is estimated with a least squares criterion. These ratios are denoted with grey lines in Fig. 5.2.

5.3.2 Main experiment

Fig. 5.3 shows a typical response for two reduced spectrum disturbances. For both disturbances the amplitudes in force, position and activation are comparable. The power of the spectral density of the muscle activation at the excited frequencies

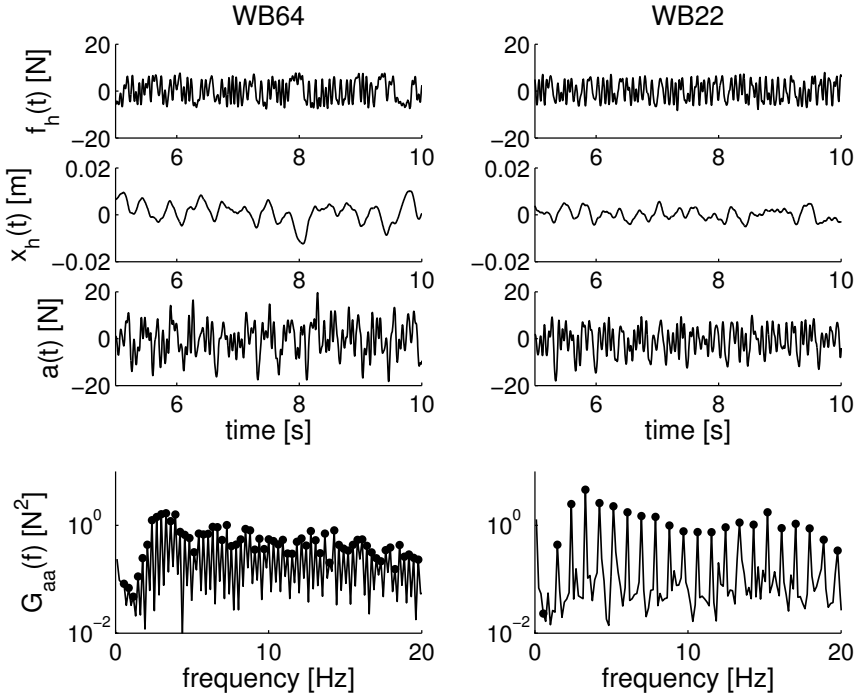


Figure 5.3: Time plots of reduced spectrum signals (left: WB64; right: WB22). First row: force at the handle $f_h(t)$; second row: position deviations $x_h(t)$; third row: muscle activation $a(t)$. Time plots of muscle activation are filtered (low pass, 20 Hz, 3th order Butterworth, forwards and backwards) for display purposes only. Bottom row: spectral density of the muscle activation $\hat{G}_{aa}(f)$. Dots denote the frequencies in the disturbance with signal power.

increased when the number of clusters reduces. This was expected since the input power increased with decreasing number of clusters (Fig. 5.1). However the muscle activation had substantial power in between the clusters, indicating the presence of noise. The noise decreased with decreasing number of clusters. Both effects, i.e. increased signal power and decreased noise, contribute to a better SNR with decreasing number of clusters.

Fig. 5.4 shows the FRFs and coherences for two disturbances for one subject. For clearance only two of the six conditions are shown, the other four had similar behaviour. The FRF of the mechanical admittance (left) did not change with the number of clusters. The coherence for the position (left) was high for all frequencies, indicating that the relation was linear and did not contain substantial noise. The coherence for the muscle activation was relatively low for frequencies below 2 Hz and increased with decreasing number of frequencies. The gain and phase of the estimated FRF of the reflexive impedance were similar for all disturbances,

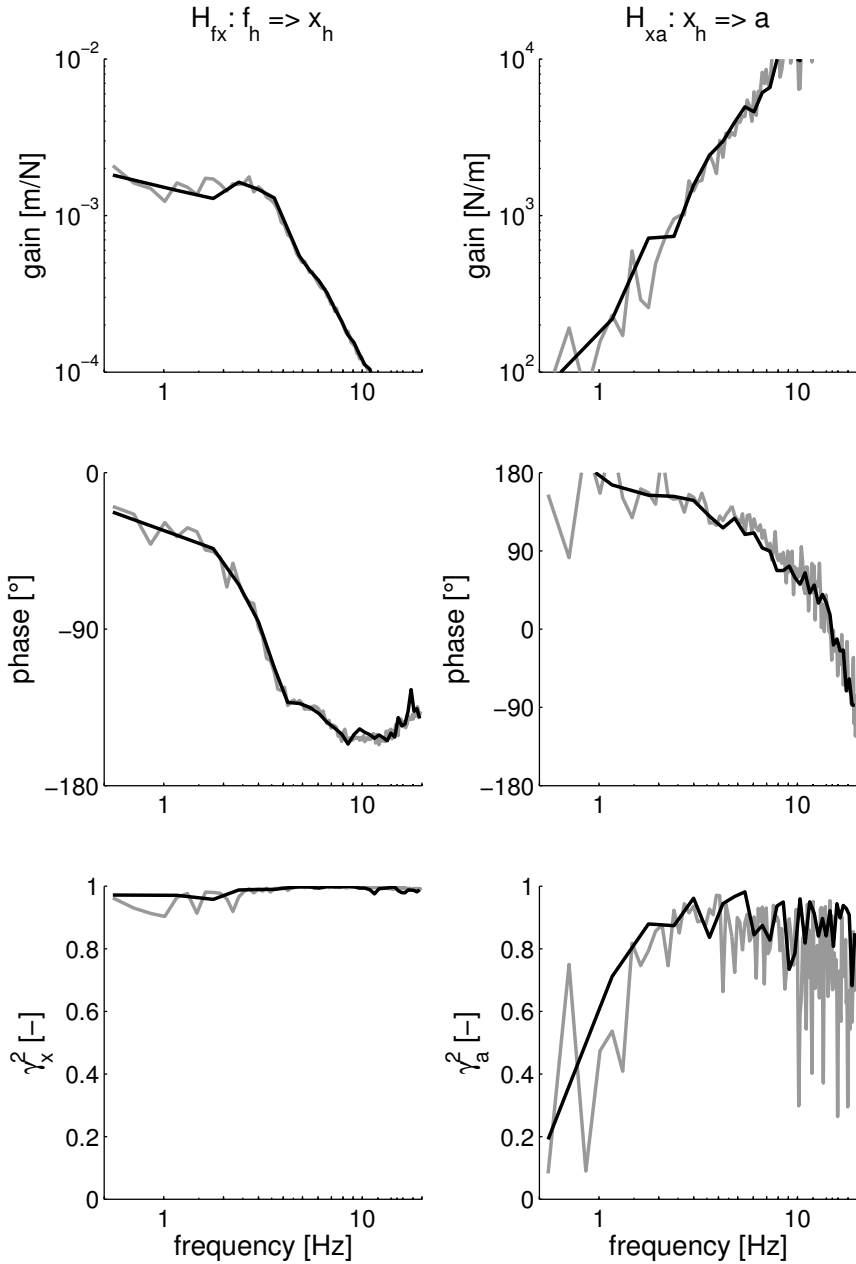


Figure 5.4: Gain (upper row) and phase (middle row) of the FRFs for the mechanical admittance (left) and the reflexive impedance (right) for WB127 (grey) and WB32 (black). Bottom row: coherences.

Table 5.1: Mean EMG u_0 , global coherence $\bar{\gamma}_a^2$, and SNR. Means with standard deviation (SD) over all subjects.

number of clusters	u_0 [-]	$\bar{\gamma}_a^2$ [-]	SNR [dB]
127 (=full)	1 (-)	0.63 (0.09)	- (-)
64	0.99 (0.06)	0.67 (0.09)	5.2 (2.2)
43	0.99 (0.10)	0.69 (0.12)	6.3 (3.2)
32	0.99 (0.10)	0.70 (0.14)	10.3 (5.1)
26	0.97 (0.05)	0.76 (0.08)	10.6 (4.3)
22	0.99 (0.09)	0.75 (0.11)	12.9 (6.2)

however the variance of the estimator was reduced as the lines become smoother with less clusters. In Table 5.1 the mean EMG for each disturbance is shown. The mean EMG did not show significant differences between the disturbances, indicating that the muscle cocontraction is constant over the conditions.

To compare the coherences of the muscle activation the global coherence was calculated for each perturbation. The global coherence $\bar{\gamma}_a^2$ is defined as the average of the coherence over the clusters with signal power and is given in Table 5.1. The last column shows the SNR for the muscle activation. The SNR was calculated by dividing the average signal S by the average noise N according to:

$$S = \frac{1}{k} \sum \hat{G}_{aa}(f_k) \quad (5.9)$$

$$N = \frac{1}{n} \sum \hat{G}_{aa}(f_n) \quad (5.10)$$

$$\text{SNR} = 10 \log \left(\frac{S}{N} \right) \quad (5.11)$$

where f_k denotes all frequencies between 0.5 and 10 Hz where the disturbance signal contains power, and f_n all frequencies between 0.5 and 10 Hz where the disturbance signal does not contain power. Note that for the full spectrum condition (WB127) the SNR can not be obtained as no estimate for the noise can be made.

The mechanical admittance (left plots in Fig. 5.4) resembled a damped second order system similar to those found in previous studies (Van der Helm et al., 2002; De Vlugt et al., 2002). The stiffness is equal to the inverse of the admittance at 0 Hz and was approximately 700 N/m. The eigenfrequency of the arm was around 3 Hz

From the increasing gain with frequency of the reflexive impedance (upper-right plots in Fig. 5.4), it appears that the reflexive feedback was dominated by velocity feedback (first derivative of the position, corresponding to a slope of +1 in the gain and 90 degrees phase lead) and even acceleration feedback (second derivative, slope of +2, 180 degrees phase lead). The time delay of the proprioceptive reflexes can be derived from the phase of the reflexive impedance. A time delay has unity gain and the phase decreases linearly with increasing frequency. Assuming that the reflexive feedback is only velocity sensitive, the time delay will be around

30 ms, indicating that the observed behaviour resulted from short latency, or spinal, reflexes. A time delay of 30 ms gives approximately 180 degrees phase lag at 17 Hz, the velocity sensitivity gives 90 degrees phase lead for all frequencies, explaining the observed 90 degrees phase lag at 17 Hz.

5.4 Discussion

In this study a method was developed to assess the dynamic relation between position and muscle activation (via EMG), i.e. the reflexive impedance. The reflexive impedance was obtained along with the mechanical admittance, while continuous random force perturbations were applied. The use of continuous random force perturbations is natural for the subject and results in an unambiguous task. Several wide bandwidth signals were designed and used as a force disturbance. The reliability of the estimated reflexive impedance is expressed in the coherence and signal-to-noise ratio (SNR). The reflexive impedance is a direct expression of the muscle activation resulting from reflexes. The reflexive impedance is a useful contribution to investigate the contribution of reflexes to the joint admittance. A succeeding study will use the signal design procedure to investigate the effect of disturbance bandwidth and external environment on proprioceptive reflexes, by fitting a model onto the admittance and reflexive impedance simultaneously (Schouten et al., 2004b, see Chapter 6).

The disturbances applied contain power between 0.5 and 20 Hz, which is sufficient to capture all relevant shoulder dynamics (Van der Helm et al., 2002). The signals used as force disturbance were designed in the frequency domain as multisine signals (Schoukens et al., 1993; Pintelon and Schoukens, 2001). Multisine signals as a disturbance have three important advantages over other continuous random signals: 1) no bias is introduced in the spectral estimators, 2) signal properties can be explicitly controlled, and 3) due to its periodicity no random errors are introduced.

In the reference signal all frequencies within the bandwidth (0.5-20 Hz) contained power. By distributing the power over less frequencies within the bandwidth, the power per frequency increased. The mechanical admittance nor the mean EMG did change with the signal, indicating that the subjects responded equally to all signals. By distributing the power over less frequencies both the SNR and coherence of the muscle activation increased. Both are measures for the reliability of the estimated reflexive impedance. However the FRFs can only be evaluated over the frequencies with signal power. Distributing the power over less frequencies reduces the resolution at which FRFs and coherences can be estimated. One has to weight the increased reliability against reduced frequency resolution.

Chapter 6

Quantifying spinal reflexes in vivo during postural control

Alfred C. Schouten, Erwin de Vlugt, J.J. (Bob) van Hilten,
Frans C.T. van der Helm
Submitted to *Journal of Neuroscience Methods*

This study aimed to analyse the dynamic properties of the muscle spindle feedback system of shoulder muscles during a posture task. External continuous force disturbances were applied at the hand while subjects had to minimize their hand displacements. The results were analysed using two frequency response functions (FRFs) from which the model parameters were derived, being (a) the mechanical admittance and (b) the reflexive impedance. These FRFs were analysed by a neuromusculoskeletal model that implicitly separates the reflexive feedback properties (position, velocity and acceleration feedback gains) from intrinsic muscle viscoelasticity. The results show substantial changes in estimated reflex gains under conditions of variable bandwidth of the applied force disturbance or variable degrees of external damping. Position and velocity feedback gains were relatively larger when the force disturbance contained only low frequencies. With increasing damping of the environment, acceleration feedback gain decreased, velocity feedback gain remained almost constant and position feedback gain increased. It is concluded that under the aforementioned circumstances, the reflex system adapts its gains to maximize the mechanical resistance to external force disturbances while preserving sufficient stability.

6.1 Introduction

Studies addressing the role of spinal reflexes in the regulation of movement and posture have been informative in understanding the impact of diseases with abnormal muscle tone including spasticity, dystonia or Parkinson's disease (Mirbagheri et al., 2001; Schouten et al., 2003; Lee and Tatton, 1975). Studies on the role of spinal reflexes in the regulation of muscle tone have mainly applied qualitative approaches (Doemges and Rack, 1992a,b; Akazawa et al., 1983; Kanosue et al., 1983). From these studies important features of the proprioceptive reflex system emerged showing the influence of position and force tasks on proprioceptive reflex magnitude. However these studies have not provided insight into the functional contribution of proprioceptive reflexes to the dynamic relation between force and position (mechanical admittance), which is crucial in the understanding of how these reflexes control stable movement and posture. Few studies have focussed on qualitative characterisation of proprioceptive reflex regulation (Zhang and Rymer, 1997; Kearney et al., 1997; Van der Helm et al., 2002). These studies have used quantification methods that basically rely on specific neuromuscular models and optimisation algorithms to minimize the difference between measured and predicted variables. Hitherto, all studies have used an indirect approach by estimating reflex parameters from the mechanical admittance. In the mechanical response, intrinsic muscle visco-elasticity and reflexive contributions coexist. Therefore assumptions on the reflexive component were necessary to separate the intrinsic and reflexive contributions. Such assumptions on reflex behaviour may introduce a bias in the model. Consequently, there is a need for methods that directly quantify reflex behaviour. In a recent study (Schouten et al., 2004a, see Chapter 5) a method was introduced to estimate the frequency response functions (FRFs) of the mechanical admittance and the reflexive impedance, i.e. the dynamic relation between position and muscle activation. This study aims to quantify spinal reflexes directly by fitting a neuromusculoskeletal (NMS) model of the arm on both the mechanical admittance and reflexive impedance, obtained simultaneously during posture tasks.

6.2 Materials and methods

6.2.1 Subjects

Two experiments were carried out. In the main experiment ten healthy subjects (4 women, 3 left handed) participated with a mean (standard deviation, SD) age of 25.8 (7.0) years. In a second experiment, to estimate the muscle activation dynamics, five subjects (2 women, 2 left handed) participated with a mean (SD) age of 25.4 (3.2) years. All subjects gave informed consent prior to the procedure. All experiments were conducted on the right arm.

6.2.2 Apparatus

Force disturbances were applied to the hand by means of a linear manipulator. The manipulator is extensively described in Chapter 2 and is introduced briefly. The subjects sat in a chair and had to hold a handle with their right hand. Movement of the handle resulted in ante-/retroflexion movements of the shoulder-joint. To the subject the manipulator behaved like a mass-spring-damper system. The parameters of the spring (k_e), damper (b_e), and mass (m_e) are adjustable. In this study the mass m_e was set to a fixed value of 1 kg. The damping b_e was varied between the trials, see Procedures. No stiffness was used ($k_e = 0$ N/m).

6.2.3 Procedures

Main experiment

In the main experiment subjects had to hold the handle and were instructed to '*minimize the displacements*' of the handle, while continuous random force disturbances were applied for 30 s (task *stiff*). The actual position of the handle was shown on a display to assist the subjects and to prevent drift. Only a few trials were necessary to get the subject acquainted with the task. The following experimental conditions were applied:

- Wide bandwidth (WB) disturbance without external damping (WB *stiff*). The WB disturbance signal had power between between 0.5 and 20 Hz. This condition is referred to as the reference condition.
- WB disturbance without external damping and the task *slack* (WB *slack*). Here the task instruction was different from the other: the subject was asked to relax the arm muscles and not to react to the disturbance. This task was only used to improve to estimate of the arm mass.
- WB disturbance with external damping. The damping was assigned values of 50, 100, 150, 200 Ns/m (B50, B100, B150, B200).
- Narrow bandwidth disturbance type 1 (NB1) without external damping. The disturbance signals had a variable bandwidth; the lowest frequency was fixed at 0.5 Hz and the highest frequency f_h varied between 1.2 and 3.7 Hz (1.2, 1.5, 1.8, 2.4, 3.1, 3.7 Hz).
- Narrow bandwidth disturbance type 2 (NB2) without external damping. The signals had a bandwidth of 0.3 Hz concentrated around a variable centre frequency f_c of 1.3 up to 7 Hz (1.3, 1.8, 2.3, 3, 4, 5, 6, 7 Hz).

The twenty different conditions were repeated four times, resulting in eighty trials of 30 s each. The trials were presented in a random order. In between the trials the subject could rest as long as he/she wanted to prevent fatigue. All disturbance signals were designed in the frequency domain as so-called multisine signals with optimized crest factor (Schoukens et al., 1993; Pintelon and Schoukens, 2001; Schouten

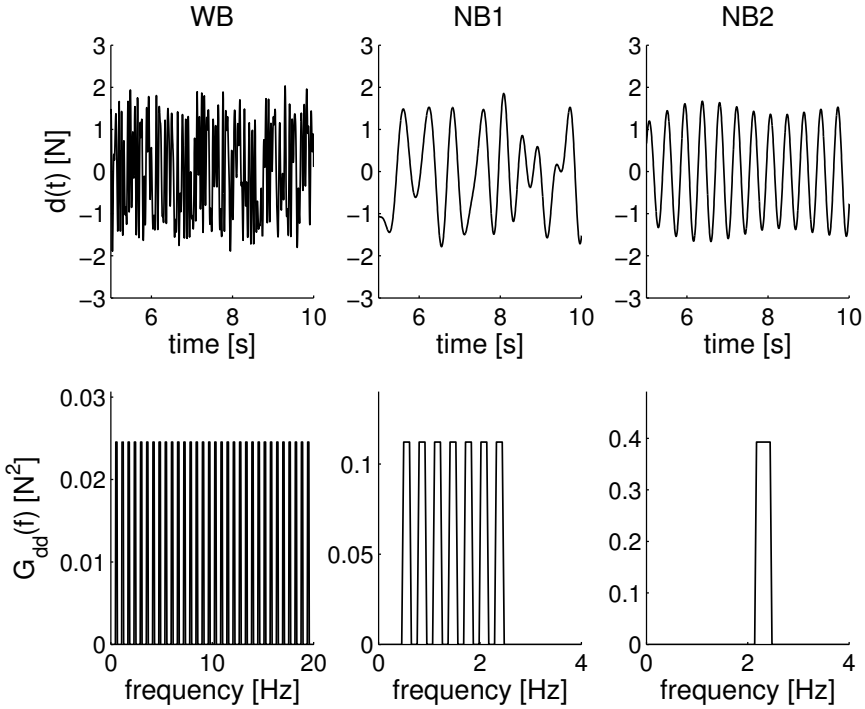


Figure 6.1: Examples of disturbance signals; left: WB; middle: NB1 $f_h = 2.4$ Hz; right: NB2 $f_c = 2.3$ Hz. Upper plots: 5 s fragment of the signals; lower plots: power spectral densities of the signals. The signals are scaled to a root-mean-square (RMS) value of one. Each peak in the power spectral densities represents a cluster of 4 (WB, NB1) or 8 (NB2) adjacent frequencies.

et al., 2004a). Because multisine signals are deterministic, no bias and variance were introduced in the estimated spectral densities (Pintelon and Schoukens, 2001; De Vlugt et al., 2003a).

To improve the signal-to-noise ratio (SNR) of the EMG and to allow reliable identification of the reflexive impedance, the power of the disturbance signal was distributed over a limited number of frequencies within the bandwidth. For the WB disturbance the signal power was uniformly distributed over 32 equidistantly spaced clusters of 4 adjacent frequencies, i.e. 25% of the frequencies within the bandwidth were excited (Schouten et al., 2004a). The data analysis required clusters of 4 adjacent frequencies for averaging. For the NB1 disturbances 50% of the frequencies within the bandwidth were excited, and consequently each NB1 signal contained a different number of clusters (ranging from 3 clusters for $f_h = 1.2$ Hz up to 11 clusters for $f_h = 3.7$ Hz). For the NB2 disturbances the power was distributed in one cluster of 8 adjacent frequencies. Fig. 6.1 shows examples of the disturbance

signals, the lower plots show the power spectral densities of the signals.

To justify the use of linear model approximations the position deviations must be kept small within each condition. Prior to the trials each condition was tested and the amplitude of the force disturbance was adjusted for each condition to obtain a root-mean-square (RMS) value for the position of approximately 3 mm.

Since recorded EMG is an electric signal which is meaningless to the mechanical properties, the EMG to force ratio was determined to obtain a relative measure of the muscle force. Therefore, subjects were required to perform isometric push and pull tasks, prior and after the main experiment. The subjects had to maintain constant force levels for 10 s (-25, -20, -15, 0, 15, 20, 25 N) by pushing or pulling against the handle, which was controlled to be in a fixed (rigid) position. During these isometric trials the reference force together with the actual force at the handle were shown on the display to assist the subject in performing the task. The EMG to force ratio was determined by linear regression.

Activation dynamics

The EMG to force ratio provides the static relation between muscle activation and muscle force. The dynamic relation between muscle activation and muscle force was determined in a secondary isometric experiment. The secondary experiment started and ended with the same push/pull tasks as the main experiment. The experiment consists of 8 trials of 30 s. During these trials the subjects performed isometric tasks and were asked to make block-shaped forces between approximately 25 N push and pull.

6.2.4 Data processing

Signal recording and processing

During a trial the force disturbance $d(t)$, the position of the handle $x_h(t)$, the force at the handle $f_h(t)$, and the EMG of four relevant shoulder muscles (e_1 : m. pectoralis major, e_2 : m. deltoideus anterior, e_3 : m. deltoideus posterior, and e_4 : m. latissimus dorsi) were recorded at 2500 Hz sample frequency with a 16 bit resolution. Before recording, the EMG signals were high pass filtered to remove DC components and movement artefacts (20 Hz, 3th order Butterworth), and low pass filtered to prevent aliasing (1 kHz, 3th order Butterworth). This study investigates stationary behaviour and to remove any initial transient effect the first 9464 samples (≈ 4 s) were eliminated, leaving 2^{16} samples (≈ 26 s) for further processing.

The EMG signals were used (1) to estimate the amount of co-activation expressed by the mean EMG and (2) to construct the (lumped) muscle activation $a(t)$. The procedure of EMG treatment is described previously in Schouten et al. (2004a) and will be briefly summarized. To improve the quality of the EMG signals a prewhitening filter is implemented, following the procedures as described in Clancy et al. (2002). The power spectral densities of the EMGs during the maximum isometric push and pull tasks (25 N) are used to obtain the parameters of the prewhitening filter (6th order). For small variations in muscle co-activation it

reasonable to assume that the intrinsic muscle visco-elasticity linearly scale with the co-activation level (Agarwal and Gottlieb, 1977). Therefore mean EMG u_0 was determined as a measure for muscle co-activation. To calculate the mean EMG the integrated rectified EMG (IEMG) of each muscle during a trial was calculated.

$$\text{IEMG}_i = \frac{1}{n} \sum_{k=1}^n |e_{w,i}(t_k)| \quad (6.1)$$

in which $e_{w,i}$ is the prewhitened EMG of muscle i , k indexes the time vector, and n is the number of samples. The mean EMG was calculated, according to:

$$u_0 = \frac{1}{4} \sum_{i=1}^4 \frac{\text{IEMG}_i}{\text{IEMG}_{ref,i}} \quad (6.2)$$

where $\text{IEMG}_{ref,i}$ denotes the IEMG for muscle i of the reference condition averaged over the four repetitions.

To calculate the muscle activation $a(t)$ the EMG signals are scaled and expressed into Newtons. The EMG to force ratio of each muscle K_i is estimated from the push/pull tasks by linear regression. The (lumped) muscle activation is obtained by combining the rectified prewhitened EMGs of the four recorded muscles:

$$a(t) = \frac{1}{2} (K_1 |e_{w,1}(t)| + K_2 |e_{w,2}(t)|) + \frac{1}{2} (K_3 |e_{w,3}(t)| + K_4 |e_{w,4}(t)|) \quad (6.3)$$

In this equation it is assumed that both 'push' muscles (1 and 2) have equal relevance and consequently the total push force is equal to the mean of both muscles. The same holds for the 'pull' muscles (3 and 4). Note that K_1 and K_2 are positive and K_3 and K_4 are negative, as the muscles operate in opposite direction.

Nonparametric analysis

The time records ($x_h(t)$, $f_h(t)$, $d(t)$, and $a(t)$) of the four repetitions for one condition are averaged to reduce the variance due to noise in the signals. The signals are transformed to the frequency domain using the fast Fourier transform (FFT). Because force disturbances are applied, interaction between the subject and manipulator existed, i.e. the position of the handle depends on both the dynamics of the subject and the external environment imposed by the manipulator. Because of this interaction closed loop identification algorithms are required to estimate the FRFs of the mechanical admittance $\hat{H}_{fx}(f)$ and reflexive impedance $\hat{H}_{xa}(f)$ (Schouten et al., 2004a).

$$\hat{H}_{fx}(f) = \frac{\hat{G}_{dx}(f)}{\hat{G}_{df}(f)} \quad (6.4)$$

$$\hat{H}_{xa}(f) = \frac{\hat{G}_{da}(f)}{\hat{G}_{dx}(f)} \quad (6.5)$$

where $\hat{G}_{dx}(f)$ is the estimated cross spectral density between d and x_h (hat denotes estimate). The spectral densities are averaged over 4 adjacent frequencies to reduce the variance of the estimations (Jenkins and Watts, 1968). As a measure for linearity between the signals the coherence for the position $\hat{\gamma}_x^2(f)$ and muscle activation $\hat{\gamma}_a^2(f)$ were estimated.

$$\hat{\gamma}_x^2(f) = \frac{|\hat{G}_{dx}(f)|^2}{\hat{G}_{dd}(f)\hat{G}_{xx}(f)} \quad (6.6)$$

$$\hat{\gamma}_a^2(f) = \frac{|\hat{G}_{da}(f)|^2}{\hat{G}_{dd}(f)\hat{G}_{aa}(f)} \quad (6.7)$$

The coherence varies between 0 and 1 and decreases due to external noise and nonlinearities. The FRFs and coherences were only evaluated at the frequencies where the perturbation signal had non-zero power.

Quantification of activation dynamics

During isometric experiments the relationship between the muscle activation $a(t)$ and handle force $f_h(t)$ depends on the activation dynamics only. As the muscle activation was scaled to force the muscle dynamics have unity static gain. The activation dynamics $\hat{H}_{act}(f)$ were estimated by dividing the appropriate spectral densities with the aid of an independent instrument variable (Pintelon and Schoukens, 2001):

$$\hat{H}_{act}(f) = \frac{\hat{G}_{wf}(f)}{\hat{G}_{wa}(f)} \quad (6.8)$$

$$\hat{\gamma}_{af}^2(f) = \frac{|\hat{G}_{af}(f)|^2}{\hat{G}_{aa}(f)\hat{G}_{ff}(f)} \quad (6.9)$$

with w as the instrument variable for which a signal with power uniformly distributed between 0.1-20 Hz was used. To improve the estimations the spectral densities are averaged over 4 adjacent frequencies.

The activation dynamics are described by with a second order model (Olney and Winter, 1985; Bobet and Norman, 1990; Potvin et al., 1996):

$$H_{act}(s, p_{act}) = \frac{1}{\frac{1}{\omega_0^2}s^2 + \frac{2\beta}{\omega_0}s + 1} \quad (6.10)$$

in which s the Laplace operator equals $j2\pi f$, f_0 is the eigenfrequency ($f_0 = \frac{\omega_0}{2\pi}$), β the relative damping of the activation dynamics model, and p_{act} is the parameter vector.

$$p_{act} = [f_0, \beta] \quad (6.11)$$

The activation dynamics were obtained by fitting the model (Eq. 6.10) onto the estimated activation dynamics (Eq. 6.8) by minimizing the criterion function:

$$L_{act}(p_{act}) = \sum_k \frac{\hat{\gamma}_{af}^2(f_k)}{1 + f_k} \left| \ln \hat{H}_{act}(f_k) - \ln H_{act}(f_k, p_{act}) \right|^2 \quad (6.12)$$

where k indexes the frequency vector. Only frequencies till 10 Hz were used in the criterion. For higher frequencies the force signal contained little power such that the activation dynamics can not be estimated reliably. This is reflected by the low coherence above 10 Hz, see Results. Because of the large range of the gain in the FRFs a least squares criterion with logarithmic difference was used (Pintelon et al., 1994). The criterion was weighted with the coherence to reduce emphasis on less reliable frequencies and with $(1 + f_k)^{-1}$ to prevent excessive emphasis on the higher frequencies. To obtain a better fit one set of parameters was used to fit the model simultaneously on all 8 trials for each subject. Finally the activation parameters were averaged over all subjects and used to quantify the intrinsic and reflexive parameters.

Quantification of intrinsic and reflexive properties

The model used to quantify the proprioceptive reflexes along with the intrinsic muscle visco-elasticity and limb mass is given in Fig. 6.2. The position of the handle $X_h(s)$, results from (1) the external force disturbance $D(s)$, (2) human arm admittance $H_{fx}(s)$, and (3) the admittance of the external environment $H_e(s)$.

$$H_e(s) = \frac{1}{m_e s^2 + b_e s + k_e} \quad (6.13)$$

The parameters of the model are summarized in Table 6.1. $H_g(s)$ represents the grip dynamics of the hand.

$$H_g(s) = b_g s + k_g \quad (6.14)$$

The intrinsic model $H_{int}(s)$ includes the visco-elasticity of the cocontracted muscles and the (lumped) arm mass. For small displacements the intrinsic visco-elastic properties of muscles can be described by a linear spring-damper system (Winters et al., 1988).

$$H_{int}(s) = \frac{1}{m s^2 + b s + k} \quad (6.15)$$

The reflexive dynamics $H_{ref}(s)$ represents the muscle spindle sensory system modelled by an acceleration (k_a), velocity (k_v), and position (k_p) gain in series with neural time delay τ_d .

$$H_{ref}(s) = \left(k_a s^2 + k_v s + k_p \right) e^{-\tau_d s} \quad (6.16)$$

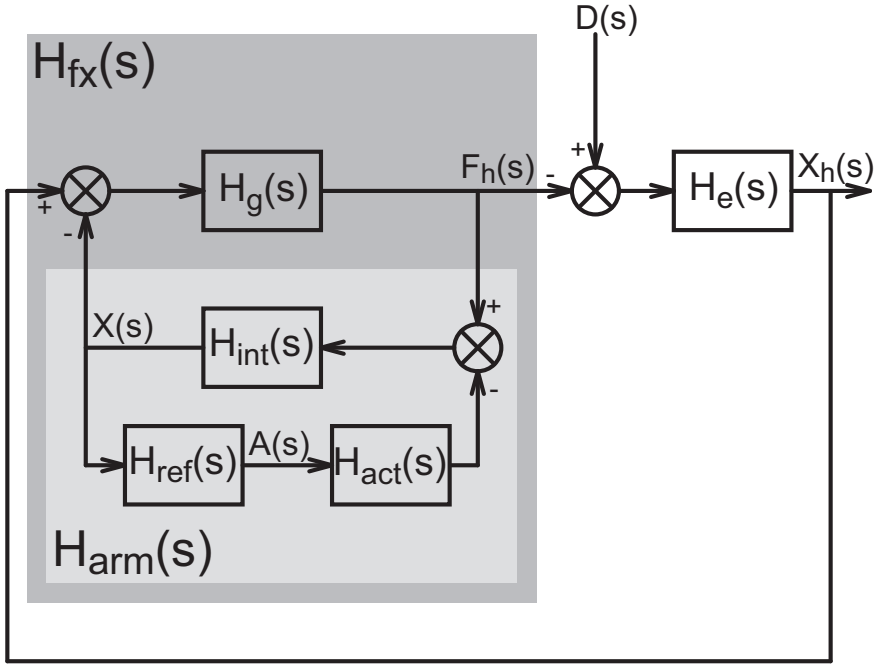


Figure 6.2: NMS model $H_{fx}(s)$ in conjunction with the environment $H_e(s)$. The external force disturbance $D(s)$, hand force $F_h(s)$, position of the handle $X_h(s)$, and muscle activation $A(s)$ are measured. $H_g(s)$ represents grip dynamics, $H_{int}(s)$ intrinsic properties, $H_{act}(s)$ activation dynamics, $H_{ref}(s)$ reflexive feedback, and $X(s)$ position of the arm. The light grey box ($H_{arm}(s)$) represents the arm model without grip.

From the equations (Eqs. 6.10-6.16) the arm dynamics, excluding grip dynamics, can be derived:

$$\begin{aligned}
 H_{arm}(s) &= \frac{X(s)}{F_h(s)} = \frac{H_{int}(s)}{1 + H_{int}(s)H_{ref}(s)H_{act}(s)} \\
 &= \frac{1}{ms^2 + bs + k + (k_a s^2 + k_v s + k_p) e^{-\tau_d s} H_{act}(s)}
 \end{aligned} \tag{6.17}$$

where $X(s)$ and $F_h(s)$ are the Laplace transforms of the arm position and hand force respectively. Finally the mechanical admittance and the reflexive impedance are modelled by:

$$H_{fx}(s, p) = \frac{X_h(s)}{F_h(s)} = H_{arm}(s) + H_g^{-1}(s) \tag{6.18}$$

$$H_{xa}(s, p) = \frac{A(s)}{X_h(s)} = H_{ref}(s) \frac{H_g(s)}{H_g(s) + H_{arm}^{-1}(s)} \tag{6.19}$$

Table 6.1: Model parameters to be quantified.

	description
m [kg]	arm mass
b [Ns/m]	muscle damping
k [N/m]	muscle stiffness
b_g [Ns/m]	grip damping
k_g [kN/m]	grip stiffness
k_a [Ns ² /m]	acceleration feedback gain
k_v [Ns/m]	velocity feedback gain
k_p [N/m]	position feedback gain
τ_d [ms]	neural time delay

in which p is the parameter vector:

$$p = [m, b, k, b_g, k_g, k_a, k_v, k_p, \tau_d] \quad (6.20)$$

Note that when the grip becomes very stiff, $H_g^{-1}(s)$ approaches to zero, such that the mechanical admittance $H_{fx}(s)$ equals $H_{arm}(s)$, while the reflexive impedance $H_{xa}(s)$ equals $H_{ref}(s)$.

The model parameters are quantified by fitting the models (Eqs. 6.18 and 6.19) to the corresponding FRFs (Eqs. 6.4 and 6.5) simultaneously, by minimizing the following criterion function:

$$L(p) = \sum_k \frac{\hat{\gamma}_x^2(f_k)}{1 + f_k} \left| \ln \hat{H}_{fx}(f_k) - \ln H_{fx}(f_k, p) \right|^2 + q \sum_k \frac{\hat{\gamma}_a^2(f_k)}{1 + f_k} \left| \ln \hat{H}_{xa}(f_k) - \ln H_{xa}(f_k, p) \right|^2 \quad (6.21)$$

with q as a weighting factor. Only frequencies where the perturbation signal contained power were included in the criterion. A weighting factor of 0.09 was chosen such that both terms in Eq. (6.21) had approximately equal values in the optimal fit.

The parameters of the conditions with WB disturbances, i.e. with and without damping and WB task *slack*, were estimated simultaneously (six conditions). During this simultaneous model fit one variable for the mass and one for the neural time delay were used for all six conditions. Except for the WB condition task *slack*, the damping and stiffness for the arm and the grip scaled between the conditions simultaneously with the mean EMG u_0 .

$$b = u_0 \cdot b_{ref} \quad (6.22)$$

$$k = u_0 \cdot k_{ref} \quad (6.23)$$

$$b_g = u_0 \cdot b_{g,ref} \quad (6.24)$$

$$k_g = u_0 \cdot k_{g,ref} \quad (6.25)$$

in which ref denotes the parameter value in the reference condition (*WB stiff*). For the condition with task *slack* only the admittance was fitted ($q = 0$) and the reflexive parameters were omitted. The only function of the *slack* condition was to get a better estimate for the mass. Finally the number of parameters was reduced from 54 (6 condition with 9 parameters) to 25 (1 mass, 1 time delay, 4 muscle and grip parameters for the reference condition, 4 idem for task *slack* and 3 reflex gains for 5 conditions).

For the NB conditions the FRFs can only be estimated for the limited bandwidth and therefore contain not enough information to estimate the nine model parameters. To overcome this, it was assumed that the intrinsic parameters (muscle and grip) scaled with mean EMG using the intrinsic parameters estimated from the reference condition (*WB stiff*), see Eqs. 6.22-6.25. Furthermore the mass and the neural time delay were fixed to the values found with the WB conditions, reducing the parameter vector for the NB conditions to the reflexive parameters only:

$$p = [k_a, k_v, k_p] \quad (6.26)$$

Model validation

The variance accounted for (VAF) is calculated to obtain a validity index for the quantified parameters. A VAF of 100% indicates that the linear model fully predicts the measurements. Noise, nonlinearities and other unmodelled behaviour reduce the VAF. Note that a low coherence (noise or nonlinearities) always results in a low VAF values.

To calculate the VAF the model is simulated in time with the disturbance $d(t)$ as input, and the simulated position $\hat{x}_h(t)$ and simulated muscle activation $\hat{a}(t)$ as the outputs. Because both the hand position and muscle activation are available from measurements, the VAF is calculated for both:

$$VAF_x = 1 - \frac{\sum_{k=1}^n |x_h(t_k) - \hat{x}_h(t_k)|^2}{\sum_{k=1}^n |x_h(t_k)|^2} \quad (6.27)$$

$$VAF_a = 1 - \frac{\sum_{k=1}^n |a(t_k) - \hat{a}(t_k)|^2}{\sum_{k=1}^n |a(t_k)|^2} \quad (6.28)$$

in which k indexes the time sampled vector. All signals are high pass filtered to remove drift, before calculating the VAF (3th order Butterworth, 1 Hz). The lumped muscle activation signal is reconstructed from rectified EMG signals and consequently contains high frequency components. To remove these components the lumped muscle activation is low pass filtered (3th order Butterworth, 10 Hz) before calculating the VAF.

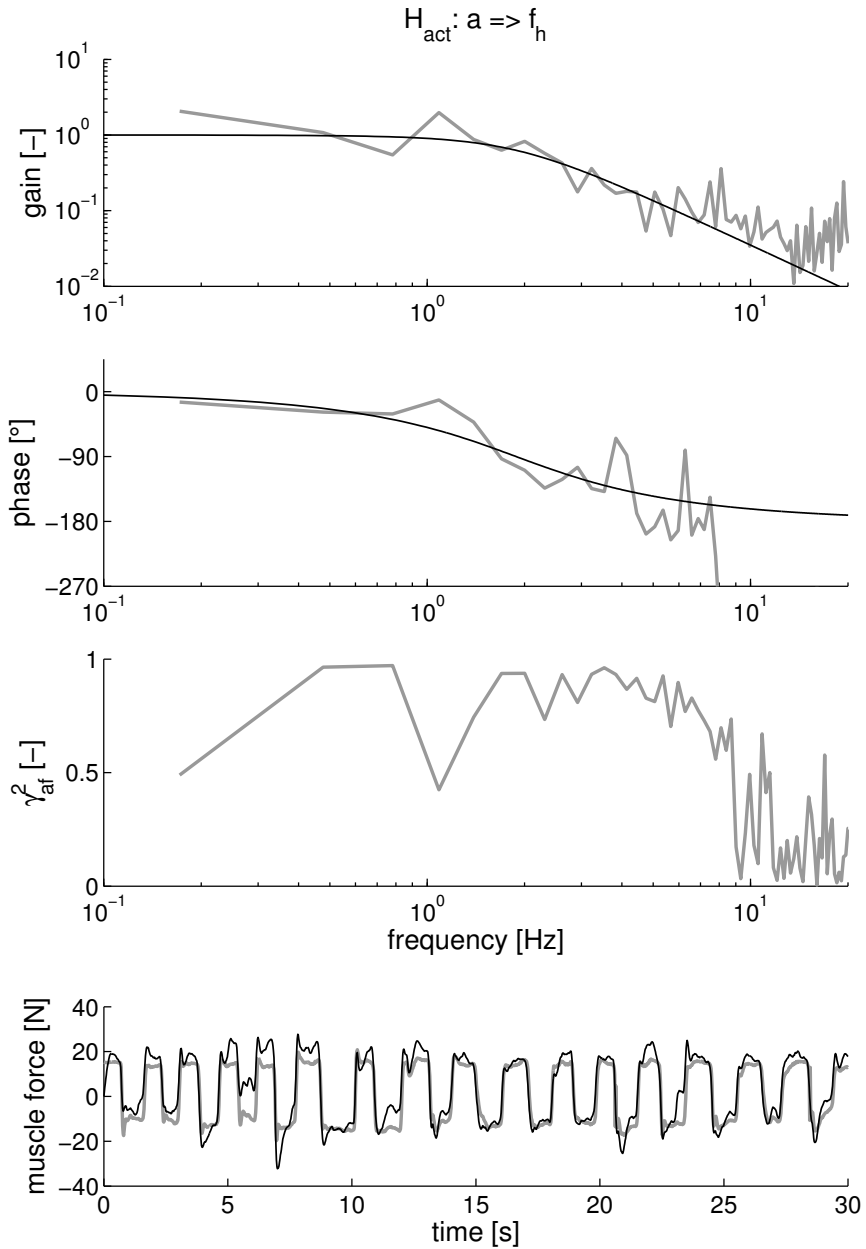


Figure 6.3: From top to bottom: gain and phase of the FRF of activation dynamics, coherence, and a 10 s fragment of the recorded hand force. Black lines: model/simulation; grey lines: estimation/measurement.

Table 6.2: *Estimated eigenfrequency, f_0 , and relative damping, β , of the activation dynamics for all subjects.*

subject	f_0 [Hz]	β [-]
1	1.88	0.80
2	2.58	0.77
3	2.03	0.74
4	2.00	0.74
5	2.37	0.64
mean (SD)	2.17 (0.29)	0.74 (0.06)

6.3 Results

6.3.1 Activation dynamics

Fig. 6.3 shows the estimated FRFs of the activation dynamics and the coherence for a typical trial of one subject. For this trial the coherence was relatively high up to 8 Hz, meaning that the estimate of the FRF is reliable up to this frequency. For frequencies beyond 8 Hz the coherence dropped, which likely resulted from low input power at these frequencies. Similar figures were found for other trials and subjects. Fig. 6.3 also shows the fitted model for the activation dynamics for this subject. The lower plot of Fig. 6.3 shows the time course of the measured and predicted hand force. The predicted force resembled the recorded force very well, only at the sharp transits, i.e. higher frequencies, the force slightly deviated from the measurements. However during the main experiment these higher frequencies were dominated by the arm mass and the mismatch will be of little concern.

In Table 6.2 the estimated parameters are given for all subjects. The average values over the subjects were 2.17 Hz for the eigenfrequency and 0.74 for the relative damping. These values were used for the estimation of the intrinsic and reflexive parameters.

6.3.2 Nonparametric FRFs

In Table 6.3 the average RMS of the hand position over the subjects is given. The RMS of the hand position was always approximately 3 mm, except for NB2 disturbances with centre frequencies higher than 5 Hz. These disturbances only contained power above the eigenfrequency of the arm, which is approximately 3 Hz. The admittance at these frequencies was primarily determined by the arm mass, which would require uncomfortably large forces to accelerate the arm. For this reason the amplitude of the force disturbance was reduced explaining the smaller amplitudes. The mean EMG varied slightly around one, indicating that the co-activation of the muscles was almost equal for all *stiff* conditions (Table 6.3).

Figs. 6.4 - 6.6 show the FRFs and coherences for one and the same subject during the damping, NB1, and NB2 conditions respectively. For all conditions the coherence of the handle position was higher than 0.95 for the frequencies within the

Table 6.3: RMS values of the handle position and muscle activity per conditions. Mean (SD) over all subjects.

condition		RMS [mm]	u_0 [-]
WB	reference	3.3 (0.4)	1 (-)
B50	50 Ns/m	3.1 (0.6)	1.02 (0.05)
B100	100 Ns/m	3.1 (0.4)	0.95 (0.05)
B150	150 Ns/m	3.2 (0.5)	0.96 (0.09)
B200	200 Ns/m	3.2 (0.5)	0.93 (0.10)
NB1	1.2 Hz	3.1 (0.8)	0.95 (0.11)
NB1	1.5 Hz	3.2 (0.8)	0.94 (0.11)
NB1	1.8 Hz	3.2 (0.7)	0.95 (0.12)
NB1	2.4 Hz	3.5 (0.9)	1.01 (0.11)
NB1	3.1 Hz	3.7 (0.6)	1.01 (0.09)
NB1	3.7 Hz	3.3 (0.6)	0.99 (0.12)
NB2	1.3 Hz	3.0 (0.5)	0.98 (0.12)
NB2	1.8 Hz	2.9 (0.7)	1.05 (0.11)
NB2	2.3 Hz	3.0 (0.8)	0.99 (0.10)
NB2	3.0 Hz	2.7 (0.5)	1.03 (0.13)
NB2	4.0 Hz	3.0 (0.7)	1.06 (0.16)
NB2	5.0 Hz	2.5 (0.4)	0.95 (0.11)
NB2	6.0 Hz	2.1 (0.4)	0.97 (0.16)
NB2	7.0 Hz	1.8 (0.3)	0.98 (0.16)

disturbance bandwidth. The coherence of the muscle activation was relatively high for the frequencies between 1 and 10 Hz. With external damping the admittance decreased at low frequencies compared to the reference condition (i.e. the arm became stiffer), and the peak at the eigenfrequency around 3 Hz increased. Note that the combined arm-environment system remained well damped due to the external damping. The gain of the reflexive impedance increased with damping (upper-right plot in Fig. 6.4). The phase of the reflexive impedance is primarily determined by velocity feedback (differential action introducing 90 degrees phase advance at all frequencies), position feedback (zero degrees for all frequencies) and a time delay (zero phase lag at 0 Hz and increasing lag with higher frequencies). With the reference condition (WB *stiff*) the phase advance at 0.5 Hz was approximately 70 degrees, indicating that at these frequencies velocity feedback was substantial. With the increase of the external damping the phase advance at 0.5 Hz decreased, indicating that position feedback was more pronounced.

For NB1 conditions the admittance decreased with decreasing disturbance bandwidth (see Fig. 6.5). A peak around the eigenfrequency could not be observed since the eigenfrequency was not excited by the NB1 disturbances. The reflexive impedance increased for smaller disturbance bandwidth and was almost 3 times larger for the smallest bandwidth compared to the reference condition.

For all NB2 conditions the gain of the admittance was lower compared to the reference condition (Fig. 6.6). However the reflexive impedance was increased for

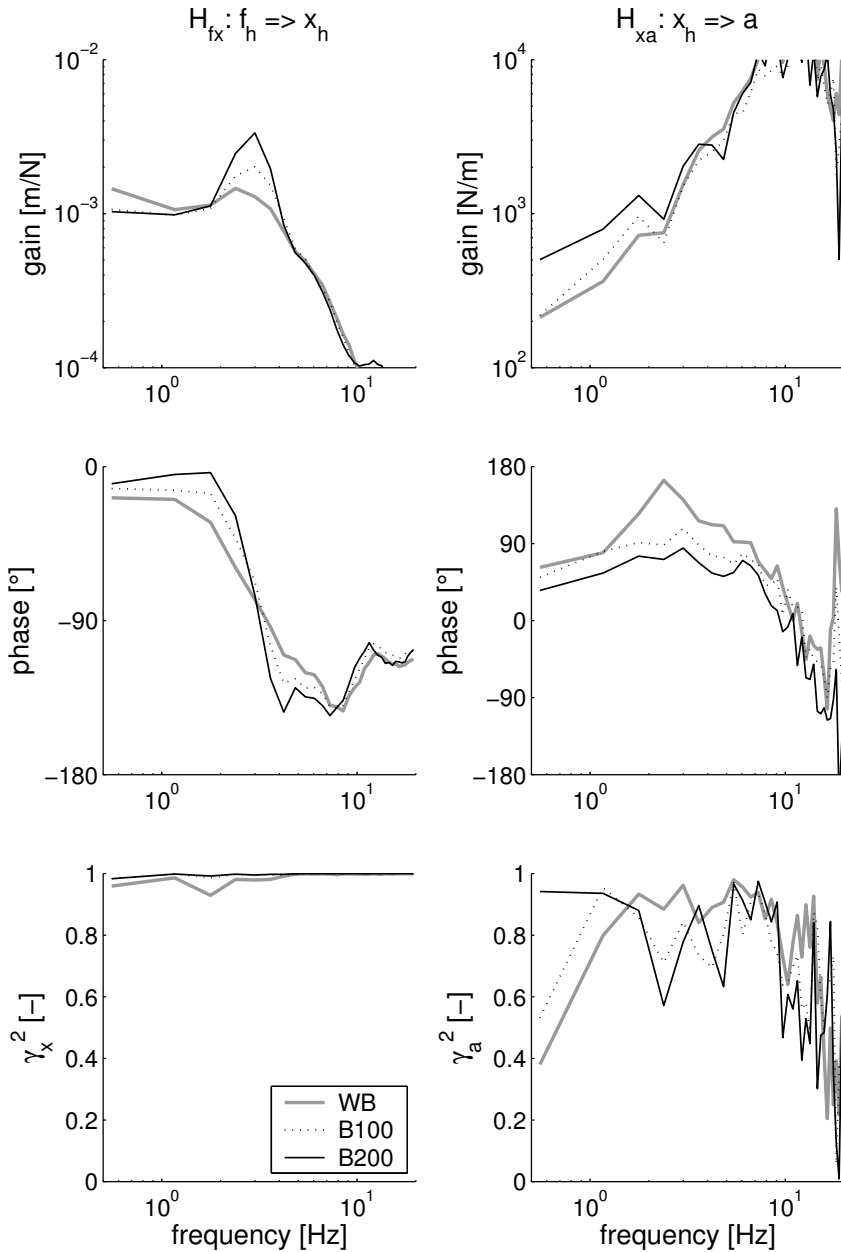


Figure 6.4: The FRFs of a typical subject for the mechanical admittance (left) and the reflexive impedance (right) together with corresponding coherences for WB disturbances with increasing damping. Upper row: gain; middle row: phase; bottom row: coherence. The grey line (WB) denotes the reference condition

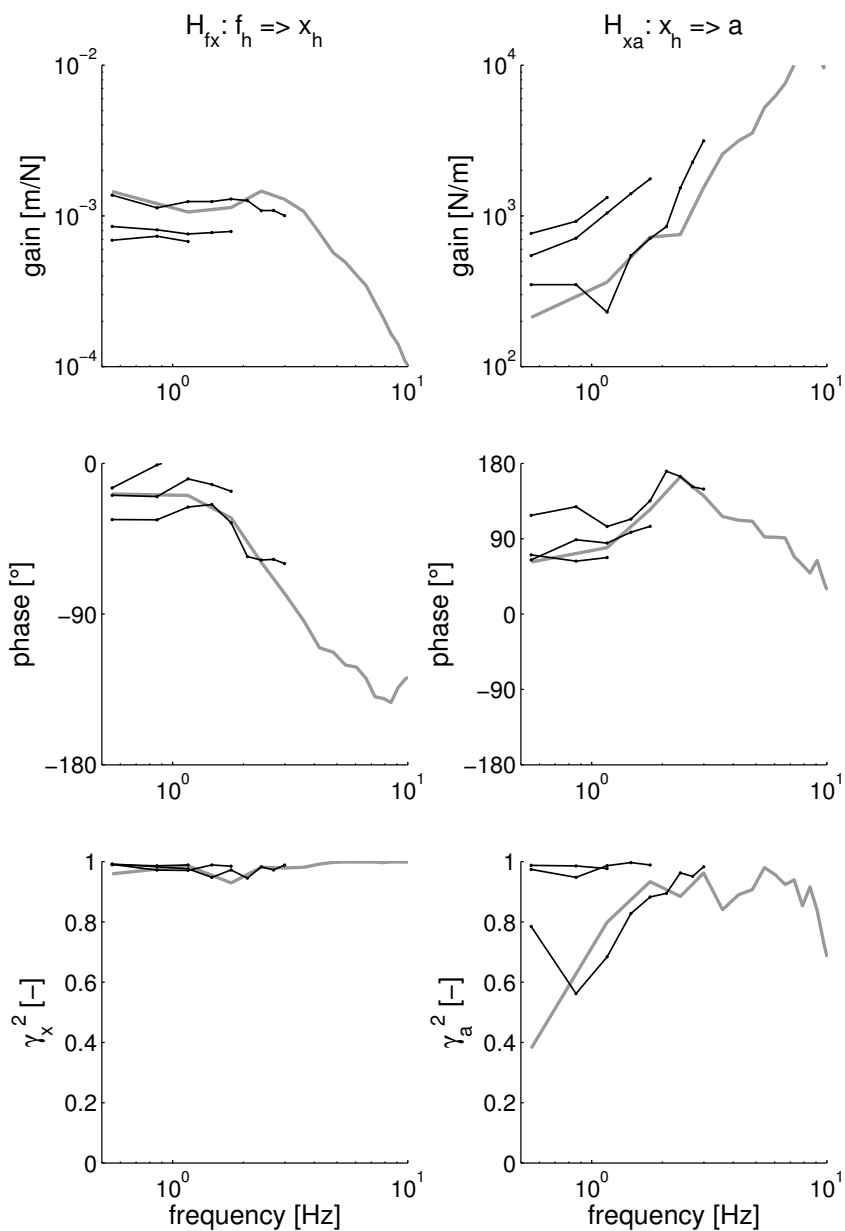


Figure 6.5: The FRFs of a typical subject for the mechanical admittance (left) and the reflexive impedance (right) together with corresponding coherences for NB1 disturbances. Upper row: gain; middle row: phase; bottom row: coherence. The grey line denotes the reference condition

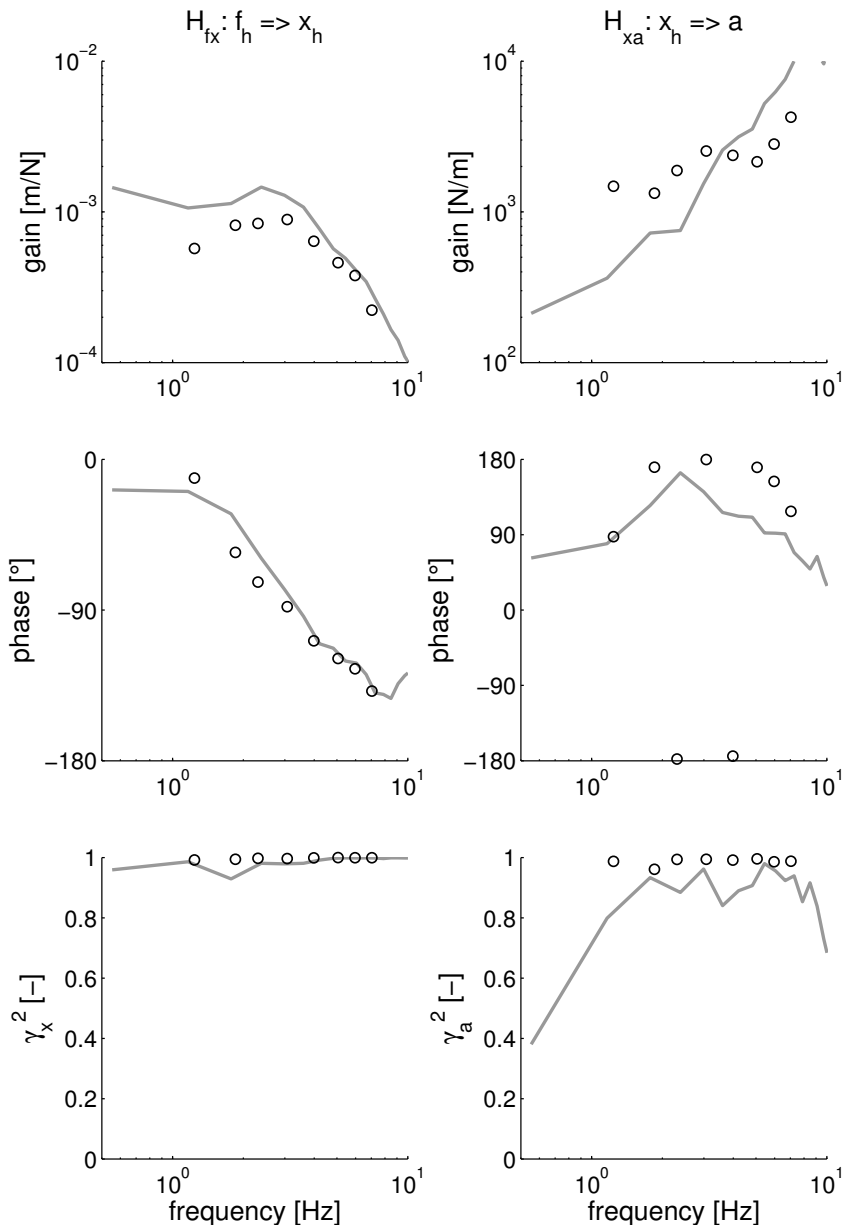


Figure 6.6: The FRFs of a typical subject for the mechanical admittance (left) and the reflexive impedance (right) together with corresponding coherences for NB2 disturbances. Upper row: gain; middle row: phase; bottom row: coherence. The power of the disturbances is concentrated in a small bandwidth around a centre frequency denoted with the circles. The grey line denotes the reference condition

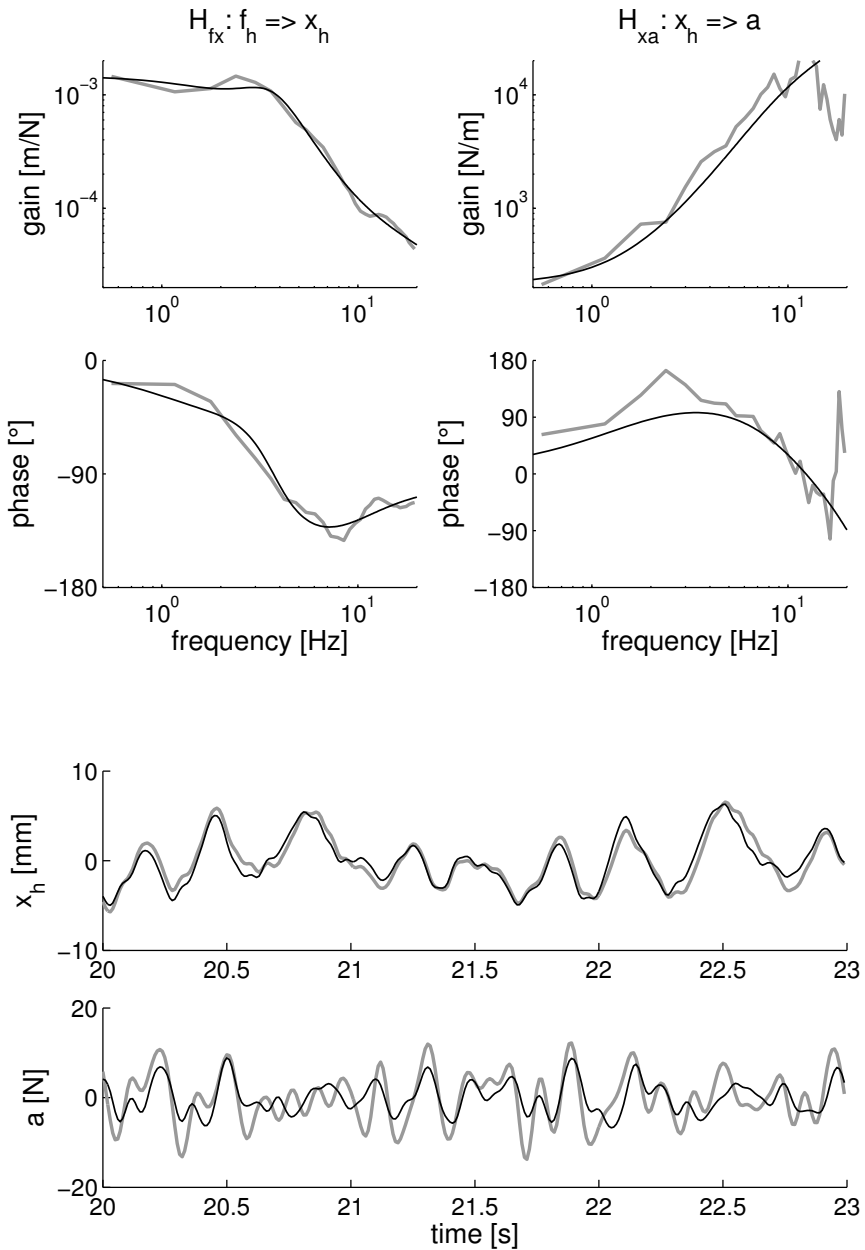


Figure 6.7: Top: FRFs of the admittance (left) and reflexive impedance (right) for reference condition for a typical subject. Grey lines: estimates; black lines: model fits. Bottom: a 3 s time fragment of handle position $x_h(t)$ and muscle activation $a(t)$. Grey lines: measurements; black lines: model simulations.

Table 6.4: *Estimated parameters for the reference condition and the condition with task slack. Mean (SD) over the subjects.*

	reference (WB stiff)	\longleftrightarrow	WB slack
m [kg]	2.02 (0.39)		2.02 (0.39)
b [Ns/m]	32.5 (10.1)		14.4 (4.2)
k [N/m]	382 (181)		169 (45)
b_g [Ns/m]	228 (94)		44 (32)
k_g [kN/m]	11.7 (6.0)		2.6 (1.9)
k_a [Ns ² /m]	2.3 (0.5)		zero
k_v [Ns/m]	37.4 (16.3)		zero
k_p [N/m]	91 (145)		zero
τ_d [ms]	28.4 (4.9)		-

centre frequencies up to 3 Hz, and smaller for higher centre frequencies. The phase lead of the reflexive impedance was larger compared to the reference condition at nearly all frequencies.

6.3.3 Intrinsic and reflexive parameters

In Fig. 6.7 the model fit is shown for a typical subject during the reference condition. In Table 6.4 the estimated parameters for the reference condition are given, together with the parameters for the condition with task *slack*. Fig. 6.8 shows the quantified parameters averaged over all subjects for all conditions together with the VAF values for position and muscle activation. The values for VAF_x (solid lines in Fig. 6.8) were generally high, i.e. higher than 90%. Only for the NB1 conditions with f_h smaller than 2 Hz the VAF_x was slightly smaller. The values for VAF_a varied around 50% for most conditions. Both the coherence and the VAF for the muscle activation were smaller than one, most likely due to the presence of noise in the EMG recordings. To severely reduce the noise in the signals all irrelevant frequencies, i.e. not excited by the force disturbance, were removed from the measured position and muscle activation. Noise reduction was performed by applying FFT, setting power to zero at all irrelevant frequencies, and then inverse transformation to time domain (by inverse FFT). The VAF values for these noise-reduced signals are indicated with grey lines in Fig. 6.8. The usage of the noise-reduced signals increased the VAF_a to values around 60% for the damping conditions and even to 90% for the NB2 conditions. The VAF_x increased to values above 90% for all conditions.

The acceleration feedback decreased with damping from around 2 Ns²/m for the reference condition to 1 Ns²/m for the highest external damping. As expected from the FRFs of the reference condition, the reflexive impedance was dominated by velocity feedback, which was approximately equal to the intrinsic damping. The position feedback gain increased with external damping, while velocity feedback remained almost constant. For the condition with the highest external damping the position feedback was in the same size as the intrinsic stiffness. This implicates that for this condition approximately 50% of the overall stiffness is of reflexive origin.

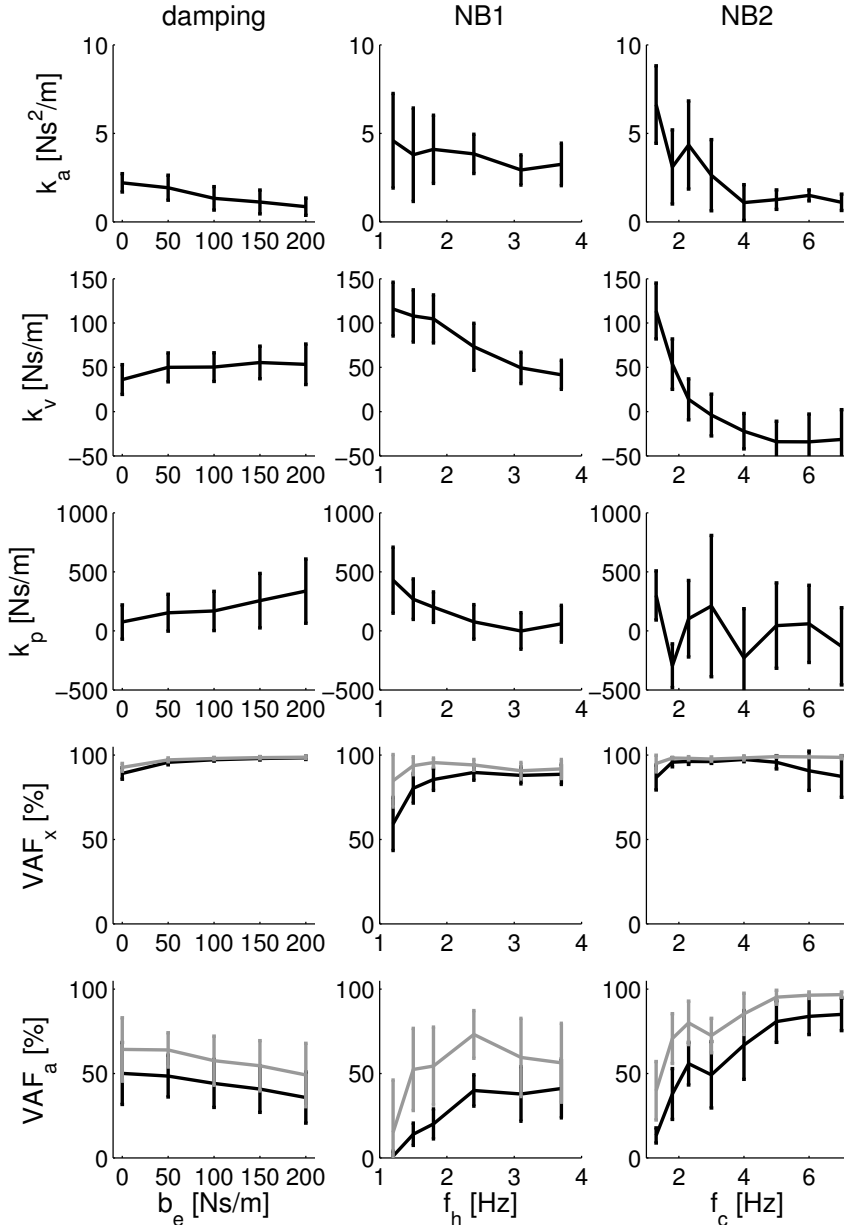


Figure 6.8: Estimated reflex gains (k_a , k_v , k_p) and corresponding VAF values (VAF_x , VAF_a). Shown are the means over the population; the error bars denote SD. Grey lines in the VAFs are the VAFs after noise reduction. Left column: external damping conditions; middle column: NB1 conditions; right column: NB2 conditions. Note that the damping condition with $b_e = 0$ Ns/m is the reference condition.

For the NB1 conditions both position and velocity feedback increased with decreasing bandwidth. For the largest bandwidth the reflex gains approached to the values corresponding to the reference condition. The mean values for the acceleration feedback gains did not show a clear trend with external damping. For the smallest bandwidth the SD was relatively high, most likely as acceleration feedback has minor effect on low frequencies.

For the NB2 conditions both the acceleration and velocity feedback increased with decreasing centre frequency. The SD of the position feedback is high and no trend is seen over the conditions. The high standard deviation indicates that the position feedback gain (1) can not be quantified accurately for these conditions and (2) has minor effect for these disturbances.

6.4 Discussion

6.4.1 Methodology

In this study a method is developed to quantify the (dynamic) properties of proprioceptive reflexes in vivo. This method is an important tool to evaluate the regulation of spinal reflexes during posture tasks. The use of force disturbances appeared natural to the subjects, facilitating the application of an unambiguous position task. Reflex gains were quantified by fitting linear models onto estimated input-output behaviour. Both the mechanical admittance and reflexive impedance were estimated on which a linear NMS model was fitted. The incorporation of the reflexive impedance into the quantification method is new and gives direct insight into the contribution of the underlying reflexive feedback system to the overall mechanical behaviour of the arm. The method has the advantage that intrinsic and reflexive parameters, including the neural time delay, can be estimated simultaneously.

The estimated coherences were high, justifying the usage of linear models. Below 1 Hz and above 10 Hz the coherence of the muscle activation was relatively low, which is likely the result of uncorrelated corrective muscle contractions to prevent drifting of the hand position and noise inherent to EMG. The estimated FRFs of the arm admittance showed that reflexes are effective in increasing the mechanical resistance to external force disturbances, as indicated by smaller mechanical admittance and higher reflexive impedance (Figs. 6.4 - 6.6). The quantified parameters resulted in accurate model predictions of both hand position and muscle activation, as proved by the high VAF values for almost all experimental conditions. The small intersubject variability of the estimated time delay indicates that this parameter is obtained with high accuracy. A mean value of ± 29 ms indicates that the identified reflexive feedback system is mediated via monosynaptic neural connections, i.e. short latency spinal pathways. Clear trends in the estimated reflex gains were seen which indicate that the reflex system adapts to the external conditions applied. This study shows that for some conditions half of the joint stiffness is of reflexive origin.

6.4.2 Functionality of reflexes

The findings of this study add to understanding of the functionality of proprioceptive reflexes. The feedback controller is the series conjunction of muscle activation dynamics, muscle spindle dynamics and a time delay. The effect of the feedback controller is explained graphically from the feedback model shown in Fig. 6.9, using two different estimated parameter sets corresponding to the reference condition (black lines) and to a NB1 ($f_h = 1.2$ Hz) condition (grey lines). The muscle spindles tend to increase the feedback gain with frequency (left column) while activation dynamics causes attenuation with increasing frequency (middle column). As a result, length and velocity feedback are most effective because these properties are manifest within the bandwidth of the activation dynamics (± 2 Hz). Beyond this bandwidth, high frequency gain from acceleration feedback (10^2 amplification per frequency decade) is cancelled due to the same amount of attenuation from the activation dynamics. Hence, the feedback system acts as a proportional-differential-proportional (PDP) controller in series with a time delay, as can be seen from Fig. 6.9 (right column). The effectiveness of the reflexive controller is strongly limited by substantial phase lag at higher frequencies due to the neural time delay. Attenuation of the gain at higher frequencies by the activation dynamics is therefore advantageous to facilitate position and velocity feedback, which are effective at low and intermediate frequencies. Without such an attenuation, position and velocity feedback gains would be severely limited to avoid unstable behaviour.

Besides stability as an ultimate bound, the feedback gains are determined by performance demands. High position and velocity feedback gains decrease the admittances at frequencies below the eigenfrequency of the arm (± 3 Hz), i.e. decrease the sensitivity to external force disturbance (De Vlugt et al., 2001; Schouten et al., 2001). However, due to the presence of phase lags from neural time delays and activation dynamics, high feedback gains also result in oscillatory behaviour around the eigenfrequency which worsens performance. In the case of the NB1 condition containing only low frequencies, the eigenfrequency is not excited and oscillations will not occur. Therefore large feedback gains are beneficial to the performance for NB1 conditions (Fig. 6.9, grey lines). Furthermore, external damping suppresses the oscillation of the arm such that large feedback gains are also beneficial for these conditions (see Fig. 6.4). Taken together, high feedback gains improve performance at low frequencies but tend to destabilize the arm around the eigenfrequency. Apparently, the central nervous system (CNS) modulates the feedback gains by trading off performance against stability. Future model optimisation studies could determine to what extent the quantified feedback gains found in this study are optimal.

6.4.3 Comparison with previous work

The experimental conditions applied in the present study were similar to those used in previous studies by our group (De Vlugt et al., 2002; Van der Helm et al., 2002). The main trends in the quantified position and velocity feedback gains are similar, albeit that in the previous studies the velocity feedback gains were under-

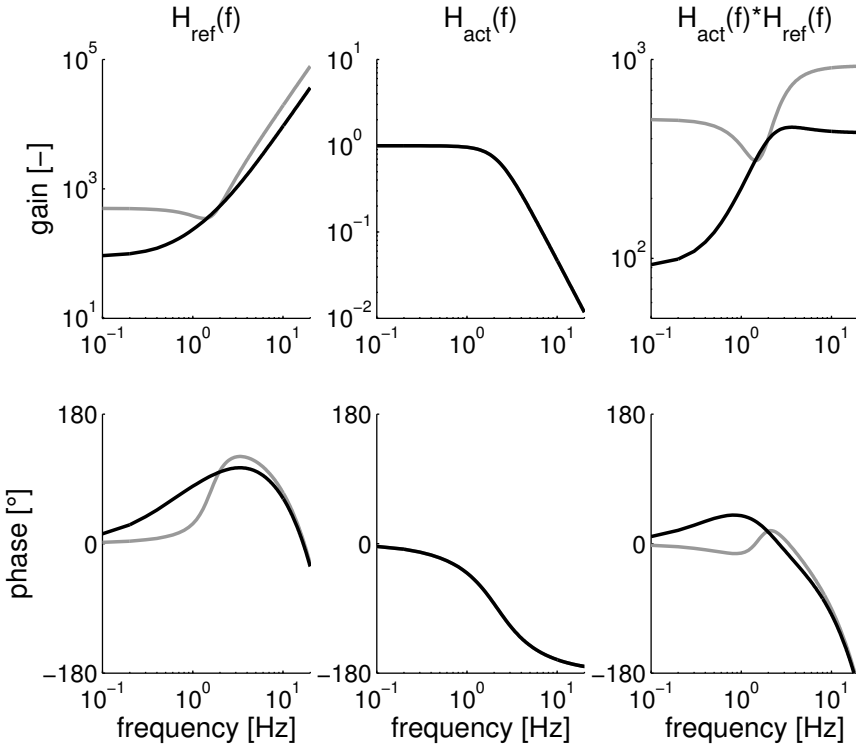


Figure 6.9: Gain (upper row) and phase (bottom row) of the reflexive feedback $H_{ref}(f)$ (left column), the activation dynamics $H_{act}(f)$ (middle column) and the combined feedback controller as the cascade of both models $H_{act}(f) \cdot H_{ref}(f)$ (right column). Parameter sets corresponding to the estimated values for the reference condition (black lines) and the NB1 ($f_h = 1.2$ Hz) condition (grey lines).

estimated. The explanation is twofold. The first is presence of reflexive feedback during the reference condition and the second is the smaller bandwidth of the muscle activation dynamics. In the previous studies the reflexive feedback could not be identified directly and therefore it was assumed that reflexes were negligible for wide bandwidth disturbances (reference condition) in order to separate the intrinsic and reflexive contributions. This study showed that velocity feedback was indeed present during the reference condition, hence velocity feedback was underestimated in the previous studies. In this study the activation dynamics were quantified, where in the previous studies a general model was adopted a-priori from literature, having a bandwidth of 5 Hz. This study proves that such a bandwidth is too high, and therefore the previously estimated velocity feedback gains were lower as a compensation.

In this study muscle activation dynamics was modelled as a second order sys-

tem. The quantified cut off frequency is 2.17 Hz and the relative damping is 0.75. These values are similar to those found in the literature. Potvin et al. (1996) found a rather wide range for trunk extensor muscles (2.0-3.3 Hz) while Bobet and Norman (1990) identified the elbow flexor and extensor muscles and found values of 1.9-2.8 Hz. Olney and Winter (1985) estimated values of 1.0-2.8 Hz for lower limb muscles during walking.

In this study, an acceleration feedback gain was included in the reflexive feedback to describe the reflexive impedance at higher frequencies. Kukreja et al. (2003) showed that linearisation of a unidirectional velocity sensitivity results in higher order terms including a pronounced acceleration term. In a recent study, the reflexive impedance was estimated from a nonlinear NMS model including unidirectional velocity sensitivity (Stienen et al., 2003, see Chapter 10). The gain and phase characteristics were comparable to those found in this study (Figs. 6.4 - 6.6) showing a clear second order (acceleration) response. This suggests that acceleration feedback is an artefact of muscle spindle unidirectionality rather than a distinct sensory function.

Chapter 7

Design of a torque-controlled wrist manipulator

Alfred C. Schouten, Erwin de Vlugt, J.J. (Bob) van Hilten,
Frans C.T. van der Helm
Submitted to *Applied Bionics and Biomechanics*

Torque disturbances are useful to analyse the functionality of proprioceptive reflexes. This paper describes the design of a torque controlled manipulator to identify the dynamics of the wrist joint during postural control. The device consists of an electromotor, a lever and a handle. A haptic controller is implemented to apply torque disturbances, such that the subject can actively control the wrist angle. To let the subject 'feel' the torque disturbance as good as possible the apparent, or virtual, dynamics of the device must be small. The minimal apparent inertia of the device is 1.6 gm^2 , which is in the same order of a normal wrist, the minimal damping and stiffness are negligible. To judge the performance of the manipulator, loads with known physical properties are attached and their parameters were quantified. The parameters of the loads were estimated with deviations of 5% at maximum. Finally the wrist dynamics of a human subject are quantified. The haptic controller has a bandwidth of 50 Hz, meaning that the apparent dynamics are realistically felt till 50 Hz. As the eigenfrequency of a (co)-contracted human wrist is approximately 15 Hz, a 50 Hz bandwidth of the haptic device is sufficient to measure all relevant dynamics of the human wrist.

7.1 Introduction

This paper describes the design of a high performance torque controlled manipulator to measure the admittance at the wrist joint. A recent study quantifying proprioceptive reflexes at the shoulder with force disturbances showed that the method of Van der Helm et al. (2002) is useful to get insight in the pathophysiology of CRPS (Schouten et al., 2003, see Chapter 3). The motoric features of neurological disorders like CRPS and Parkinson's disease however, mostly develop in distal joints and slowly progress proximal. To measure changes in reflex settings in the early stages of these disorders it is desirable to quantify reflexes around a distal joint like the wrist.

The joint admittance will be assessed by perturbing the subject's wrist with torque disturbances and measuring the angular deviations. To minimize the inertia apparent to the subject the manipulator needs to be light-weight. To further reduce the apparent dynamics a haptic controller is implemented, which replaces the real dynamics with a virtual, or external, environment. To analyse the performance of the haptic device, systems with known physical properties are attached to the manipulator and perturbed with use of continuous torque disturbances. To judge the performance of the manipulator, the parameters of the test loads are quantified by modelling the dynamic response. Finally the wrist dynamics of a human subject are quantified.

7.2 Materials and methods

7.2.1 Apparatus

Manipulator design

The manipulator is designed to apply flexion and extension torques to the wrist, resulting in an one degree-of-freedom (1-DOF) manipulator, see Fig. 7.1. The manipulator consists of an electromotor, a lever and, a handle. The torque applied by the subject is measured by a torque transducer mounted approximately halfway the lever. To prevent movement of the forearm the subject is supported by an arm support.

A brushless disc motor (Baumüller, DSM130N) is chosen to drive the manipulator. These disc motors are designed for very low cogging and the absence of brushes results in very low friction. The motor has a special winding design to generate high torques at low speed (8.0 Nm continuous, max. 500 rpm). High torques are required because the manipulator must be able to operate even when the subject maximally resists (*'maintain the deviations'* task). Because the motor can operate at low speeds there is no need for a gearbox, avoiding friction and tolerance. The motor is equipped with a SinCos encoder to measure the angle accurately (Stegmann SRS50). The current needed to drive the motor is supplied by a combined amplifier/control unit (Baumüller BUM60), which includes current feedback to improve motor performance.

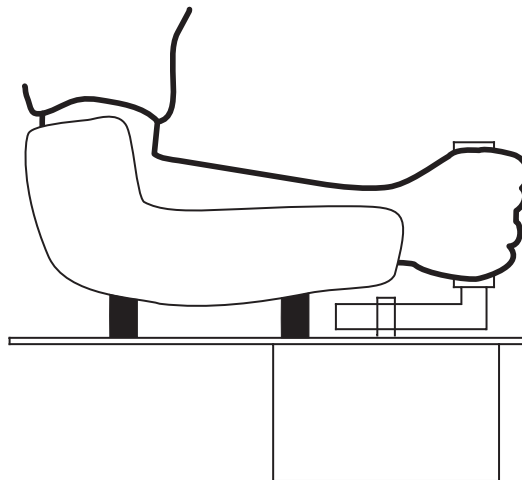


Figure 7.1: Schematic side view of the wrist manipulator. Subject holds the handle with the left or right hand, while the forearm is supported by the arm support. The subject can freely flex and extend the wrist, while the manipulator applies torque disturbances.

The lever, which transfers the torque from the motor to the handle, is attached directly to the shaft. The lever has a fixed length to align the wrist joint of an average size hand with the motor axis (axis to axis: 70 mm). To reduce weight the lever is made of a high strength aluminium alloy (7075T-6). The handle consists of two parts: a plastic grip and a core made of aluminium alloy (7075T-6). The grip has a length of 110 mm and a diameter of 32 mm giving a comfortable grip. To measure the torque exerted by the subject, the lever contains a custom-made torque transducer, consisting of strain gauges (HBM, XK13E-3/350) in a full bridge.

Manipulator control

The standard amplifier/control unit, which comes with the electromotor, is used as a velocity servo-controller, and operates at a sample frequency of 16 kHz. The velocity servo forms an inner loop within the haptic controller. The haptic controller is implemented using a digital signal processor (DSP) board (dSPACE, DS1104) within a normal PC and provides the reference velocity for the velocity servo. All relevant signals are sampled by the DSP with 16-bit resolution and 5 kHz sample frequency.

In order to apply torque disturbances, a haptic controller is used to control the manipulator. The haptic controller replaces the real manipulator dynamics with external dynamics, in this case, a (rotational) mass-spring-damper system, see Fig. 7.2. This means that to the subject the manipulator 'feels' like a mass-spring-damper system, i.e. the external environment (haptic is Greek for 'touch sense').

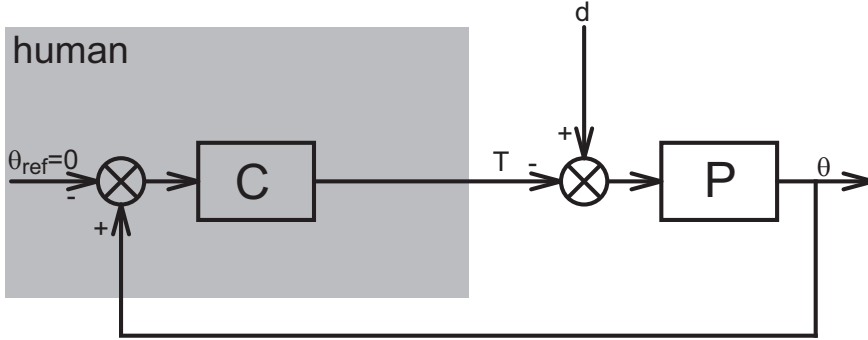


Figure 7.2: General scheme of a haptic controller. The haptic manipulator imposes a virtual, or external, environment P . Torque disturbance d together with the human (reaction) torque T inputs the external environment resulting in angle θ . As the objective of the human (grey box) during postural control is 'maintain position' the internal reference angle will be constant, or zero: $\theta_{ref} = 0$.

The desired equation of motion of the manipulator are described as follows:

$$I_e \ddot{\theta}_d(t) + b_e \dot{\theta}_d(t) + k_e \theta_d(t) = d(t) - T(t) \quad (7.1)$$

The desired (external) mass-spring-damper consist of the inertia I_e , the rotational damper b_e , and rotational spring k_e . $\theta_d(s)$ denotes the desired angle of the system; $\dot{\theta}_d(s)$ and $\ddot{\theta}_d(s)$ denote the desired angular velocity and acceleration respectively. The system is driven by the torques exerted to it: (1) the torque exerted by the subject $T(t)$ and (2) the additional disturbance torque $d(t)$, i.e. the torque disturbance. In the Laplace domain Eq. 7.1 can be rewritten to:

$$\theta_d(s) = \frac{1}{I_e s^2 + b_e s + k_e} (D(s) - T(s)) \quad (7.2)$$

in which s denotes the Laplace operator, with $s = \lambda + j2\pi f$. For the haptic controller Eq. 7.2 is rewritten to:

$$\dot{\theta}_d(s) = \frac{1}{I_e s + b_e} (D(s) - T(s) - k_e \theta(s)) \quad (7.3)$$

In this case $\dot{\theta}_d(s)$ is used as the reference angular velocity for the velocity servo-controller and the external stiffness is implemented by position feedback of the measured angle $\theta(s)$, see Fig. 7.3. Most haptic controller are implemented either as an impedance or admittance controller. Note that this controller is hybrid as, the inertia and damping are implemented via an admittance and the stiffness via an impedance.

In Fig. 7.3 the scheme of the haptic manipulator is given along. The velocity servo forms the core of the haptic manipulator. Note that in Fig. 7.3 this control

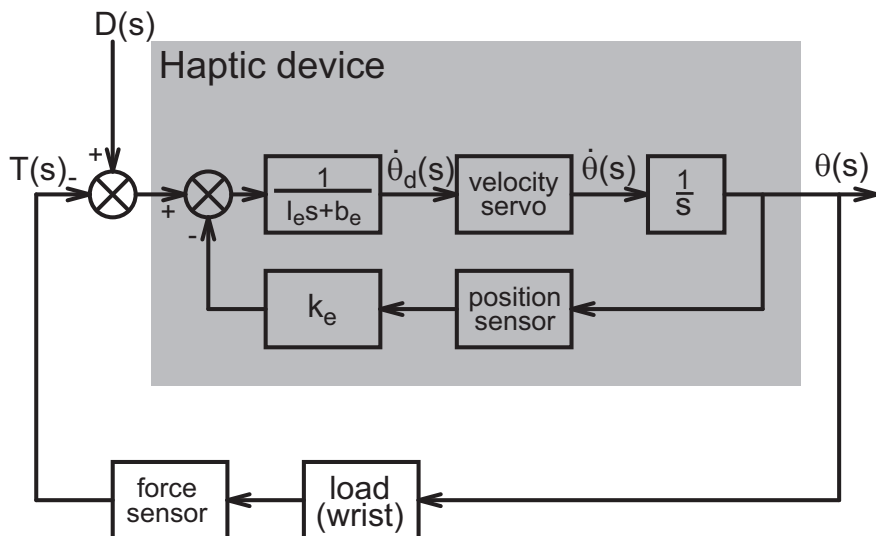


Figure 7.3: Scheme of the haptic controller used in this study. With a torque sensor the human reaction torque $T(s)$ is measured. This interaction torque together with torque disturbance $D(s)$ inputs the haptic manipulator. The haptic manipulator imposes an external inertia-spring-damper system (I_e , k_e , b_e) and controls angle $\theta(s)$.

loop is not drawn explicitly and the velocity servo is represented by one block. The velocity servo controller is implemented in the standard motor control unit as a PI-controller. The haptic controller itself is implemented in the DSP. Two torques act on the external environment, i.e. the (measured) human torque $T(s)$ and the torque disturbance $D(s)$. The (external) spring torque is subtracted from these torques and the reference velocity for the velocity servo is obtained by filtering this torque by the external inertia and damping (see Eq. 7.3 and Fig. 7.3). Since the torque transducer is implemented in the lever of the manipulator, the load of the manipulator (human wrist in Fig. 7.3) includes the inertia of the hand grip.

Safety consideration

The safety of the subjects is secured by several redundant measures taken both on a design and control level. The manipulator is designed to apply torques at the wrist and to measure the joint admittance during posture control. Because in posture control only small deviations around an equilibrium are concerned the range of motion of the lever is physically constrained with two blocks. The lever can only move plus and minus 15 degrees from its neutral position, which is much smaller than the range of motion of a human wrist.

In both the servo-controller and the DSP several safety measures are implemented. Firstly starting at 10 degrees deviation of the neutral position the damping instantaneously increases. This means that it is impossible to move the lever be-

yond 10 degrees at high speed. Secondly the DSP and the servo-controller continuously monitor the maximum speed, actuator torque, and torque in the lever. When one of the values is too high the motor automatically stops.

7.2.2 Procedures

First the servo-controller and haptic controller were tuned. Second the performance of the haptic manipulator was analysed and finally the wrist dynamics of a human subject were quantified. In this study two signals were used as a torque disturbance. The first signal contained power uniformly distributed between 1 and 500 Hz, and was used to analyse the performance of the velocity servo-controller and to tune the haptic controller. The second signal had power uniformly distributed between 1 and 50 Hz, and was used to test the performance of the haptic manipulator and to identify the admittance of the human wrist joint.

The signals used as torque disturbances were 10 s in length and consisted out of a sum of sines, the so-called multisine signals (Pintelon and Schoukens, 2001). The use of multisines in comparison with stochastic signals had several advantages for the nonparametric analysis. The main advantages of using deterministic multisines were that the variance of the nonparametric estimators was substantially reduced and free of bias (Pintelon and Schoukens, 2001; De Vlugt et al., 2003a). Because the variance of the estimators was relatively low, relatively short observation times (10 s) were possible.

Controller settings

The bandwidth of the haptic manipulator is mainly determined by the bandwidth of the velocity servo (assuming that both the velocity and torque sensor have a substantially larger bandwidth). Note that the dynamic behaviour of a velocity servo also depends on the payload, in this case the subject (payload is not drawn in Fig. 7.3). The most demanding situation is when a subject firmly holds the handle and maximally cocontracts. The controller was adjusted such that the controller had a bandwidth of 50 Hz, when a subject holds the handle with maximally voluntary cocontraction. This bandwidth of 50 Hz is approximately 3 times larger than the eigenfrequency of a human wrist.

After the velocity controller was tuned the haptic controller was adjusted. The haptic manipulator is designed to apply torque disturbances to the wrist over a wide bandwidth. As the external, or apparent, environment 'filters' the torque disturbance, it is desirable to have small external parameters. The external stiffness and damping can be set to negligibly small values, where the external inertia can never be set to zero (the gain of the external filter in Fig. 7.3 would go to infinity). If the inertia is set too low a phenomenon called contact instability occurs (Colgate, 1988; Carigan and Cleary, 2000; De Vlugt et al., 2003b). As an ultimate bound the haptic manipulator must remain stable in all cases, with and without a subject holding the handle. The stability of the haptic controller can be determined by

Table 7.1: *Applied loads to test the performance of the haptic manipulator.*

case	load	description
1	no load	0.7 gm ² (handle inertia)
2	inertia	2.8 gm ² (exclusive handle)
3	springs	2.94 Nm/rad
4	inertia with springs	combination of 2 and 3
5	subject	

calculating the loop gain ($k_e = 0$ Nm/rad, $b_e = 0$ Nms/rad):

$$H_{loop}(s) = P(s)C(s) = \frac{1}{I_e s^2} H_{servo}(s) H_{load}^{-1}(s) \quad (7.4)$$

in which $H_{servo}(f)$ is the frequency response function (FRF) of the velocity servo controller and $H_{load}^{-1}(f)$ the impedance of the load at the handle (normally a subject's wrist). The stability and stability margins are determined by plotting the loop gain in a Nyquist diagram and check the smallest M-circle (Maciejowski, 1989). If the loop gain encircles (-1,0) the system will not be stable in closed loop. The smallest M-circle denotes the stability margin and performance of the closed loop system. In this study $M = 2$ is chosen as smallest M-circle for the haptic controller. Larger values of M result in too small stability margins and smaller values of M (i.e. wider stability margins) would restrict the performance (i.e. bandwidth) of the haptic manipulator too much.

The FRFs of the velocity servo and the load were obtained by perturbing with the 500 Hz bandwidth signal, while the external environment was set to a safe setting, i.e. $I_e = 3$ gm², $b_e = 0.13$ Nms/rad, and $k_e = 3$ Nm/rad. These settings resemble a critically damped system with 5 Hz bandwidth. The FRFs were assessed for three situations: no load, an inertia (≈ 2.8 gm²), and a subject. With the aid of a Nyquist diagram the minimal external inertia was calculated, such that the system had the predetermined stability margin.

Estimation performance

The haptic manipulator will be used to measure the admittance of the human wrist. To evaluate the haptic manipulator, haptic control algorithm and sensors, several systems with known dynamics were measured and their FRFs estimated. The FRFs were parametrized by fitting an inertia-spring-damper model on to the FRFs with a least squares criterion. Because the gain of the FRFs show large variations over the frequencies the criterion uses the logarithm of the FRFs (Pintelon et al., 1994).

The estimated parameters were compared with the real values. The tested physical systems are summarized in Table 7.1. Additionally a real subject was measured. Normally the external dynamics were set to the minimal values. However when the load had no stiffness (cases 1 & 2), a small external stiffness was set to prevent

drifting (1 Nm/rad) and when the load had no damping (cases 1-4), a small external damping was set to prevent oscillation (0.1 Nms/rad). The FRFs were identified by perturbing with the 50 Hz bandwidth torque disturbance, which is sufficient to observe all relevant dynamics.

7.2.3 Data processing

During a trail force disturbance $d(t)$, motor angle $\theta(t)$, interaction force $T(t)$, and desired angular velocity $\dot{\theta}_d(t)$ were recorded with 2500 Hz sample frequency and a 16 bits resolution. By using only the last 2^{14} samples (≈ 6.55 s) of each record for analysis, initial transient effects were removed.

With a haptic manipulator interaction exists between the haptic manipulator and the subject (Fig. 7.2). Because of this interaction closed loop identification algorithms were needed to estimate the dynamics imposed by the haptic manipulator and the load of the haptic manipulator, i.e. the human wrist, separately (De Vlugt et al., 2003a). First the time records ($d(t)$, $T(t)$, $\theta(t)$, $\dot{\theta}_d(t)$) were transformed to the frequency domain ($D(f)$, $T(f)$, $\theta(f)$, $\dot{\theta}_d(f)$) via the fast Fourier transform (FFT) and used to estimate the power and cross spectral densities:

$$\hat{G}_{dT}(f) = D(-f)T(f) = D^*(f)T(f) \quad (7.5)$$

$$\hat{G}_{d\theta}(f) = D(-f)\theta(f) = D^*(f)\theta(f) \quad (7.6)$$

$$\hat{G}_{d\dot{\theta}_d}(f) = D(-f)\dot{\theta}_d(f) = D^*(f)\dot{\theta}_d(f) \quad (7.7)$$

$$\hat{G}_{dz}(f) = D(-f)Z(f) = D^*(f)Z(f) \quad (7.8)$$

$$\hat{G}_{dd}(f) = D(-f)D(f) = D^*(f)D(f) = |D(f)|^2 \quad (7.9)$$

$$\hat{G}_{\theta\theta}(f) = \theta(-f)\theta(f) = \theta^*(f)\theta(f) = |\theta(f)|^2 \quad (7.10)$$

in which \hat{G} denotes the estimated spectral densities (hat denotes estimate), the asterisk the complex conjugate, and $Z(f)$ is the input of the haptic manipulator ($Z = D - T$). The spectral densities are averaged over 4 frequency bands to reduce the variance of the estimators (Jenkins and Watts, 1968).

The FRFs for the servo-controller, the load (human wrist), and manipulator were estimated by dividing the appropriate spectral densities (De Vlugt et al., 2003a):

$$\hat{H}_{servo}(f) = \frac{\dot{\theta}(f)}{\dot{\theta}_d(f)} = \frac{\theta(f)s}{\dot{\theta}_d(f)} = \frac{\theta(f)j2\pi f}{\dot{\theta}_d(f)} = \frac{\hat{G}_{d\theta}(f)j2\pi f}{\hat{G}_{d\dot{\theta}_d}(f)} \quad (7.11)$$

$$\hat{H}_e(f) = \frac{\theta(f)}{Z(f)} = \frac{\hat{G}_{d\theta}(f)}{\hat{G}_{dz}(f)} (\equiv P) \quad (7.12)$$

$$\hat{H}_{load}(f) = \frac{\theta(f)}{T(f)} = \frac{\hat{G}_{d\theta}(f)}{\hat{G}_{dT}(f)} (\equiv C^{-1}) \quad (7.13)$$

Here $\hat{H}_{servo}(f)$ is the estimated FRF of the servo controller, $\hat{H}_e(f)$ the FRF of the external environment imposed by the haptic manipulator (P in Fig. 7.2) and $\hat{H}_{load}(f)$

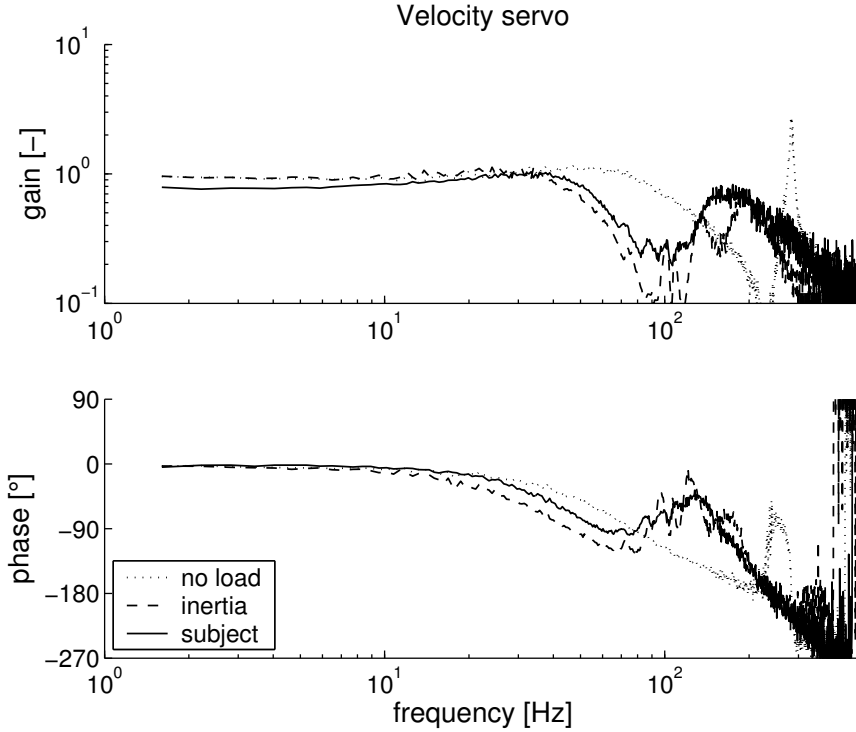


Figure 7.4: FRFs of the velocity servo controller $\hat{H}_{servo}(f)$; dotted line: no load; solid line: with subject; dashed line: with inertia.

is the FRF of the wrist, i.e. the load for the haptic manipulator (inverse of C in Fig. 7.2). In addition to the FRFs the coherence is estimated:

$$\hat{\gamma}^2(f) = \frac{|\hat{G}_{d\theta}(f)|^2}{\hat{G}_{dd}(f)\hat{G}_{\theta\theta}(f)} \quad (7.14)$$

The coherence $\hat{\gamma}^2(f)$ is a measure for the linearity and signal to noise ratio. By definition the coherence varies between 0 and 1. A value of 1 means that at that specific frequency the relationship between input and output is linear and not deteriorated by noise.

To judge the performance of the device systems with known parameters were tested. The parameters of these systems were quantified by fitting inertia-spring-damper models onto the measured FRFs of the load $\hat{H}_{load}(f)$.

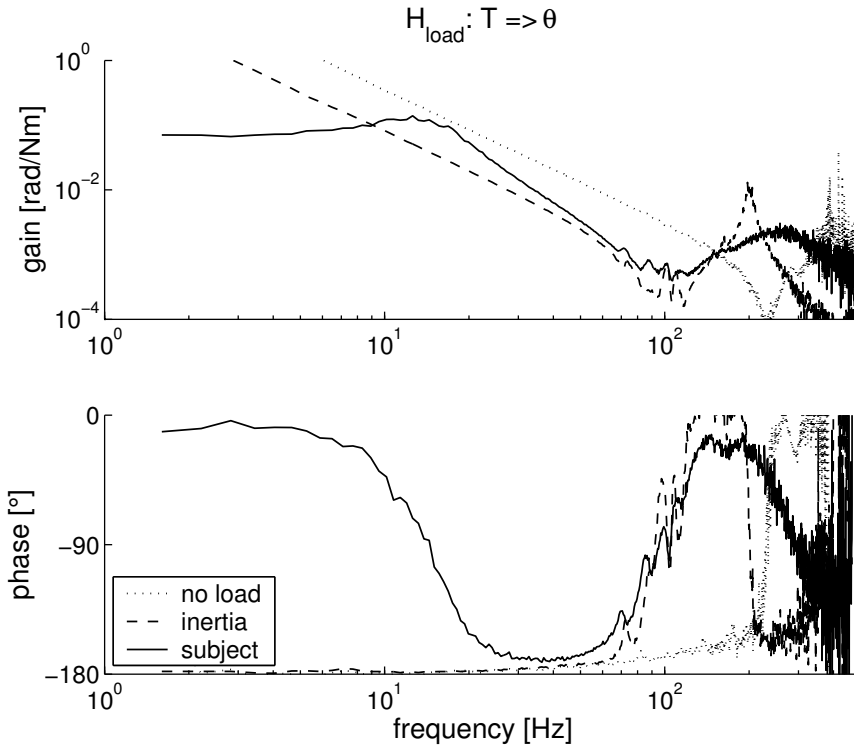


Figure 7.5: FRFs of the loads $\hat{H}_{load}(f)$; dotted line: no load; solid line: with subject; dashed line: with inertia.

7.3 Results

7.3.1 Controller settings

Three loads were tested to analyse the velocity servo: no load (i.e. handle only), an inertia and a subject (Fig. 7.4). In the first two cases (no load and an inertia) distinct troughs and peaks were present in the frequency range from 50 to 300 Hz. This behaviour is typical for mass-spring-mass systems as formed by the handle mass and rotor inertia with the torque transducer in between, which has a limited stiffness (to measure force/torque with straingauges the material stiffness must be locally reduced to allow strain). Especially the peaks are undesirable because the gain of velocity servo is large at this frequency and can result in undesired oscillatory behaviour. A subject however, will always introduce damping, and as a result the troughs and peaks will be flattened. The velocity servo remained stable for all three loads and the bandwidth of the velocity servo with a subject holding the handle and maximally cocontracting is approximately 50 Hz.

Fig. 7.5 shows the loads as measured at the handle with the 500 Hz disturbance.

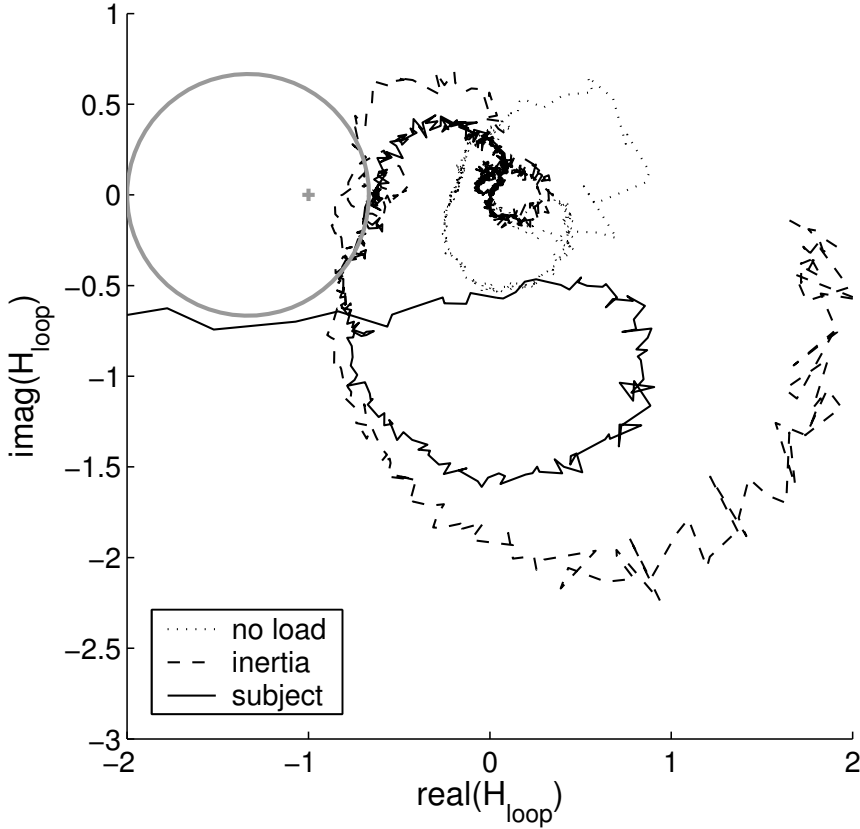


Figure 7.6: Nyquist diagram for the loop gain, $\hat{H}_{loop}(f)$, the circle denotes the $M = 2$ circle; dotted line: no load; solid line: with subject; dashed line: with inertia.

It can be seen that till approximately 70 Hz the measurements were reliable. For higher frequencies, as a result of the reduced stiffness in the torque transducer, the measurements do not fully represent the load.

With the FRFs of the servo (Fig. 7.3) and the loads (Fig. 7.5) the minimal external inertia of the haptic controller can be obtained using Eq. 7.4. For all three loads the Nyquist diagram is constructed with $I_e = 1.6 \text{ gm}^2$, see Fig. 7.6. None of the lines encircle point (-1,0) meaning that $I_e = 1.6 \text{ gm}^2$ results in a stable haptic controller for all three loads. With $I_e = 1.6 \text{ gm}^2$ and a subject the Nyquist diagram ‘touches’ the $M = 2$ circle, indicating that the prescribed stability margin is met.

7.3.2 Estimation performance

The estimated FRFs and coherences of the test loads are given in Fig. 7.7. It can be seen that the coherences for the applied bandwidth are high for all test loads

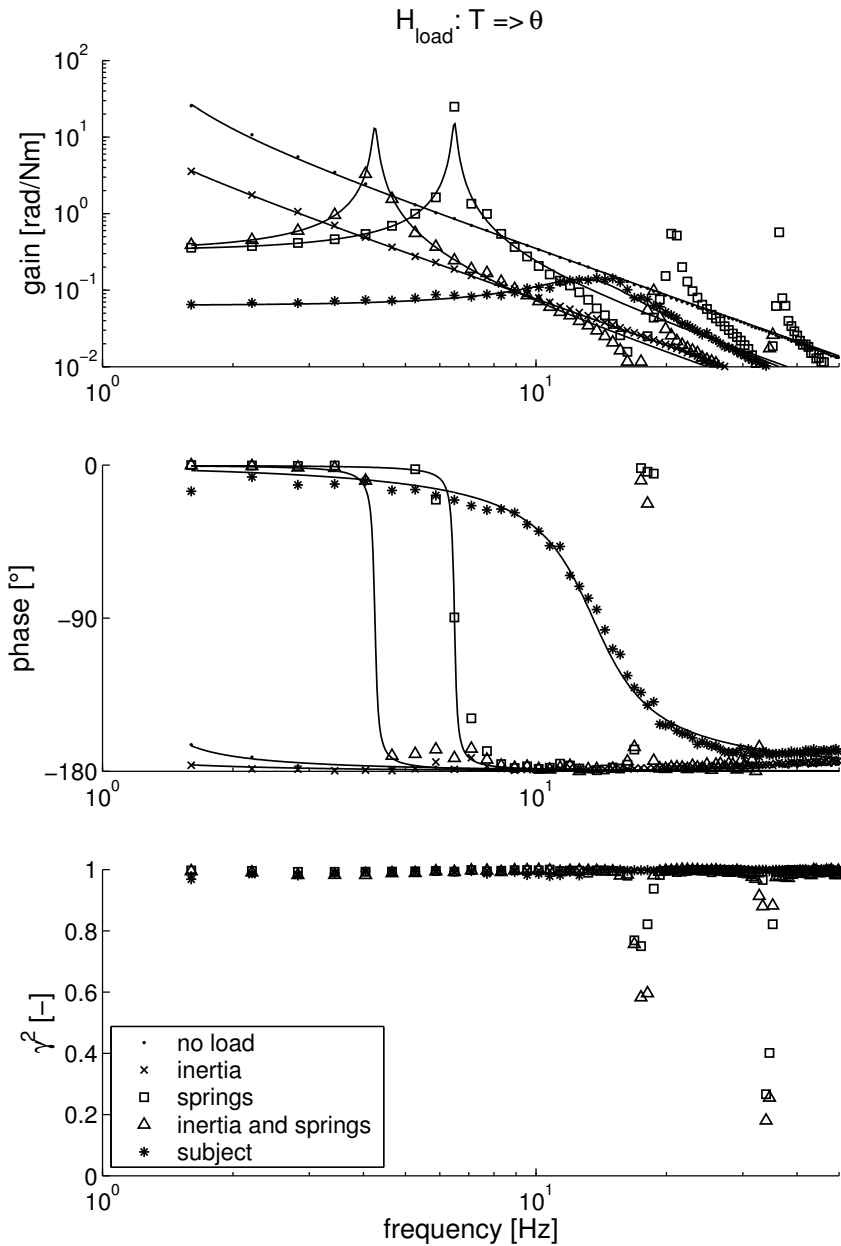


Figure 7.7: Estimated FRFs of the loads ($\hat{H}_{load}(f)$) and coherences ($\hat{\gamma}^2(f)$) given in Table 7.1, the estimated FRFs are denoted with symbols and the solid lines denote the fitted models; dots: no load; crosses: with inertia; squares: springs; triangles: springs and inertia; stars: subject.

Table 7.2: Values of the applied and estimated loads.

case	load			estimated parameters		
	I [gm ²]	b [Nms/rad]	k [Nm/rad]	I [gm ²]	b [Nms/rad]	k [Nm/rad]
1	0.7	-	-	0.73	0.0009	0.04
2	3.5	-	-	3.31	0.0018	0.06
3	0.75*	-	2.94	1.81	0.0016	3.00
4	3.62*	-	2.94	4.23	0.0028	3.02
5		subject		2.18	0.0862	15.75

* exclusive inertia of the springs

($\hat{\gamma}^2(f) > 0.95$, except for the frequencies where sharp troughs and peaks appear), meaning that the estimated FRF is reliable and the relationship between input and output is linear.

The FRFs of Fig. 7.7 were parametrized by fitting a second order model to the FRFs; the real and estimated parameters are summarized in Table 7.2. In case 3 and 4 sharp troughs and peaks appear, these resulted from vibrations in the springs, a phenomena occurring with technical springs never being ideal, e.g. having zero mass. In case 1 and 2 (no load and an inertia) only inertia is present, the inertias are estimated with an accuracy of 5%. The inertia estimated in cases 3 and 4 includes inertia, resulting from the finite mass of the springs. Because it is unclear how much mass of the springs attributes to the inertia no comparison in inertia can be made, the stiffness in this cases is estimated with 3% accuracy.

Finally in case 5 a real subject is measured. The task given to the subject to '*minimize the deviations*', resulting in high voluntary cocontraction. The estimated subject inertia given in Table 7.2 includes the handle inertia (see case 1), correction for this inertia results in a subject inertia of 1.45 gm². The eigenfrequency of this subject is 16.6 Hz (uncorrected 13.5 Hz) and the relative damping is 0.29 (uncorrected 0.23).

7.4 Discussion

In this paper the design of a torque controlled wrist manipulator is presented. With this manipulator torque disturbances can be applied by means of a haptic controller. With the haptic controller the parameters of the external environment, as felt by the subject, are adjustable and the influence of external environments on the proprioceptive reflexes can be investigated. The bandwidth of the haptic manipulator is approximately 50 Hz, which is at least 3 times larger than the eigenfrequency of the human wrist. Meaning that the haptic manipulator can mimic the external environment in a, to the human, realistic manner.

The minimal external inertia which the haptic manipulator safely can mimic is 1.60 gm². Because the torque transducer is located in the lever the handle inertia can not be compensated for, and consequently the handle inertia (0.73 gm²) add to the external inertia. The, to the subject, apparent inertia (2.33 gm²) is 14% smaller

than the real inertia of the haptic manipulator ($\approx 2.7 \text{ gm}^2$; motor only: 1.8 gm^2). The minimal external inertia is in the same order found for a normal fist human hand.

The performance of the haptic manipulator is tested by application of loads with known parameters and fitting a second order model to the measured FRFs. The manipulator was able to quantify the loads with deviations of 5% at maximum. Finally a subject was measured. The subject was instructed to '*minimize the deviations*' of the handle, an unambiguous task, resulting in high cocontraction. The wrist stiffness and damping (15.75 Nm/rad ; 0.0862 Nms/rad) are comparable to values found in Milner and Cloutier (1993) during high effort tasks.

Almost all manipulators built to identify joint dynamics are position controlled, meaning that the position, or joint angle, is imposed. In that case the subject has no influence on the position and has to maintain a constant force/torque, or EMG level (Kearney et al., 1997; Mirbagheri et al., 2000; Zhang and Rymer, 1997; Cathers et al., 1999). Only a few manipulators are force/torque controlled and consequently require a position task (Ruitenbeek and Janssen, 1984; Van der Helm et al., 2002; De Vlugt et al., 2003b). For technical systems there is no difference between identification with position or torque disturbances. However humans are highly adaptable, e.g. Doemges and Rack (1992a,b) showed that the proprioceptive reflexes at the wrist are substantially larger with force disturbances. Note that torque disturbances form a natural form of input and mimic most real life situations: the subject can actively control the position and must preserve stability in the presence of external disturbances.

Previous research on the shoulder joint have shown that force disturbances are relevant and useful to quantify proprioceptive reflexes in both healthy subjects (De Vlugt et al., 2002; Van der Helm et al., 2002) and patients with neurological disorders (Schouten et al., 2003). In future studies the high performance wrist manipulator described in this paper will be used to analyse the wrist admittance during posture tasks and to quantify the proprioceptive reflexes at the wrist joint. Because the motoric features in neurological disorders generally develop at the distal joints, it is expected that differences can be quantified earlier after disease onset and with a greater accuracy.

Chapter 8

Quantifying proprioceptive reflexes at the wrist

Alfred C. Schouten, Bastiaan C.P. Zwaan

The aim of this study is to quantify proprioceptive reflexes at the human wrist joint during postural control. From previous studies investigating reflexes at the shoulder it is known that the magnitude of proprioceptive reflexes depends on the bandwidth of the torque disturbance and on the damping and inertia of the external environment. This study investigates if the same phenomena can be observed at the wrist. The subjects were given a position task ('minimize the displacement'), while torque disturbances were applied. The high coherences indicate that for the given conditions the human wrist acts as a linear system. Reflex gains for acceleration, velocity and position along with intrinsic (muscle) properties were quantified by fitting a linear model on the estimated frequency response functions (FRFs) for the joint admittance and the reflexive impedance. High values for the variance accounted for (VAF) indicate that the model adequately predicts the observed behaviour. Especially velocity feedback varied substantially with the bandwidth of the disturbance and with the external damping. Generally spoken, smaller bandwidth and a more damped environment provoked larger reflexes. The results suggest that, given the condition, humans modulate the magnitude of the proprioceptive reflexes to maximally resist the torque disturbances.

8.1 Introduction

The aim of this study is to quantify proprioceptive reflexes at the human wrist during postural control in healthy subjects and to investigate if the magnitude of wrist reflexes depend on the frequency content of the (torque) perturbation and the (external) inertia and damping. A powerful manipulator is used to generate continuous random torque perturbations and to impose the external environment (Schouten et al., 2004c, see Chapter 7). The subjects were given a position task (*'minimize deviations'*), while continuous random torque disturbances were applied for 10 s. Joint admittance and reflexive impedance were estimated using system identification in the frequency domain. Finally intrinsic and reflexive parameters were quantified by fitting a model on the joint admittance and the reflexive impedance simultaneously.

8.2 Materials and methods

8.2.1 Subjects

Two groups of patients participated in the experiment. In the main experiment ten normal healthy subjects (1 woman) with a mean (standard deviation, SD) age of 25.3 (1.9) years. All subjects were right handed. In the second experiment to estimate the muscle activation dynamics, four subjects (1 woman) participated with a mean (SD) age of 28.3 (5.6) years (2 subjects were left handed). The experiments were carried out on the right wrist. All subjects gave informed consent prior to the procedure.

8.2.2 Apparatus

Torque disturbances were applied at the wrist by means of a manipulator. The manipulator is extensively described in Chapter 7 and is introduced briefly. Subjects were seated in a chair and had to hold a handle with the right hand, while the forearm was supported by an arm support. The handle is connected, via a lever, to a motor. The lever has a fixed length to align the wrist joint of an average size hand with the motor axis. The subject could move the handle resulting in flexion and extension of the wrist. To the subject the manipulator behaved like a rotational inertia-spring-damper system. The parameters of this external environment are fully adjustable, except that the external inertia has a minimum ($I_e \geq 1.6 \text{ gm}^2$). In this study the external inertia and damping (b_e) were altered and no value for the spring was set ($k_e = 0 \text{ Nm/rad}$).

8.2.3 Procedures

Main experiment

The main experiment consists of 26 different conditions, lasting 10 s each. The conditions were presented in randomized order to prevent anticipation and were re-

peated 4 times, giving a total of 104 trials. During a trial the subject was instructed to 'minimize the displacement' of the handle, while continuous random torque disturbances were applied. To assist the subject and to prevent drift the actual angle was shown on a display. The trials consisted of disturbances with a variable frequency content and disturbances in combination with variable external environment. The magnitude of the torque disturbances was adjusted for each condition to limit the maximum amplitude of the displacement to approximately 1 degree, facilitating linear model approximations. As the trials required high effort of the subjects, sufficient time was given between trials to prevent fatigue. The complete experiment for one subject, including instruction and pauses, lasted approximately one and a half hours.

In the experimental conditions both the frequency content of the torque disturbance ($n = 17$) and the external environment ($n = 8$) were varied from a reference condition. Random continuous torque disturbances were applied with clustered power spectra and random phase (Schouten et al., 2004a,b, see Chapters 5-6). The reference condition is:

- Wide bandwidth disturbance (WB): a disturbance signal consisting of 20 clusters of 4 sines each, linearly spaced between lowest frequency f_l of 1.4 Hz and highest frequency f_h of 49.4 Hz. ($I_e = 1.6 \text{ gm}^2$, $b_e = 0 \text{ Nms/rad}$, $k_e = 0 \text{ Nm/rad}$)

The variation in frequency content can be distinguished into two ranges (the parameters of the external environment are set to their minimal value: $I_e = 1.6 \text{ gm}^2$, $b_e = 0 \text{ Nms/rad}$, $k_e = 0 \text{ Nm/rad}$):

- Narrow bandwidth disturbance type 1 (NB1): disturbance signals with power between a fixed f_l of 1.4 Hz and a variable f_h . f_h varied from 3.1 to 16.5 Hz, i.e. 2 to 13 varying numbers of clusters of 4 sines. ($f_h = 3.1; 4.3; 5.5; 6.7; 7.9; 9.1; 10.4; 11.6; 14.0; 16.5 \text{ Hz}$)
- Narrow bandwidth disturbance type 2 (NB2): single cluster of 4 sines with fixed bandwidth of 0.45 Hz around a centre frequency f_c , which varied between 1.6 and 16.2 Hz. ($f_c = 1.6; 4.0; 6.5; 8.9; 11.3; 13.8; 16.2 \text{ Hz}$)

The variation of the external environment can be distinguished into two ranges as well (perturbation with the WB disturbance):

- Damping: external damping varied between 0.25 and 4 Nms/rad ($I_e = 1.6 \text{ gm}^2$, $b_e = 0.25; 0.5; 1; 2; 4 \text{ Nms/rad}$, $k_e = 0 \text{ Nm/rad}$)
- Inertia: external inertia varied between 3.2 and 12.8 gm^2 ($I_e = 3.2; 6.4; 12.8 \text{ gm}^2$, $b_e = 0 \text{ Nms/rad}$, $k_e = 0 \text{ Nm/rad}$).

To obtain the EMG to torque ratio isometric tasks were performed before and after the trials. For this purpose the handle was set to a fixed rigid position while the subject was asked to exert 9 predefined torque levels (4 in extensor direction, 4

in flexor direction and 1 zero torque level), presented in random order. To support the subject the target and the actual torque were shown on the display during the isometric trials.

Activation dynamics

The model parameters of the activation dynamics were determined from a secondary experiment. The experiment started and ended with the same isometric tasks as the main experiment. The experiment consists of 8 trials of 10 s. During these trials the subjects performed isometric tasks and were asked to make block-shaped torques between approximately 2.5 Nm flexion and extension.

8.2.4 Data processing

Signal recording and processing

The angle of the manipulator $\theta(t)$, the torque exerted on the handle by the subject $T(t)$, the external torque disturbance applied by the manipulator $d(t)$, and the surface EMG of the m. flexor carpi ulnaris $e_1(t)$ and the m. extensor carpi radialis $e_2(t)$ were recorded with a sample frequency of 2500 Hz and a resolution of 16 bits. Before digitizing the EMG signals were filtered using a 20 Hz high pass filter (third order Butterworth), to remove movement artefacts and DC components, amplified, and filtered using a 1 kHz low pass filter (third order Butterworth), to prevent aliasing. By using only the last 2^{14} samples (≈ 6.55 s) of each record for analysis, initial transient effects were removed.

The EMG signals of the two antagonistic muscles are used (1) to calculate the mean EMG u_0 , as a measure of the cocontraction and (2) to obtain the lumped muscle activation $a(t)$. To improve the quality of the EMG signals a prewhitening filter is implemented, following the procedures as described in Clancy et al. (2002). The power spectral densities of the EMG of the flexor during the maximum isometric flexion (2.5 Nm) and extensor during maximum extension (-2.5 Nm) were used to obtain the parameters of the prewhitening filter (6th order moving average filter).

After whitening the EMG signals, the EMG was rectified and averaged to obtain the integrated rectified EMG, or IEMG.

$$\text{IEMG}_i = \frac{1}{n} \sum_{k=1}^n |e_{w,i}(t_k)| \quad (8.1)$$

where k indexes the (sampled) time vector, $e_{w,i}$ denotes the whitened EMG of muscle i , and n is the number of samples. The cocontraction, expressed in the mean EMG u_0 , is calculated for each trial using the IEMG of the flexor and extensor. The mean EMG is normalized with respect to the IEMG during the reference condition.

$$u_0 = \frac{1}{2} \sum_{i=1}^2 \frac{\text{IEMG}_i}{\text{IEMG}_{i,ref}} \quad (8.2)$$

where $IEMG_{i,ref}$ is the IEMG of muscle i for the reference condition, averaged over the 4 repetitions.

From the isometric tasks the EMG to torque ratios were estimated. Firstly the IEMGs were calculated for each muscle and each torque level. Second the gain was estimated by minimizing a least squares criterion.

$$\hat{T}_{i,l}(p) = K_i IEMG_{i,l} + B_i \quad (8.3)$$

$$L(p) = \sum_l T_l - \hat{T}_{i,l}(p) \quad (8.4)$$

in which $\hat{T}_{i,l}$ is the predicted average torque with torque level l for muscle i , T_l is the measured average torque, K_i and B_i are the quantified ratios and offsets respectively, L is the criterion to be minimized, and p the parameter vector.

$$p = [K_i, B_i] \quad (8.5)$$

As muscles only pull the negative torques are omitted for the flexor and the positive torques for the extensor. The (lumped) muscle activation was obtained by combining the flexor and extensor EMG using their gain K_i :

$$a(t) = \sum_{i=1}^2 K_i |e_{w,i}(t)| \quad (8.6)$$

in which $a(t)$ is the muscle activation scaled in Nm by K_i and i refers to the two muscles. Note that this study investigates dynamic behaviour around an equilibrium and consequently it is not necessary to use the offsets to calculate $a(t)$.

Nonparametric analysis

For each condition of the main experiment the recorded signals ($d(t)$, $\theta(t)$, $T(t)$, $a(t)$) were averaged over the four repetitions and converted to the frequency domain by fast Fourier transform (FFT). As torque disturbances were applied, interaction between the subject and manipulator existed, see Fig. 8.1. Because of this interaction closed loop identification algorithms were required to estimate the dynamics of the subject.

The frequency response functions (FRFs) for the joint admittance $\hat{H}_{T\theta}(f)$ and the reflexive impedance $\hat{H}_{\theta a}(f)$ were estimated by dividing the appropriate spectral densities (Schouten et al., 2004b). Along with the FRFs the coherences for the

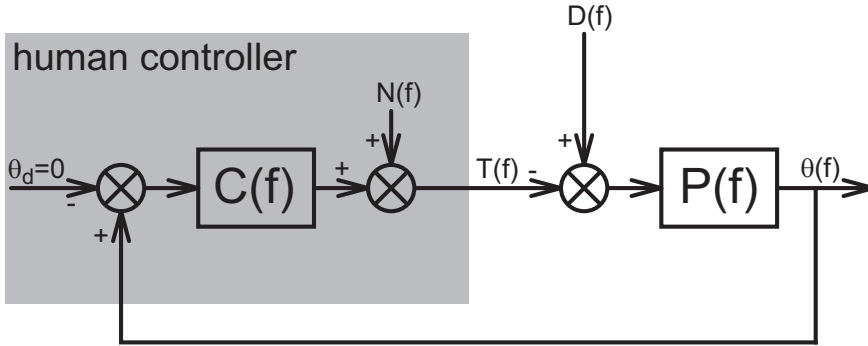


Figure 8.1: Blockscheme of human posture control expressed in the frequency domain. $C(f)$: transfer function of wrist dynamics; $P(f)$ transfer function of manipulator dynamics; $D(f)$ external torque disturbance; $T(f)$ human reaction torque; $\theta(f)$ angle of the handle; $N(f)$ model remnant; $\theta_d = 0$ reference angle. The wrist dynamics (grey box) are described by linear transfer function $C(f)$, together with the remnant $N(f)$ which is uncorrelated with $D(f)$.

joint angle $\hat{\gamma}_\theta^2(f)$ and muscle activation $\hat{\gamma}_a^2(f)$ were estimated.

$$\hat{H}_{T\theta}(f) = \frac{\theta(f)}{T(f)} = \frac{\hat{G}_{d\theta}(f)}{\hat{G}_{dT}(f)} \left(\equiv C^{-1}(f) \right) \quad (8.7)$$

$$\hat{H}_{\theta a}(f) = \frac{A(f)}{\theta(f)} = \frac{\hat{G}_{da}(f)}{\hat{G}_{d\theta}(f)} \quad (8.8)$$

$$\hat{\gamma}_\theta^2(f) = \frac{|\hat{G}_{d\theta}(f)|^2}{\hat{G}_{dd}(f)\hat{G}_{\theta\theta}(f)} \quad (8.9)$$

$$\hat{\gamma}_a^2(f) = \frac{|\hat{G}_{da}(f)|^2}{\hat{G}_{dd}(f)\hat{G}_{aa}(f)} \quad (8.10)$$

in which $\hat{G}_{d\theta}(f)$ is the cross spectral density between $d(t)$ and $\theta(t)$ (Hat denotes estimate). The spectral densities were averaged over 4 adjacent frequencies to improve the estimators (Jenkins and Watts, 1968). The FRFs and coherences were only evaluated at frequencies where the disturbance signal contained power. By definition the coherence varies between 0 and 1, where a value of 1 indicates that the signals are linearly related and no external noise exists.

Quantification of activation dynamics

In this experiment the dynamic relation between muscle activation $a(t)$ and torque $T(t)$ is sought. First the FRF and coherence between muscle activation and torque were estimated by dividing the appropriate spectral densities with the aid of an

independent instrument variable (Pintelon and Schoukens, 2001).

$$\hat{H}_{act}(f) = \frac{\hat{G}_{wT}(f)}{\hat{G}_{wa}(f)} \quad (8.11)$$

$$\hat{\gamma}_{aT}^2(f) = \frac{|\hat{G}_{aT}(f)|^2}{\hat{G}_{aa}(f)\hat{G}_{TT}(f)} \quad (8.12)$$

in which w is the instrument variable, $\hat{H}_{act}(f)$ the FRF, and $\hat{\gamma}_{aT}^2(f)$ the coherence. The instrument variable was constructed in the frequency domain having power between 1 and 50 Hz. The spectral densities were averaged over 4 adjacent frequencies to improve the estimators.

Because the experiment was isometric, i.e. there are no angular deviations, the relation between muscle activation and torque is described by the activation dynamics and does not contain reflexes or muscle visco-elasticity. The activation dynamics were modelled as a second order system (Olney and Winter, 1985; Bobet and Norman, 1990; Potvin et al., 1996):

$$H_{act}(s, p) = \frac{1}{\frac{s^2}{\omega_0^2} + 2\beta\frac{s}{\omega_0} + 1} \quad (8.13)$$

with

$$p = [f_0, \beta]$$

in which $s = j2\pi f$ is the Laplace operator, f_0 is the eigenfrequency in Hz ($f_0 = \frac{\omega_0}{2\pi}$) and β is the relative damping.

The activation dynamics were obtained by fitting the model (Eq. 8.13) onto the measured activation dynamics (Eq. 8.11) by minimizing a criterion function:

$$L(p) = \sum_k \frac{\hat{\gamma}_{aT}^2(f_k)}{1 + f_k} |\ln \hat{H}_{act}(f_k) - \ln H_{act}(f_k, p)|^2 \quad (8.14)$$

where k indexes the frequency vector. Only the frequencies upto 20 Hz were used for the criterion. For higher frequencies the torque signal contained little power such that the activation dynamics could not be estimated reliably. This is reflected by the low coherence for these frequencies, see Results. Because of the large range of the FRF gain a least squares criterion with logarithmic difference was used (Pintelon et al., 1994). The criterion was weighted with the coherence to reduce emphasis on less reliable frequencies in the FRF and with $(1 + f_k)^{-1}$ to prevent excessive emphasis on the higher frequencies. To obtain a better fit one set of parameters was used to fit the model simultaneously on all 8 trials for each subject. Finally the activation parameters were averaged over all subjects and used to quantify the intrinsic and reflexive parameters.

Quantification of intrinsic and reflexive properties

The human wrist is modelled in a similar manner as the arm in Chapter 6, except that linear terms are replaced with rotational terms. Fig. 8.2 show the model of the transfer function of the wrist.

The intrinsic properties, including muscle cocontraction, are modelled as a rotational spring-damper system around the wrist joint (Winters et al., 1988):

$$H_{int}(s) = \frac{1}{Is^2 + bs + k} \quad (8.15)$$

The inertia of the hand in fist position is modelled as I and the muscles, tendons and ligaments are modelled in damping b and stiffness k , and includes visco-elasticity as a result of cocontraction.

Muscle spindles are attached to muscle fibres and hence the stretch and stretch velocity of the muscle spindles are proportional to the stretch and stretch velocity of the muscle fibres. The muscle spindle send information via the Ia and II afferent nerves to the central nervous system (CNS) and α -motoneuron. Furthermore the Golgi tendon organs located in the tendon provide information about the muscle force and is send via Ib afferents. As it is not possible to separate these feedback paths the reflexive feedback is described with one model, $H_{ref}(s)$.

$$H_{ref}(s) = \left(k_a s^2 + k_v s + k_p \right) e^{-\tau_d s} \quad (8.16)$$

in which τ_d is the time delay due to neural transportation and processing time. The reflex gains k_a , k_v , and k_p describe the acceleration, velocity and position feedback gain respectively.

The model of the wrist, including activation dynamics, intrinsic muscle properties and reflexive feedback equals:

$$H_w(s) = \frac{\theta_w(s)}{T(s)} = \frac{H_{int}(s)}{1 + H_{int}(s)H_{ref}(s)H_{act}(s)} \quad (8.17)$$

The (external) environment $H_e(s)$ can be described by a rotational inertia-spring-damper system.

$$H_e(s) = \frac{1}{I_e s^2 + b_e s + k_e} \quad (8.18)$$

The complete model consists of two submodels: one for the wrist, $H_w(f)$, and one for the environment, $H_e(f)$. In between the wrist and the environment is the visco-elasticity of the grip, including the stiffness of the transducer in the lever.

$$H_g(s) = b_g s + k_g \quad (8.19)$$

in which b_g is the damping and k_g is the stiffness of the grip, including handle and lever. The grip visco-elasticity is relatively high ($b_g = 1$ Nms/rad; $k_g = 1500$

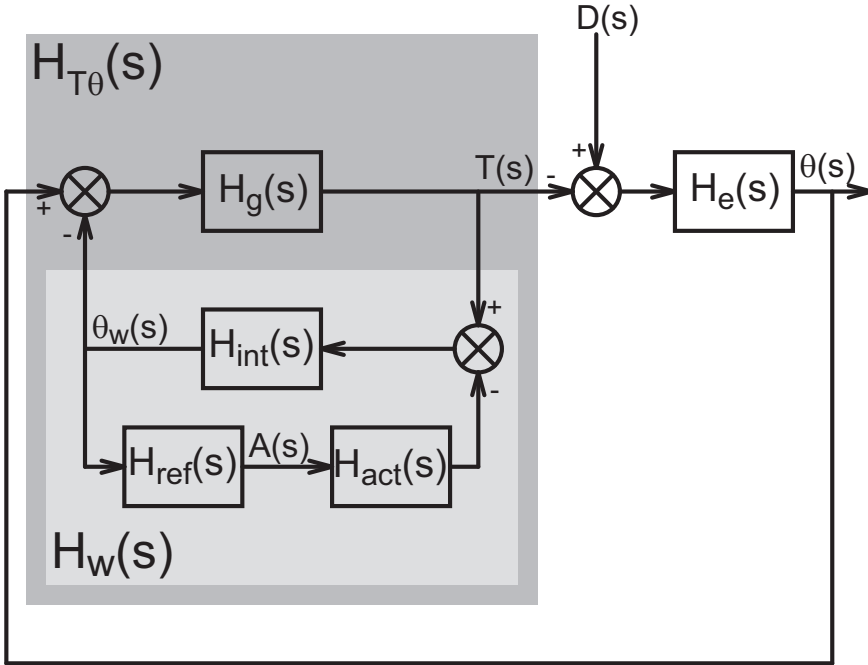


Figure 8.2: Model of the wrist $H_{T\theta}(s)$ in conjunction with the environment $H_e(s)$. The external torque disturbance $D(s)$, wrist reaction torque $T(s)$, angle of the handle $\theta(s)$, and muscle activation $A(s)$, are measured. $H_g(s)$ represents grip dynamics, $H_{int}(s)$ intrinsic properties, $H_{act}(s)$ activation dynamics, $H_{ref}(s)$ reflexive feedback, and $\theta_w(s)$ angle of the wrist. The light grey box represents the model for only the wrist $H_w(s)$.

Nm/rad) and mainly determined by the (reduced) stiffness of the custom made force sensor in the lever. The grip dynamics are necessary to accurately describe the measured admittance, especially at the higher frequencies. Furthermore the grip dynamics are necessary to simulate the complete system because both the wrist and the environment need to be causal, i.e. having torque as input.

Finally two transfer function can be obtained from Fig. 8.2 to describe the joint admittance $H_{T\theta}(s)$ and the reflexive impedance $H_{\theta a}(s)$ respectively:

$$H_{T\theta}(s, p) = \frac{\theta(s)}{T(s)} = \frac{1 + H_w(s)H_g(s)}{H_g(s)} = H_w(s) + H_g^{-1}(s) \quad (8.20)$$

$$H_{\theta a}(s, p) = \frac{a(s)}{\theta(s)} = H_{ref}(s) \frac{H_w(s)}{H_w(s) + H_g^{-1}(s)} \quad (8.21)$$

with p as the parameter vector:

$$p = [I, b, k, k_a, k_v, k_p, \tau_d] \quad (8.22)$$

Note that when the grip visco-elasticity is high the joint admittance ($H_{T\theta}(s)$) approaches the wrist dynamics ($H_w(s)$) and the reflexive impedance ($H_{\theta a}(s)$) the reflexive feedback ($H_{ref}(s)$).

The intrinsic and reflexive parameters were quantified by fitting the model (Eqs. 8.20-8.21) onto the FRFs (Eqs. 8.7-8.8) using a least squares minimization procedure.

$$L_{\theta}(p) = \sum_k \frac{\hat{\gamma}_{\theta}^2(f_k)}{1 + f_k} |\ln \hat{H}_{T\theta}(f_k) - \ln H_{T\theta}(f_k)|^2 \quad (8.23)$$

$$L_a(p) = \sum_k \frac{\hat{\gamma}_a^2(f_k)}{1 + f_k} |\ln \hat{H}_{\theta a}(f_k) - \ln H_{\theta a}(f_k)|^2 \quad (8.24)$$

$$L(p) = L_{\theta}(p) + qL_a(p) \quad (8.25)$$

in which k indexes the frequency vector and q a weighting factor. The criterion was only evaluated at the frequencies where the disturbance contained power. Factor q was chosen such that L_{θ} and qL_a were approximately equal in the optimal solution of the reference condition ($q = 0.16$). For the reflexive impedance all frequencies above 16 Hz in the FRF were omitted, because of the low reliability, see Results.

In the fitting procedure two steps can be distinguished. First the parameters of the experiments using the WB disturbance (reference condition, damping environment and inertia environment, $n = 9$) were quantified simultaneously. It was assumed that the inertia of the hand I and time delay τ_d were constant over all trials, so I and τ_d were identical for all conditions. Furthermore it was assumed that the intrinsic visco-elasticity (b and k) linearly scaled with the mean EMG (Agarwal and Gottlieb, 1977).

$$b = u_0 \cdot b_{ref} \quad (8.26)$$

$$k = u_0 \cdot k_{ref} \quad (8.27)$$

where k_{ref} and b_{ref} are the intrinsic stiffness and damping during the reference condition. The number of parameters that need to be quantified reduces from 63 (9 condition with 7 parameters) to 31 (1 inertia, 1 time delay, 2 muscle parameters and 3 reflex gains for the 9 condition).

Second for the NB1 and NB2 disturbances, the hand inertia I and time delay τ_d were fixed to the values of the reference condition (WB disturbance) and again the intrinsic parameters b and k scaled with the mean EMG. This implicates that only the reflexive parameters k_a , k_v , and k_p had to be quantified for each NB condition:

$$p = [k_a, k_v, k_p] \quad (8.28)$$

Model validation

The quantified parameters were used for forward simulation of the wrist response in time domain with the model of Fig. 8.2. This simulation used the same perturbation signals as the experiments. The validity of the quantified parameters is expressed in the variance accounted for (VAF) for both the angular position and the

muscle activation:

$$\text{VAF}_\theta = 1 - \frac{\sum_{k=1}^n |\theta(t_k) - \hat{\theta}(t_k)|^2}{\sum_{k=1}^n |\theta(t_k)|^2} \quad (8.29)$$

$$\text{VAF}_a = 1 - \frac{\sum_{k=1}^n |a(t_k) - \hat{a}(t_k)|^2}{\sum_{k=1}^n |a(t_k)|^2} \quad (8.30)$$

in which $\hat{\theta}(t_n)$ and $\hat{a}(t_n)$ are the forward simulated angular handle position and activation respectively and $\theta(t_n)$ and $a(t_n)$ are the measured angular handle position and activation respectively averaged over the four repetitions. The index of the time vector is n . Before calculating the VAF all signals were high pass filtered to remove drift (1.4 Hz, 3th order Butterworth). Furthermore the muscle activation signals were low pass filtered to remove noise (16 Hz, 3th order Butterworth).

8.3 Results

8.3.1 Isometric experiments

The result of a typical subject for the isometric tasks is shown in Fig. 8.3. During flexion (positive torque) the flexor carpi ulnaris was active and the extensor carpi radialis was relatively silent, and vice versa. From the active part of the EMG to torque relation the EMG to torque ratio was estimated with a least squares criterion. The EMG to torque ratios are denoted by the grey lines in Fig. 8.3.

8.3.2 Activation dynamics

Fig. 8.4 shows the FRF of the muscle activation, the coherence, and the torque of a typical subject during a trial. The estimated parameters for all subjects of the muscle activation model are given in Table 8.1. With use of the estimated EMG to torque ratios, the muscle activation model, and the recorded EMG, the torque was predicted. The model predicted the measured torque well (Fig. 8.4, bottom). The average parameters of the four subjects were used for the main experiment as the muscle activation model.

8.3.3 Nonparametric FRFs

In Table 8.2 the root-mean-square (RMS) of the handle angle and the mean EMG u_0 are shown, averaged over the population. The RMS of the handle angle was around 0.85 degrees for all conditions. The mean EMG was around one indicating that the variations in muscle cocontraction over the conditions were small.

Fig. 8.5 shows the FRFs and coherences for the damped and inertial environments and Fig. 8.6 for the NB1 and NB2 perturbations, for one typical subject. For all conditions the coherence of the angular position is high, indicating that external

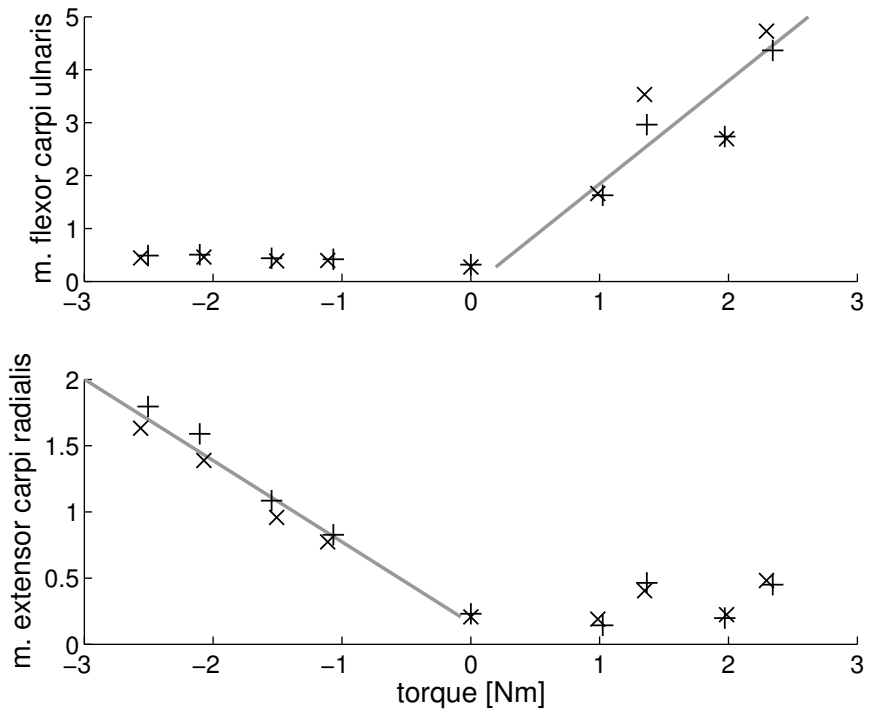


Figure 8.3: EMG to torque ratios for a typical subject. Top: *m. flexor carpi ulnaris*; bottom: *m. extensor carpi radialis*. Average torque is given on the X-axis, the corresponding IEMG on the Y-axis. The 'x' and '+' denotes the IEMG of the push/pull tasks before and after the main experiment respectively; the slope of the line denotes the estimated EMG to torque ratio.

Table 8.1: Estimated eigenfrequency, f_0 , and relative damping, β , of the activation dynamics for all subjects. In the lower row the average and SD over the subjects are given.

subject	f_0 [Hz]	β [-]
1	2.06	0.94
2	2.34	0.46
3	2.36	0.72
4	2.07	0.87
mean (SD)	2.21 (0.16)	0.75 (0.21)

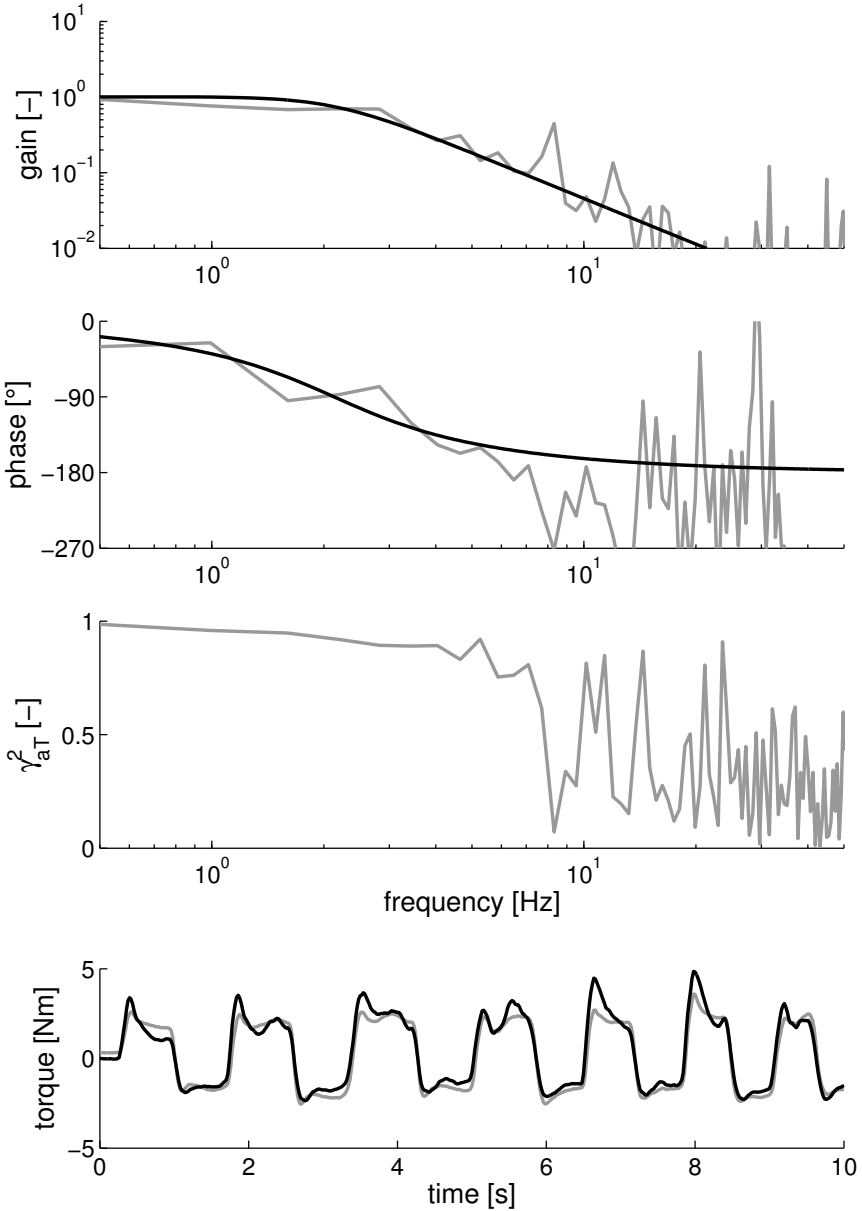


Figure 8.4: From top to bottom: gain and phase of the FRF of the muscle activation $\hat{H}_{act}(f)$, coherence $\hat{\gamma}_{aT}^2(f)$, and torque $T(t)$. Black lines: model; grey lines: measurements.

Table 8.2: RMS values of the handle angle and the mean EMG u_0 per condition. The values are averaged over the population (SD).

condition	RMS [°]	u_0 [-]
WB reference	0.74 (0.10)	1 (-)
b_e 0.25 Nms/rad	0.79 (0.12)	1.11 (0.12)
b_e 0.50 Nms/rad	0.83 (0.10)	1.17 (0.13)
b_e 1 Nms/rad	0.83 (0.07)	1.21 (0.13)
b_e 2 Nms/rad	0.78 (0.09)	1.27 (0.12)
b_e 4 Nms/rad	0.61 (0.06)	1.16 (0.13)
I_e 3.2 gm ²	0.84 (0.09)	1.08 (0.14)
I_e 6.4 gm ²	0.85 (0.12)	1.13 (0.13)
I_e 6.4 gm ²	0.84 (0.12)	1.05 (0.11)
NB1 3.1 Hz	0.74 (0.12)	1.10 (0.14)
NB1 4.3 Hz	0.86 (0.18)	1.09 (0.15)
NB1 5.5 Hz	0.89 (0.23)	1.06 (0.23)
NB1 6.7 Hz	0.93 (0.18)	1.10 (0.13)
NB1 7.9 Hz	0.92 (0.13)	1.01 (0.16)
NB1 9.1 Hz	0.94 (0.16)	0.99 (0.11)
NB1 10.4 Hz	0.93 (0.15)	1.04 (0.12)
NB1 11.6 Hz	0.92 (0.12)	1.02 (0.16)
NB1 14.0 Hz	0.90 (0.10)	0.97 (0.11)
NB1 16.5 Hz	0.89 (0.13)	0.96 (0.16)
NB2 1.6 Hz	0.78 (0.23)	1.19 (0.15)
NB2 4.0 Hz	0.91 (0.17)	1.02 (0.11)
NB2 6.5 Hz	1.04 (0.19)	1.06 (0.17)
NB2 8.9 Hz	0.82 (0.14)	0.86 (0.11)
NB2 11.3 Hz	0.81 (0.16)	0.95 (0.12)
NB2 13.8 Hz	0.82 (0.21)	0.79 (0.17)
NB2 16.2 Hz	0.85 (0.18)	0.92 (0.21)

noise is low and a linear relation exists between the joint angle and torque. The coherence of the muscle activation is relatively high for frequencies from 2 to 20 Hz.

With increased damping of the environment the joint admittance decreased at low frequencies (Fig. 8.5). The decreased admittance implicates that the wrist joint was stiffer with a damped environment. The gain of the reflexive impedance increased with external damping, indicating enhanced reflexes. The phase of the reflexive impedance at low frequencies gives an indication of the most important feedback gain, position feedback gives 0 degrees phase advance, velocity 90 degrees, and acceleration 180 degrees. The phase advance is around 120 degrees, indicating that the reflexive feedback was a combination of primarily velocity and acceleration term. The phase lag with increasing frequency results from the neural time delay.

The joint admittance at low frequencies decreased with increased external in-

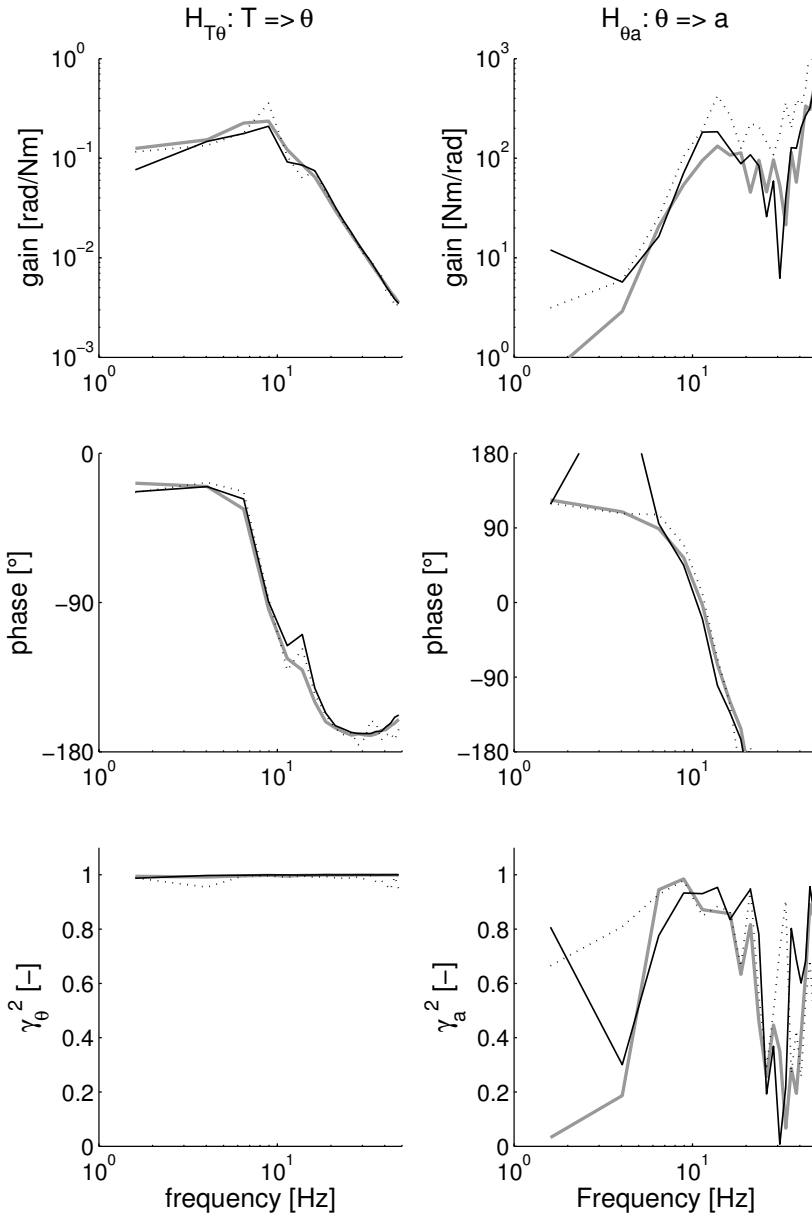


Figure 8.5: Gain and phase of the estimated FRF of the joint admittance $\hat{H}_{T\theta}(f)$ (left) and the reflexive impedance $\hat{H}_{\theta a}(f)$ (right), and the coherences of the angular wrist position $\hat{\gamma}_\theta^2(f)$ (left) and the activation $\hat{\gamma}_a^2(f)$ (right). Shown are three condition for one typical subject. Grey lines: reference condition; black: $b_e = 40$ Nms/rad; dotted: $I_e = 12.8$ gm².

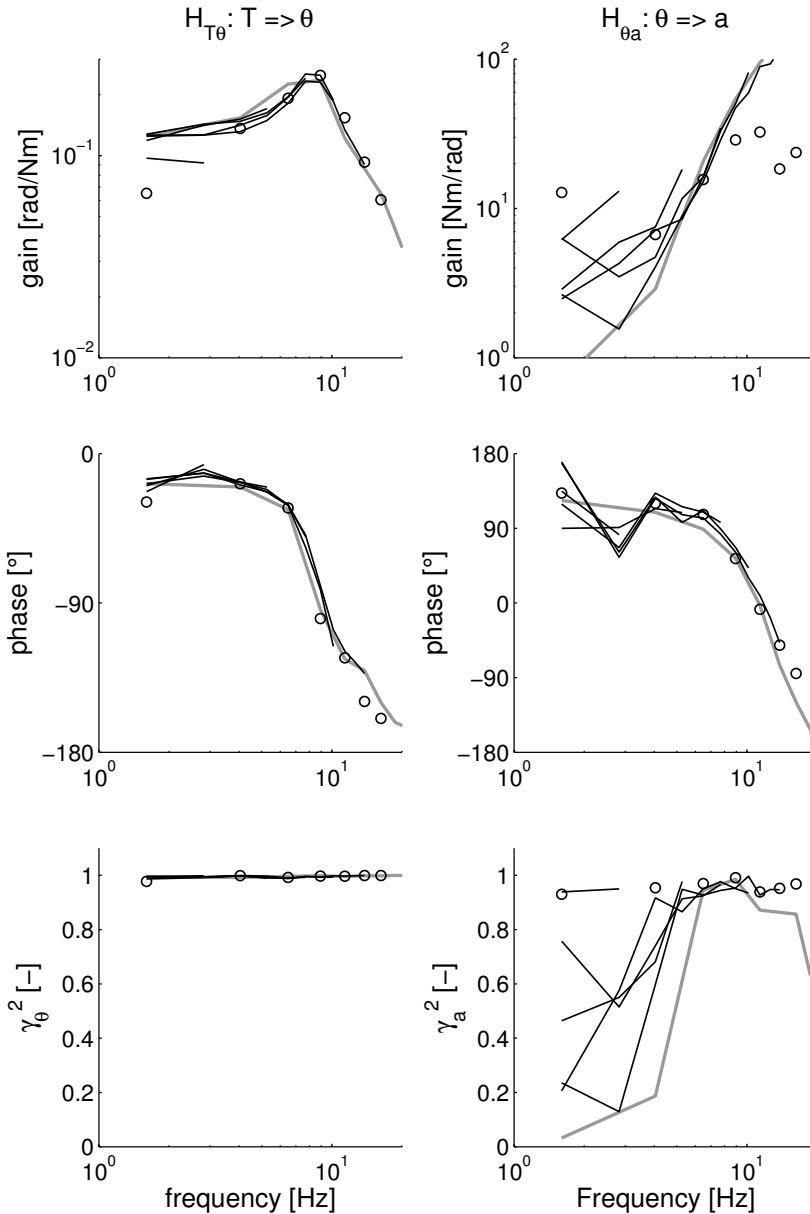


Figure 8.6: Gain and phase of the estimated FRF of the joint admittance $\hat{H}_{T\theta}(f)$ (left) and the reflexive impedance $\hat{H}_{\theta a}(f)$ (right), and the coherences of the angular wrist position $\hat{\gamma}_\theta^2(f)$ (left) and the muscle activation $\hat{\gamma}_a^2(f)$ (right). Grey lines: reference condition; black lines: NB1; circles: NB2.

Table 8.3: Quantified parameters for the reference condition. Means (SD) over the ten subjects.

	description	
I [gm ²]	inertia	2.13 (0.03)
b [Nms/rad]	intrinsic damping	0.088 (0.009)
k [Nm/rad]	intrinsic stiffness	9.7 (3.1)
k_a [Nms ² /rad]	acceleration feedback gain	0.009 (0.004)
k_v [Nms/rad]	velocity feedback gain	0.15 (0.15)
k_p [Nm/rad]	position feedback gain	0.4 (2.4)
τ_d [ms]	time delay	42.7 (5.8)

ertia (Fig. 8.5). The oscillation around the eigenfrequency, i.e. the peak, increased. Furthermore the reflexive impedance increased with the environmental damping.

Fig. 8.6 shows the estimated FRFs and coherences for the NB1 perturbation. The frequency range is visible by the length of the curve. The joint admittance decreased as the bandwidth of the disturbance f_h decreased, while the reflexive impedance increased. NB2 perturbations consist of a small bandwidth around centre frequency f_c , visualized with the circles in Fig. 8.6. Up to 5 Hz the joint admittance was low compared to the reference condition. The reflexive impedance was low for centre frequencies beyond 10 Hz compared with the reference condition, while the phase advance is larger at all centre frequencies.

8.3.4 Intrinsic and reflexive parameters

The quantified parameters for the reference condition are given in Table 8.3. The reflexive parameters for all conditions are shown in Figs. 8.7 and 8.8. Note that the reference condition is also given twice in Fig. 8.7 ($b_e = 0$ Ns/m, $I_e = 1.6$ gm²). The corresponding VAF values are given in the lower two rows of the figures. The VAF values for the handle angle VAF_θ are high for all conditions, indicating that the model describes the observed mechanical behaviour well. The VAF values of the muscle activation VAF_a are around 40-50% for the environmental damping and inertia conditions. This can be considered high given the fact that EMG contains substantial noise. To severely reduce the noise in the signals all irrelevant frequencies, i.e. not excited by the torque disturbance, were removed from the measured angle and muscle activation. Noise reduction was performed by applying FFT, setting power to zero at all irrelevant frequencies, and then inverse transformation to time domain (by inverse FFT). The VAF values for these noise-reduced signals are indicated with grey lines in Figs. 8.7 and 8.8. By removing the irrelevant frequencies the VAF_a increased to values around 60% for the environment condition and even to 80% for the NB2 disturbances. The VAF_a for NB2 disturbances is reduced primarily by movements around the eigenfrequency and removing the irrelevant frequencies, including the not excited eigenfrequency, improved the VAF substantially.

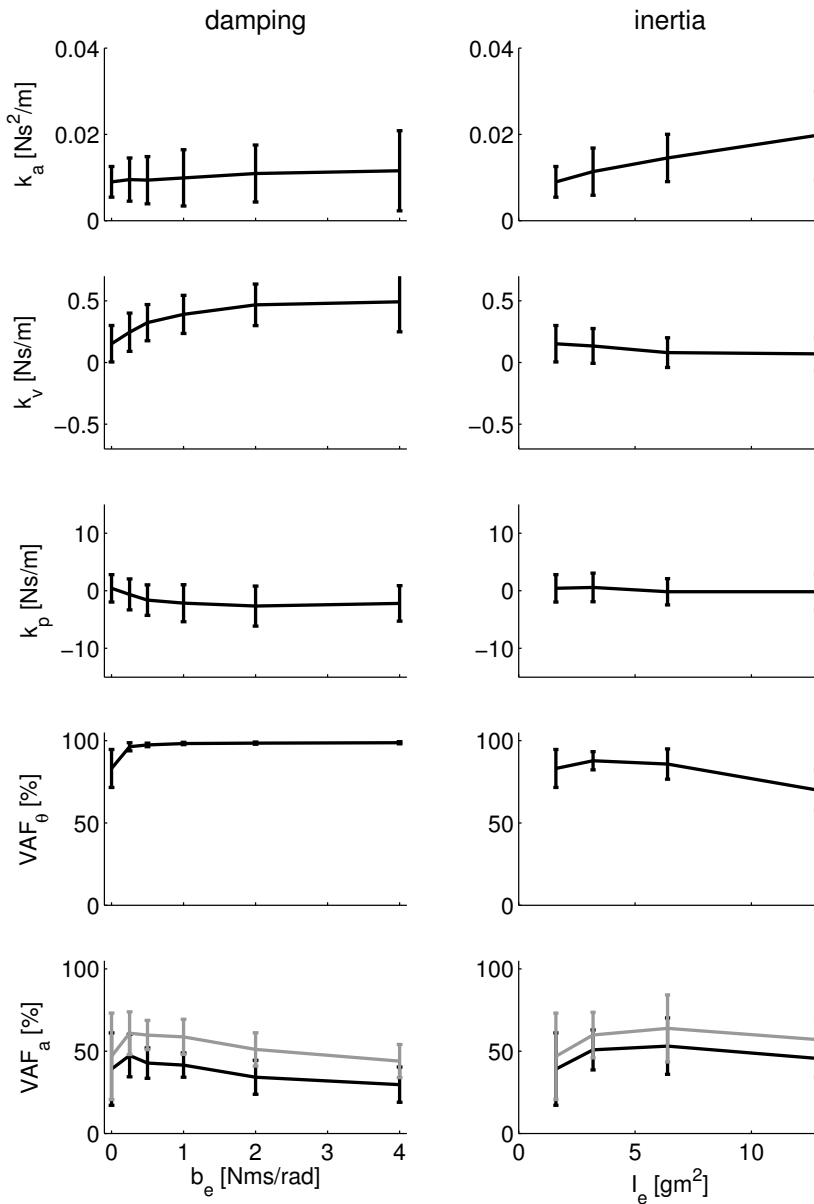


Figure 8.7: Quantified reflexive parameters (k_a , k_v , k_p) and corresponding VAF values (VAF_θ , VAF_a) of the damping (left) and inertia (right) environment. The lines denote the means over the population, error bars denote the SD. Grey lines in the VAFs are the VAFs after noise reduction. Note that the both $b_e = 0$ Nms/rad and $I_e = 1.6$ gm² refer to the reference condition.

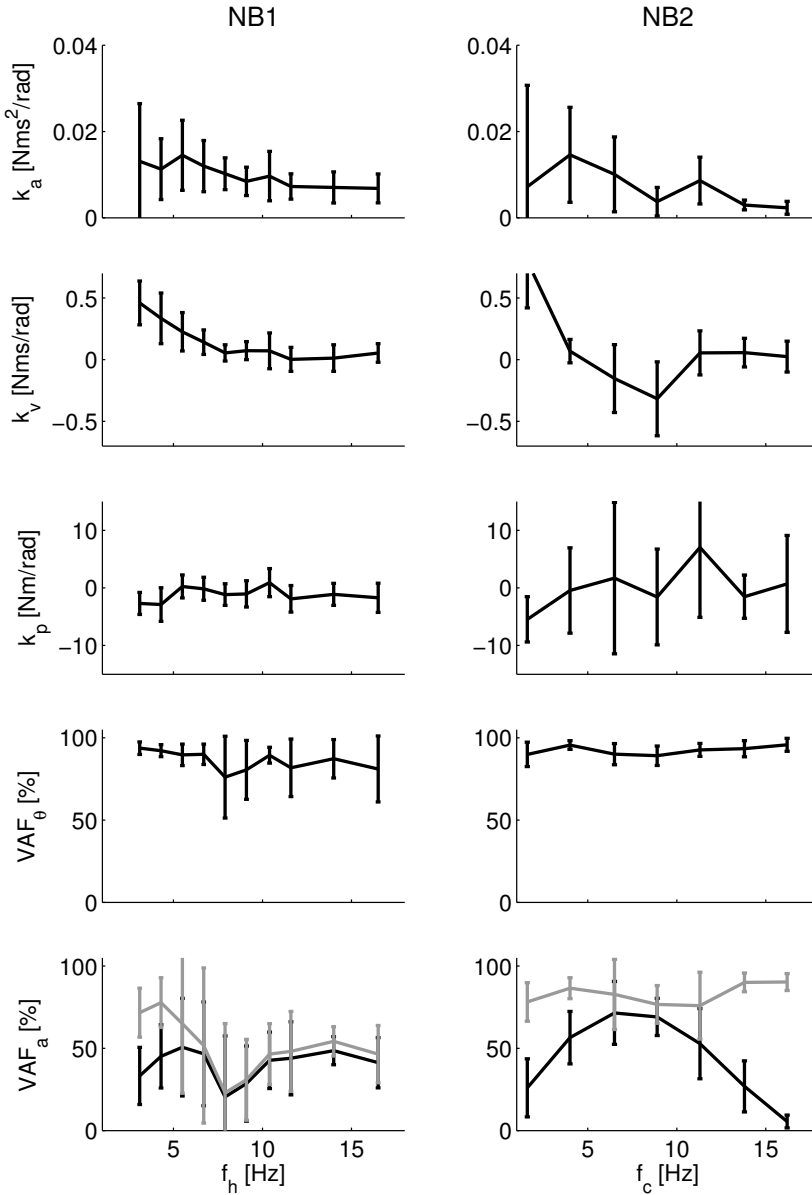


Figure 8.8: Quantified reflexive parameters (k_a , k_v , k_p) and corresponding VAF values (VAF_θ , VAF_a) for the NB1 perturbation (left, as a function of frequency f_h) and NB2 perturbation (right, as a function of frequency f_c). The lines denote the means over the population, error bars denote the SD. Grey lines in the VAFs are the VAFs after noise reduction.

As the torque transducer was mounted in the lever of the manipulator, the quantified inertia includes the inertia of the handle ($\approx 0.73 \text{ gm}^2$, Schouten et al., 2004c). Correcting for the handle inertia gives the real inertia of a fisted hand, 1.40 gm^2 . The stiffness of the wrist during the reference condition is around 10 Nm/rad ($k + k_p$). The acceleration and position feedback are relatively small during the reference condition. The velocity feedback is approximately 70% larger than the intrinsic damping, indicating that velocity feedback had a substantial contribution to the performance.

The velocity feedback gain increased with external damping (Fig. 8.7, left). Both the variations in gain of acceleration and position feedback with the environmental damping were small. The acceleration feedback gain increased with external inertia (Fig. 8.7, right), while velocity and position feedback have small and constant values.

Fig. 8.8 (left) shows that with NB1 perturbations the velocity feedback decreased when the disturbance bandwidth increased. The right column of Fig. 8.8 shows the quantified reflexive parameters of the NB2 perturbation. The velocity feedback gain is high for low centre frequencies and decreased for increasing centre frequencies, the velocity feedback gain even became negative for some centre frequencies. The variations in acceleration feedback are small and the high SD on the position feedback suggests that the position feedback gain has a minor effect on the performance for these disturbances and can not be reliably estimated.

8.4 Discussion

In this study the magnitude of proprioceptive reflexes is assessed at the wrist by means of torque disturbances. The use of torque disturbances facilitates an unambiguous position task (*'minimize deviations'*), which is natural and appealing for the subjects. As the task requires minimal joint admittance proprioceptive reflexes will have a relevant contribution to the performance. Furthermore by changing the condition (external damping/inertia and disturbance bandwidth) different reflex magnitudes are provoked.

The method is an important tool to evaluate the regulation of spinal reflexes and useful to investigate the contribution of reflexes in disorders with abnormal muscle tone. Abnormalities of muscle tone are an integral component of many chronic neurological disorders, like complex regional pain syndrome (CRPS). A previous study evaluation reflexes at the shoulder showed that the method gives insight in to the pathophysiology of CRPS (Schouten et al., 2003, see Chapter 3). For most neurological disorders the motor features starts at distal joints and may affect more proximal joints as the disease develops. To measure changes in reflex settings in the early stages of these disorders it is desirable to quantify reflexes around a distal joint like the wrist. Future studies can use the methods of this study to investigate reflexes at the wrist in neurological disorders.

For each condition the FRFs of the joint admittance and reflexive impedance are estimated, describing the input-output behaviour from torque to angle and an-

gle to muscle activity (EMG) respectively. By fitting a linear model on to the FRFs the intrinsic (muscle) and reflexive properties are estimated. The high coherence for the angular deviations show that the behaviour is linear under the given circumstances. Below 2 Hz and above 20 Hz the coherence for the muscle activation was lowered, which likely results from low frequent corrective actions uncorrelated with the disturbance and the low signal power for higher frequencies relative to the noise inherent with EMG recordings.

The muscle cocontraction showed small variations, indicating that the intrinsic muscle visco-elasticity was approximately constant over the conditions. The variations in the joint admittance between the conditions were larger than the variations in muscle cocontraction, indicating that the reflexive contribution varied over the conditions. Furthermore for all conditions hold that when the joint admittance decreased the reflexive impedance increased, indicating that the changes in mechanical behaviour result from enhanced reflexes.

The high VAF values for the angular position show that the wrist joint was adequately described with the given linear model. The quantified inertia, intrinsic muscle visco-elasticity, and neural time delay showed intersubject variability; this makes these parameters reproducible and well interpretable. It was found that during the reference condition the reflex gain for velocity feedback was substantially larger than the intrinsic damping, indicating that reflexes play an important role during the reference condition (i.e. minimal external inertia, no external damping and a wide bandwidth disturbance). The reflexive parameters (k_a , k_v , k_p) varied between the conditions, although the variations in the velocity feedback are the most prominent. Increasing external damping and decreasing disturbance bandwidth increases the velocity feedback gain to values 3 times larger than during the reference condition. For disturbances around a centre frequency the velocity feedback became even negative. Increasing the external inertia increased the acceleration feedback. The position feedback seemed marginally affected by the applied conditions.

De Vlugt et al. (2002) investigated reflexes at the shoulder with varying external environments and found that the length feedback gain increased when the environmental damping or inertia increased. Velocity feedback remained constant. In this study, investigating the wrist joint, the velocity feedback gain increased with external damping or inertia and position feedback remained constant. Van der Helm et al. (2002) studied the effect of perturbation bandwidth on reflexes of the shoulder. With NB1 perturbations the position feedback gain increased as the bandwidth decreased and the velocity feedback gain was almost constant. At the wrist again the opposite was seen increasing velocity feedback gain with decreasing bandwidth and constant position feedback gain.

The observed differences between reflexes at the shoulder and at the wrist can be explained from the higher eigenfrequency of the wrist (15 Hz) compared to the shoulder (3 Hz). Above the eigenfrequency the joint admittance is dominated by the mass/inertia and reflexes are of low value. Reflexive feedback can decrease the joint stiffness, but its effectiveness is limited by the activation dynamics. Activation

dynamics have a bandwidth around 2.2 Hz, hence the position feedback is only effective below 2.2 Hz. This all implicates that position feedback is effective at the shoulder. At the wrist position feedback does only cover a small frequency range below the eigenfrequency and higher order terms, like velocity, will be more effective.

Chapter 9

Proprioceptive reflexes at the wrist in patients with Parkinson's disease

The goal of this study is to test if the wrist manipulator can be used to quantify reflexes in patients with Parkinson's disease. Quantification of reflex magnitudes can be an important tool to investigate the how reflexes contribute to the motoric features of Parkinson's disease. External torque disturbances were applied at the wrist and the subjects had to 'minimize the deviations' of the handle of the manipulator. Intrinsic (muscle) and reflexive properties are assessed by fitting a model onto the input-output behaviour. Modulation of reflex magnitude was provoked by changing the external damping, imposed by the manipulator, or the disturbance bandwidth. This study showed that parkinsonian patients can perform the task well and that intrinsic and reflexive parameters can be reliably quantified. It was found that the neural time delay of proprioceptive reflexes in patients was significantly larger compared to controls (patients: 55 ms; controls 43 ms). The differences in modulation of the reflex magnitude were most pronounced for the external damping conditions. Future studies with large populations of Parkinson patients should focus on the protocol with damping conditions. By reducing the number of experimental conditions the experiment time will reduce substantially and lighten the experiment for the subjects.

9.1 Introduction

Parkinson's disease (PD) is a neurodegenerative disorder characterized by tremor, bradykinesia, rigidity, and impaired postural reflexes. The symptoms develop with the loss of dopamine producing cells in the central nervous system (CNS). Current studies indicate that the proprioceptive reflexes are modulated by presynaptic inhibition of muscle spindle afferents in the spinal cord, under control of higher centres in the CNS (Stein and Capaday, 1988). As patients with PD progressively lose the coordination and activation of the muscles, it is hypothesized that also the ability to modulate the proprioceptive reflexes deteriorates.

In a recent study spinal reflexes at the wrist joint are quantified during postural control tasks (Chapter 8). In that study continuous random torque disturbances were applied to the wrist, via a handle. The subjects were requested to keep the handle in an equilibrium position and to '*minimize deviations*', resulting from the torque disturbances. Goal of this study is to quantify reflexes at the wrist and to investigate if and how spinal reflexes are disturbed in parkinsonian patients. To provoke different reflexive setting the bandwidth of the disturbance and the damping, imposed by the manipulator, are altered. As the number of trials is relatively large it is important to find a subset of the applied conditions, which is able to mark the differences between patients and controls. This subset can be used for large clinical trials.

9.2 Materials and Methods

9.2.1 Subjects

In this study six parkinsonian patients (1 woman, all subjects right handed) were assessed with a mean (standard deviation, SD) age of 52.7 (8.4) years. The characteristics of the patients are summarized in Table 9.1. All patients were scored according to the Hoehn & Yahr scale (Hoehn and Yahr, 1967). Where zero on the Hoehn & Yahr scale indicates that no difference existed compared to healthy subjects, and four indicate severe impairment. All patients were on medication during the experiments. The results were compared with a group of 12 controls (2 woman, all right handed). The controls had a mean (SD) age of 31.4 (14.4) years. The experiments were conducted on the right wrist. All subjects gave informed consent to the experimental procedure.

9.2.2 Apparatus

Torque disturbances were applied at the wrist by means of a manipulator. The manipulator is extensively described in Chapter 7 and is introduced briefly. Subjects were seated in a chair and had to hold a handle with the right hand, while the forearm was supported by an arm support. The handle is connected, via a lever, to a motor. The lever has a fixed length to align the wrist joint of an average size

Table 9.1: Characteristics of the parkinsonian patients participating in this study.

patient	gender	age	Hoehn & Yahr
1	M	47	2
2	M	54	2
3	M	54	2
4	M	68	2
5	M	48	2
6	M	45	2

hand with the motor axis. The subject could move the handle resulting in flexion and extension of the wrist. To the subject the manipulator behaved like a rotational inertia-spring-damper system. The parameters of this external environment are fully adjustable, except that the external inertia has a minimum ($I_e \geq 1.6 \text{ gm}^2$). In this study the external damping (b_e) was altered, the inertia was set to the minimum value, and no value for the spring was set ($k_e = 0 \text{ Nm/rad}$).

9.2.3 Procedures

The experiment consisted of eighteen different conditions. Each condition was applied four times, resulting in seventy-two trials of 10 s each. The conditions applied in this study are a subset of the conditions presented in a similar study on healthy subjects (Chapter 8). For each condition the magnitude of the torque disturbance was adjusted such that the root-mean-square (RMS) value of the handle angle was approximately 1 degree. The trials were presented in a randomized order to prevent anticipation. The following conditions were applied:

- Wide bandwidth disturbance (WB): a disturbance signal consisting of 20 clusters of 4 sines each, linearly spaced between lowest frequency f_l of 1.4 Hz and highest frequency f_h of 49.4 Hz. ($I_e = 1.6 \text{ gm}^2$, $b_e = 0 \text{ Nms/rad}$, $k_e = 0 \text{ Nm/rad}$). This condition is referred to as the reference condition.
- Narrow bandwidth disturbance type 1 (NB1): disturbance signals with power between a fixed f_l of 1.4 Hz and a variable f_h . f_h varied from 3.1 to 16.5 Hz, i.e. 2 to 13 varying numbers of clusters of 4 sines. ($f_h = 3.1; 4.3; 6.7; 9.1; 11.6; 16.5 \text{ Hz}$). The parameters of the environment are equal to the reference condition.
- Narrow bandwidth disturbance type 2 (NB2): single cluster of 4 sines with a fixed bandwidth of 0.45 Hz around a centre frequency f_c , which varied between 1.6 and 16.2 Hz. ($f_c = 1.6; 4.0; 6.5; 8.9; 11.3; 16.2 \text{ Hz}$). The parameters of the environment are equal to the reference condition.
- Damping: external damping b_e varied between 0.25 and 4 Nms/rad ($I_e = 1.6 \text{ gm}^2$, $b_e = 0.25; 0.5; 1; 2; 4 \text{ Nms/rad}$, $k_e = 0 \text{ Nm/rad}$). The WB disturbance from the reference condition was used as the disturbance.

The signals used as torque disturbances are so-called multisine signals with clustered power spectra (Pintelon and Schoukens, 2001; Schouten et al., 2004a, see Chapter 5). Multisine signals are deterministic signals consisting of a large number of sines. The use of multisine signals as a disturbance improves the estimates for the frequency response functions (FRFs) substantially (Pintelon and Schoukens, 2001; De Vlugt et al., 2003a). By clustering the power and cresting the signal the estimates are further improved. The procedure to construct these signals is given in Schouten et al. (2004a).

To obtain the EMG to torque ratio isometric tasks were performed before and after the trials. During the isometric tasks the motor angle was fixed and the subjects were asked to exert nine predefined torque levels presented in random order (-2.5, -2, ..., 2.5 Nm/rad). During these isometric tasks the reference torque level was shown on the display along with the actual torque level to assist the subject in performing the task.

9.2.4 Data processing

Signal recording and processing

The angle of the manipulator $\theta(t)$, the torque exerted on the handle by the subject $T(t)$, the external torque disturbance applied by the manipulator $d(t)$, and the surface EMG of the m. flexor carpi ulnaris $e_1(t)$ and the m. extensor carpi radialis $e_2(t)$ were recorded with a sample frequency of 2500 Hz and a resolution of 16 bits. Before digitizing the EMG signals were filtered using a 20 Hz high pass filter (third order Butterworth), to remove movement artefacts and DC components, amplified, and filtered using a 1 kHz low pass filter (third order Butterworth), to prevent aliasing. By using only the last 2^{14} samples (≈ 6.55 s) of each record for analysis, initial transient effects were removed.

The EMG signals of the two antagonistic muscles are used (1) to calculate the mean EMG u_0 , as a measure of the cocontraction and (2) to obtain the lumped muscle activation $a(t)$, followin the procedures in Chapter 8.

Nonparametric analysis

For each condition the angle $\theta(t)$, torque $T(t)$, and muscle activation $a(t)$ were averaged over the four repetitions. The signals, including the disturbance $d(t)$ were then transformed to the frequency domain via fast Fourier transform (FFT). The FRFs for the joint admittance $\hat{H}_{T\theta}(f)$ and the reflexive impedance $\hat{H}_{\theta a}(f)$ were estimated by dividing the appropriate spectral densities, see Chapter 8. The joint admittance describes the mechanical behaviour of the human wrist in the frequency domain (ratio of angle and torque per frequency) and comprises the joint inertia, muscle visco-elasticity and proprioceptive reflexes. The reflexive impedance describes the reflexive muscle activity relative to the angular deviations (ratio of EMG and angle per frequency) and only includes proprioceptive reflexes.

Along with the FRFs the coherences for the angle $\hat{\gamma}_{\theta}^2(f)$ and the muscle activation $\hat{\gamma}_a^2(f)$ were estimated. The coherence varies between 0 and 1 by definition,

where a value of 1 indicates that the signal is linearly related to disturbance and noise free.

Quantification of intrinsic and reflexive properties

To obtain the intrinsic and reflexive parameters a model is fitted onto the joint admittance and the reflexive impedance simultaneously, see Chapter 8. The intrinsic model consists of inertia I , intrinsic stiffness k , and intrinsic damping b . The stiffness and damping describe the joint visco-elasticity, including the muscle visco-elasticity resulting from muscle cocontraction. The reflexive feedback is modelled as a feedback gain for position k_p , velocity k_v , acceleration k_a in series with neural time delay τ_d , describing the neural transportation and processing time.

Model validation

To get an impression of the goodness of the model structure and model fit the variance accounted for (VAF) was used. The VAF was calculated for the joint angle VAF_θ and the muscle activation VAF_a as both are available from measurements. To obtain the VAF the model is simulated with the estimated parameters and applied torque disturbance. The angle and muscle activation of the model are compared to the real recordings, see Chapter 8.

Note that a low coherence will always result in a low VAF. Low coherence indicate that nonlinearities and noise are present in the signals. Both effects will also reduce the VAF. A low VAF with a high coherence suggests that the chosen (linear) model structure is inappropriate. A high coherence indicates that the behaviour is linear and so a linear model must exist, but the chosen model structure is not able to fit the observed behaviour.

Statistical analysis

Differences in intrinsic parameters between patients and healthy subjects were evaluated using unpaired two-sample Student's t -tests for samples with unequal variances. Differences for the reflexive parameters were evaluated with 2-way ANOVA. p -values smaller than 0.05 were considered significant.

9.3 Results

9.3.1 Nonparametric FRFs

In Table 9.2 the RMS value for the handle angle and the mean EMG are shown. For both the patients and the subjects the mean EMG is around one indicating that the variation in muscle co-activation over the conditions is small. The deviations of the handle are around 0.8-0.9 degrees for the controls. The higher SD over the parkinsonian subjects shows that the patients had difficulties with the task.

In Fig. 9.1 the joint admittance and the reflexive impedance are shown for the healthy subjects and the parkinsonian patients during the reference condition. The

Table 9.2: The RMS value for the handle angle and the mean EMG u_0 per condition for the healthy subjects and the parkinsonian patients. The values are averaged over the populations (SD).

condition		controls ($n = 12$)		patients ($n = 6$)	
		RMS $_{\theta}$ [°]	u_0 [-]	RMS $_{\theta}$ [°]	u_0 [-]
WB	reference	0.79 (0.15)	1 -	0.96 (0.36)	1 -
b_e	0.25 Nms/rad	0.78 (0.12)	1.07 (0.14)	0.62 (0.09)	0.86 (0.07)
b_e	0.5 Nms/rad	0.83 (0.09)	1.14 (0.13)	0.80 (0.07)	1.01 (0.15)
b_e	1 Nms/rad	0.81 (0.07)	1.17 (0.15)	0.81 (0.12)	1.03 (0.19)
b_e	2 Nms/rad	0.76 (0.09)	1.20 (0.20)	0.72 (0.06)	0.90 (0.15)
b_e	4 Nms/rad	0.60 (0.06)	1.12 (0.16)	0.65 (0.08)	0.93 (0.12)
NB1	3.1 Hz	0.80 (0.17)	1.09 (0.13)	0.99 (0.42)	1.22 (0.28)
NB1	4.3 Hz	0.91 (0.21)	1.09 (0.13)	1.06 (0.51)	1.19 (0.22)
NB1	6.7 Hz	1.01 (0.31)	1.11 (0.13)	1.31 (0.46)	1.19 (0.22)
NB1	9.1 Hz	0.96 (0.17)	0.98 (0.10)	1.11 (0.23)	1.09 (0.16)
NB1	11.6 Hz	0.91 (0.11)	1.01 (0.15)	1.01 (0.28)	1.04 (0.18)
NB1	16.5 Hz	0.88 (0.12)	0.96 (0.15)	0.86 (0.18)	0.97 (0.13)
NB2	1.6 Hz	0.79 (0.21)	1.17 (0.14)	0.74 (0.22)	1.14 (0.27)
NB2	4.0 Hz	0.95 (0.23)	1.02 (0.10)	1.03 (0.41)	1.05 (0.17)
NB2	6.5 Hz	1.10 (0.28)	1.07 (0.16)	1.16 (0.52)	1.16 (0.22)
NB2	8.9 Hz	0.82 (0.17)	0.86 (0.10)	0.71 (0.20)	0.87 (0.15)
NB2	11.3 Hz	0.77 (0.19)	0.92 (0.15)	0.52 (0.07)	0.81 (0.16)
NB2	16.2 Hz	0.76 (0.26)	0.90 (0.22)	0.29 (0.03)	0.72 (0.20)

FRF of the joint admittance comprises the joint inertia, the muscle visco-elasticity and the proprioceptive reflexes. The coherence for the joint angle is high for all frequencies, indicating that the FRF is relevant at all frequencies. For healthy subjects the eigenfrequency of the wrist is approximately 12 Hz, above this frequency the mechanical behaviour is dominated by the inertia. For low frequencies (1-8 Hz) the admittance of the controls is lower, meaning that the controls are stiffer and consequently perform the task better (*'minimize deviations'*). As the inertia does not differ and the stiffness is lower the eigenfrequency is lower in patients.

The FRF of reflexive impedance describes the muscle activation as a result of angular deviation and results from the proprioceptive feedback. The coherence for the muscle activation is low at two frequency ranges. First for the frequencies below 2 Hz, probably the result from (small) voluntary contractions, i.e. drift. Note that the coherence for the joint angle also has its lowest values at these frequencies. Second the coherence gradually decreases for frequencies above 20 Hz. This is likely the result of the decreased power in both the muscle activation and the angular position, i.e. the variation in these frequencies are very small. Consequently noise dominates the recordings at these high frequencies, reducing the coherence.

The increasing gain with frequency in the reflexive impedance show that velocity feedback dominates the proprioceptive feedback. Velocity feedback gives a

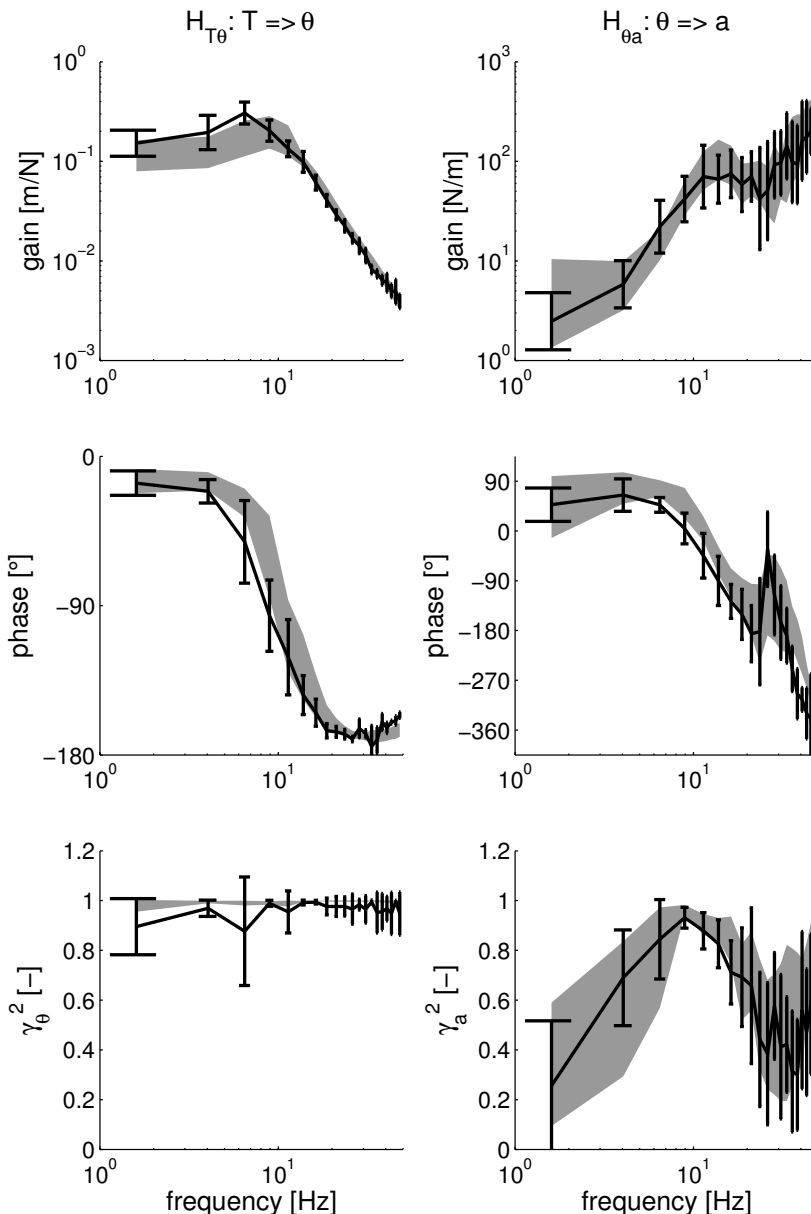


Figure 9.1: Gain and phase of the estimated FRFs of the joint admittance $\hat{H}_{T\theta}(f)$ (left) and the reflexive impedance $\hat{H}_{\theta a}(f)$ (right), and coherences of the angular position $\hat{\gamma}_\theta^2(f)$ (left) and the muscle activation $\hat{\gamma}_a^2(f)$ (right) for the reference condition. The grey area show the mean of the controls (\pm SD) and the black line with error bars denote the mean \pm SD over the patients .

Table 9.3: Quantified inertia, intrinsic damping and stiffness, time delay and reflexive feedback gains during the reference condition. Mean (SD) over the populations. *Italic boldface type indicates a significant difference between patients and controls*

	description	controls ($n = 12$)	patients ($n = 6$)
I [gm^2]	inertia	2.07 (0.03)	2.08 (0.02)
b [Nms/rad]	intrinsic damping	0.086 (0.010)	0.095 (0.028)
k [Nm/rad]	intrinsic stiffness	9.1 (3.2)	6.6 (2.5)
k_a [Nms^2/rad]	acceleration feedback gain	0.009 (0.004)	0.008 (0.003)
k_v [Nms/rad]	velocity feedback gain	0.13 (0.14)	0.11 (0.05)
k_p [Nm/rad]	position feedback gain	0.1 (2.2)	0.0 (0.9)
τ_d [ms]	time delay	42.8 (6.2)	54.6 (8.8)

slope of +1 in the gain and a phase advance of 90 degrees. The neural time delay does not effect the gain, but introduces a phase lag. The phase lag resulting from a delay increases with frequency and the rate depends on the delay. A larger delay will lag the phase more steeply. Remarkable phase lags more steeply in the patients.

The FRFs for the other conditions are not shown (damping, NB1, NB2) as the differences between the condition are better indicated in the estimated parameters.

9.3.2 Intrinsic and reflexive parameters

In Table 9.3 the quantified parameters are given for both the healthy subjects and the patients during the reference condition. In Fig. 9.2 the reflexive parameters are given for all conditions, along with the corresponding VAF values. For readability only the VAF values for the patients are shown in the Figure. The values for the controls are comparable or even better. The coherences for the angular position were generally high, proving that the behaviour was linear and noise free. The VAF values for the angular position were above 90% for all condition, showing that the chosen linear model structure was able to describe the observed behaviour well. The VAF values for the muscle activation are around 50-60% as could be expected for the coherence for the muscle activation. EMG signals contain substantial noise, which reduces both the coherence and the VAF.

To severely reduce the noise in the signals all irrelevant frequencies, i.e. not excited by the torque disturbance, were removed from the measured angle and muscle activation, see Chapter 8. The VAF values for these noise-reduced signals are indicated with grey lines in Fig. 9.2. By removing the irrelevant frequencies the VAF_a increased to values around 60%.

For the inertia, intrinsic damping and stiffness no statistical significant differences emerged. Although the results suggest that intrinsic stiffness is somewhat lower in patients ($p < 0.10$), this is also seen in the joint admittance (Fig. 9.1). The neural time delay for the patients is significantly larger (Student's t -test, $p < 0.02$). This effect is also seen in the phase of the reflexive impedance, see Fig. 9.1. Differences between patients and controls in the reflexive parameters are tested with

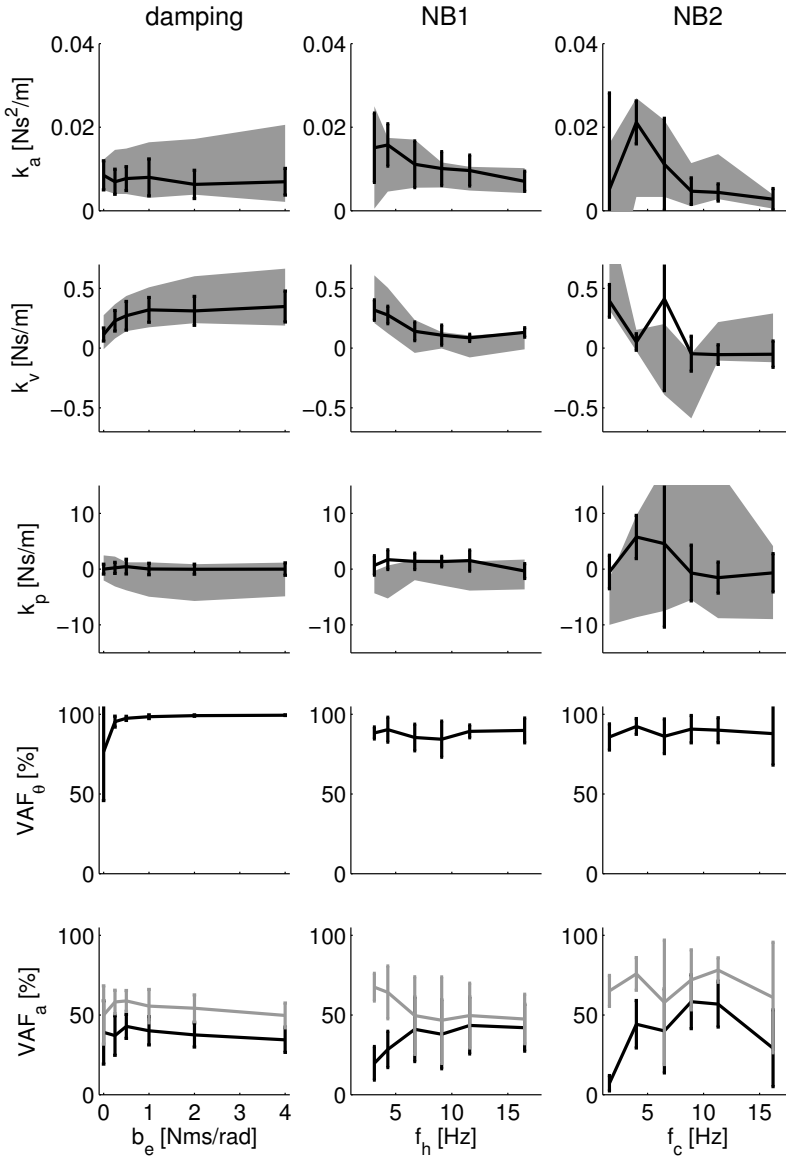


Figure 9.2: Mean quantified reflexive parameters k_a , k_v and k_p and corresponding VAF_θ and VAF_a for the damping environment (left), NB1 disturbances (middle), and NB2 disturbances (right). The grey area denote the mean \pm SD over the controls. The lines denote the means over the patients, error bars denote the SD. Grey lines in the VAFs are the VAFs after noise reduction. For readability the VAFs of the controls are not given. The VAFs for the controls are comparable or have even higher values.

2-way ANOVA. For the damping conditions the trend in both k_a and k_p are significantly different between patients and controls; for NB1 conditions trends in k_p are significantly different. For NB2 conditions no significant differences are expected since the variance on the reflexive parameters is large.

9.4 Discussion

In this study the proprioceptive reflexes at the wrist in patients suffering from Parkinson's disease are assessed with use of the method described in Chapter 8. Both in patients and controls the coherences and VAF values are high, indicating that the method is relevant and applicable. In healthy subjects the magnitude of the reflexes depends on the bandwidth of the torque disturbance and the external damping. In this study these conditions were applied to patients suffering from PD. Despite the small populations (12 controls and 6 parkinsonian patients) it is found that the neural time delay in patients was significantly larger. Furthermore it was found that with external damping the range of modulation of the reflexive feedback gains was confined in patients. Future studies with large groups of patients should focus on the external damping conditions. The number of conditions can be reduced from eighteen in this study to five, substantially experiment time. Damping has an additional advantage that patients with tremor can be assessed as the external damping will reduce the tremor.

Torque perturbations with a position task are a relevant protocol to investigate proprioceptive reflexes. During postural control it is desirable to have a low admittance for all frequencies, to suppress the influence of the torque disturbance onto the deviations. The admittance comprise the joint admittance and the external environment. Both intrinsic properties and proprioceptive reflexes influence the joint admittance. The reflexive impedance is the dynamic relationship between angle and muscle activation, indicating the reflexive activity as a result to the deviations, and describes the proprioceptive reflexes. A high reflexive impedance indicates that the magnitude of the proprioceptive reflexes is high. Strong reflexes also decrease the joint admittance. However the effectiveness of the proprioceptive reflexes is limited by the neural time delays. Feedback with a time delay, like proprioceptive reflexes, an oscillatory peak around the eigenfrequency occurs when the feedback is (too) high. This means that there is a trade-off between low joint admittance for frequencies below the eigenfrequency at the cost of an oscillatory peak at the eigenfrequency. With NB disturbances this peak is not excited and so does not deteriorate the performance. With external damping the peak is damped out by the environment and the increased stiffness remains.

Chapter 10

Analysis of reflex modulation with a biological neural network

Arno H.A. Stienen, Alfred C. Schouten, Frans C.T. van der Helm
Submitted to *Biological Cybernetics*

The neuromusculoskeletal (NMS) model of this study was built to give insight into the mechanisms behind negative position and velocity feedback gains as identified in human postural control. Specifically, neural deficiencies were sought which could explain why complex regional pain syndrome (CRPS) patients with tonic dystonia are unable to set negative gains, although they are still to modulate the gains in the positive range. The model is an integration of a biological realistic neural network (BNN), modelling all relevant spinal neurons, and a one degree-of-freedom (DOF) musculoskeletal model. Muscle proprioceptors provide the neural network with feedback. Literature suggests that the inability to set negative gains results from neurotransmitter deficiencies in inhibiting synapses in the spinal neural network. Two synaptic connections were selected for possible dysfunctioning: (1) the synapse which presynaptically inhibits the monosynaptic stretch reflex synapse, and (2) the synapse connecting the inhibitory interneuron to the motoneuron. A lack of presynaptic inhibition resulted in an overly dominant monosynaptic stretch reflex with high, positive feedback gains. Disabling the second prevented several major proprioceptive feedback paths from providing the motoneurons with negative stimulation, making the setting of negative feedback gains next to impossible. It is concluded that both synapses play an important role in obtaining negative feedback gains and that dysfunctioning of these synapses could account for the motor features in CRPS patients. However the presynaptically inhibiting of the monosynaptic stretch is a prerequisite for feedback gain modulation.

10.1 Introduction

Complex regional pain syndrome (CRPS), also known as reflex sympathetic dystrophy, is a painful condition typically following a minor injury to a limb. The symptoms may include movement disorders (Van Hilten et al., 2001), of which the most common form in patients with CRPS is tonic dystonia (Bhatia et al., 1993; Schwartzman and Kerrigan, 1990). Dystonia is characterised by involuntary muscle contractions forcing the affected limbs into abnormal postures. The mechanisms responsible for tonic dystonia are still unknown, but involvement of inhibiting synapses in the spinal cord was suggested (Van Hilten et al., 2000).

In Van der Helm et al. (2002) a method was developed that allows the quantitative assessment of circuits that modulate the gain of proprioceptive reflexes of the upper extremities during postural control. Force disturbances were applied at the hand while subjects had to '*minimize the deviations*' resulting from the force disturbance. Healthy subjects modulate the magnitude of their reflexes based on the frequency content of the force disturbance. For disturbances containing only frequencies in a small bandwidth around a centre frequency even negative feedback gains were found. However, quantification of reflex gains in CRPS patients with tonic dystonia revealed their inability to achieve negative gains, although modulation of positive gains was still possible (Schouten et al., 2003, see Chapter 3).

Literature concerning the neural mechanisms to generate negative feedback gains is scarce. The goal of this study is to develop a biological realistic neural network (BNN) controlling a musculoskeletal model to find and elucidate mechanisms involved in the setting of negative feedback gains. Dysfunction of such mechanisms could give insight into the pathophysiology of CRPS.

10.2 Method

First, a BNN, modelling all relevant spinal neurons, was integrated with a musculoskeletal model of the human arm with proprioceptors, creating a complete neuromusculoskeletal (NMS) model. The musculoskeletal model consists of a single one degree-of-freedom (1 DOF) limb on which two antagonistic muscles act, representing the shoulder joint in the experimental set-up of Van der Helm et al. (2002) and Schouten et al. (2003). The BNN is based on the model of Bashor (1998). General data for the models for the muscle spindles and Golgi tendon organs were derived from literature.

Second, the NMS model was stimulated by force disturbances in computer simulations. The scheme of the model is given in Fig. 10.1. In the simulations, the force disturbance $d(t)$ acted on the endpoint of the limb resulting in position deviations $x(t)$. The BNN blended tonic supraspinal excitatory commands from the brain and proprioceptive feedback from muscle spindles and Golgi tendon organs into activation signals for both muscles.

Third and finally, the reflex gains were quantified by applying the procedure of Van der Helm et al. (2002). By varying synaptic connection strengths, neural mecha-

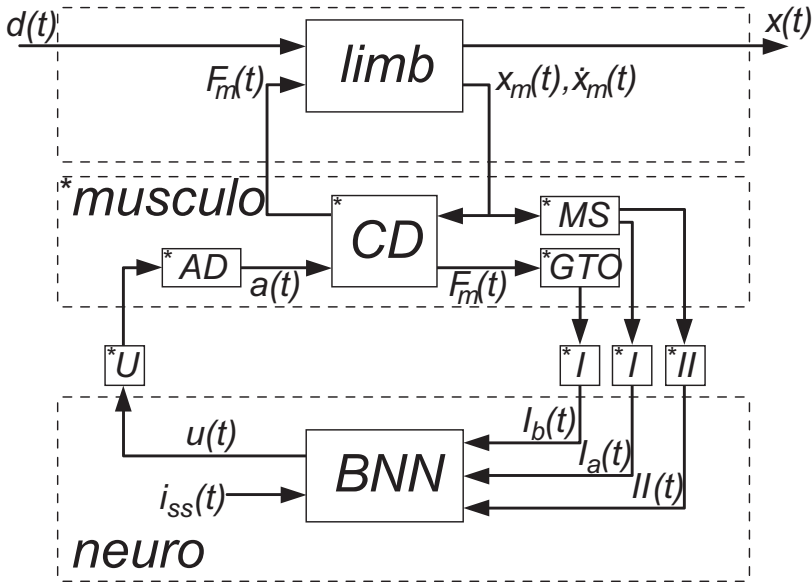


Figure 10.1: Scheme of the NMS model. $d(t)$ external force disturbance which act to the limb; $x(t)$ endpoint position; $i_{ss}(t)$ supraspinal excitatory commands; $F_m(t)$ muscle force from the contraction dynamics (CD); $x_m(t)$ muscle stretch; $\dot{x}_m(t)$ muscle stretch velocity; $u(t)$ motoneuron activation. The muscle spindles (MS) and Golgi tendon organs (GTO) sense the muscle stretch, stretch velocity and force resulting in afferent signals on the $I_a(t)$, $I_b(t)$, and $II(t)$ afferents respectively. These afferent signals require a conduction time τ_I or τ_{II} , depending on the afferent path, before reaching the BNN. After the conduction time $\tau_u(t)$, $u(t)$ reaches the muscle and is converted into the muscle activation $a(t)$ by the activation dynamics (AD). The “*” denotes the necessity to double the components for the flexor and the extensor muscles.

nisms were analysed for their ability to generate or prevent negative feedback gains in the neural network.

10.2.1 Simulation model

Musculoskeletal model

Fig. 10.2 shows the geometrical model representation of the human shoulder for postural control tasks with one limb and two muscles. The model has 1 DOF and comprise a lumped mass m_l of 2 kg on the endpoint of a 0.3 m long limb (l_l), on which two antagonistic muscles (normal length $l_m = 0.3$ m) act with a constant moment arm l_a of 0.04 m (Stroeve, 1999).

The muscles were represented with a second order model with activation a , muscle stretch x_m and stretch velocity \dot{x}_m as inputs. In the reference position, the

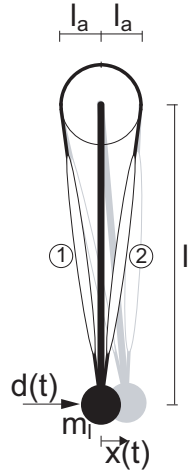


Figure 10.2: Geometrical representation of the 1 DOF model of the human shoulder. The limb with concentrated mass m_l is actuated by two antagonistic muscles, (1) and (2), and disturbed by a force $d(t)$ resulting in the position deviation $x(t)$. The limb length is represented by l_l and the constant moment arm of the muscle force by l_a . The black figure is the limb in equilibrium or reference position; the grey figure is the limb after a small deviation.

stretch is defined as zero. The muscle force $F_m(t)$ is given by:

$$F_m(t) = a(t) (F_{max} + K_m x_m(t) + B_m \dot{x}_m(t)) \quad (10.1)$$

with the maximum contraction force F_{max} of 800 N (Stroeve, 1999), muscle stiffness K_m and damping B_m , and the activation dynamics:

$$\frac{da(t)}{dt} = \frac{-a(t) + u(t)}{\tau_a} \quad (10.2)$$

where τ_a is the muscle activation time constant of 30 ms (Winters and Stark, 1985), $u(t)$ the motoneuron activation, and $a(t)$ the muscle activation. Both $u(t)$ and $a(t)$ are normalised, ranging from 0 to 1.

In the study of (Van der Helm et al., 2002) an endpoint stiffness of 800 N/m and an endpoint damping of 40 Ns/m were found, representing the visco-elastic properties of the (cocontracted) muscles and surrounding tissues. Note that in the musculoskeletal model all the visco-elastic properties are accounted for in the muscles. The above mentioned endpoint values were converted to muscle stiffness K_m and damping B_m . It is assumed that muscle activation is 40% of maximum, resulting in a K_m of 56.3 kN/m and a B_m of 2.81 kNs/m. Abbink (2002) showed that healthy human subjects keep their muscles cocontracting at roughly 40% of maximum contraction during maximum performance postural control tasks. Because this observation required subjects to perform an 'apply maximum force' task and this

task is undesirable and/or impossible for CRPS patients, it was not possible to quantify their activation level in a percentage. However, a constant cocontraction level was observed for different disturbances (Schouten et al., 2003).

Proprioceptors

Vital to any feedback control network is the quality of the sensory input. Prochazka and Gorassini (1998a,b) compared several mathematical models for their ability to predict the firing characteristics of muscle spindle primary afferents recorded chronically during normal stepping in cats. Jankowska and Hammar (2002) argued that the essential properties and organisations of spinal interneuronal systems in cat and man are similar, and therefore relevant cat data and models are used in the NMS model of this study when human data and models are unavailable.

Muscle spindles output muscle length and velocity information via two separate spike train channels: Ia afferent for both length and velocity information (conduction delay $\tau_I = 15$ ms, Winters and Stark (1985)) and the slower II afferent for pure length information ($\tau_{II} = 30$ ms, Winters and Stark (1985)). Two equations are needed to determine the spike rate (in sp/s) for both channels (Prochazka and Gorassini, 1998a,b):

$$I_a(t) = p_m + p_p x_m(t) + p_{v1} \dot{x}_m^{p_{v2}}(t) \quad (10.3)$$

$$II(t) = p_m + p_p x_m(t) \quad (10.4)$$

where $x_m(t)$ is the muscle stretch (in mm) and $\dot{x}_m(t)$ the muscle stretch velocity (in mm/s). The constant p_m represents the mean firing rate and is arbitrarily set to 80 sp/s. The length change constant p_p and velocity constants p_{v1} and p_{v2} scale the length and velocity information. Although Prochazka and Gorassini (1998a,b) kept the p_p at 2 for the Ia afferent channel, in this study it is set to 13.5, equal to their choice for the II afferent channel. This increases the static component of the Ia afferent channel, as is expected for postural control tasks. Values for p_{v1} and p_{v2} (4.3 and 0.6) are claimed to be valid for both humans and cats and therefore used unaltered (Prochazka and Gorassini, 1998a,b).

Golgi tendon organ models are far more scarce, but available literature suggest that the firing rate is linear with the force (Crago et al., 1982). The Ib afferent spike rate output is linear from zero to maximum isometric muscle force:

$$I_b(t) = p_f \frac{F_m(t)}{F_{max}} \quad (10.5)$$

where F_m is the muscle force (in N) and F_{max} the before mentioned maximum muscle force (800 N). With a mean muscle force of 40% of maximum, the Ib afferent output is arbitrarily set to the muscle spindles' firing mean of 80 sp/s, hence giving the constant p_f a value of 200 sp/s.

Biological neural network

Bashor (1998) created a large-scale BNN model to study the dynamic interactions in neuron populations. Bashor calibrated the model by examining its ability to reproduce known aspects of the reflexes, but without linking it to a musculoskeletal model. Here this BNN model is used to control a musculoskeletal model during postural control tasks. Early simulations showed that three adaptations to Bashor's BNN model were required.

Firstly, projections inside neuron population resulted in mass synchronised firing which disrupted the motoneuron to muscle connections. Bashor (1998) noted the synchronised firing and applied a moving average filter (100 ms) before plotting the signals. Disabling the projections inside the neuron population made the neurons less responsive when the neurons are of the excitatory kind, and more when inhibitory. However, model wide behaviour was unaffected by these static gain changes and the disabling largely reduced synchronised firing.

Secondly, the default connection strength to one specific group of interneurons, the inhibitory interneurons (IN, see Fig. 10.3), were too weak to generate any significant background firing on which (downwards) modulation was possible. Increasing all the synaptic connection strengths to the inhibitory interneurons provided a level of background activity comparable to the other interneurons, but did make them more responsive to input changes. Model wide behaviour was unaffected by these adaptations, while the lack of significant firing was eliminated.

And thirdly, there were no II afferent paths, important for the length information feedback from muscle spindles. II afferent paths are polysynaptic and possibly also reciprocally coupled to the motoneurons (Jankowska and Hammar, 2002). A pair of II afferent paths was added including synaptic connections to the Ia and excitatory interneurons (EX). The synaptic connection strengths were made approximately equal to the Ia and Ib afferent connections.

The BNN generates the motoneuron activation $u(t)$ by combining supraspinal excitations $i_{ss}(t)$ and afferent signals from the muscle spindles and Golgi tendon organs. The network consist of motoneurons and several types of interneurons. The motoneurons directly drive the muscles; the interneurons are exciting or inhibiting, possibly recurrent or reciprocal, intermediates for passing the Ia, II, and Ib afferent information received from the proprioceptors on to the motoneurons.

The BNN model (Fig 10.3) consists of a large population of 2298 neurons (Bashor, 1998). The neurons in the model are grouped in six antagonistic population pairs, representing motoneurons (MN, $n = 169$, for both the agonistic and the antagonistic population), Renshaw cells (RC, $n = 196$), and intermediating interneurons (Ia, Ib, inhibitory and excitatory interneurons, abbreviated by IA, IB, IN, EX respectively, $n = 196$ each). Pairs of Ia, II, and Ib afferent ($n = 121$ each) and supraspinal excitation paths ($n = 98$) provide further input to the neurons.

Cell and network algorithms and synaptic mechanism of the BNN are based on the SYSTM22 program using the PTNRN10 neuron model of MacGregor (1987), see also Bashor (1998). The neuron model uses discrete equations with a time-step Δt of 1 ms, based on the following first order differential equations to calculate the

potassium conductance $G_p(t)$ (times resting conductance), the membrane potential $V_m(t)$ (in mV) and the threshold potential $V_t(t)$ (in mV) for every neuron k at time t (in ms):

$$\frac{dG_p^k(t)}{dt} = \frac{-G_p^k(t) + B^{\tilde{k}}S^k(t)}{\tau_r^{\tilde{k}}} \quad (10.6)$$

$$\begin{aligned} \frac{dV_m^k(t)}{dt} = & \frac{-V_m^k(t) + G_p^k(t) \left(V_p^{\tilde{k}} - V_m^k(t) \right)}{\tau_m^{\tilde{k}}} \\ & + \frac{\sum_{\tilde{m}=1}^5 G_i^{k,\tilde{m}}(t) (V_e^{\tilde{m}} - V_m^k(t))}{\tau_m^{\tilde{k}}} \end{aligned} \quad (10.7)$$

$$\frac{dV_t^k(t)}{dt} = \frac{-\left(V_t^k(t) - V_0^{\tilde{k}} \right) + C^{\tilde{k}}V_m^k(t)}{\tau_t^{\tilde{k}}} \quad (10.8)$$

where:

$$\frac{dG_i^{k,\tilde{m}}(t)}{dt} = \frac{-G_i^{k,\tilde{m}}(t) + \sum_{m=1}^{3558} \frac{G_s^{k,\tilde{m},m} S^m(t)}{1 - e^{-\Delta/\tau_s^{\tilde{m}}}}}{\tau_s^{\tilde{m}}} \quad (10.9)$$

and resulting in the spiking output:

$$S^k(t) = \begin{cases} 0 & \text{if } V_m^k(t) < V_t^k(t) \\ 1 & \text{if } V_m^k(t) \geq V_t^k(t) \end{cases} \quad (10.10)$$

where the superscript k denotes the neuron number (out of 2298 network neurons), \tilde{k} the type of neuron (motoneuron, Renshaw cell or general interneuron), m the origin of the synaptic connection to neuron k (out of 3558 neural, afferent or tonic descending sources), and \tilde{m} the type of synaptic connection (ESTC, DESTC, TESTC, ELTC, or ISTC). All potentials are relative to the resting potential of a neuron (≈ -70 mV). See Table 10.1 for the parameter names and values of neurons and synapses and Fig. 10.3 for the synaptic connection strengths and numbers. Conductance change $G_i(t)$ produced by afferent and tonic descending excitation fibre input and cell to cell connections increase or decrease the membrane potential $V_m(t)$. The potential $V_m(t)$ determines the threshold potential $V_t(t)$. When the membrane potential $V_m(t)$ is higher than the threshold potential $V_t(t)$, the cell fires a spike on its output channel $S(t)$ and the potassium conductance $G_p(t)$ rises, creating a refractory period.

The synaptic connections from neural, afferent or tonic descending sources to targeted neuron populations are randomly distributed in these populations in the MacGregor SYSTM22 program. Fig. 10.3 shows the average number of connections a single neurons receives from the projecting population and the type of synapse used to make that connection. Furthermore, the spikes generated by the central nervous system (CNS) and the proprioceptors are randomly distributed to their tonic descending excitation and afferent channels.

Table 10.1: Properties of neuron and synapse types in the PTNRN10 neuron model and SYSTM22 program (MacGregor, 1987) based on Bashor (1998, and personal communications). All potentials are relative to the resting potential of a neuron (≈ -70 mV).

Description		neuron type				
		MN	RC	IA,IB,IN,EX		
B [-]	sensitivity to potassium conductance	70	4	35		
C [-]	threshold sensitivity	0.6	0.7	0.6		
V_0 [mV]	initial threshold	10	10	10		
V_p [mV]	resting potassium potential	-10	-10	-10		
τ_m [ms]	membrane time constant	5	5	5		
τ_r [ms]	refractory time constant	20	3	10		
τ_t [ms]	time constant for accommodation	25	25	25		
		synapse type				
		ESTC	DESTC	TESTC	ELTC	ISTC
G_s [-]	conductance change per transmission	0.01	0.02	0.03	0.01	0.01
V_e [mV]	equilibrium potential for synaptic type	70	70	70	70	-10
τ_s [ms]	time constant for synaptic action	1	1	1	50	1

Normalised muscle activation

The motoneuron activation $u(t)$ provides the input for the muscle activation dynamics, and is constructed by taking the average output over the motoneurons in either the agonistic or antagonistic population and then applying a moving average filter (20 ms) to smooth the signals. The motoneuron output requires a conductance time τ_u of 10 ms before it reaches the muscle activation dynamics (Winters and Stark, 1985).

With a tonic supraspinal excitatory input of 80 sp/s, the motoneurons have an mean firing rate of 25 sp/s, the Renshaw cells 100 sp/s and the interneurons from 15 to 40 sp/s. These firing rates are biologically realistic, while allowing for both up- and downwards variations. The average 25 sp/s output firing rate of the motoneurons is therefore set to equal the 40% of maximum activation into the muscle activation model (see Sec. 10.2.1).

Mono-, di- and trisynaptic feedback paths

The proprioceptive information reaches the motoneurons directly or via one or more intermediating interneurons. These paths can be classified by the number of synaptic connections. For instance, the monosynaptic stretch reflex includes the Ia

Table 10.2: Mono-, di- and trisynaptic paths in the BNN (see Fig. 10.3). Ia, Ib and II denote the type of afferent (first column: aff.), MN, RC, IA, IB, IN and EX the type of neuron (nrn.), and e.. and i.. the synaptic type of the connection (syn.), respectively excitatory and inhibitory, together with the synapse identifying number. A \rightarrow corresponds to a connection within the agonistic or antagonistic populations, whereas a \Rightarrow represents a connection from the agonistic to the antagonistic populations or vice versa. The last column (stimulus) indicates whether the stimulation on the motoneuron will be positive or negative.

aff.	syn.	nrn.	syn.	nrn.	syn.	nrn.	stimulus
monosynaptic feedback path							
Ia	$\xrightarrow{e5}$	MN					positive
disynaptic feedback paths							
Ia	$\xrightarrow{e14}$	IA	$\xrightarrow{i2}$	MN			positive
Ia	$\xrightarrow{e20}$	IN	$\xrightarrow{i3}$	MN			negative
Ib	$\xrightarrow{e21}$	IN	$\xrightarrow{i3}$	MN			negative
II	$\xrightarrow{e15}$	IA	$\xrightarrow{i2}$	MN			positive
II	$\xrightarrow{e23}$	EX	$\xrightarrow{e4}$	MN			positive
trisynaptic feedback paths							
Ia	$\xrightarrow{e14}$	IA	$\xrightarrow{i10}$	RC	$\xrightarrow{i1}$	MN	negative
Ia	$\xrightarrow{e14}$	IA	$\xrightarrow{i13}$	IA	$\xrightarrow{i2}$	MN	positive
Ia	$\xrightarrow{e17}$	IB	$\xrightarrow{e19}$	IN	$\xrightarrow{i3}$	MN	negative
Ia	$\xrightarrow{e17}$	IB	$\xrightarrow{e22}$	EX	$\xrightarrow{e4}$	MN	negative
Ib	$\xrightarrow{e18}$	IB	$\xrightarrow{e19}$	IN	$\xrightarrow{i3}$	MN	negative
Ib	$\xrightarrow{e18}$	IB	$\xrightarrow{e22}$	EX	$\xrightarrow{e4}$	MN	negative
II	$\xrightarrow{e15}$	IA	$\xrightarrow{i10}$	RC	$\xrightarrow{i1}$	MN	negative
II	$\xrightarrow{e15}$	IA	$\xrightarrow{i13}$	IA	$\xrightarrow{i2}$	MN	positive

afferent channel coming from the muscle spindles and goes directly to the motoneurons, thereby crossing only one synapse. All available mono-, di- and trisynaptic paths in the spinal reflex model are given in Table 10.2. Information from the afferents reaches the motoneurons over many paths. Note that for this network the direct influence decreases with the number of synapses due to information dilution. Therefore paths which cross more than three synapses are ignored.

Whether the paths provide positive or negative stimuli to the motoneurons is another interesting aspect. The total stimulation effect of the path on the motoneuron is given in Table 10.2. Positive stimulation of an agonistic afferent means that the activation of the agonistic motoneuron increases relative to antagonistic motoneuron, either by increased activation of the agonistic motoneurons or de-

creased activation of the antagonistic motoneurons. Crossing one reciprocal or one inhibitory synapse will make the stimulus negative; crossing another makes the stimulus positive again.

Dysfunctional mechanism candidates

To investigate whether inhibitory neurotransmitter deficiencies can prevent the setting of negative feedback gains (Van Hilten et al., 2000; Jankowska and Hammar, 2002), two inhibiting synaptic connections are selected for possible disfunctioning.

The primary candidate is the synapse that presynaptically inhibits the monosynaptic stretch reflex, caused by a specific neurotransmitter deficiency. Stein and Capaday (1988), amongst others, suggested that this presynaptic inhibition is the main neural mechanism to modulate the strength of the stretch reflex. In the BNN of the present study, the effect of presynaptic inhibition is simulated by directly modulating the strength of the synapse of the monosynaptic stretch reflex (see Fig. 10.3, synapse $e5$). When presynaptic inhibition is high, this synaptic strength is low and vice versa.

Any other type of neurotransmitter could be deficient too. Therefore a second candidate is selected for its ability to disable some, but not all, di- or trisynaptic feedback paths. Some further assumptions are needed. Firstly, the presynaptic inhibition is assumed to be functional and therefore the monosynaptic stretch reflex synapse can be set to a strength of 0 (when presynaptic inhibition is at its maximum), disabling the existing dominance of the monosynaptic stretch reflex connection (see Results). Secondly, negative feedback gains can only be achieved by negatively stimulating feedback paths in the neural network. Therefore, a dysfunctional synapse should normally be guiding many more negative than positive stimuli. Giving the synapse between the inhibitory interneuron and motoneuron (synapse $i3$, see Fig. 10.3) a strength of 0 disables both the disynaptic negatively stimulating paths and two out of six trisynaptic negatively stimulating paths, leaving three disynaptic positively stimulating paths, two trisynaptic positively stimulating paths and four trisynaptic negatively stimulating paths still working (see Table 10.2).

Together they might shed light on ‘the problem of the relative importance of the deficient inhibition of α -motoneurons as one of the main causes of the hyperexcitability of these [motoneurons]’ (Jankowska and Hammar, 2002).

10.2.2 Procedures

The two candidates are tested by gradually increasing the monosynaptic stretch reflex synapse $e5$ (i.e. reducing the presynaptic inhibition) from simulation to simulation between 0 to 3 times the default strength in steps of 0.25, while the synapse between the inhibitory interneuron and motoneuron ($i3$) is either normal or disabled. For each setting, the NMS model is simulated with a force disturbance applied to the endpoint of the limb and the resulting position deviations are recorded. The reflexive feedback gains are estimated by fitting a linear model to allow com-

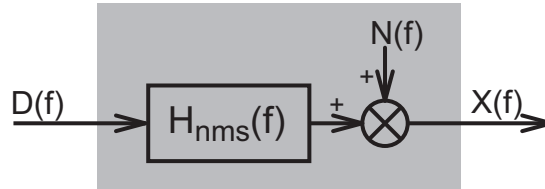


Figure 10.4: Block scheme of human postural control expressed in the frequency domain. $H_{nms}(f)$: transfer function of the dynamics of the NMS model; $D(f)$: external force disturbance; $X(f)$: skeletal bone endpoint position; $N(f)$: model remnant. The NMS dynamics (grey box) are described by the linear transfer function $H_{nms}(f)$, together with the remnant $N(f)$, which is uncorrelated with $D(f)$.

parisons with experimental results of Van der Helm et al. (2002) and Schouten et al. (2003).

Disturbance signal

The force disturbances $d(t)$ used in this study are continuous wide-bandwidth signals, with a length of 9 s, a uniform power distribution between 0.6 Hz and 20 Hz and a random phase. The signals are designed in the frequency domain, inverse fast Fourier transformed to time domain and then stored to be used for all synaptic set-ups. To allow linear model approximations, the force signal is scaled such that the root-mean-square (RMS) of the endpoint position is around 5 mm.

Data recording and processing

The force disturbance $d(t)$ and position deviation $x(t)$ are sampled at 1 kHz. From the 9 s over which each realisation is simulated, only the last 8192 samples are used. This removes any transient response coming from the NMS model. The signals are transformed to the frequency domain by fast Fourier transform (FFT) and the frequency response function (FRF) for the joint admittance $\hat{H}_{nms}(f)$ of the NMS model (see Fig. 10.4) is estimated from the appropriate spectral densities.

$$\hat{H}_{nms}(f) = \frac{\hat{G}_{dx}(f)}{\hat{G}_{dd}(f)} \quad (10.11)$$

where \hat{G} denotes the auto ($\hat{G}_{dd}(f)$, $\hat{G}_{xx}(f)$) and cross ($\hat{G}_{dx}(f)$) spectral densities (hat denotes estimate). To improve the estimate and to reduce the variance of the estimators, each setting is simulated eight times with eight different disturbance realisations. The spectral densities resulting from these eight realisations are then averaged, whereafter another improvement of the estimate is achieved by averaging the spectral densities over four frequency bands (Jenkins and Watts, 1968). After the averaging step, the spectral densities have a frequency resolution of $\frac{4}{8.192s} \approx 0.49$ Hz

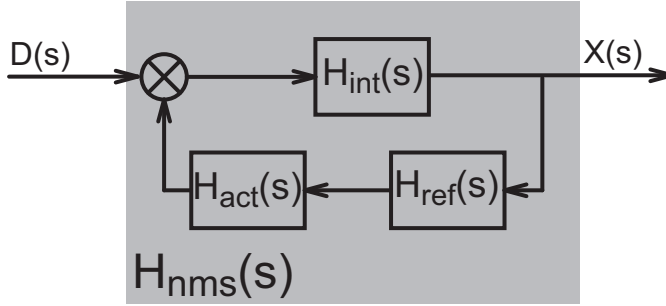


Figure 10.5: Block scheme of the linear arm model of which the transfer function $H_{nms}(s)$ is derived. $D(s)$: external force disturbance; $X(s)$: skeletal bone endpoint position; $H_{int}(s)$: intrinsic (muscle) dynamics; $H_{ref}(s)$: reflexive dynamics; $H_{act}(s)$: muscle activation dynamics.

As a measure for the reliability of the estimated FRF the coherence is estimated:

$$\hat{\gamma}^2(f) = \frac{|\hat{G}_{dx}(f)|^2}{\hat{G}_{dd}(f)\hat{G}_{xx}(f)} \quad (10.12)$$

By definition the coherence ranges between 0 and 1. A coherence of 1 at a specific frequency means that a linear relationship exists between the signals and the measurements contains no noise or nonlinearities at that frequency. Possible causes of low coherence must be found in nonlinearities in the BNN.

Fitting the linear model

Fitting a linear arm model on the estimated FRF of the joint admittance $\hat{H}_{nms}(s)$ quantifies the feedback gains in the linear model. These gains can then be compared with the results of Van der Helm et al. (2002) and Schouten et al. (2003).

In the study of Van der Helm et al. (2002) a linear model is developed to describe the joint admittance (see Fig. 10.5). The muscle visco-elasticity (including cocontraction) and the limb mass are described by a mass-spring-damper system, $H_{int}(s)$:

$$H_{int}(s) = \frac{1}{ms^2 + bs + k} \quad (10.13)$$

with mass m , intrinsic damping b , and intrinsic stiffness k . The Laplace operator s equals $\lambda + j2\pi f$ where $\lambda = 0$ because the initial transient response in the first second of simulation is removed from the recordings. The reflexive feedback is described by feedback gains for position k_p , velocity k_v , and acceleration k_a in series with a neural time delay τ_d .

$$H_{ref}(s) = (k_a s^2 + k_v s + k_p) e^{-\tau_d s} \quad (10.14)$$

The muscle activation dynamics are modelled as a first order process $H_{act}(s)$ with activation time constant τ_a .

$$H_{act}(s) = \frac{1}{\tau_a s + 1} \quad (10.15)$$

Combining above equations gives the complete linear arm model, $H_{nms}(s)$:

$$\begin{aligned} H_{nms}(s) &= \frac{X(s)}{D(s)} = \frac{H_{int}(s)}{1 + H_{int}(s)H_{ref}(s)H_{act}(s)} \\ &= \frac{1}{ms^2 + bs + k + (k_a s^2 + k_v s + k_p) \frac{e^{-\tau_d s}}{\tau_a s + 1}} \end{aligned} \quad (10.16)$$

In this study the values for the intrinsic properties, neural time delay and activation dynamics are a priori known. The reflex gains (k_a , k_v , k_p) are quantified by fitting the FRF of the joint admittance $\hat{H}_{nms}(s)$ (Eq. 10.11) on the linear arm model H_{nms} (Eq. 10.16), while keeping the intrinsic parameters, neural time delay and time constants fixed ($m = 2$ kg, $b = 40$ Ns/m, $k = 800$ N/m, $\tau_d = 25$ ms, $\tau_a = 30$ ms). To fit the linear model on the measured data, the following criterion function is minimised:

$$L(p) = \sum_k \hat{\gamma}^2(f_k) |\ln \hat{H}_{nms}(f_k) - \ln H_{nms}(f_k, p)|^2 \quad (10.17)$$

where k indexes the frequency vector f_k , and p is the parameter vector (k_p , k_v , k_a). The criterion function is evaluated over the bandwidth of the disturbance signal. Because the FRFs have a large range of gain logarithmic differences are used (Pintelon et al., 1994).

Linear model validation

The variance accounted for (VAF) is calculated to give an indication of the goodness of the model fit, where the maximum VAF score of 1 indicates that the observed behaviour is completely described by the linear model.

$$\text{VAF} = 1 - \frac{\sum_{i=1}^n |x(t_i) - \hat{x}(t_i)|^2}{\sum_{i=1}^n |x(t_i)|^2} \quad (10.18)$$

where i indexes the sampled time vector. $x(t_i)$ is the simulated output of the NMS model. $\hat{x}(t_i)$ is the forward simulated skeletal endpoint position using the original disturbance signals, the linear arm model and the estimated feedback parameters.

10.2.3 Tools and languages

The NMS model was developed using Matlab (© 2003 The MathWorks). All Fortran code in the SYSTM22 program (MacGregor, 1987) was translated to Matlab code, as were the proprioceptor models. Simulating a single run of the NMS model took roughly ten times the simulation length on a 900 MHz Windows (© 2003 Microsoft) machine, so a 9 s simulation run took 90 s in real time. Note that each neural network set-up was simulated eight times, therefore taking 12 minutes to complete.

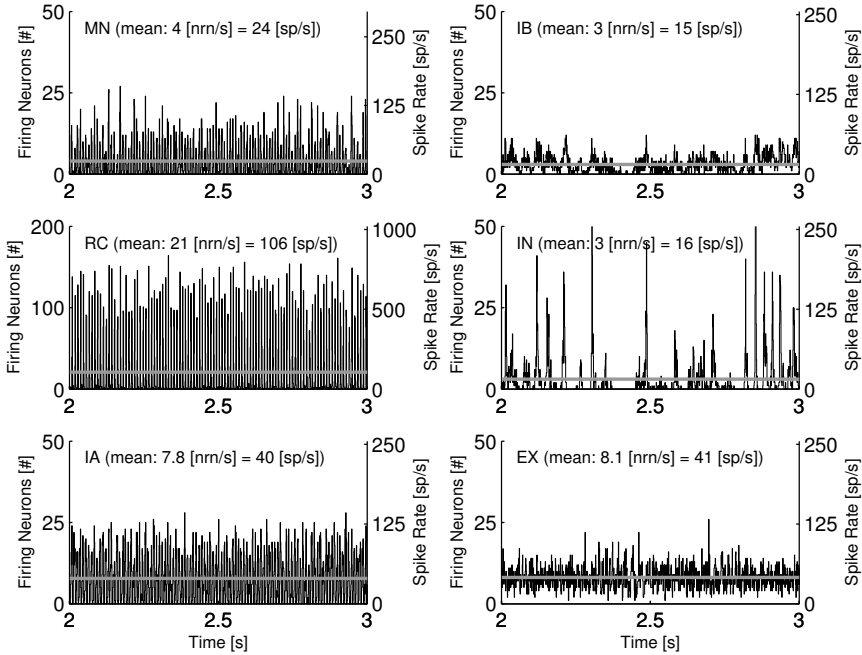


Figure 10.6: Typical neuron activity for the six agonistic neuron populations. Left y-axis: number of neurons firing a spike; right y-axis: related spiking frequency, averaged over the population. The grey horizontal lines indicates the number of neurons firing a spike and the spiking frequency, averaged over the entire simulation run. The signals were recorded on the flexor side of the BNN during a single simulation with the default BNN setting. To improve readability, only a single second of the simulation is plotted.

10.3 Results

Typical neuron activity during the default BNN setting is given in Fig. 10.6. Typical muscle stretch, stretch velocity and muscle force signals together with the resulting II, Ia and Ib afferent activity are given in Fig. 10.7.

10.3.1 Presynaptic inhibition candidate

By increasing the connection strength of the monosynaptic stretch reflex synapse (synapse $e5$), a decrease of presynaptic inhibition on this synapse was simulated. Fig. 10.8 gives the input force disturbance and output endpoint position deviation of three presynaptic inhibition settings (0, 1.5, and 3 times default strength). With increasing synaptic strength (decreasing synaptic inhibition) the deviation amplitude decreases, i.e. the stiffness increases, while high-frequency oscillations appear (dashed line). Fig. 10.9 gives the FRF for the joint admittance and the coherence for the same three settings. Increasing synaptic strength decreases the admittance at

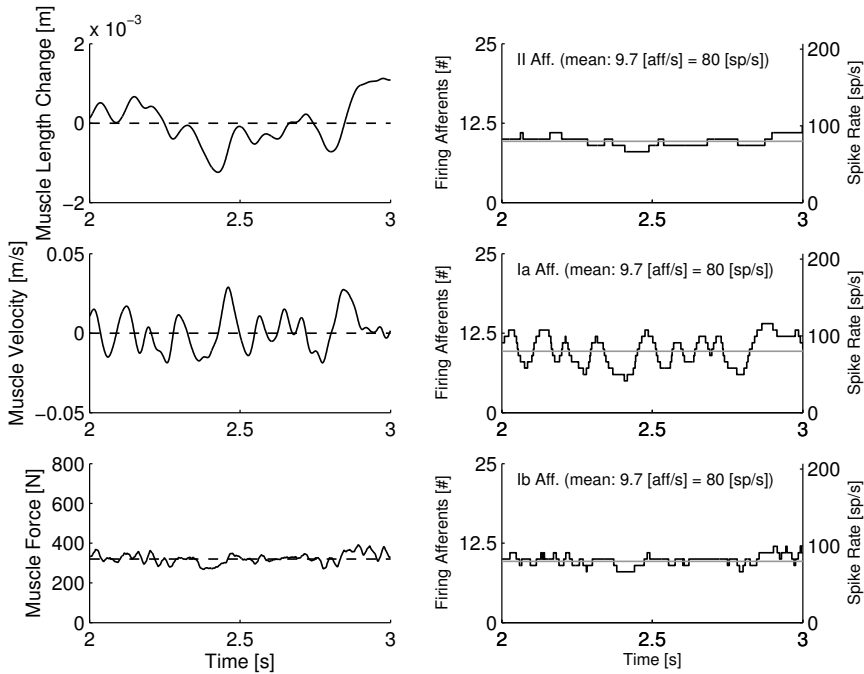


Figure 10.7: Typical muscle stretch, stretch velocity and muscle force signals (left plots) and the resulting II, Ia and Ib afferent activity (right plots). Dashed line indicates the average signal. The signals were recorded on the flexor side of the BNN during a single simulation with the default BNN setting. To improve readability, only a single second of the simulation is plotted.

low frequencies (increased stiffness), while a peak in the gain at the eigenfrequency appears (oscillations).

Plotting the results for the thirteen presynaptic inhibition settings displays a clear rising trend for all three feedback gains (Fig. 10.10, black lines), with negative gains for low synaptic strengths and thus for high presynaptic inhibition. This plot shows that modulation of the feedback gains in a healthy subject is possibly by the presynaptic inhibition mechanism, and even negative gains are achievable. Furthermore it appears that all three feedback gains increase simultaneously with the strength of the monosynaptic stretch reflex.

10.3.2 Alternative deficiency candidate

To verify the importance of negatively stimulating feedback paths for achieving negative feedback gains, the procedure of simulating presynaptic inhibition on the monosynaptic stretch reflex synapse was repeated. This time, the main supplier of negative stimulation, the synapse between the inhibitory interneuron and the

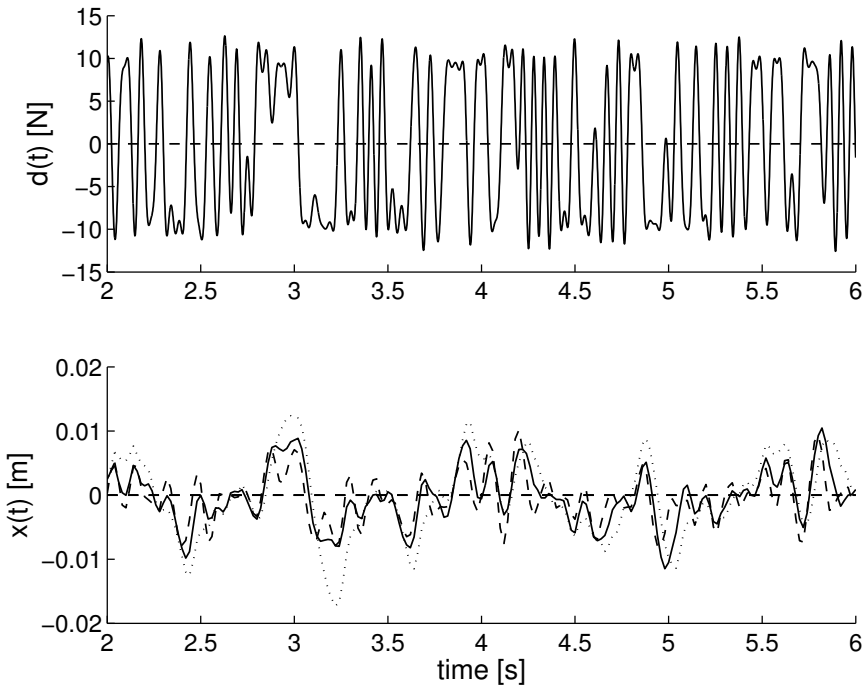


Figure 10.8: Force disturbance (above) and endpoint position displacement (below) of three different simulation runs. Monosynaptic stretch reflex synaptic strengths of 0 (dotted), 1.5 (solid) and 3 (dashed) times the default synaptic strength, simulating decreasing presynaptic inhibition on this synapse. To improve readability, only 4 s of a simulation are plotted.

motoneuron (synapse $i3$), was disabled. Plotting for the presynaptic inhibition settings again displays a clear rising trend for all three feedback gain types (Fig. 10.10, grey lines). However, the negative feedback gains are unreachable, even at high presynaptic inhibition. Restricted feedback modulation by the presynaptic inhibition mechanism was still possible.

10.4 Discussion

The NMS model of this study was built to better understand the mechanisms behind the negative position and velocity feedback gains as identified in human posture control (Van der Helm et al., 2002). The model is an integration of a BNN based on Bashor (1998) into an one DOF musculoskeletal model derived from human shoulder studies (Stroeve, 1999; Van der Helm et al., 2002; Schouten et al., 2003). Muscle proprioceptors obtained from the comparative studies of Prochazka and Gorassini (1998a,b) provide the neural network with muscle length, velocity and

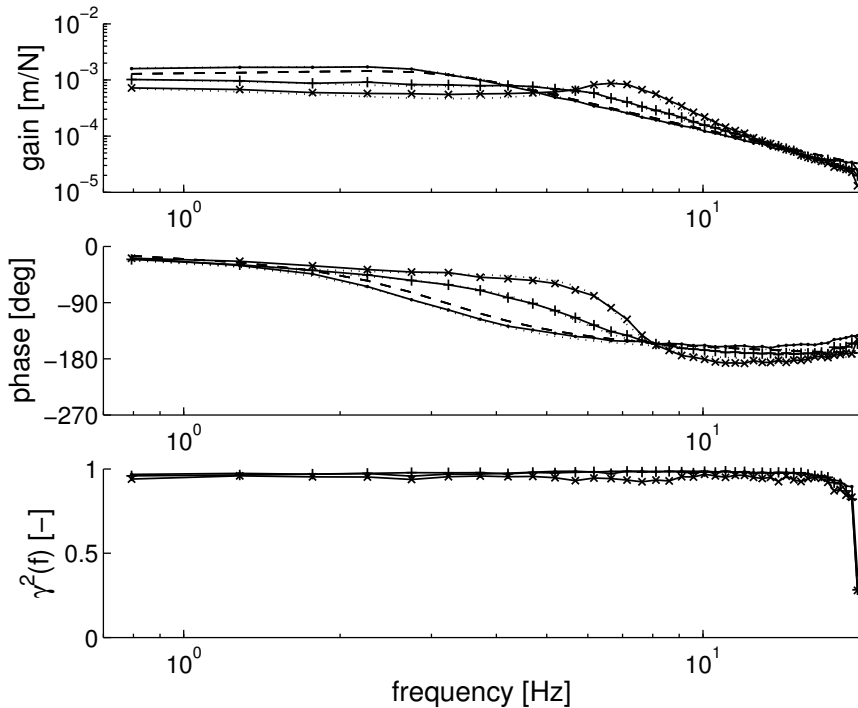


Figure 10.9: Gain (above), phase (middle) of the joint admittance, and the coherence $\hat{\gamma}^2(f)$ (below). Monosynaptic stretch reflex synaptic strengths of 0 (dots), 1.5 (pluses) and 3 ('x'-marks) times the default synaptic strength, simulating decreasing presynaptic inhibition on this synapse. Solid line: simulation; dotted line: linear model fit; and dashed line: simulation without afferent feedback.

force feedback from the musculoskeletal model.

Schouten et al. (2003) observed the inability of CRPS patients with dystonia to set negative feedback gains even though optimal posture control dictates these gains as desirable (Schouten et al., 2001; De Vlugt et al., 2001). However, the patients were still able to modulate the positive feedback gains (Schouten et al., 2003). Suggestions that the inability to set negative gains is due to neurotransmitter deficiencies of inhibitory interneurons in the spinal neural network (Van Hilten et al., 2000; Jankowska and Hammar, 2002) were investigated in this study.

The primary candidate for involvement in the negative feedback gains was the synapse which presynaptically inhibits the monosynaptic stretch reflex synapse. Stein and Capaday (1988) and others suggested that this presynaptic inhibition is the main neural mechanism to modulate the strength of the stretch reflex. A neurotransmitter deficiency here could disrupt the modulation (see Sec. 10.4.2).

A second candidate was selected for its ability to disable some, but not all, di- or trisynaptic feedback paths, possibly preventing negative feedback gains from being

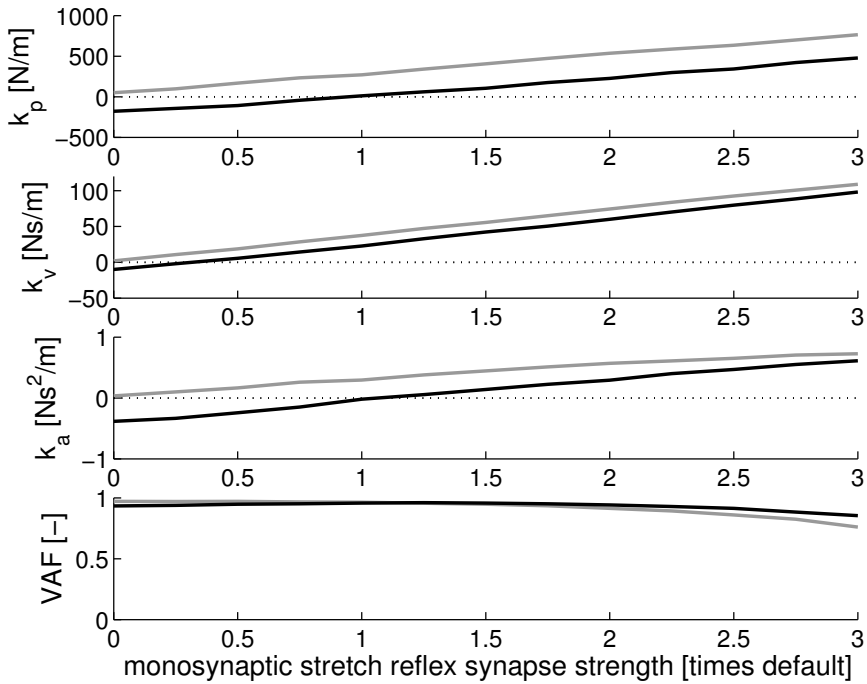


Figure 10.10: Feedback gain values for the position (k_p), velocity (k_v) and acceleration (k_a), together with the VAF scores, plotted against the monosynaptic stretch reflex synapse strength (relative to default strength). By increasing the monosynaptic stretch reflex synapse strength, a decreasing presynaptic inhibition is simulated; for maximum presynaptic inhibition, the monosynaptic stretch reflex synapse strength is 0. Black lines: normal situation; grey lines: pathological situation, synapse i_3 was disabled.

achievable by presynaptic inhibition of the monosynaptic stretch reflex synapse. The synapse connecting the inhibitory interneuron to the motoneuron fitted the profile, as it guides many more negative than positive stimuli and these negative stimuli are essential for the generation of the negative feedback gains (see Sec. 10.4.3).

10.4.1 Model verifications

Validating the NMS was restricted by the unavailability of biological data for the components. The approach used here was to keep all parameters within biological supposed correct boundaries while verifying the components in black-box simulations where possible. Bashor (1998) summarised that his large-scale spinal segmental model, mainly based on cat data, produced predictable reflex responses when compared with stretch and Golgi tendon organ reflexes studies, and behaviours such as agonist excitation and reciprocal inhibition were both predictable and ex-

pected. The proprioceptors derived from the comparative analysis in Prochazka and Gorassini (1998a,b) were reported to give a good prediction of the firing characteristics of muscle spindle primary afferents recorded chronically during normal stepping in cats, with the key variable in achieving good predictions being muscle velocity. The problem of whether the above studies are valid for a human model was addressed by Jankowska and Hammar (2002). Their general impression arising from results of studies on human and cat reflex interneuronal systems was that these systems have more features in common than differing. They hypothesised that not only the properties investigated so far, but also other basic properties of human spinal interneurons, such as their membrane properties and their sensitivity to various chemical compounds, are similar to those found in the cat.

The available black-box verifications for this NMS model do not suggest any abnormalities. Fig. 10.6 and Fig. 10.7 show that neuron firing rates stay within biological plausible boundaries, and, as can be seen in the following sections, changing parameters in the BNN mechanisms produces many wanted or unwanted states, but all with counterparts as observed in human subjects. The presumption that feedback gains can be controlled by presynaptic inhibition on the monosynaptic stretch reflex synapse (Stein and Capaday, 1988) was corroborated with the results for the normal situation in Fig. 10.10. Therefore the assumption is made that the model of this study is indeed valid for interpreting human postural control behaviour.

The spike based signals in the BNN may not have to contain the same frequency information as continuous time signals do. This was explored in Appendix A, but no differences were found in the frequency ranges used for the force disturbances (0-20 Hz).

10.4.2 Presynaptic inhibition candidate

Fig. 10.10 shows that to achieve negative feedback gains for position and velocity information, a high presynaptic inhibition of the monosynaptic stretch reflex synapse (synapse $e5$ in Fig 10.3) is required, disabling the transfer from the Ia afferents to the motoneurons. The weaker this connection, the lower the feedback gains and vice versa. In effect, the high presynaptic inhibition disables the dominant monosynaptic stretch reflex path and allows negatively stimulating paths in the BNN to achieve the negative feedback gains. Therefore a dysfunctional presynaptic inhibition in CRPS patients with dystonia, can indeed prevent them from achieving the required negative feedback gains necessary for specific postural control tasks. However, a completely disabled presynaptic inhibition also severely disables the modulation of feedback gains, which contradicts with the results on CRPS patients with dystonia of Schouten et al. (2003): these patients are still able to modulate their feedback gains in the positive range.

10.4.3 Alternative deficiency candidate

Presynaptic inhibition on its own does not cause the negative feedback gains, it can just prevent the monosynaptic stretch reflex from being dominant over other feed-

back paths in the BNN. Therefore, other paths must be present which do provide negative stimulation to the motoneuron.

By identifying all present mono-, di- and trisynaptic paths (see Table 10.2), and classifying them as either positively or negatively stimulating, it was clear that the main paths for negative stimulation all pass the inhibitory interneuron (IN), and thereby the synapse between this interneuron and the motoneuron (synapse *i3* in Fig. 10.3). Although other synapses convey negatively stimulating feedback, none are both disynaptic and coming from the Ia afferent channel. These last two conditions are important because: (a) every synaptic connection a path has to cross dilutes the information with information coming from other paths, and (b) the Ia afferent information has a stronger amplitude compared to the two other afferent channels (see Fig. 10.7).

Disabling the synapse between the inhibitory interneuron and the motoneuron, should prevent negative feedback gains. Fig. 10.10 shows that even with maximum presynaptic inhibition, the identified position and velocity feedback gains did not become negative. Therefore it is concluded that a dysfunctional synapse in an (important) negatively stimulating feedback path, likely the result of a neurotransmitter deficiency, can prevent the setting of negative feedback gains. Modulation of the positive feedback gains is still possible by the regular control of presynaptic inhibition on the monosynaptic stretch reflex synapse.

10.4.4 Conclusion

This study shows that: (a) both the monosynaptic stretch reflex synapse and the synapse between the inhibitory interneuron and the motoneuron, play an important role in obtaining negative feedback gains and that disfunctioning of these synapses could account for the previously unexplainable feedback gain quantification results for healthy subjects and CRPS patients, and (b) a disabled synapse between the inhibitory interneuron (IN) and the motoneuron would still allow limited feedback gain modulation.

Chapter 11

Reflections

11.1 Introduction

The prime goal of this project was to get insight into the pathophysiology of neurological disorders with abnormal muscle tone. This goal was met by quantification of proprioceptive reflexes during posture tasks *in vivo*. The reflex gains were parametrised by fitting a model onto the mechanical response after continuous force perturbations. Previous studies showed that the magnitude of the reflexes modulate with task and conditions (Van der Helm et al., 2002; De Vlugt et al., 2002). One of the objectives was to investigate the feasibility of the application of the methods to patients with neurological disorders. This thesis shows that the methods are relevant, as reflexes can be reliably estimated in patients with neurological disorders.

Abnormal high muscle tone, or hypertonia, (described as dystonia, rigidity, or spasticity) is seen in many neurological disorders and is often associated with an exaggerated sensitivity of the stretch reflexes. Although many studies measured reflexes this thesis is one of the first to *quantify* proprioceptive reflexes in patients with hypertonia *in vivo*. The major advantage of the methods presented in this thesis is that reflexes are assessed during an unambiguous and relevant task: force perturbations are applied and subjects were asked to '*minimize the deviations*'. Many studies seem to ignore the fact that task instruction and conditions influence reflex magnitude.

Quantifying proprioceptive reflexes in terms of position and velocity sensitivity contributes to the understanding of human motion control. And quantification of reflexes in patients with hypertonia gives insight in pathophysiology of the disorders. The methods are relatively new and strongly based on control engineering techniques. The quantification method and manipulator described in this thesis could be standard diagnostic tools for neurological departments. The wrist manipulator can be a prototype for the diagnostic devices of the future.

11.2 Results and conclusions

No negative feedback gains in CRPS patients with tonic dystonia

One of the main findings of this thesis is that CRPS patients with tonic dystonia are unable to modulate negative feedback gains (Chapter 3), while modulation in the positive range is still possible. In healthy control subjects and CRPS patients without tonic dystonia negative feedbacks were found when specific force disturbances with power in a small bandwidth around a centre frequency were applied. Theoretical studies have shown that negative feedback gains are optimal for these conditions (Schouten et al., 2001; De Vlugt et al., 2001). Although dystonia in the evaluated CRPS patients mainly affected the distal musculature, the results indicate involvement of the proximal musculature as well. Dystonia of CRPS generally progresses in the extremities from distal to proximal musculature (Schwartzman and Kerrigan, 1990). This suggests that, despite that the musculature of the whole upper extremity is affected, the dystonia will present first in the distal musculature

and develops to proximal as CRPS progresses. Note that the neural time delay of the spinal reflex is larger for distal joints, as the neural delay of the spinal reflex is directly related to the length of the feedback path. Larger time delay gives smaller stability margins, and consequently instabilities caused by exaggerated reflex magnitude will present first in distal joints.

The inability to modulate negative reflex gains raises the question which neural mechanism(s) is(/are) responsible for negative feedback gains at all. Positive feedback gains result primarily from monosynaptic feedback of muscle spindle afferents to motoneurons. The magnitude of the afferent information can be reduced by presynaptic inhibition, decreasing the feedback gains (Stein and Capaday, 1988). The neural mechanism for negative feedback gains must have either an inhibitory effect on the agonistic motoneuron (autogenic inhibition), an excitatory effect on the antagonistic motoneuron (reciprocal excitation), or both. Literature describing the aforementioned paths are scarce; one elaborate review mentioned only the interneuronal circuits that mediate postsynaptic inhibition of the motoneuron (Jankowska, 1992). To get insight into the neural mechanisms responsible for negative feedback gains a neuromusculoskeletal model was built, based on a biological realistic neural network (BNN) containing all relevant spinal neurons (Chapter 10). With such a BNN the effect of impairment of specific neural mechanisms and connections were investigated to explore the mechanism(s) behind negative reflex gains. The BNN contains several populations of interneurons and many connection between these populations and the motoneurons. Analysis of the BNN model revealed that the connection from the inhibitory interneuron to the motoneuron mediates many inhibitory paths to the motoneuron. Disabling the synapses of these inhibitory interneurons to the motoneurons, removed the possibility to generate negative feedback gains.

Incorporation of the reflexive impedance improves the method

In the first chapters of this thesis, spinal reflexes were quantified by fitting a model onto the mechanical admittance during disturbance experiments. The mechanical admittance comprises intrinsic muscle visco-elasticity and reflexive contributions. Assumptions on the intrinsic and reflexive component were necessary to separate the individual contributions. The estimation of the reflexive impedance (dynamic relation between muscle activation, assessed with EMG, and position deviations) gave a direct measure for the reflexive muscle activation (Chapters 5-6). The incorporation of the reflexive impedance into the quantification method is new and gives direct insight into the contribution of the underlying reflexive feedback system to the overall mechanical behaviour of the arm. Including the reflexive impedance in the quantification method has the advantage that intrinsic and reflexive parameters, including the neural time delay, can be estimated simultaneously without prior assumptions on the relative contributions.

Measuring spinal reflexes at the wrist

At the start of the project patients were measured on the shoulder manipulator at the shoulder laboratory of the Delft university of technology. As this hydraulic manipulator is not mobile, patients had to travel from the Leiden University Medical Centre to Delft. This had severe implications on the procedures: it was practical impossible to measure patients off medication or to follow the progress of individual patients. Furthermore there was the need to measure a more distal joint, as tonic dystonia with CRPS generally progresses in the extremities from distal to proximal musculature (Schwartzman and Kerrigan, 1990).

Half-way the project it was decided to build a mobile electric-powered wrist manipulator, facilitating experiments at the LUMC (Chapter 7). Early 2003 the wrist manipulator was operational and because of the restricted time only a small study on healthy and parkinsonian subjects was performed in Delft. With this manipulator torque disturbances are applied at the wrist and the admittance of the wrist can be estimated. For the shoulder joint it was already shown that healthy subjects vary the magnitude of the proprioceptive reflex gains, depending on the bandwidth of the disturbance or the external damping imposed by the manipulator (Van der Helm et al., 2002; De Vlugt et al., 2002). Generally it was found that the reflex magnitude increases with decreasing disturbance bandwidth or increasing external damping. In this thesis it is shown that the same phenomena exist for the wrist joint, showing that the wrist manipulator is a relevant manipulator for investigating reflexes (Chapter 8).

In the both the shoulder and the wrist the reflex magnitude varies with disturbance bandwidth or external damping. Two distinct differences exist between the shoulder and wrist: the neural time delay of spinal reflexes and the eigenfrequency. The measurements show that the neural time delay at the wrist is 50% larger than that for the shoulder (43 against 28 ms). As the inertia around the wrist is much smaller than that of the shoulder, the eigenfrequency of a (cocontracted) wrist is approximately 4 times higher than the eigenfrequency of the (cocontracted) wrist (12 Hz for the wrist vs. 3 Hz for the shoulder). Both phenomena have an effect on the stability margins. More time delay in a feedback loop reduces the stability margins, thus allowing smaller feedback gain. Higher eigenfrequency has an opposite effect, allowing larger feedback gains.

Neural time delay is larger in patients with Parkinson's disease

In Chapter 4 and 9 proprioceptive reflexes in patients with Parkinson's disease (PD) are assessed at respectively the shoulder and the wrist. Tremor is one of the major symptoms of PD. As in this thesis force disturbances are applied, tremor would dominate the recorded position deviations, deteriorating the measurements. In Chapter 4 the protocol with external damping is used to quantify proprioceptive reflexes, as external damping reduces tremor. It was found that the range of reflex gain modulation at the shoulder is confined in parkinsonian patients. Furthermore, the high coherence and low relative damping in patients with tremor suggests that

the observed tremor is a property of the system and not (directly) induced by the central nervous system (CNS).

To estimate the reflex gain from the mechanical admittance assumptions were needed to separate the reflexive and intrinsic contribution. In parkinsonian patients (Chapter 4) this probably led to an underestimation of the reflex gains. To overcome this the method was extended with the reflexive impedance, such that no prior assumptions about the separate contributions (Chapters 5-6). In Chapter 9 the reflexive feedback gains are assessed at the wrist with this improved method, based on the mechanical admittance and the reflexive impedance. Again it was found that with external damping the range of reflex gain modulation was confined. Furthermore it was found that the neural time delay in patients was $\approx 25\%$ larger. Larger time delay results in smaller stability margins and oscillation are more likely to occur. Future research with large numbers of subjects should focus on the neural time delay. Note that with the previous method the neural time delay could not be estimated and fixed values were taken from literature.

11.3 Recommendations and future directions

11.3.1 Medical applications

Clinimetric evaluation

In this thesis small groups of patients have been measured to show that the methods are applicable and useful to get insight in the pathophysiology of neurological disorders. The next step will be the clinimetric evaluation of the method. Firstly a large number of healthy subjects needs to be measured to build up a large and representative control group and to check the sensitivity of the method. Secondly a large number of patients needs to be measured to get a good indication of the typical differences, to test the specificity of the method, and to compare the results with standard neurological scores. When indicators are found, it is possible to track patients with disease progress and to evaluate the impact of medication onto the proprioceptive reflexes in specific disorders. The development of the wrist manipulator will facilitate the clinimetric evaluation as the manipulator is mobile such that data acquisition can be performed inside the hospital (LUMC).

Other disorders

This thesis focusses on hypertonia as seen in CRPS and PD. But is well applicable to get insight into the pathophysiology of other disorders with hypertonia and other motor disorders with suggested disturbed proprioceptive reflexes, e.g. cerebrovascular attack (CVA, or stroke), repetitive strain injury (RSI) and paralysis. What happens with the proprioceptive reflexes after paralysis caused by spinal cord injury, stroke or other central nervous system disorders?

11.3.2 Effect of tasks and conditions

In this thesis methods are developed to quantify spinal reflexes during postural control in vivo. Reflexes were quantified by analysing the mechanical behaviour in response to a continuous random force disturbance, while the subject is asked to '*minimize the deviations*'. Note that the role of the disturbance is twofold. Firstly the disturbance is necessary to provoke a mechanical response, allowing identification of the mechanical behaviour. And secondly the disturbance is part of the task: '*minimize deviations*' given the properties of the force disturbance. In other words the subject has to optimize its mechanical behaviour by modulating the reflexive feedback such that the given force disturbance has minimal effect onto the deviations. This brings up four important issues for future investigations: position disturbances, submaximal tasks, transient disturbances, and movement.

Force vs. position disturbances

Force disturbances were applied and subjects were asked to '*minimize the deviations*'. Hence feedback of the position (i.e. muscle spindles) is relevant for the task. The task and the force disturbance require an optimal disturbance rejection, i.e. minimum sensitivity for the force disturbance (low admittance, or high stiffness), demanding high muscle cocontraction and strong position feedback from muscle spindles. Another important class of proprioceptors are the Golgi tendon organs. Literature about the functionality of GTO is scarce. From a theoretical viewpoint force feedback from the Golgi tendon organs is undesirable during position tasks, as force feedback reduces the stiffness.

Another type of input is position perturbations. Position perturbations leaves the force as a controlled variable for the subject, e.g. *press with a specific force (and minimize the force deviation)*. Such tasks require a low stiffness (the effect of a change in position to the force must be small). From an optimal viewpoint feedback from muscle spindle is undesirable and strong force feedback from Golgi tendon organs is desired. Force tasks are unnatural and it would be interesting to investigate how humans perform during force tasks.

In disorders with hypertonia, patients have exaggerated reflexive feedback, i.e. the (muscle spindle, or position) feedback gains are (too) high, where normal subjects have the ability to reduce the reflex magnitude. As with force tasks position feedback from the muscles is undesirable, force tasks may be valuable protocol to investigate patients with hypertonia.

Reflexes with submaximum tasks

Minimizing position deviations requires a maximum effort, and energy (oxygen) consumption is relatively unimportant. Two independent strategies contribute to the performance of the tasks: muscle cocontraction and proprioceptive reflexes. Muscle cocontraction is very energy consuming as the muscles are constantly activated compared to proprioceptive reflexes where energy is only used when in response to a deviation. During submaximal tasks a weighting between performance

(effort) and energy will be required, favouring reflexes over cocontraction. Sub-maximal also implies that multiple solutions are available. Is it possible to uniquely formulate a submaximal task, such that all subjects interpret the task equally. Or will every subject respond differently, or will a few solutions emerge.

During submaximum tasks there will likely be an interplay between force feedback (Golgi tendon organs), position/velocity feedback (muscle spindles), and muscle cocontraction. Feedback from Golgi tendon organs decreases the stiffness but increases the effective bandwidth of the muscle, making muscle spindle feedback effective for higher frequencies (Rozendaal, 1997).

Continuous vs. transients signals

In this thesis continuous disturbances are applied. This thesis and previous studies (Van der Helm et al., 2002; De Vlugt et al., 2002) have shown that humans adapt the reflex magnitude within seconds after the start of the perturbation (to remove any transient effect the first few seconds are omitted). How do humans anticipate to transient perturbations (steps, ramps, etc). The possibility to adapt on-line to the disturbance is lacking. Likely during the first transient disturbance the reflexive setting from before the disturbance is measured, the settings adapt after each following perturbation (learning), and maybe after many perturbations the setting is adapted to the transient. This would implicate that the behaviour is different for each step, making comparisons between and within subjects difficult, and only after many perturbations the response converges to an optimum.

Posture tasks vs. movement

This thesis considers postural control, a specific case within human motion control. How do reflexes contribute during movement? Reflexive feedback clearly tends to keep the system in a posture, or equilibrium. During movement the reflex gains will likely be small to facilitate movement, but likely play an important role during homing-in. How can you measure reflexes during movement?

11.3.3 Future challenges

Neural mechanisms behind disturbed reflexes

With the methods provided in this thesis the magnitude of proprioceptive reflexes can be assessed and differences in reflex magnitudes between patients and healthy controls were found. This brings up the question which neural mechanisms are disturbed with a specific neurological disorder. The models used in this study to describe the spinal feedback are relatively simple black-box observations, describing input-output behaviour of the spinal cord in terms of a summation and some feedback gains. With a more detailed physiological model describing all relevant neuron populations of the spinal cord, i.e. a biological realistic neural network (BNN), more insight could be gained.

Chapter 10 gives a complete new approach by integrating a novel biological realistic neural network (BNN) with a musculoskeletal model of the human arm

and proprioceptors, creating a complete neuromusculoskeletal model. This model study showed the relevance of this approach and directed to possible disturbed neural connections in CRPS. To assess the real synapse strengths and the modulation of the synaptic strengths during experiments, the BNN must be incorporated in the quantification method of Chapter 6. However to validate the BNN and to use the BNN for quantification more variables (signals), likely from inside the spinal cord, are necessary. During the experiments force, position and EMG are recorded. With microneurography, a needle is put inside a nerve and the signal of a single afferent can be recorded. This would facilitate recording of Ib (GTO), Ia (muscle spindle: stretch velocity), II (muscle spindle: stretch) afferents.

How are reflexes controlled?

This thesis shows that people modulate the magnitude of reflexes depending on task and conditions. Previous studies showed that these modulations are optimal (De Vlugt et al., 2001; Schouten et al., 2001). In short, the strength of the synapse (i.e. the modulation of the magnitude) is set such that the performance is optimal, i.e. the human behaves as an optimal controller, weighting performance. This leaves the most intriguing question: how are reflexes controlled? What is the neural mechanism behind the adaptation of these feedback gains? What triggers the CNS to alter the feedback settings? Are the optimal control settings a priori learned by the CNS, or are they continuously adapted in order to minimize a certain variable, or a combination of variables? Or formulated otherwise, if there is an optimal controller where is it and how does it work?

11.4 Epilogue

In this thesis spinal reflexes are assessed by means of disturbance experiments. By analysing the mechanical behaviour and the EMG signals from the muscles the position and velocity feedback gains are quantified. The use of force disturbances is natural for the subjects and facilitates an unambiguous task (*'minimize the deviations'*), while reflexive feedback is functional for the task. Modelling the mechanical response is important as it gives direct insight to the mechanisms behind the observed behaviour. The application of (control) engineering techniques in the field of neuroscience is innovative and also necessary to understand the function of spinal reflexes. The quantification methods and manipulators described in this thesis could be standard diagnostic tools for neurological departments, where the wrist manipulator can be a prototype for future diagnostic devices.

References

- Abbink DA (2002) The effect of position and force tasks on human arm admittance. MSc-thesis, Delft University of Technology, Delft, The Netherlands.
- Agarwal GC, Gottlieb CL (1977) Compliance of the human ankle joint. *J Biomech Eng* 99:166-170.
- Akazawa K, Milner TE, Stein RB (1983) Modulation of reflex EMG and stiffness in response to stretch of human finger muscle. *J Neurophysiol* 49:16-27.
- Amadio PC, Mackinnon SE, Merritt WH, Brody GS, Terzis JK (1991) Reflex sympathetic dystrophy syndrome: consensus report of an ad hoc committee of the American Association for Hand Surgery on the definition of reflex sympathetic dystrophy syndrome. *Plast Reconstr Surg* 87:371-375.
- Bashor DP (1998) A large-scale model of some spinal reflex circuits. *Biol Cybern* 78:147-157.
- Bhatia KP, Bhatt MH, Marsden CD (1993) The causalgia-dystonia syndrome. *Brain* 116:843-851.
- Bobet J, Norman RW (1990) Least-squares identification of the dynamic relation between the electromyogram and joint moment. *J Biomech* 23:1275-1276.
- Brouwn GG (2000) Postural control of the human arm. PhD-thesis. Delft University of Technology, Delft, The Netherlands.
- Carignan CR, Cleary KR (2000) Closed-loop force control for haptic simulation of virtual environments. *Haptics-e 1* (<http://www.haptics-e.org>).
- Carter RR, Crago PE, Keith MW (1990) Stiffness regulation by reflex action in the normal human hand. *J Neurophysiol* 64:105-118.
- Cathers I, O'Dwyer N, Neilson P (1999) Dependence of stretch reflexes on amplitude and bandwidth of stretch in human wrist muscle. *Exp Brain Res* 129:278-287.
- Clancy EA, Morin EL, Merletti R (2002) Sampling, noise-reduction and amplitude estimation issues in surface electromyography. *J Electromyogr Kinesiol* 12:1-16.
- Colgate JE (1988) The Control of Dynamically Interacting Systems. PhD-thesis. Massachusetts Institute of Technology, Cambridge, USA.

- Crago PE, Houk JC, Hasan Z (1976) Regulatory actions of human stretch reflex. *J Neurophysiol* 39:925-935.
- Crago PE, Houk JC, Rymer WZ (1982) TSampling of total muscle force by tendon organs. *J neurophysiol* 47:1069-1083.
- De Vlugt E, Van der Helm FCT, Schouten AC, Brouwn GG (2001) Analysis of the reflexive feedback control loop during posture maintenance. *Biol Cybern* 84:133-141.
- De Vlugt E, Schouten AC, Van der Helm FCT (2002) Adaptation of reflexive feedback during arm posture to different environments. *Biol Cybern* 87:10-26.
- De Vlugt E, Schouten AC, Van der Helm FCT (2003a) Closed-loop multivariable system identification for the characterization of the dynamic arm compliance using continuous force disturbances: a model study. *J Neurosci Meth* 122:123-140.
- De Vlugt E, Schouten AC, Van der Helm FCT, Teerhuis PC, Brouwn GG (2003b) A force controlled planar haptic manipulator for posture control analysis of the human arm. *J Neurosci Methods* 129:151-168.
- De Vlugt E (2004) Identification of spinal reflexes. PhD-thesis. Delft University of Technology, Delft, The Netherlands.
- Doemges F, Rack PMH (1992a) Changes in the stretch reflex of the human first dorsal interosseous muscle during different tasks. *J Physiol* 447:563-573.
- Doemges F, Rack PMH (1992b) Task-dependent changes in the response of human wrist joints to mechanical disturbance. *J Physiol* 447:575-585.
- Hill AV (1938) The heat of shortening and the dynamic constants of muscle. *Proc R Soc Lond B Biol Sci* 126:136-195.
- Hoehn MM, Yahr MD (1967) Parkinsonism: onset, progression and mortality. *Neurology* 17:427-442.
- Huxley HE (1969) The mechanism of muscular contraction. *Science* 164:1356-1366.
- Illert M, Kummel H, Scott JJ (1996) Beta innervation and recurrent inhibition: a hypothesis for manipulatory and postural control. *Pflugers Arch* 432:R61-67.
- Jankowska E (1992) Interneural relay in spinal pathways from proprioceptors. *Prog Neurobiol* 38:335-378.
- Jankowska E, Hammar I (2002) Spinal interneurons; how can studies in animals contribute to the understanding of spinal interneuronal systems in man? *Brain Res Rev* 40:19-28.
- Jenkins GM, Watts DG (1968) Spectral analysis and its applications. Holden-Day, San Francisco, USA.

- Kandel ER, Schwartz JH, Jessell TM (2000) Principles of neural science, fourth edition. McGraw-Hill, New York, USA.
- Kanosue K, Akazawa K, Fujii K (1983) Modulation of reflex activity of motor units in response to stretch of a human finger muscle. *Jpn J Physiol* 33:995-1009.
- Katz R, Mazzocchio R, Penicaud A, Rossi A (1993) Distribution of recurrent inhibition in the human upper limb. *Acta Physiol Scand* 149:183-198.
- Kearney RE, Stein RB, Parameswaran L (1997) Identification of intrinsic and reflex contributions to human ankle stiffness dynamics. *IEEE Trans Biomed Eng* 44:493-504.
- Kirsch RF, Kearney RE, MacNeil JB (1993) Identification of time-varying dynamics of the human triceps surae stretch reflex, I: Rapid isometric contraction. *Exp Brain Res* 97:115-127.
- Kukreja SL, Galiana HL, Kearney RE (2003) NARMAX representation and identification of ankle dynamics. *IEEE Trans Biomed Eng* 50:70-81.
- Lee RG, Tatton WG (1975) Motor responses to sudden limb displacements in primates with specific CNS lesions and in human patients with motor system disorders. *Can J Neurol Sci* 2:285-293.
- MacGregor RJ (1987) Neural and brain modeling. Academic Press, New York, USA.
- Maciejowski JM (1989) Multivariable feedback design. Addison Wesley, New York, USA.
- Milner TE, Cloutier C (1993) Compensation for mechanically unstable loading in voluntary wrist movement. *Exp Brain Res* 94:522-32.
- Mirbagheri MM, Barbeau H, Kearney RE (2000) Intrinsic and reflex contributions to human ankle stiffness: variation with activation level and position. *Exp Brain Res* 135:423-436.
- Mirbagheri MM, Barbeau H, Ladouceur M, Kearney RE (2001) Intrinsic and reflex stiffness in normal and spastic, spinal cord injured subjects. *Exp Brain Res* 141:446-459.
- Olney SJ, Winter DA (1985) Predictions of knee and ankle moments of force in walking from EMG and kinematic data. *J Biomech* 18:9-20.
- Paice E (1995) Reflex sympathetic dystrophy. *BMJ* 310:1645-1648.
- Perreault EJ, Crago PE, Kirsch RF (2000) Estimation of intrinsic and reflex contributions to muscle dynamics: a modeling study. *IEEE Trans Biomed Eng* 47:1413-1421.

- Pintelon R, Guillaume P, Rolain Y, Schoukens J, Van Hamme H (1994) Parametric identification of transfer functions in the frequency domain - A survey. *IEEE Trans Autom Contr* 39:2245-2260.
- Pintelon R, Schoukens J (2001) *System identification: a frequency domain approach*. IEEE Press, New York, USA.
- Potvin JR, Norman RW, McGill SM (1996) Mechanically corrected EMG for the continuous estimation of erector spinae muscle loading during repetitive lifting. *Eur J Appl Physiol* 74:119-132.
- Prochazka A, Gorassini M (1998a) Models of ensemble firing of muscle spindle afferents recorded during normal locomotion in cats. *J Physiol (Lond)* 507:277-291.
- Prochazka A, Gorassini M (1998b) Ensemble firing of muscle afferents recorded during normal locomotion in cats. *J Physiol (Lond)* 507:293-304.
- Ribbers G, Geurts ACH, Mulder T (1995) The reflex sympathetic dystrophy syndrome: a review with special reference to chronic pain and motor impairments. *Int J Rehabil Res* 18:277-295.
- Rozendaal LA (1997) *Stability of the shoulder*. PhD-thesis. Delft University of Technology, Delft, The Netherland.
- Ruitenbeek JC, Janssen RJ (1984) Computer-controlled manipulator/display system for human-movement studies. *Med Biol Eng Comput* 22:304-308.
- Schoukens J, Guillaume P, Pintelon R (1993) Design of broadband excitation signals In: Godfrey KR (ed.), *Perturbation Signals for System Identification*. Prentice-Hall, Englewood Cliffs, USA.
- Schouten AC, De Vlught E, Van der Helm FCT, Brouwn GG (2001) Optimal posture control of a musculo-skeletal arm model. *Biol Cybern* 84:143-152.
- Schouten AC, Van de Beek WJT, Van Hilten JJ, Van der Helm FCT (2003) Proprioceptive reflexes in patients with Reflex Sympathetic Dystrophy. *Exp Brain Res* 151:1-8.
- Schouten AC, De Vlught E, Van der Helm FCT (2004a) Estimating the reflexive impedance during posture tasks. Submitted.
- Schouten AC, De Vlught E, Van Hilten JJ, Van der Helm FCT (2004b) Quantifying reflexes with mechanical admittance and reflexive impedance. Submitted.
- Schouten AC, De Vlught E, Van Hilten JJ, Van der Helm FCT (2004c) Design of a force-manipulator to analyse the admittance of the wrist joint. Submitted.
- Schwartzman RJ, Kerrigan J (1990) The movement disorder of reflex sympathetic dystrophy. *Neurology* 40:57-61.

- Stein RB, Capaday C (1988) The modulation of human reflexes during functional motor tasks. *Trend Neurosci* 11:328-332.
- Stienen AHA, Schouten AC, Van der Helm FCT (2003) Integrating a biological neural network into a musculoskeletal model to analyse postural control reflex modulation. MSc-thesis, Delft University of Technology, Delft, The Netherlands.
- Stroeve SH (1999) Impedance characteristics of a neuromusculoskeletal model of the human arm. I. Posture control. *Biol Cybern* 81:475-494.
- Van der Helm FCT, Schouten AC, De Vlugt E, Brouwn GG (2002) Identification of intrinsic and reflexive components of human arm dynamics during postural control. *J Neurosci Meth* 119:1-14.
- Van Hilten BJ, Van de Beek WJT, Hoff JI, Voormolen JH, Delhaas EM (2000) Intrathecal Baclofen for the Treatment of Dystonia in Patients with Reflex Sympathetic Dystrophy. *N Engl J Med* 343:625-630.
- Van Hilten JJ, van de Beek WJT, Vein AA, van Dijk JG, Middelkoop HAM (2001) Clinical aspects of multifocal or generalized tonic dystonia in reflex sympathetic dystrophy. *Neurology* 56:1762-1765.
- Winters JM, Stark L (1985) Analysis of fundamental human movement patterns through the use of in-depth antagonistic muscle models. *IEEE Trans Biomed Eng* 32:826-839.
- Winters J, Stark L, Seif-Naraghi A (1988) An analysis of musculoskeletal system impedance. *J Biomech* 21:1011-1025.
- Zhang LQ, Rymer WZ (1997) Simultaneous and nonlinear identification of mechanical and reflex properties of human elbow joint muscles. *IEEE Trans Biomed Eng* 44:1192-209.

Appendix A

Spiking vs. continuous time-signals

In a biological realistic neural network (BNN) the information in the signals is contained in spike rates. One concern of using the fast Fourier transform (FFT), is whether these binary spike based signals convey the same frequency information as continuous signals. Information could be lost in the process of signal transformation (e.g. the muscle spindles receive continuous muscle force as input and return spiking signals as output). Therefore the transfer functions are investigated of the conversion from continuous signals to spike based signals and back again.

Continuous random signals are designed in the frequency domain, with uniformly power from 0.12 to 20 Hz and random phase. The signal was transformed to time domain via inverse FFT. Staying within biological boundaries, this continuous signal (in spike rate, sp/s) varied between 0 and 300 sp/s. The conversion from a spike rate to a spike train sums the input (spike rate) and fires a spike whenever the threshold is reached, after which the summation restarts. The return conversion was done in a noncausal process by taking the inverse of the interspike interval length and using this as the rate during the interval. At each stage, the spectral densities are calculated and the analysis performed on the input and output of the signal converters:

$$\hat{H}_{conv}(f) = \frac{\hat{G}_{ii}(f)}{\hat{G}_{io}(f)} \quad (\text{A.1})$$

where $\hat{G}_{ii}(f)$ is the estimate for the auto spectral density of the converter input signal and $\hat{G}_{io}(f)$ the estimate for the cross spectral density between the input and output signals, resulting in the estimate for the frequency response function (FRF) of the conversion process $\hat{H}_{conv}(f)$. The estimates of the spectral densities are averaged over four frequency bands to improve the estimates (Jenkins and Watts, 1968).

This procedure clearly shows that spike rates can be converted to and from spike trains without loss of relevant frequency information (see Fig. A.2). The 'discrete' look of the second spike rate signal in Fig. A.1, is caused by the finite sampling time (1 ms) and introduces high frequency components. These high frequency components are irrelevant for the neuromusculoskeletal model used in this study as the information contained in lower frequencies is unaffected.

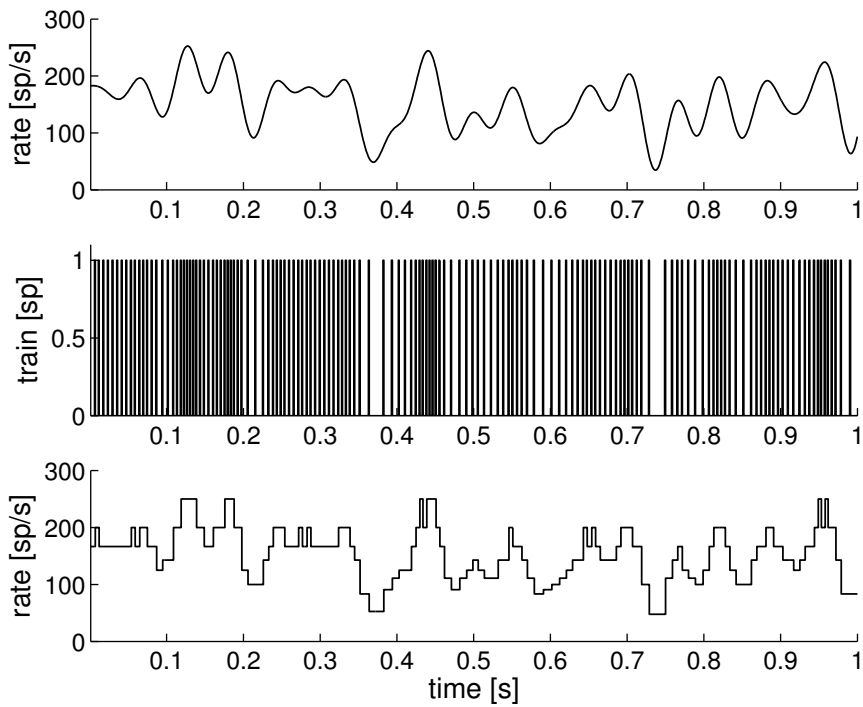


Figure A.1: The original spike-rate signal (above), the converted spike-train signal (middle) and the return converted spike-rate signal (below). To improve readability only the first second of the 8.192 s is shown.

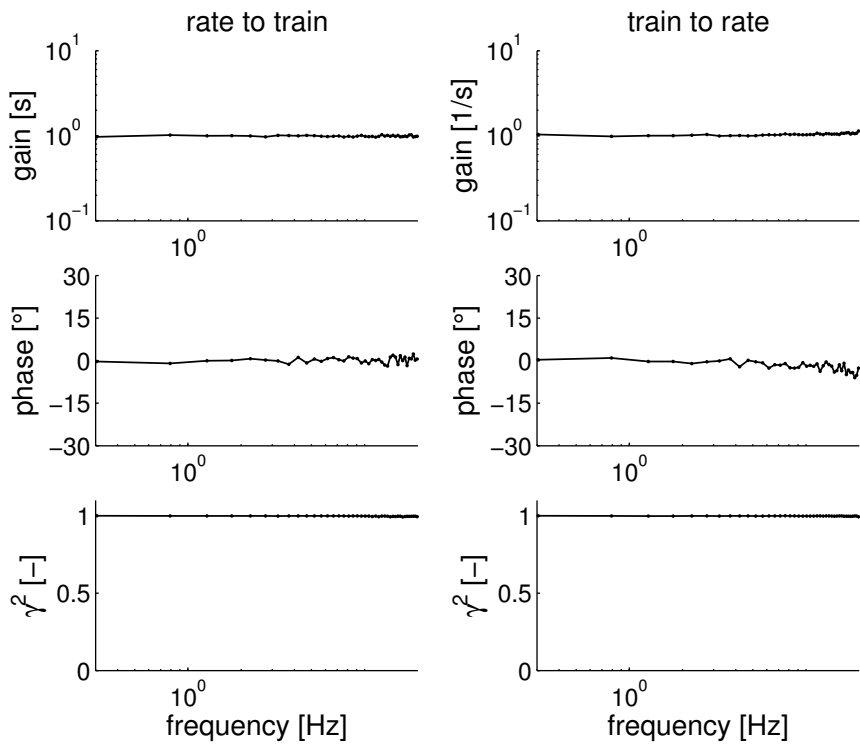


Figure A.2: Gain and phase of the FRF of the signal conversions. Left: conversion from spike-rate to spike-train; right: return conversion from spike-train to spike-rate.

Summary

Chapter 1: Proprioceptive reflexes play an important role during the control of movement and posture. Many studies suggest disturbed modulation of proprioceptive reflexes as the cause for the motor features present in neurological disorders. However no quantitative data exist to support the hypothesis. In this thesis methods are developed and evaluated to quantify proprioceptive reflexes in vivo during postural control. The prime goal of this thesis is to gain insight in the pathophysiology of motor disorders and to evaluate the method as a diagnostic tool.

Chapter 2: To quantify the proprioceptive reflex gains continuous random force disturbances were applied by means of a manipulator, while the subjects were instructed to '*minimize the deviations*' of the handle. The results were analysed in frequency domain with the frequency response function (FRF) of the mechanical admittance, expressing the dynamic relation between force disturbance and handle position. The mechanical response to an external force disturbance comprises intrinsic (muscle) and reflexive properties. The parameters of the intrinsic viscoelasticity and proprioceptive reflex gains are obtained by fitting a model onto the mechanical admittance. By either changing the bandwidth of the force disturbance or the external dynamics imposed by the manipulator different reflex settings are provoked.

Chapter 3: Complex regional pain syndrome (CRPS) is a syndrome that frequently follows an injury and is characterized by sensory, autonomic and motor features of the affected extremities. One of the more common motor features of CRPS is tonic dystonia, which is caused by impairment of inhibitory interneuronal spinal circuits. In this study the proprioceptive reflex gains of the shoulder musculature are quantitatively assessed in nineteen CRPS patients, nine of whom presented with dystonia. The proprioceptive reflexes are quantified by applying two types of force disturbances: (1) disturbances with a fixed low frequency and a variable bandwidth and (2) disturbances with a small bandwidth around a prescribed centre frequency. Compared to controls, patients have lower reflex gains for velocity feedback in response to the disturbances around a prescribed centre frequency. Additionally, patients with dystonia lack the ability to generate negative reflex gains for position feedback, for these disturbances. Proprioceptive reflexes to the disturbances with a fixed low frequency and variable bandwidth present no difference between patients and controls. Although dystonia in the CRPS patients was limited to the distal musculature, the results suggest involvement of interneuronal circuits that mediate postsynaptic inhibition of the motoneurons of the proximal musculature.

Chapter 4: Parkinson's disease (PD) is a neurodegenerative disorder and is characterized by tremor, bradykinesia, rigidity, and impaired postural reflexes. With the gradual loss of dopamine producing brain cells the smooth initiation of movements and fine control of muscles vanish and subsequently the symptoms develop. It is hypothesized that also the modulation of proprioceptive reflexes is involved in the development of the symptoms. Several settings for the external damping, imposed by the manipulator, are applied. It is found that the intrinsic muscle stiffness is significantly larger in patients compared to healthy control subjects. In patients the position feedback gain does increase with external damping but not as steeply as in controls, indication that the range of reflex gain modulation is confined with PD.

Chapter 5: Previous studies used the mechanical admittance to quantify reflex gains during postural control tasks. The method is extended with the reflexive impedance, expressing the dynamic relation between position and muscle activation (assessed via electromyography, EMG). The reflexive impedance describes the muscle activation resulting from the position deviations and hence is a direct measure for proprioceptive reflexes. To record all relevant dynamical characteristics of the arm, wide bandwidth signals were used as force disturbance. Distributing the power of the signal over less frequencies within the bandwidth improved the signal-to-noise ratio (SNR) of the EMG recordings, facilitating reliable estimation of the reflexive impedance.

Chapter 6: With the availability of the FRFs of the mechanical admittance and the reflexive impedance simultaneously, intrinsic and reflexive parameters can be estimated without prior assumptions about their relative contributions. The FRFs were analysed by a neuromusculoskeletal model that implicitly separates the reflexive properties (position, velocity and acceleration feedback gains) from intrinsic muscle visco-elasticity. The results show substantial changes in estimated reflex gains under conditions of variable bandwidth of the applied force disturbance or variable degrees of external damping. Position and velocity feedback gains were relatively larger when the force disturbance contained only low frequencies. With increasing damping of the environment, acceleration feedback gain decreased, velocity feedback gain remained constant and position feedback gain increased. It is concluded that under the aforementioned circumstances, the reflex system adapts its gains to maximize the mechanical resistance to external force disturbances while preserving sufficient stability.

Chapter 7: For most neurological disorders, like CRPS and PD, the motoric features starts at distal joints and may affect more proximal joints as the disease develops. To measure changes in reflex settings in the early stages of these disorders it is desirable to quantify reflexes around a distal joint like the wrist. A wrist manipulator is developed consisting of an electromotor, a lever and a handle. A haptic controller is implemented to apply torque disturbances, such that the subject can actively control the wrist angle. To let the subject 'feel' the torque disturbance as good as possible the apparent dynamics of the device must be small. The minimal apparent inertia of the device is 1.6 gm^2 , which is in the same order of a normal wrist, the minimal damping and stiffness are negligible. To judge the performance of the

manipulator, loads with known physical properties are attached and their parameters were quantified. The parameters of the loads were estimated with deviations of 5% at maximum. Finally the wrist dynamics of a human subject were quantified. The haptic controller has a bandwidth of 50 Hz, meaning that the apparent dynamics are realistically felt till 50 Hz. As the eigenfrequency of a cocontracted human wrist is approximately 15 Hz, a 50 Hz bandwidth of the haptic device is sufficient to measure all relevant dynamics of the human wrist.

Chapter 8: From previous studies investigating reflexes at the shoulder it is known that the magnitude of proprioceptive reflexes depends on the bandwidth of the torque disturbance and on the damping and inertia of the external environment. This study investigates if the same phenomena can be observed at the wrist. The subjects were given a position task (*'minimize the displacement'*), while torque disturbances were applied. The high coherences indicate that for the given conditions the human wrist acts as a linear system. Reflex gains for acceleration, velocity and position along with intrinsic (muscle) properties were quantified by fitting a linear model on the estimated FRFs for the joint admittance and the reflexive impedance. Especially velocity feedback varied substantially with the bandwidth of the disturbance and with the external damping. Generally spoken, smaller bandwidth and a more damped environment provoked larger reflexes. The results suggest that, given the condition, humans modulate the magnitude of the proprioceptive reflexes to maximally resist the torque disturbances.

Chapter 9: The wrist manipulator is used to quantify reflexes in patients with PD to test if the wrist manipulator can be used for patients with Parkinson's disease. Modulation of reflex magnitude was provoked by changing the external damping, imposed by the manipulator, or the disturbance bandwidth. This study showed that parkinsonian patients can perform the task well and that intrinsic and reflexive parameters can be reliably quantified. It was found that the neural time delay of proprioceptive reflexes in patients was significantly larger compared to controls (patients: 55 ms; controls 43 ms). The differences in modulation of the reflex magnitude were most pronounced for the external damping conditions. Future studies with large populations of Parkinson patients should focus on the protocol with damping conditions. By reducing the number of experimental conditions the experiment time will reduce substantially and lighten the experiment for the subjects.

Chapter 10: To give insight into the mechanisms behind negative feedback gains as identified in human postural control, a neuromusculoskeletal (NMS) model was built. Specifically, neural deficiencies were sought which could explain why CRPS patients with tonic dystonia are unable to set negative gains, although they are still to modulate the gains in the positive range. The model is an integration of a biological realistic neural network (BNN), modelling all relevant spinal neurons, and a one degree-of-freedom musculoskeletal model. Muscle proprioceptors provide the neural network with feedback. Literature suggests that the inability to set negative gains results from neurotransmitter deficiencies in inhibiting synapses in the spinal neural network. Two synaptic connections were selected for possible dysfunctioning: (1) the synapse which presynaptically inhibits the monosynaptic stretch reflex,

and (2) the synapse connecting the inhibitory interneuron to the motoneuron. A lack of presynaptic inhibition resulted in an overly dominant monosynaptic stretch reflex with high, positive feedback gains. Disabling the second prevented several major proprioceptive feedback paths from providing the motoneurons with negative stimulation, making the setting of negative feedback gains next to impossible. It is concluded that both synapses play an important role in obtaining negative feedback gains and that dysfunctioning of these synapses could account for the motor features in CRPS patients. However the presynaptically inhibiting of the monosynaptic stretch is a prerequisite for feedback gain modulation.

Chapter 11: In this thesis spinal reflexes are assessed by means of disturbance experiments. By analysing the mechanical behaviour and the EMG signals from the muscles the position and velocity feedback gains are quantified. The use of force disturbances is natural for the subjects and facilitates an unambiguous task (*'minimize the deviations'*), while reflexive feedback is functional for the task. Modelling the mechanical response is important as it gives direct insight to the mechanisms behind the observed behaviour. The application of (control) engineering techniques in the field of neuroscience is innovative and also necessary to understand the function of spinal reflexes. The quantification methods and manipulators described in this thesis could be standard diagnostic tools for neurological departments, where the wrist manipulator can be a prototype for future diagnostic devices.

Alfred Schouten, 2004

Samenvatting

Hoofdstuk 1: Proprioceptieve reflexen spelen een belangrijke rol bij de regulatie van houding en beweging. Vele studies suggereren verstoorde modulatie van proprioceptieve reflexen als oorzaak voor de motorische afwijkingen in neurologische aandoeningen. Er zijn echter geen kwantitatieve gegevens om deze hypothese te ondersteunen. In dit proefschrift zijn methoden ontwikkeld en geëvalueerd om de reflexieve bijdrage tijdens houdingsregulatie te kwantificeren. Het primaire doel van dit proefschrift is het verkrijgen van inzicht in de pathofysiologie van motorische afwijkingen bij neurologische aandoeningen en het evalueren van de methode als een diagnostisch middel.

Hoofdstuk 2: Om proprioceptieve reflexen te kwantificeren worden willekeurige krachtverstoringen opgelegd, met behulp van een manipulator, terwijl de proefpersonen wordt gevraagd de uitwijkingen van het handvat te minimaliseren. De resultaten worden geanalyseerd in frequentiedomein met de frequentie response functie (FRF) van de mechanische admittantie, welke de dynamische relatie tussen krachtverstoring en positie van het handvat uitdrukt. De mechanische reactie op een externe krachtverstoring bestaat uit intrinsieke (spier) en reflexieve eigenschappen. De parameters van de intrinsieke visco-elasticiteit en de proprioceptieve reflex bijdragen worden verkregen door de mechanische admittantie met een model te beschrijven. Verschillende reflex sterkten worden uitgelokt door de bandbreedte van de krachtverstoring of de externe dynamica, welke door de manipulator wordt opgelegd, te veranderen.

Hoofdstuk 3: Complex regional pain syndrome (CRPS), ookwel posttraumatische dystrofie, is een syndroom dat volgt na een trauma en zich kenmerkt door sensorische, autonome en motorische afwijkingen aan de betrokken ledematen. Een veelvoorkomende motorische afwijkingen bij CRPS is een tonische dystonie, veroorzaakt door een stoornis van inhiberende interneuronale circuits in het rugmerg. In deze studie worden de proprioceptieve reflexen rond de schouder gekwantificeerd in negentien CRPS patiënten, van wie negen met dystonie. De proprioceptieve reflexen worden gekwantificeerd door twee soorten krachtverstoringen toe te passen: (1) verstoringen met een beperkte bandbreedte en (2) verstoringen met een smalle bandbreedte rond een bepaalde centrum frequentie. Vergeleken met gezonde proefpersonen hebben de patiënten een lagere reflex sterkte voor snelheidsterugkoppeling bij verstoringen rond een centrumfrequentie. Bovendien, kunnen de patiënten met dystonie geen negatieve reflex sterkte voor positieterugkoppeling genereren bij deze storingen. Proprioceptieve reflexen bij de verstoringen met een beperkte bandbreedte geven geen verschil tussen patiënten en gezonde proefper-

sonen. Hoewel de dystonie in de patiënten tot het distale spierstelsel beperkt was, blijkt uit de resultaten dat interneuronale circuits verantwoordelijk voor postsynaptische inhibitie van de motoneuronen van proximale spieren zijn aangedaan.

Hoofdstuk 4: De ziekte van Parkinson (ZvP) is een neurodegeneratieve aandoening, welke wordt gekenmerkt door tremor, bradykinesia, rigiditeit, en verstoorde houdingsreflexen. Met het geleidelijke verlies van de dopamine producerende hersencellen verdwijnt de vlotte initiatie van bewegingen en ontwikkelen de symptomen. De hypothese wordt gesteld dat ook de modulatie van proprioceptieve reflexen bij de ontwikkeling van de ZvP betrokken is. Verscheidene waarden voor de externe demping, opgelegd door de manipulator, zijn toegepast. De intrinsieke spierstijfheid is bij patiënten beduidend groter in vergelijking met gezonde proefpersonen. In patiënten stijgt de sterkte van de positieterugkoppeling met externe demping, echter niet zo steil als in gezonde proefpersonen, wat er op wijst dat de bereik van de reflex modulatie met de ZvP beperkt is.

Hoofdstuk 5: In de eerdere hoofdstukken is alleen de mechanische admittantie gebruikt om proprioceptieve reflexen te kwantificeren tijdens houdingstaken. De methode wordt uitgebreid met de reflexieve impedantie, welke de dynamische relatie tussen positie en spieractivatie (verkregen middels electromyografie, EMG) uitdrukt. De reflexieve impedantie beschrijft de spieractivatie als gevolg van de positie uitwijkingen en is daardoor een directe maat voor de proprioceptieve reflexen. Om alle relevante dynamische kenmerken van de arm te registreren werden breedbandige signalen gebruikt als krachtverstoring. Verdeling van het signaalvermogen over minder frequenties binnen de bandbreedte verbeterde de signal ruis verhouding van de EMG signalen, wat een betrouwbare schatting van de reflexieve impedantie bevordert.

Hoofdstuk 6: Met de beschikbaarheid van de FRFs van de mechanische admittantie en de reflexieve impedantie kunnen de intrinsieke en reflexieve parameters zonder aannamen over hun relatieve bijdragen worden geschat. De FRFs werden geanalyseerd door een neuromusculair model dat impliciet de reflexieve eigenschappen (positie-, snelheids- en versnellingsterugkoppeling) van de intrinsieke spiervisco-elasticiteit scheidt. De resultaten tonen aanzienlijke veranderingen in reflex sterkte bij beperkte bandbreedte van de toegepaste krachtverstoring of bij veranderlijke mate van externe demping. De reflexieve positie- en snelheidsterugkoppeling waren groter wanneer de krachtverstoring slechts lage frequenties bevatte. Met stijgende externe demping, verminderde de versnellingsterugkoppeling, bleef de snelheidsterugkoppeling bijna constant en steeg de positieterugkoppeling. De resultaten duiden erop dat onder de genoemde omstandigheden, het reflex systeem zijn sterkte aanpast om de mechanische weerstand tegen externe krachtverstoringen te maximaliseren met behoud van stabiliteit.

Hoofdstuk 7: Voor de meeste neurologische aandoeningen, zoals CRPS en de ZvP, beginnen de motorische symptomen bij distale gewrichten en met de progressie van de ziekte kunnen ook proximale gewrichten worden aangedaan. Om veranderingen in reflexen in een vroege stadium te kunnen meten is het wenselijk om reflexen rond een distaal gewricht zoals de pols te kwantificeren. Een pols

pertubator is ontwikkeld, welke bestaat uit een electromotor, een hefboom en een handvat. Een haptisch controller is geïmplementeerd om torsieverstoreningen aan te kunnen bieden, zodat de proefpersoon zijn/haar polshoek actief kan beïnvloeden. Om de proefpersoon de aangeboden verstoring zo goed mogelijk te 'voelen' moet de dynamica van het apparaat klein zijn. De minimale inertie van het apparaat is $1,6 \text{ gm}^2$, wat in de zelfde orde van een normale pols is, de minimale demping en stijfheid zijn te verwaarlozen. Om de prestaties van het haptische apparaat te analyseren, zijn de parameters van systemen met bekende fysieke eigenschappen gekwantificeerd door de gemeten dynamische reacties te modelleren. De parameters van deze systemen werden geschat met een afwijking van maximaal 5%. Tot slot werd de dynamica van de pols van een proefpersoon gekwantificeerd. De pols perturbator heeft een bandbreedte van 50 Hz, m.a.w. de opgelegde dynamica wordt tot 50 Hz realistisch gevoeld. Aangezien de eigenfrequentie van een menselijke pols ongeveer 15 Hz is, volstaat een bandbreedte van 50 Hz om alle relevante dynamica van de menselijke pols te meten.

Hoofdstuk 8: Uit eerdere studies naar reflexen bij de schouder is het bekend dat de sterkte van de proprioceptieve reflexen varieert met de bandbreedte van de verstoring en met de externe demping en inertie opgelegd door de manipulator. Deze studie onderzoekt of dezelfde fenomenen bij de pols kunnen worden waargenomen. Aan de proefpersonen werd een positietaak gegeven (*'minimiliseer de uitwijkingen'*), terwijl torsieverstoreningen werden opgelegd. De hoge coherenties wijzen erop dat onder de gegeven condities de menselijke pols als lineair systeem is te beschrijven. De reflex sterkten voor versnelling, snelheid en positie samen met intrinsieke (spier) eigenschappen werden gekwantificeerd door de FRFs van de mechanische admittantie en de reflexieve impedantie met een lineair model te beschrijven. Vooral de snelheidsterugkoppeling varieerde met de bandbreedte van de verstoring en de externe demping. Over het algemeen veroorzaakten kleinere bandbreedte en meer externe demping grotere reflexen. De resultaten laten zien dat, onder de gegeven condities, mensen proprioceptieve reflexen instellen om de verstoringen maximaal te onderdrukken.

Hoofdstuk 9: De polsmanipulator is gebruikt om reflexen in patiënten met de ZvP te kwantificeren om te testen of de polsmanipulator kan worden gebruikt bij patiënten met de ZvP. Modulatie van de reflex sterkte werd uitgelokt door de externe demping of de bandbreedte van de verstoring te veranderen. Deze studie toont aan dat Parkinson patiënten de taak goed kunnen uitvoeren en dat de intrinsieke en reflexieve parameters betrouwbaar kunnen worden gekwantificeerd. De neurale tijdvertraging van proprioceptieve reflexen in patiënten was beduidend groter in vergelijking met gezonde proefpersonen (patiënten: 55 ms; gezonde proefpersonen 43 ms). De verschillen in modulatie van de reflex sterkte waren het meest uitgesproken voor de externe dempingscondities. Toekomstige studies met grote groepen patiënten zouden zich op het protocol met dempingscondities moeten concentreren. Door het aantal experimentele condities te verminderen zal de experimenttijd wezenlijk verkorten, wat de belasting voor de patiënt aanzienlijk verlicht.

Hoofdstuk 10: Om inzicht te geven in de mechanismen achter negatieve reflex

sterkte, zoals die bij houdingsregulatie is gevonden werd een neuromusculair model ontwikkeld. Specifiek, werd gezocht naar de neurale deficiënties die kunnen verklaren waarom CRPS patiënten met tonische dystonie geen negatieve reflexen kunnen genereren, hoewel zij wel in positieve reflexen kunnen moduleren. Het neuromusculaire model is de integratie van een biologisch realistisch neuraal netwerk (BNN) en een één graad-van-vrijheid spierskelet model. De proprioceptoren van de spier voorzien het BNN van terugkoppeling. Literatuur suggereert dat het onvermogen om negatieve reflexen in te stellen volgt uit deficiënties van neurotransmitter in het ruggemerg. Twee synaptische verbindingen werden geselecteerd voor het mogelijke disfunctioneren: (1) de synaps die presynaptisch de monosynaptic rek reflex inhibeert, en (2) de synaps die inhiberende interneuronen verbindt met de motoneuronen. Uitschakelen van de presynaptische inhibitie resulteerde in een overdreven dominante monosynaptic rekreflex met een hoge positieve reflex sterkte. Uitschakelen van de tweede synaps onderbreekt verscheidene belangrijke proprioceptieve terugkoppelingbanen welke de motoneuronen van negatieve stimuli voorzien en maakt negatieve reflex sterkte onmogelijk. Beide synapsen spelen een belangrijke rol in het verkrijgen van negatieve reflexen. Echter presynaptische inhibitie is eerste vereiste voor modulatie van de reflexen.

Hoofdstuk 11: In dit proefschrift worden de proprioceptieve reflexen gekwantificeerd middels verstoringsexperimenten. Door het mechanische gedrag en de EMG signalen van de spieren te analyseren worden de positie- en snelheidsterugkoppelfactoren gekwantificeerd. Het gebruik van krachtverstoringen is natuurlijk voor de proefpersonen en leidt tot een ondubbelzinnige taak (*'minimaliseer de uitwijkingen'*), terwijl reflexen functioneel zijn voor de taak. Het modelleren van de mechanische reactie is belangrijk aangezien het direct inzicht geeft in de mechanismen achter het gemeten mechanische gedrag. Het toepassen van regeltechnische technieken binnen de neurologie is zinvol, maar ook noodzakelijk om de functie van ruggemerg reflexen te begrijpen. De kwantificatie methoden en manipulatoren die in dit proefschrift worden beschreven kunnen standaard diagnostisch middelen voor neurologische afdelingen worden, waar de polsmanipulator een prototype voor toekomstige diagnostische apparatuur kan zijn.

Dankwoord

Eindelijk na jaren van zwoegen, doorgaan, maar vooral ook plezier, is het eindelijk zover: het proefschrift is voltooid. Het onderzoek had en zal nog jaren doorgaan, maar nu is de tijd om mijn bijdrage hierin op te schrijven. Zo'n project van vele jaren is zelden het werk van een enkeling en op deze plaats wil ik een aantal mensen danken, zonder wie dit proefschrift er in deze vorm nooit geweest zou zijn.

In de eerste plaats wil ik mijn promotoren, Frans van der Helm en Bob van Hilten, bedanken. Ze hebben mij het vertrouwen gegeven om te onderzoek uit te voeren, stonden altijd klaar voor vragen en advies, maar hebben me ook de vrijheid gegeven om het werk om mijn eigen manier uit te voeren.

Het onderzoek beschreven in dit proefschrift volgt op het promotiewerk van Guido Brouwn en ik ben blij dat ik bij Guido heb mogen afstuderen. Hij heeft me tijdens het afstuderen laten zien hoe leuk onderzoek is en heeft daarmee mijn enthousiasme voor onderzoek aangewakkerd.

De pols pertubator is grotendeels gebouwd binnen de faculteit werktuigbouwkunde. De inbreng van Ad van der Geest, John Dukker en Kees Slinkman was hierin onontbeerlijk. Niet alleen hebben zij bijgedragen aan het omzetten van de tekeningen tot een echt apparaat, ook heb ik dankbaar gebruik gemaakt van hun kritische en opbouwende opmerkingen tijdens het ontwerp van de pertubator.

Tijdens het project heb ik met diverse studenten samengewerkt. Leen, Klaske, Joris, Jan-Pieter, Edwin, Pieter, Niek en Marc bedankt. Al staat jullie werk niet in dit proefschrift, het heeft zeker bijgedragen aan het begrip en inzicht. Drie studenten heb ik mogen begeleiden tijdens hun afstuderen: David Abbink, Arno Stienen en Bas Zwaan. Afstudeerders begeleiden kost tijd, maar levert ook veel op, zie o.a. hoofdstuk 8 en 10. Het was prettig om met jullie samen te werken en het heeft me geleerd om onderzoek op een heldere manier uit te leggen.

Verder wil ik Erwin de Vlugt bedanken. Bijna gelijktijdig zijn we elk aan een promotie onderzoek begonnen, beide in het schouderlab, en we delen al vele jaren hetzelfde kantoor. Je bent altijd bereid om ideeën en inzichten te bediscussieren en dat heeft zeker geleid tot de convergentie die nodig is om een proefschrift te kunnen schrijven. Het is me een genoegen om op dezelfde dag te promoveren.

En als laatste wil ik bedanken Yvonne, Lisa en Karlijn, door simpelweg te laten zien dat er meer is in het leven dan wetenschap alleen.

Alfred, april 2004

Curriculum vitae

22 oktober 1972

geboren te Dordrecht.

1985-1991

HAVO, scholengemeenschap 'S.G. de Krimpenerwaard' te Krimpen aan den IJssel.

1991-1995

HTS werktuigbouwkunde te Dordrecht.

1995-1999

TU Delft, werktuigbouwkunde. Afgestudeerd bij de sectie Mens-machine systemen met een scriptie getiteld 'Optimal control of a neuromusculoskel-et al arm model'.

1999-2003

TU Delft, werktuigbouwkunde. Promovendus bij de sectie Mens-machine systemen. Titel proefschrift: 'Proprioceptive reflexes and neurological disorders'.

2004-

TU Delft, werktuigbouwkunde. Postdoc bij de sectie Mens-machine systemen in het TREND project (Traume RELated Neurological Disorders).

